



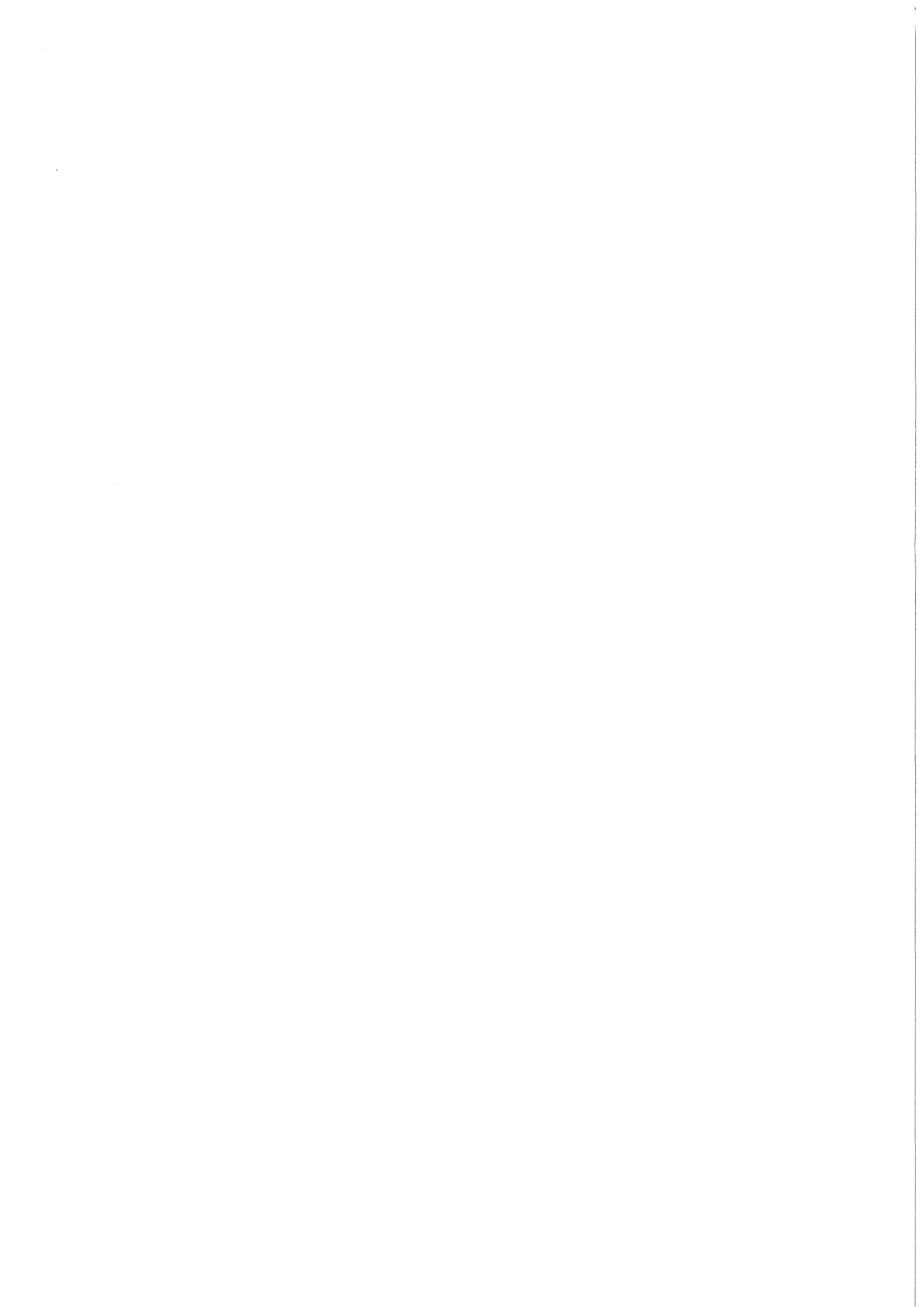
KfK 4405  
Februar 1988

# **Annual Report on Nuclear Physics Activities**

**July 1, 1986 - June 30, 1987**

**Editors:  
W. Heeringa, F. Voss  
Institut für Kernphysik**

**Kernforschungszentrum Karlsruhe**



KERNFORSCHUNGSZENTRUM KARLSRUHE

Institut für Kernphysik

KfK 4405

ANNUAL REPORT

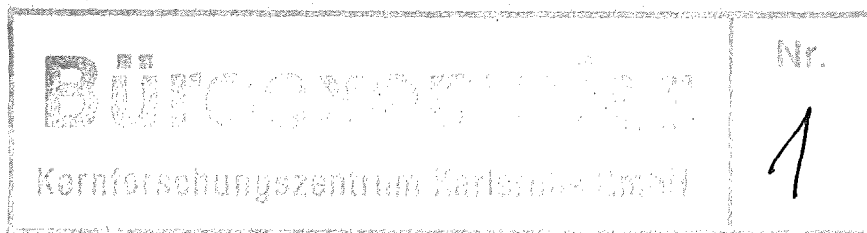
ON

NUCLEAR PHYSICS ACTIVITIES

July 1, 1986 - June 30, 1987

Editors:

W.Heeringa, F.Voss



Kernforschungszentrum Karlsruhe GmbH, Karlsruhe

Als Manuskript vervielfältigt  
Für diesen Bericht behalten wir uns alle Rechte vor

Kernforschungszentrum Karlsruhe GmbH  
Postfach 3640, 7500 Karlsruhe 1

ISSN 0303-4003

## ABSTRACT

This report surveys the activities in basic research from July 1, 1986 to June 30, 1987 at the Institute for Nuclear Physics (IK) of the Kernforschungszentrum Karlsruhe. The research program of this institute comprises laser spectroscopy, nuclear reactions with light ions, neutron physics, neutrino physics and high energy physics, as well as detector technology.

## ZUSAMMENFASSUNG

Der vorliegende Bericht gibt einen Überblick über die Arbeiten am Institut für Kernphysik (IK) des Kernforschungszentrums Karlsruhe im Zeitraum vom 1. Juli 1986 bis zum 30. Juni 1987. Das Forschungsprogramm umfaßt die Gebiete Laserspektroskopie, Kernreaktionen mit leichten Ionen, Neutronenphysik, Neutrinophysik und Hochenergiephysik sowie Detektor-Technologie.

## P R E F A C E

This annual report on nuclear physics activities at the Kernforschungszentrum Karlsruhe describes experiments carried out in sections I and III of the Institut für Kernphysik (IK). Work in the field of intermediate energy physics is no longer included since it was decided in 1987 to transfer these activities completely to Karlsruhe University which had made a considerable contribution to this work in the past years.

The groups in Section IK I are working in experimental nuclear and particle physics:

- Fast Neutron Physics: Scattering experiments on very light nuclei are carried out using the polarized neutron beam of the facility POLKA at the Karlsruhe Cyclotron. The main goal is to determine precise nucleon-nucleon phase shifts from experiments with polarized neutrons on (polarized) protons. The structure of light nuclear systems is studied in neutron scattering experiments and in neutron induced reactions. Measurements of fast polarized neutron capture on light nuclei have been started. The cryogenic polarization facility KRYPTA has been used successfully to produce polarized targets for spin-spin interaction experiments. Prototype studies deal with the use of cryogenic methods for high resolution, low threshold particle detection.

- Neutrino Physics: The group is preparing neutrino physics experiments in the energy range between appr. 10 and 50 MeV. This work is done at the Spallation Neutron Source ISIS at the Rutherford Appleton Laboratory (RAL) in England. The program involves experimental studies of fundamental questions in the fields of particle physics, nuclear physics and astrophysics. A collaboration of KfK, University of Erlangen, University of Karlsruhe, University of Oxford and Queen Mary College of London is going to use the 60 t scintillator detector system KARMEN 1 (Karlsruhe-Rutherford-Medium-Energy-Neutrinoexperiment), which has been installed in a massive blockhouse of steel set up by KfK at ISIS. This work, carried out in cooperation with Karlsruhe University, was partly supported by BMFT through the "Verbund Mittelenergiephysik".

- High Energy Physics: The group is mainly working on the data analysis for the experiments performed with an international collaboration using the CELLO detector at the PETRA accelerator (DESY). Emphasis is laid on the analysis of hadronic final states in  $e^+e^-$  annihilation for QCD tests and for the determination of the coupling constant  $\alpha_s$ . In the study of electroweak interactions the analysis of inclusive leptons in multihadronic events yields information on the heavy c- and b-quarks. A search for new particles in  $e^+e^-$  annihilations was performed. Hardware activities are the development of trigger counters for the em calorimeter of the DELPHI detector at LEP (CERN) and tests of their performance.

- Detector Development: The work is concentrating on liquid ionization chambers using either liquid argon or molecular, room temperature liquids as active media. With liquid argon, the time projection chamber (TPC) was successfully tested. For the room temperature calorimeters, different materials were tested. For tetramethylsilane (TMS) and for neopentane prototype studies have been performed. The investigations will be continued to enable the use of this type of detectors in large scale calorimeters for particle physics and astrophysics experiments.

Section IK III is mainly working in the following fields:

- Nuclear Astrophysics: Capture cross sections of fast neutrons in the keV to MeV range are measured in order to understand in detail the synthesis of heavy elements in stars. In this work, a considerable increase in accuracy is expected from a novel  $4\pi$ -BaF<sub>2</sub> scintillation detector which is nearing completion. For the interpretation of these data, additional nuclear structure information is required. This has initiated a series of experiments at the high flux reactor of the Institut Laue Langevin, Grenoble.

- Nuclear Reactions: Work in this field makes use of the 26 MeV/nucleon <sup>6</sup>Li beam from the Karlsruhe Isochronous Cyclotron and of the magnetic spectrometer for investigating continuous spectra in break-up reactions. Theoretical studies have shown that Coulomb break-up should allow the determination of radiative capture cross sections between light nuclei at very low relative velocities. Such cross sections are of great importance in astrophysics. Experiments in order to verify these considerations are under way.

- Laser Spectroscopy: This technique is applied to sub-ng amounts of radioactive atoms in order to determine hyperfine structure and isotopic shifts of atomic transitions. The results yield information on nuclear moments and on the change of nuclear charge radii due to varying neutron number. At present nuclides of thorium are studied by a new experimental technique the spectroscopy of ions stored in electromagnetic fields.

- Applied Gamma-Ray Spectroscopy: Here instruments are developed to determine concentration and isotopic composition of fissile materials. The instruments make use either of the intrinsic radioactivity or of X-ray absorption and fluorescence. Their main applications are in the safeguards of nuclear fuel and in process control during fabrication and reprocessing.

- Section IK III is also responsible for operating the three accelerators of our institute. The Karlsruhe Isochronous Cyclotron which is mainly used for fast neutron physics and nuclear reaction experiments; the 3.75 MeV Van-de-Graaff accelerator which serves mainly as a source of keV neutrons for the nuclear astrophysics studies; and a compact cyclotron which is basically a commercial installation to produce radioactive isotopes for nuclear medicine and mechanical engineering.

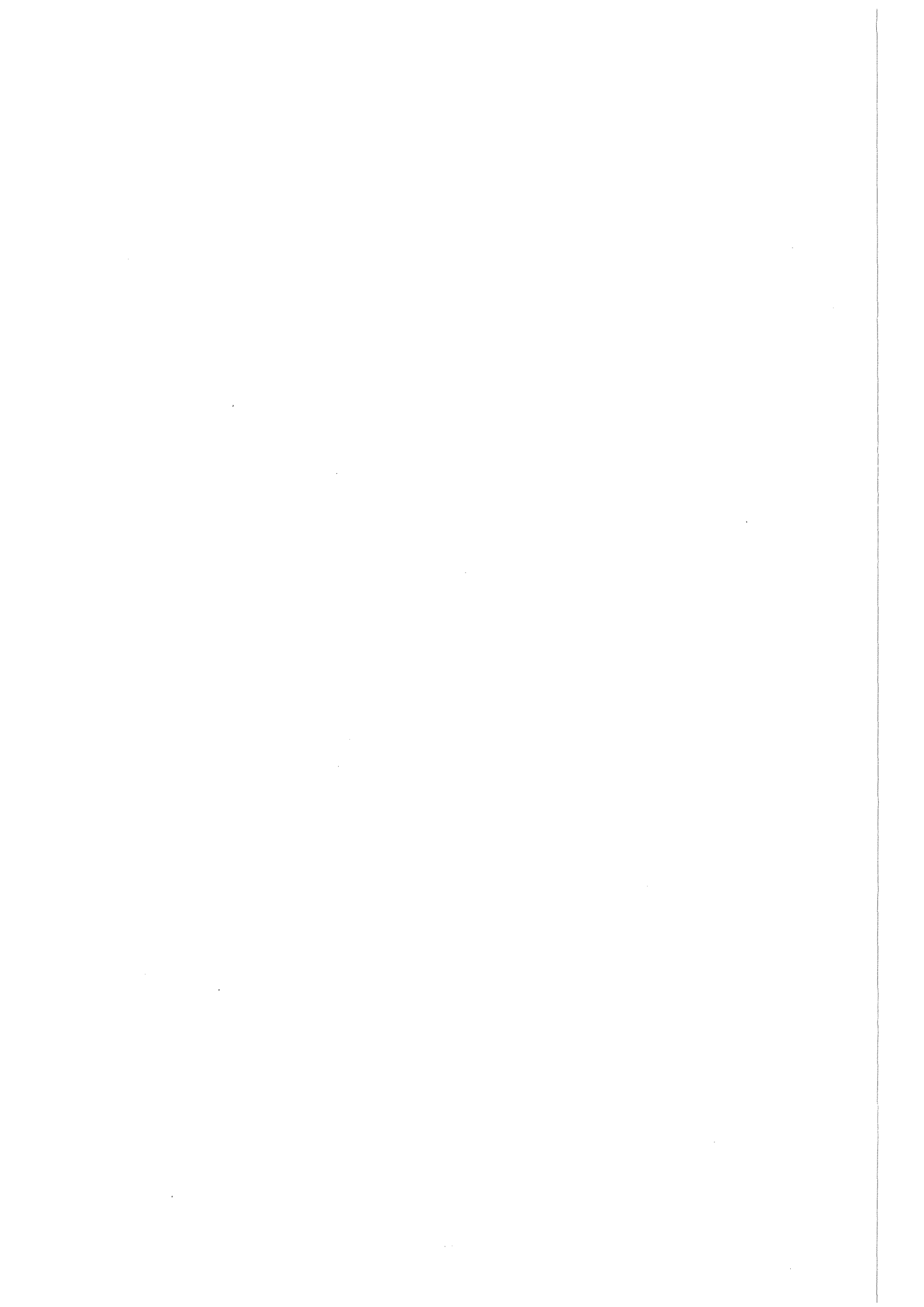


(B. Zeitnitz)



(G. Schatz)





CONTENTS

	PAGE
1. NUCLEAR PHYSICS	
1.1 NUCLEAR ASTROPHYSICS	
1.1.1 The $^{14}\text{N}(n,p)^{14}\text{C}$ reaction at keV neutron energies	1
1.1.2 Measurement of the neutron capture cross section of $^{40}\text{Ar}$ and an s-process analysis from $^{34}\text{S}$ to $^{42}\text{Ca}$	2
1.1.3 The s-process branching at $^{79}\text{Se}$	3
1.1.4 Stellar krypton cross sections at $kT = 25$ and $52$ keV	3
1.1.5 Measurement of the $^{85,87}\text{Rb}$ capture cross sections for s-process studies	4
1.1.6 Activation of short lived isotopes - a measurement of the $^{107,109}\text{Ag}$ capture cross sections	5
1.1.7 The $^{151}\text{Sm}$ branching, a probe for the irradiation time scale of the s-process	6
1.1.8 Extension of the level scheme of $^{176}\text{Lu}$	7
1.1.9 Neutron capture in $^{185,187}\text{Re}$ - a measurement at $kT = 25$ keV	9
1.1.10 The stellar capture cross section of $^{197}\text{Au}$ - an absolute measurement at $kT = 25$ keV	10
1.1.11 Activation studies near the end of the s-process path	13
1.1.12 Status of the classical s-process	15
1.1.13 S-process studies using single and pulsed neutron sources	16
1.1.14 An ionization chamber for studies of stellar (n,p) and (n, $\alpha$ ) reactions	16
1.1.15 Neutron capture cross sections for s-process studies	18
1.1.16 Beta-decay rates of highly ionized heavy atoms in stellar interiors	18
1.2 NEUTRON SCATTERING	
1.2.1 Measurement of the n-p spin correlation parameter $A_{yy}$ at forward angles	20

1.2.2	Results from n-p analyzing power measurements at backward angles	21
1.2.3	Model calculations for the neutron-proton system	23
1.3 NEUTRON INDUCED REACTIONS		
1.3.1	Neutron spin-spin cross sections of $^{27}\text{Al}$ and $^{93}\text{Nb}$	24
1.3.2	Measurement of the analyzing power of the reactions $^3\text{He}(\vec{n},p)t$ and $^3\text{He}(\vec{n},d)d$	25
1.3.3	Preliminary results of neutron capture on $^1\text{H}$ and $^{12}\text{C}$ in the energy range from 18 MeV to 50 MeV	27
1.3.4	Test run for calibrating NaI detectors at 14.24 MeV	28
1.3.5	Study of neutron capture reactions at light nuclei	29
1.4 NUCLEAR REACTIONS BY CHARGED PARTICLES		
1.4.1	Experimental methods for studying nuclear density distributions	31
1.4.2	Density dependent effective interactions in analyses of elastic alpha-particle scattering	34
1.4.3	Inclusive energy spectra and angular distributions of $^6\text{Li}$ -projectile break-up fragments and the Serber model	37
1.4.4	Break-up of 29.6 MeV $^7\text{Li}$ -projectiles on $^{27}\text{Al}$ and $^{59}\text{Co}$	39
1.4.5	Energy dependence of the sequential and direct Coulomb break-up of light ions	41
1.4.6	Looking for nonresonant Coulomb break-up of 156 MeV $^6\text{Li}$ -projectiles	43
1.4.7	A realistic signature of final state interaction in direct Coulomb break-up	45
1.4.8	Manifestation of the internal momentum distribution in $^6\text{Li}$ break-up reactions ?	46
1.4.9	Intermediate mass fragments in the reaction $^6\text{Li} + ^{46}\text{Ti}$ at $E/A = 26$ MeV	49
1.4.10	Intermediate mass fragments from the reactions $^6\text{Li} + \text{natCu}$ and $^6\text{Li} + \text{natAg}$ at $E/A = 26$ MeV	49

1.4.11	A semiclassical multistep evaporation model for intermediate mass fragment emission	53
1.4.12	$E_0$ strength in $^{12}\text{C}$ from $^6\text{Li}$ scattering	54
1.4.13	Isoscalar giant monopole resonances in Sn- isotopes from $^6\text{Li}$ scattering	54
1.4.14	The ( $^6\text{Li}, ^6\text{He}$ ) reaction at small angles to study spin-isospin strength	57
1.4.15	Gamow-Teller strength and other spin-isospin modes in the reaction $^{90}\text{Zr}(^6\text{Li}, ^6\text{He})^{90}\text{Nb}$	59
1.4.16	Empirical relationships between low energy antiproton-nucleon and antiproton-nucleus in- teractions	61
2. LASER SPECTROSCOPY		
2.1	Charge radii and moments of strontium nuclei by laser spectroscopy	64
2.2	Hyperfine splitting of the $^{242\text{m}}\text{Am}$ ground state from atomic beam laser spectroscopy	64
2.3	Nuclear quadrupole moment of $^{243}\text{Am}$ from a hyperfine structure analysis of the Am I level spectrum	66
2.4	Laser spectroscopic investigations of isotope shifts and hyperfine structure of thorium isotopes in an RF ion trap	69
2.5	Attempts to produce a beam of radioactive platinum atoms	73
2.6	A test of the accuracy of atomic beam laser spectroscopy	73
2.7	System for the detection and determination of laser beat frequencies in the E-band range	74
2.8	A frequency stabilized cw ring dye laser with high effi- ciency	75
3. NEUTRINO PHYSICS		
3.1	Status of the project	
3.1.1	Neutrino area	78
3.2	The scintillator calorimeter KARMEN	79
3.3	Electronics and data handling	82
3.4	Prototype results	82

4.	HIGH ENERGY PHYSICS	84
4.1	HARDWARE ACTIVITIES	
4.1.1	Development and tests of triggercounters for the electromagnetic calorimeter of the DELPHI-detector (CERN/LEP)	85
4.2	ANALYSIS OF HADRONIC FINAL STATES AND TEST OF QCD	
4.2.1	Model independent limits of the QCD scale parameter $\Lambda_{\text{MS}}$ from $e^+e^-$ annihilation data in the energy range from 14 to 46 GeV	87
4.2.2	Determination of $\alpha_s$ with energy correlations	91
4.2.3	A model independent study of the shape of the third jet in $e^+e^-$ annihilation into multihadrons at 35 GeV	95
4.3	STUDY OF ELECTROWEAK INTERACTION	
4.3.1	Study of inclusive leptons from b-quark production in $e^+e^-$ annihilations	97
4.4	SEARCH FOR NEW PARTICLES IN $e^+e^-$ ANNIHILATIONS	
4.4.1	Single photon search with the CELLO-detector	100
5.	DEVELOPMENTS AND INSTRUMENTATION	
5.1	DETECTORS	
5.1.1	Status and tests of the Karlsruhe $4\pi$ BaF <sub>2</sub> detector	103
5.1.2	Gamma-ray spectroscopy with a cooled barium-fluoride crystal	104
5.1.3	Electronic components for the $4\pi$ BaF <sub>2</sub> detector	107
5.1.4	Acceptance detector for the magnetic spectrograph "Little John"	111
5.1.5	A modification of the magnetic spectrograph "Little John" for high angular resolution measurements	113
5.1.6	Production of superconductive tunnel junctions for particle detection	116

5.1.7	MWPC set-up for neutron induced reactions on $^{12}\text{C}$	117
5.1.8	Liquid argon time projection chamber	119
5.1.9	Ionization chambers using room temperature liquids	120
5.2 INSTRUMENTATION		
5.2.1	A $^3\text{He}$ evaporation cryostat	122
5.2.2	Scalar multiplexer: the first layout attempt using the sophisticated layout system	124
5.2.3	A CAMAC controlled linear gate	125
5.2.4	Extension and improvement of the data acquisition system for the magnetic spectrograph "Little John"	126
5.3 ACCELERATORS		
5.3.1	Operation of the Karlsruhe Isochronous Cyclotron (KIZ)	128
5.3.2	Operation of the compact cyclotron (KAZ)	131
5.3.3	Status of external ion sources	131
5.3.4	The new computer control system of the KIZ beam lines	133
5.4 APPLICATIONS		
5.4.1	Elemental and trace element distribution in medical samples: Analysis by proton induced X-ray emission	136
5.4.2	$\text{Ca}^{2+}$ -metabolism in arteries of spontaneously hypertensive rats: Assessment by proton induced X-ray emission (PIXE)	137
5.4.3	Distribution of trace element concentrations in Morris hepatoma 7777	137
5.4.4	Elemental composition of human aorta in Marfan syndrome	138
5.4.5	Trace element metabolism in liver cells after copper sulfate uptake	138
5.4.6	Three-dimensional lithium microanalysis by the $^7\text{Li}(p,\alpha)$ -reaction	139
5.4.7	Reprocessing output verification by K-edge densitometry	139

5.4.8	Field demonstration of an X-ray densitometer for uranium and plutonium input verification in re-processing	140
5.4.9	Energy-dispersive X-ray techniques for accurate heavy element assay	140
5.4.10	Demonstration of NDA technology for reprocessing input analytical measurements	141
5.4.11	Evaluation of high-rate pulse processing in K-edge densitometry	141
5.4.12	Design of a wavelength-dispersive prefilter for improved sensitivity of EDXRFA	142
5.4.13	Participation in the interlaboratory exercise REIMEP-86 for the determination of the <sup>235</sup> U abundance in UF <sub>6</sub> samples	143
5.4.14	Energy-dispersive XRF analyzers for uranium monitoring in a reprocessing plant	145
5.4.15	Application of the hybrid X-ray instrument for the measurement of thorium-plutonium mixed solutions	148
5.4.16	A comparison of methods for the net peak area determination from XRF spectra of the KfK hybrid instrument	150
5.4.17	Production of isotopes for medical applications	151
5.4.18	Blood flow measurements using ultra-pure- <sup>81</sup> Rb	154
5.4.19	Radionuclide technique for mechanical engineering (RTM)	155
6.	LIST OF PUBLICATIONS	
6.1	PUBLICATIONS AND REPORTS	157
6.2	CONFERENCE CONTRIBUTIONS	161
7.	PERSONNEL	165

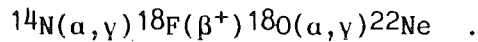
1. NUCLEAR PHYSICS

1.1. NUCLEAR ASTROPHYSICS

1.1.1 THE  $^{14}\text{N}(n,p)^{14}\text{C}$  REACTION AT keV NEUTRON ENERGIES

K. Brehm<sup>\*</sup>, H.P. Trautvetter<sup>\*</sup>, F. Käppeler

Because of its small  $(p,\gamma)$  rate,  $^{14}\text{N}$  is the most abundant product of hydrogen burning in the CNO cycle. When  $^{14}\text{N}$  is exposed to the high temperatures during helium burning it is efficiently converted to  $^{22}\text{Ne}$  via the reaction chain



This isotope then may release enough neutrons by the  $^{22}\text{Ne}(\alpha,n)^{25}\text{Mg}$  reaction for the s-process to operate. However,  $^{14}\text{N}$  must also be considered as a neutron poison because of its sizeable  $(n,p)$  cross section. As no experimental data for this cross section existed in the relevant energy range below 150 keV, the present measurement was intended to replace the rather uncertain extrapolation from higher energies (1).

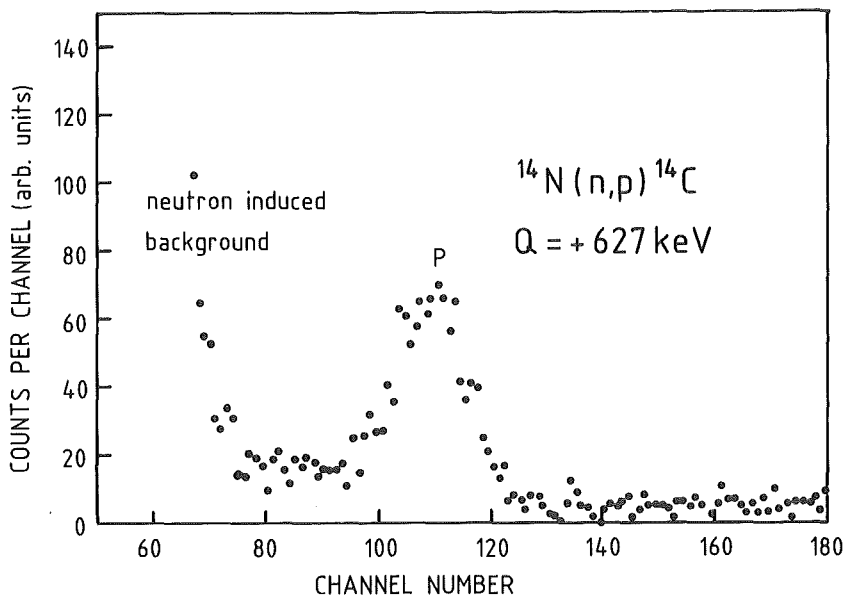


Fig. 1 Pulse height spectrum from the  $^{14}\text{N}(n,p)^{14}\text{C}$  reaction as measured with a 15  $\mu\text{m}$  thick surface barrier detector. The nitrogen sample consisted of a 2 mm wide air gap in front of the detector.



The measurement was carried out at the Karlsruhe 3.75 MV Van de Graaff accelerator using the quasi stellar neutron spectra at  $kT \sim 25$  and 52 keV that can be obtained from the  ${}^7\text{Li}(p,n){}^7\text{Be}$  and  ${}^3\text{H}(p,n){}^3\text{He}$  reactions. It was found that very thin surface barrier detectors ( $<30 \mu\text{m}$ ) were required to resolve the proton peak at  $E_p = 630$  keV from neutron induced backgrounds (Fig. 1). The nitrogen target was simply the air in front of the detector, that was confined in a well defined volume. The rear side of the detector was in an argon atmosphere.

First preliminary results for the  ${}^{14}\text{N}(n,p)$  cross section are  $0.74 \pm 0.05$  mb and  $0.58 \pm 0.07$  mb at  $kT = 25$  and 52 keV, respectively. These values are about three times smaller than assumed in previous stellar model calculations; hence, their impact on the neutron balance is less stringent and the problem of  ${}^{16}\text{O}$  overproduction is reduced (2).

- (1) C.H. Johnson, H.H. Barschall, Phys. Rev. 80 (1950) 818
- (2) M. Arnould, A. Jorissen, Advances in Nuclear Astrophysics, eds. E. Vangioni-Flam, J. Audouze, M. Cassé, J.P. Chièze, J. Tran Thanh Van (Editions Frontières: Gif sur Yvette 1986) p. 419

\* Institut für Kernphysik, Universität Münster

#### 1.1.2 MEASUREMENT OF THE NEUTRON CAPTURE CROSS SECTION OF ${}^{40}\text{Ar}$ AND AN s-PROCESS ANALYSIS FROM ${}^{34}\text{S}$ TO ${}^{42}\text{Ca}$

H. Beer, R.-D. Penzhorn\*(1)

The neutron capture cross section of  ${}^{40}\text{Ar}$  has been measured using the activation technique. A Maxwellian averaged capture cross section of  $2.55 \pm 0.15$  mb at a thermal energy of  $kT = 25$  keV has been obtained. With the present result and additional new data from literature an s-process analysis in the mass region from  $A = 34$  to 42 has been carried out. A two component s-process with exponential neutron exposures has been used assuming continuous and pulsed neutron irradiations. The calculation yielded the s-process abundances of the isotopes in this mass region. The  ${}^{40}\text{Ar}$  and  ${}^{40}\text{K}$  abundances are sensitive to a branching at  ${}^{39}\text{Ar}$ . For  ${}^{40}\text{Ar}$  values can range between 5 and 30 ( $\text{Si} \equiv 10^6$ ). The analysis with the classical unpulsed s-process yielded  $N({}^{40}\text{Ar}) = 24 \pm 7$  ( $\text{Si} \equiv 10^6$ ).

- (1) Astron. Astrophys. 174 (1987) 323

\* Institut für Radiochemie, Kernforschungszentrum Karlsruhe

### 1.1.3 THE s-PROCESS BRANCHING AT $^{79}\text{Se}$

G. Walter, H. Beer, F. Käppeler, G. Reffo\* and F. Fabbri\* (1)

Neutron capture cross section measurements have been carried out for the isotopes  $^{75}\text{As}$ ,  $^{79,81}\text{Br}$ ,  $^{71}\text{Ga}$ , and  $^{74}\text{Ge}$  by the activation method and for  $^{\text{nat}}\text{Ga}$  and  $^{80}\text{Se}$  by the time-of-flight technique and Maxwellian averaged capture cross sections were derived. The measurements were supplemented by capture cross section calculations with the statistical model especially for the radioactive nuclei  $^{79}\text{Se}$  and  $^{81,85}\text{Kr}$ . The analysis of the s-process branching at  $^{79}\text{Se}$  with a two component model of exponential neutron exposures provides the last missing link for a determination of allowed ranges of s-process neutron densities and temperatures. The solar Kr abundance was determined in the frame of this calculation to  $N_{\odot}(\text{Kr}) = 50 \pm 8$  ( $\text{Si}=10^6$ ) and the solar abundances from  $A = 69$  to  $88$  were decomposed into the s- and r-process contributions.

(1) Astron. Astrophys. 167 (1986) 186

\* E.N.E.A., Bologna, Italy

### 1.1.4 STELLAR KRYPTON CROSS SECTIONS AT $kT = 25$ AND $52$ keV

F. Käppeler, A.A. Naqvi\*, M. Al-Ohali\* (1)

Studies of neutron capture nucleosynthesis in the s-process usually refer to a thermal energy of  $kT = 30$  keV, corresponding to a temperature of  $T = 3.5 \times 10^8$  K. This convention is justified as stellar neutron capture rates are in general not sensitive to temperature because of the approximate  $E_n^{-1/2}$  dependence of most capture cross sections. But several important exceptions of this rule require more detailed information on the variation of the average stellar cross section with temperature. We show that activation measurements can be performed in a quasi stellar neutron spectrum for  $kT = 52$  keV, using kinematically collimated neutrons from the  $^3\text{H}(p,n)$  reaction. Neutron capture cross sections were measured in this spectrum and at  $kT = 25$  keV for  $^{86}\text{Kr}(n,\gamma)$  and for the reaction  $^{84}\text{Kr}(n,\gamma)^{85\text{m}}\text{Kr}$ , which populates the isomeric state in  $^{85}\text{Kr}$ . In this way, the respective 30 keV cross sections of  $3.5 \pm 0.3$  and  $16.7 \pm 1.2$  mb could be derived by interpolation.

(1) Phys. Rev. C35 (1987) 936

\* Univ. of Dhahran, Saudi Arabia

### 1.1.5 MEASUREMENT OF THE $^{85,87}\text{Rb}$ CROSS SECTIONS FOR s-PROCESS STUDIES

H. Beer, R.L. Macklin\*

For estimating an upper bound of the neutron burst width of a pulsed s-process, the  $^{87}\text{Rb}$  capture cross section turned out to be of crucial importance (1). In view of the discrepancies observed in previous experiments, a high resolution time-of-flight measurement on  $^{85,87}\text{Rb}$  was carried out at the Oak Ridge Electron Linear Accelerator, covering the energy range between 2.6 and 500 keV. For  $^{87}\text{Rb}$ , single resonances could be resolved up to 40 keV (Fig. 1).

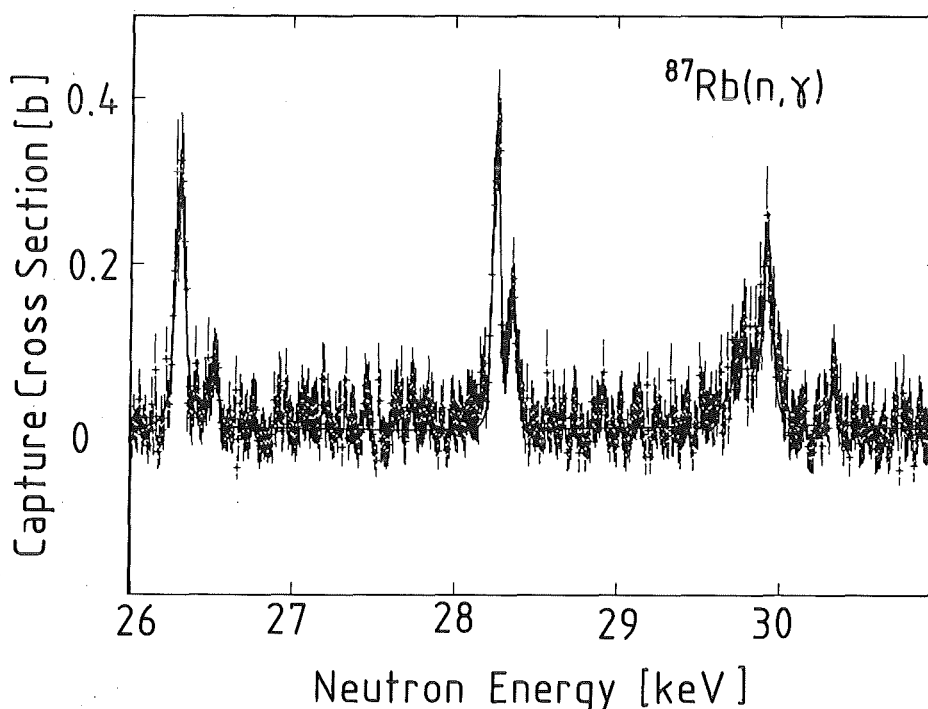


Fig. 1  $^{87}\text{Rb}(n,\gamma)$  yield data. The solid line is generated from the least squares fitting code.

The Maxwellian averaged capture cross section of  $^{87}\text{Rb}$  determined from the new data is in disagreement with the activation result used in ref. (1). It was found that the activation measurement was incorrect because of difficulties with the decay scheme of  $^{88}\text{Rb}$  reported in literature. The analysis of the  $^{85}\text{Kr}$  branching as a test for a pulsed s-process will now be repeated.

- (1) H. Beer, in *Advances in Nuclear Astrophysics*, eds. E. Vangioni-Flam, J. Audouze, M. Cassé, J.P. Chièze, J. Tran Thanh Van (Editions Frontières: Gif-sur-Yvette 1986) p. 375

\* Oak Ridge National Laboratory, Oak Ridge, USA

### 1.1.6 ACTIVATION OF SHORT LIVED ISOTOPES - A MEASUREMENT OF THE 107,109Ag CAPTURE CROSS SECTIONS

H. Beer, F. Voss, F. Käppeler, G. Rupp

A new setup for activation measurements on isotopes with short-lived residual activities ( $> 1$  sec) has been tested, consisting of a fast sample changer and a Ge(Li) detector ( $154 \text{ cm}^3$ , 2.6 keV resolution at 1.332 MeV). Neutrons are produced in the  ${}^7\text{Li}(p,n){}^7\text{Be}$  reaction at  $E_p = 1912$  keV, kinematically collimated with an opening angle of  $120^\circ$ . The Ge(Li) detector is located outside the neutron beam and shielded by lead, Cd sheets, and boron loaded paraffin.

During the irradiation phase, the proton beam current and the neutron flux are monitored; in addition, the neutron flux is recorded as a function of time. Data accumulation from the Ge(Li) detector is blocked by a signal for the analog-to-digital converter. During the counting phase, neutron production is turned off by a beam stop and the induced activities are recorded via the Ge(Li) detector.

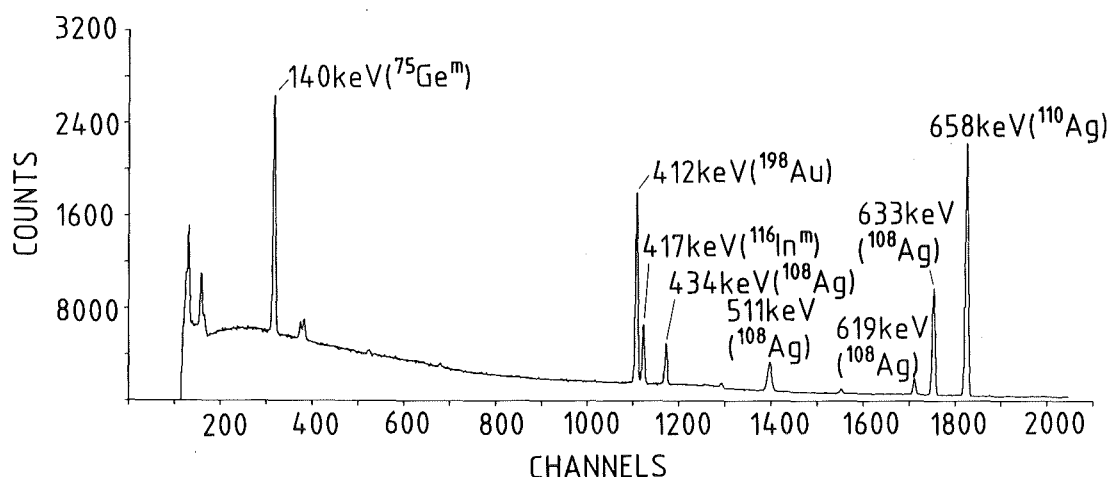


Fig. 1 The Ge(Li) spectrum accumulated in 640 activation cycles of a natural silver sample.

The experimental setup is designed for a determination of the  ${}^{22}\text{Ne}(n,\gamma){}^{23}\text{Ne}$  (38sec) cross section and was tested by a measurement of the cross sections for  ${}^{107}\text{Ag}(n,\gamma){}^{108}\text{Ag}$  (2.41 min) and  ${}^{109}\text{Ag}(n,\gamma){}^{110}\text{Ag}$  (24.6 sec). First results are presented in Fig. 1. The plotted spectrum was accumulated in 640 cycles, each consisting of 26 sec intervals for irradiation and counting, respectively. Besides the gamma activities from the silver sample and the gold standard, prominent background lines from

$^{116}\text{mIn}$  and  $^{75}\text{mGe}$  were also observed, resulting from capture of scattered neutrons in the Ge(Li) detector.

The result on  $^{109}\text{Ag}(n,\gamma)^{110}\text{Ag}$  (24.8 sec) was used to estimate the sensitivity of the setup for the  $^{22}\text{Ne}(n,\gamma)$  reaction: With a 6mg  $^{22}\text{Ne}$  sample the cross section limit would be 0.3 mb.

### 1.1.7 THE $^{151}\text{Sm}$ BRANCHING, A PROBE FOR THE IRRADIATION TIME SCALE OF THE s-PROCESS

H. Beer, R.L. Macklin\*

The excitation functions for the reactions  $^{152,154,155,157}\text{Gd}(n,\gamma)$  have been measured over the neutron energy range from 3 to 500 keV. In Fig. 1 the capture cross sections for  $^{152,154}\text{Gd}$  are shown. Maxwellian averaged capture cross sections for thermal energies  $kT = 5-100$  keV have

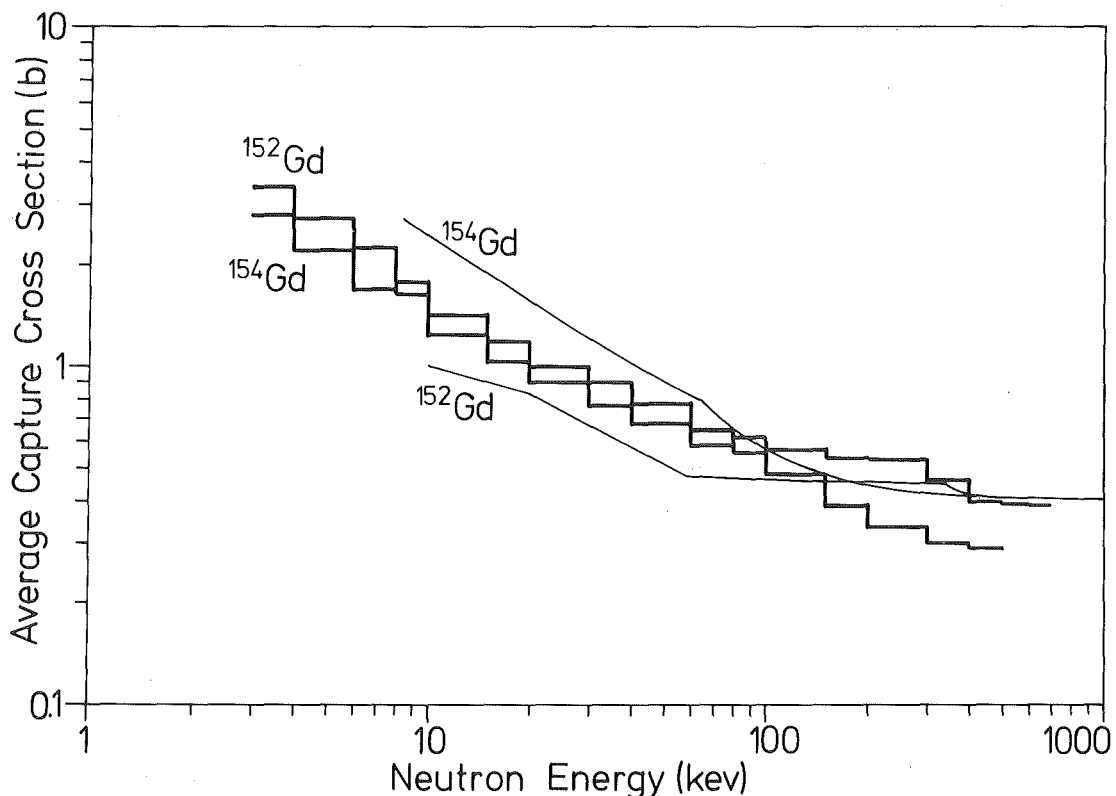


Fig. 1 Effective cross sections of  $^{152,154}\text{Gd}(n,\gamma)$  as a function of neutron energy. Solid lines are theoretical estimates.

been calculated. At  $kT = 30$  keV we have found:  $\sigma(^{152}\text{Gd}) = 1003 \pm 30$  mb,  $\sigma(^{154}\text{Gd}) = 878 \pm 27$  mb,  $\sigma(^{155}\text{Gd}) = 2721 \pm 90$  mb,  $\sigma(^{157}\text{Gd}) = 1355 \pm 39$  mb. The data, in conjunction with other cross sections and solar abundances, were used to carry out an s-process analysis of the branchings in the Sm to Gd mass range. The s-process is treated in the classical as well as in the pulsed model. The solution of the classical model is contained in the pulsed model as the asymptotic solution for large pulse widths. It is shown that this solution is the only one which can reproduce the abundance pattern of the different branchings. Pulse durations are thus limited to values larger than about 3 yr.

\* Oak Ridge National Laboratory, Oak Ridge, USA

#### 1.1.8 EXTENSION OF THE LEVEL SCHEME OF $^{176}\text{Lu}$

N. Klay, H. Beer, H. Börner\*, F. Hoyler\*, F. Käppeler,  
B. Krusche\*, S. Robinson, G. Schatz, K. Schreckenbach\*

In the present study we are searching for electromagnetic links between ground state and isomer of  $^{176}\text{Lu}$  (1), which are important for thermal effects during s-process nucleosynthesis (2,3). Experimentally we have measured the gamma-rays and conversion electrons emitted after thermal neutron capture in  $^{175}\text{Lu}$  using the spectrometers GAMS and BILL at the ILL, Grenoble. These measurements have been finished in March 1987, but data evaluation is still in progress.

Using the information of our first gamma-ray measurement (1) we could already construct an extended level scheme via the Ritz combination principle. This level scheme is still separated into two parts based on the ground state and the isomer, respectively. The internal energy precision of both parts is about 10 eV near 1 MeV level energy and even  $\sim 1$  eV for level energies below 200 keV. This high precision results from the outstanding energy resolution of the GAMS spectrometers.

Compared to this high internal precision, the energy of the isomer is only known within  $\pm 2$  keV from a (t, $\alpha$ ) measurement (4). A recent (d,p) measurement (5) provided a more precise position of the isomer, but should be confirmed with better statistics.

Our present level scheme contains some levels which allow for gamma transitions of low multipolarity between isomer and ground state

without K-forbiddness. In view of the 2 keV uncertainty of the isomer the assignment of these transitions is still ambiguous as many lines of the measured gamma-ray spectrum fall into an interval of this width.

A significant improvement should be possible after the conversion electron spectra are completely evaluated. Up to  $\sim 200$  keV, we have measured the corresponding electron lines for practically all of the significant gamma-ray lines. For the stronger transitions, conversion electrons were even recorded up to  $\sim 880$  keV gamma-ray energy. The momentum resolution in this measurement was  $\Delta p/p \approx 4 \cdot 10^{-4}$ , and therefore admixtures of K, L, M lines could be resolved in most cases in spite of the high line density at lower energies (Fig. 1). Consequently, the multipolarity of most of the  $\sim 550$  gamma-ray transitions should be obtained.

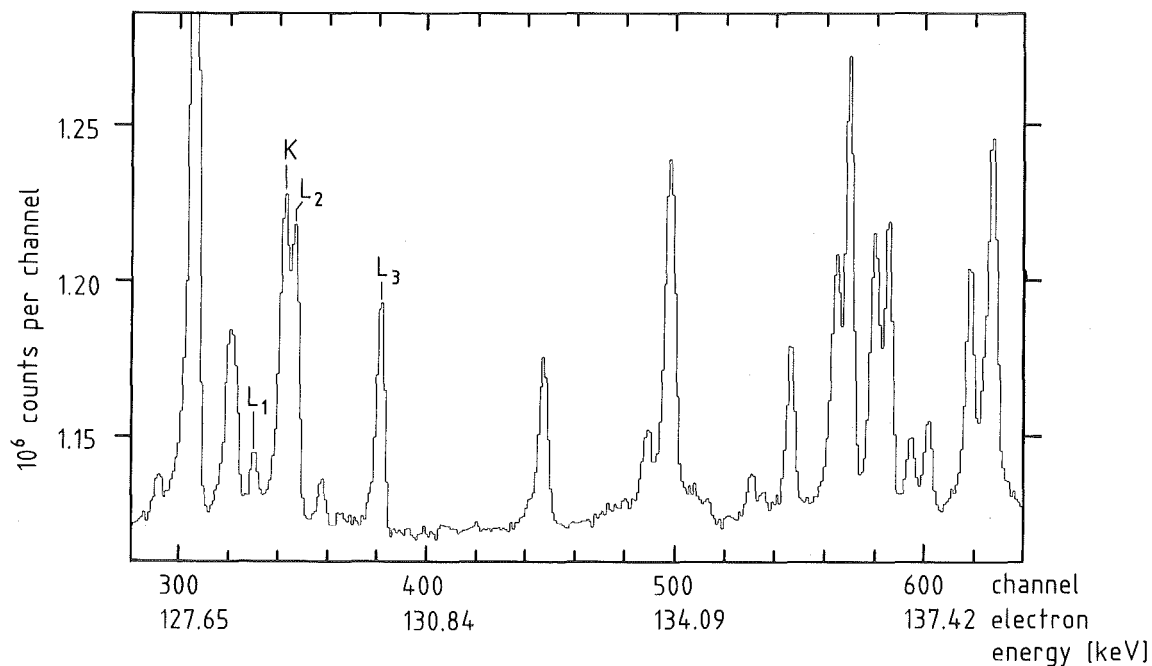


Fig. 1 Part of the conversion electron spectrum from thermal neutron capture in  $^{175}\text{Lu}$ . The corresponding subshells are given for some lines; all L lines result from the same transition.

With this additional information the present level scheme has to be checked. In a next step both parts of the level scheme can be extended with high confidence. This should result in a situation where several mediating transitions can be expected between both parts. A consistent set of such transitions with proper multipolarity can then be used to fix the

energy of the isomer within  $\sim 10$  eV. As a further consistency check this energy should fall into the 300 eV window expected from an improved (d,p) measurement (5).

After all, we expect to establish the level scheme up to  $\sim 1$  MeV, no longer separated into two parts. The information about the mediating transitions will then be used to investigate the thermal effects on the  $^{176}\text{Lu}$  cosmic clock.

- (1) N. Klay, H. Beer, H. Börner, F. Hoyler, F. Käppeler, G. Schatz, K. Schreckenbach, Report KfK 4159, Kernforschungszentrum Karlsruhe, (1986) p. 7
- (2) H. Beer, F. Käppeler, K. Wisshak, R. Ward, Ap. J. Suppl. 46 (1981) 295
- (3) H. Beer, G. Walter, R.L. Macklin, P.J. Patchett, Phys. Rev. C30 (1984) 464
- (4) R.A. Dewberry, R.K. Sheline, R.G. Lander, L.G. Mann, G.L. Struble, Phys. Rev. C24 (1981) 1628
- (5) U. Mayerhofer, G. Hlawatsch, T. v. Egidy (1987) , private communication

\* Institut Laue - Langevin, Grenoble, France

#### 1.1.9 NEUTRON CAPTURE IN $^{185,187}\text{Re}$ - A MEASUREMENT AT $kT = 25$ keV

F. Käppeler, Z.Y. Bao\*, M. Heil

The interpretation of the chronometric pair  $^{187}\text{Re} - ^{187}\text{Os}$  has been shown (1,2,3) to be complicated by various effects, e.g. electron capture in  $^{187}\text{Os}$  which may invalidate the local approximation commonly used in analyses of this clock. The above problem is related to the s-process mass flow through the branching at  $A = 185, 186$ . Apart from the difficult question of the stellar neutron capture rate of  $^{187}\text{Os}$  (4), the status of some other involved cross sections is also not satisfactory (5). As long as the experimental data in this mass range are incomplete, calculations of the cross sections for the unstable branching isotopes  $^{185}\text{W}$  and  $^{186}\text{Re}$  cannot be based on reliable systematics.

To improve this situation, we started a measurement on  $^{185,187}\text{Re}$ . The cross sections of both isotopes can be derived simultaneously by activation of a natural rhenium sample. The decay of the product nuclei  $^{186,188}\text{Re}$  yields gamma-rays of 137 and 155 keV, respectively. The activations are performed in the quasi stellar neutron spectrum obtained with the  $^7\text{Li}(p,n)^7\text{Be}$  reaction, corresponding to a thermal energy of  $kT=25$  keV.



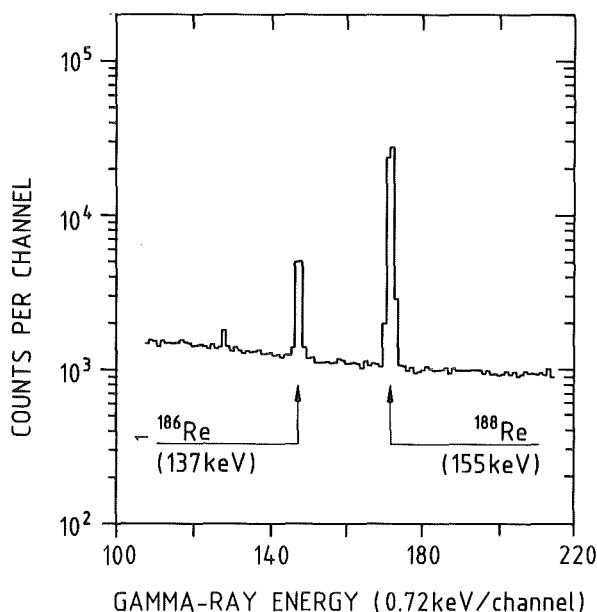


Fig. 1  
Gamma-ray spectrum  
recorded after activation  
of a natural Re sample

Fig. 1 shows the gamma-ray spectrum measured after activation of a 14.7 mg sample for 5.4 h. The background due to beta decay electrons appears rather high because the related gamma-ray intensities are relatively weak. Preliminary results from a first series of activations indicates a significantly smaller cross section for <sup>187</sup>Re as compared to previous data (4).

- (1) J. Conrad, H.D. Zeh, Z. Naturforsch. 33a (1978) 887
- (2) K. Yokoi, K. Takahashi, M. Arnould, Astron.Astrophys. 117(1983)6
- (3) M. Arnould, K. Takahashi, K. Yokoi, Astron.Astrophys. 137(1984)51
- (4) R.R. Winters, R.F. Carlton, J.A. Harvey, N.W. Hill, Phys. Rev. C34 (1986)840
- (5) Z.Y. Bao, F. Käppeler, Atomic Data and Nuclear Data Tables 36 (1987)411

\* Institute of Atomic Energy, Academia Sinica, Beijing, Peoples Republic of China

#### 1.1.10 THE STELLAR CAPTURE CROSS SECTION OF <sup>197</sup>Au - AN ABSOLUTE MEASUREMENT AT kT = 25 keV

W. Ratynski\*, F. Käppeler

The importance of the neutron capture cross section of gold as a standard in the keV region initiated a number of measurements. In the energy range of astrophysical interest around 30 keV neutron energy, differential data obtained with the time-of-flight (TOF) technique as well as data obtained with the activation technique are available. As these data show signifi-

cant discrepancies we found it worthwhile to reinvestigate this cross section via the activation technique.

Neutron production by means of the  ${}^7\text{Li}(p,n){}^7\text{Be}$  reaction has the unique feature that the  ${}^7\text{Be}$  activity directly represents the time-integrated neutron yield, thus allowing absolute cross section measurements. If the proton beam energy is kept close to the reaction threshold at  $E_p = 1881$  keV all neutrons are kinematically collimated in a forward cone, providing for a 'good' experimental geometry. Neutron capture in gold leads to  ${}^{198}\text{Au}$  with a convenient half-life of 2.6 d, so that the capture cross section can be determined completely by activation (1,2). As we were mainly interested in the stellar neutron capture rate, the simulated Maxwell spectrum from the  ${}^7\text{Li}(p,n){}^7\text{Be}$  reaction was chosen for the activations, which was shown to almost perfectly imitate a Maxwellian energy distribution for  $kT = 23.4$  keV (3); this value was later revised to  $kT = 25$  keV (4). This quasi stellar spectrum was remeasured with improved sensitivity and over a larger energy range. The experimental setup was almost identical to that of Beer and Käppeler (3), consisting of two  ${}^6\text{Li}$  glass detectors. One detector served as a stationary monitor to normalize the spectra obtained at various angles with the second movable detector. The angle-dependent neutron spectra were measured with the TOF technique with the accelerator operated in pulsed mode at a repetition rate of 1 MHz and a pulse width of  $\sim 1$  ns. A proton energy of 1912 keV was chosen as in the previous study (3), leading to kinematic neutron collimation into a cone of  $\sim 120$  deg opening angle. The spectrum measurement was carried out in two steps: The energy range  $5 < E_n < 120$  keV was measured with the movable detector located at a flight path of 51.5 cm, which was then reduced to 27.8 cm for better sensitivity down to 1 keV. Integration over the entire neutron cone yields the final spectrum, which is well represented by a Maxwell distribution for  $kT = 25.0 \pm 0.5$  keV.

The activation measurements were carried out in three steps: of definition of the Au samples, irradiation in the above defined neutron spectrum, and determination of the induced  ${}^7\text{Be}$  and  ${}^{198}\text{Au}$  activities.

(i) The shape of the Au samples is determined by the experimental technique: In order that all neutrons pass through the sample and that the sample appears equally thick to all neutrons, a homogeneous spherical gold segment (0.05 mm thick) was used covering the entire neutron beam (Fig.1). The samples were shaped in a precise tool to achieve good homogeneity.

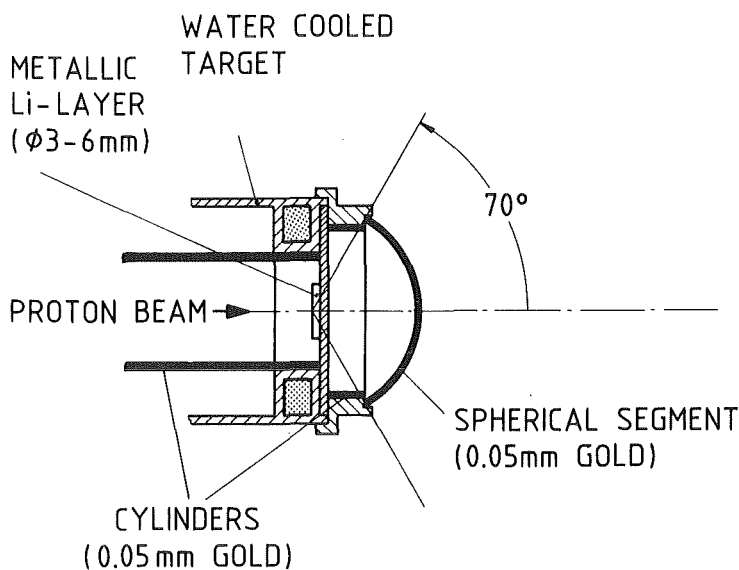


Fig. 1  
Experimental setup during  
the activations.

(ii) All irradiations were carried out at the standard proton energy  $E_p = 1912$  keV. It was verified in a number of tests that  ${}^7\text{Be}$  losses from the target were negligible at the applied beam currents of less than  $1 \mu\text{A}/\text{mm}^2$ . Together with the spherical Au sample two cylindrical Au samples were used during the activations. These are intended to cover practically all of the remaining solid angle, thus directly detecting neutrons, which are scattered in the target backing. This effect required only small corrections (1.8% for 1 mm Cu and 0.5% for 0.2 mm Ag backings) almost entirely due to the cylinder in the forward hemisphere.

(iii) The induced activities were determined via the 412 and 478 keV gamma-ray lines of  ${}^{198}\text{Au}$  and  ${}^7\text{Be}$  using a coaxial, high purity Ge detector with a peak/Compton ratio of 32 and an energy resolution of 1.7 keV at 1.33 MeV. The efficiency ratio for the two gamma-ray lines was determined with standard sources to a precision of 0.3%. The measured gamma-ray intensities were corrected for different solid angle (1%) and self-absorption (2 to 7%), whereas dead time effects were always negligible.

The scatter of the results from 8 activations is fully consistent with the compilation of all systematic and statistical uncertainties. As systematic effects clearly dominate the overall uncertainty of 1.4%, combination of the individual results do not allow for a significantly smaller uncertainty in the final cross section. For the quasi stellar experimental spectrum we quote the neutron capture cross section of gold to be  $\sigma = 586 \pm 8$  mb. This experimental result must be slightly modified before it can be used in an astrophysical context. Conversion to a true stellar cross section requires multiplication with the normalization

factor  $2/\sqrt{\pi}$  and a correction for the difference of the experimental neutron spectrum from the true Maxwellian shape. The latter correction can be obtained via the differential gold cross section of Macklin (5), leading to a final stellar cross section

$$\langle\sigma v\rangle/v_T = 648 \pm 10 \text{ mb} \quad \text{at} \quad kT = 25.0 \pm 0.5 \text{ keV.}$$

The present result is in good agreement with the most often used standard values for the capture cross section of gold. The differences to the data of Macklin (5) and to the previously recommended value at  $kT = 30$  keV by Bao and Käppeler (6) are 1.1 and 3.5%, respectively, and are not significant for the overall picture of s-process nucleosynthesis at the present stage. The importance of the precision achieved in the present study lies in future applications, when improved experimental techniques, (e.g. the Karlsruhe  ${}^4\text{HfBaF}_2$  detector (7)) are expected to yield cross section ratios at the 1 to 2% level.

- (1) W.P. Poenitz, Nucl. Energy 20 (1966) 825
- (2) S. Zhu, S. Jiang, Y. Chen, D. Luo, Chin. Nucl. Phys. 6 (1984) 23
- (3) H. Beer, F. Käppeler, Phys. Rev. C21 (1980) 534
- (4) H. Beer, 1985, private communication
- (5) R.L. Macklin, 1982, private communication
- (6) Z.Y. Bao, F. Käppeler, Atomic Data and Nuclear Data Tables 36 (1987) 411
- (7) F. Käppeler, G. Schatz, K. Wisshak, Report KfK 3472, Kernforschungszentrum Karlsruhe (1983)

\* Institute for Nuclear Studies, Swierk, Poland

#### 1.1.11 ACTIVATION STUDIES NEAR THE END OF THE s-PROCESS PATH

U. Ratzel, H. Beer, F. Käppeler

Neutron capture on the last stable isotope,  ${}^{209}\text{Bi}$ , results in a back-cycling of the s-process flow via alpha decay of  ${}^{210,211}\text{Po}$  to  ${}^{206,207}\text{Pb}$  (Fig. 1) (1). Another possibility is the chain  ${}^{209}\text{Bi}(n,\gamma){}^{210\text{m}}\text{Bi}(n,\gamma){}^{211}\text{Bi}$  which then also decays to  ${}^{207}\text{Pb}$ . However, this becomes only efficient, if the isomer  ${}^{210\text{m}}\text{Bi}$  is not equilibrated with the short lived ground state by thermal excitation in the hot stellar photon bath.

For analyses of the termination of the synthesis path, the stellar neutron capture cross sections for the reactions  ${}^{208}\text{Pb}(n,\gamma){}^{209}\text{Pb}$  and  ${}^{209}\text{Bi}(n,\gamma){}^{210\text{g}}\text{Bi}$  are investigated at  $kT = 25$  keV. The classical s-process model requires three different distributions of neutron exposures to

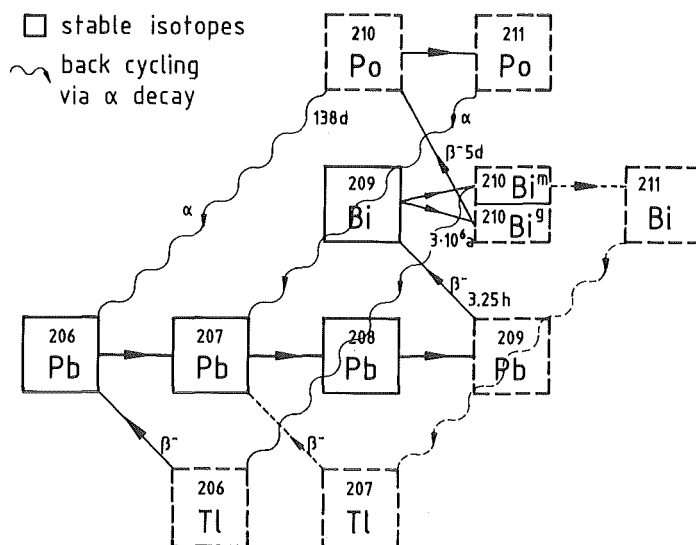


Fig. 1 The s-process flow at the end of the synthesis path.

explain the so-produced abundances. In addition to the main component which describes the abundances between  $A = 90$  and  $200$ , a strong component for  $A > 200$  and a weak component for  $A < 90$  are needed. Previous investigations showed that the abundances of  $^{206}, ^{207}\text{Pb}$  and mainly that of  $^{208}\text{Pb}$  are sensitive to the strong component (2); an accurate neutron capture cross section of  $^{208}\text{Pb}$  is therefore important. Existing measurements being discrepant by a factor 2 (3), motivated the present study. The  $^{208}\text{Pb}$  and  $^{209}\text{Bi}$  sample are activated in a neutron spectrum resembling a Maxwellian energy distribution at  $kT = 25$  keV together with suitable gold foils for monitoring the neutron flux. As the decay of the reaction product leads directly to the ground state of the daughter nuclei, the induced activities have to be determined by detection of the beta decay electrons. For this purpose we have built a  $4\pi$  beta spectrometer consisting of two Si(Li) detectors in close geometry, covering 96% of the total solid angle. The spectrometer resolution is  $\sim 0.3\%$  for the 976 keV conversion line of  $^{207}\text{Bi}$ . Alternatively, we have also considered a beta spectrometer consisting of two thin (0.5 - 1.5mm)  $\text{BaF}_2$  crystals. This solution allows for simpler operation and practically 100% efficiency, while the reduced resolution can be tolerated in case of the smooth beta spectra. However, measurements of very small activities are severely hampered by the intrinsic background of  $\text{BaF}_2$  crystals due to traces of radium, which by far exceeds the net count rate.

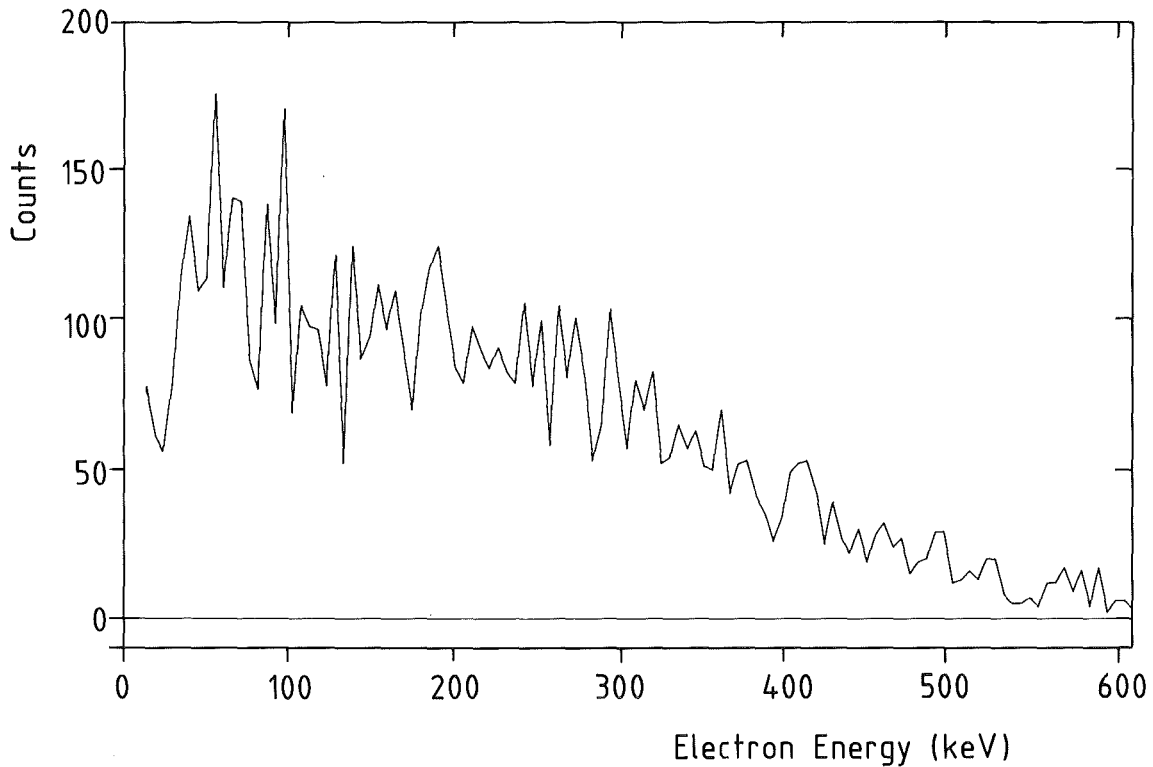


Fig. 2 Electron spectrum from the decay of  $^{209}\text{Pb}$  taken with the  $^4\text{II}$  Si(Li) spectrometer. The fluctuation at low energies results from background subtraction.

First activations showed reasonable signal-to-background ratios (Fig. 2) and seem to confirm the lower cross sections reported in literature (3).

- (1) H. Beer, R.L. Macklin, Phys. Rev. C32 (1985) 738
- (2) D.D. Clayton, M.E. Rassbach, Ap.J. 148 (1967) 69
- (3) Z.Y. Bao, F Käppeler, Atomic Data and Nuclear Data Tables 36 (1987) 411

#### 1.1.12 STATUS OF THE CLASSICAL s-PROCESS

F. Käppeler (1)

The classical s-process, which simply assumes steady neutron irradiations, provides quantitative constraints for a number of characteristic features of neutron capture nucleosynthesis. The present status of these results is summarized and discussed, in particular the product of cross section and

s-process abundance  $\sigma N_s$ , as a function of mass number, r-process residuals, and the effect of s-process branchings.

- (1) Advances in Nuclear Astrophysics, eds. E. Vangioni-Flam, J. Audouze, M. Cassé, J.P. Chièze, J. Tran Thanh Van (Editions Frontières: Gif sur Yvette 1987) p. 355

#### 1.1.13 s-PROCESS STUDIES USING SINGLE AND PULSED NEUTRON EXPOSURES

H. Beer (1)

The formation of heavy elements by slow neutron capture (s-process) is investigated. A pulsed neutron irradiation leading to an exponential exposure distribution is dominant for nuclei from  $A = 90$  to 200. For the isotopes from iron to zirconium an additional "weak" s-process component must be superimposed. Calculations using a single or another pulsed neutron exposure for this component have been carried out in order to reproduce the abundance pattern of the s-only and s-process dominant isotopes. For the adjustments of these calculations to the empirical values, the inclusion of new capture cross section data on  $^{76}\text{Se}$  and  $^{89}\text{Y}$  and the consideration of the branchings at  $^{63}\text{Ni}$ ,  $^{79}\text{Se}$ , and  $^{85}\text{Kr}$  was important. The combination of an s-process with a single and a pulsed neutron exposure yielded a better representation of empirical abundances than a two component pulsed s-process.

- (1) Advances in Nuclear Astrophysics, eds. E. Vangioni-Flam, J. Audouze, M. Cassé, J.P. Chièze, J. Tran Thanh Van (Editions Frontières: Gif sur Yvette 1987) p. 375

#### 1.1.14 AN IONIZATION CHAMBER FOR STUDIES OF STELLAR (n,p) AND (n, $\alpha$ ) REACTIONS

R. Steininger, F. Käppeler

While for the bulk of isotopes involved in neutron capture nucleosynthesis the resulting abundances are completely determined by their respective neutron capture rates, there are a few cases where (n,p) and (n, $\alpha$ ) reactions play an important role. The  $^{33}\text{S}(n,\alpha)^{30}\text{Si}$  reaction is such an example with direct impact on explosive nucleosynthesis (1). The stellar

cross section at  $kT = 30$  keV was determined by two different groups with highly discrepant results:  $\langle\sigma v\rangle/vT = 690 \pm 170$  mb (2) and  $234 \pm 20$  mb (3).

For clarification of this discrepancy and for similar investigations on unstable targets, we have built an ionization chamber. Compared to surface barrier detectors, this approach avoids radiation damage and allows for a large solid angle and, possibly, for lower backgrounds. At the same time, the energy resolution should be comparable to that of solid state detectors. We have chosen an axial chamber geometry with the sample fixed on the cathode in order to achieve a  $2\pi$  solid angle. As the counter gas should be free of hydrogen in order to avoid proton recoils, we found tetrafluormethane a good choice with respect to resolution and stopping power.

The chamber is normally operated at 200 mbar and 200 V/cm. Laboratory tests showed that a resolution of 2% could be achieved for 5 MeV alpha-particles, a value which was slightly worse when the chamber was exposed to the neutron field at the Van de Graaff. Though we are still not content with the backgrounds, the setup is ready for measurements dealing with particle energies above  $\sim 1$  MeV. Fig. 1 shows the spectrum obtained from a sample of  $1.8 \cdot 10^{16}$   $^{33}\text{S}$  atoms implanted into a carbon matrix, which was accumulated within 5 h. The preliminary analysis of this experiment strongly supports the smaller cross section quoted above.

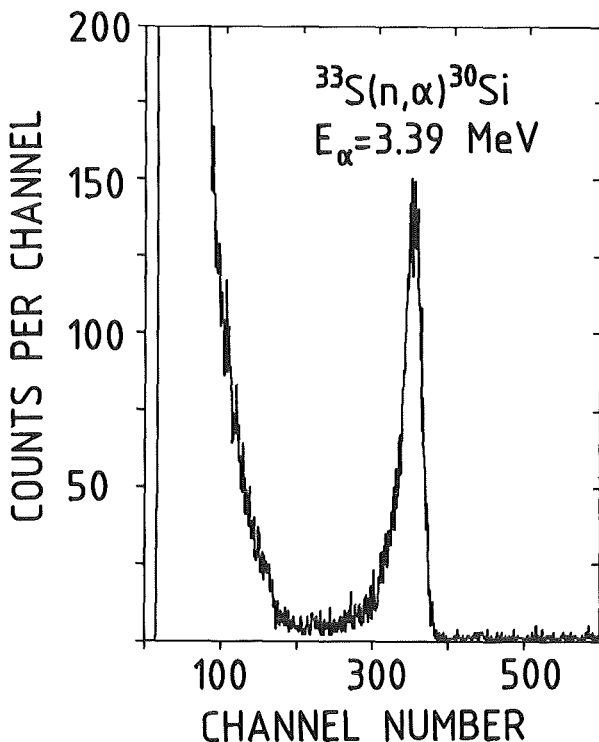


Fig. 1  
Pulse height spectrum of the reaction  $^{33}\text{S}(n, \alpha)^{30}\text{Si}$  measured with the ionization chamber at neutron energies corresponding to  $kT = 25$  keV.



- (1) W.M. Howard, W.D. Arnett, D.D. Clayton, S.E. Woosley, *Astrophys. J.* 175 (1972) 201
- (2) G.F. Auchampaugh, J. Halperin, R.L. Macklin, W.M. Howard, *Phys. Rev. C* 12 (1975) 1126
- (3) C. Wagemans, H. Weigmann, R. Barthelemy, 1986, preprint

#### 1.1.15 NEUTRON CAPTURE CROSS SECTIONS FOR s-PROCESS STUDIES

Z.Y. Bao\* and F. Käppeler (1)

Existing experimental and calculated neutron capture cross sections in the keV energy range have been surveyed, properly renormalized if necessary, and converted into Maxwellian averages over stellar neutron spectra characterized by thermal energies between 10 and 50 keV. This compilation includes all isotopes involved in the slow neutron capture process (s-process) of nucleosynthesis between  $^{12}\text{C}$  and  $^{209}\text{Bi}$  as well as the longer-lived actinide isotopes which might have been modified by the s-process. Gaps in the experimental data were covered with calculated cross sections, which are particularly important in the case of radioactive nuclei and for estimating the effect of thermally populated excited states. From the entire body of evaluated data a current best set of cross sections is recommended for use in s-process studies.

- (1) Atomic Data and Nuclear Data Tables 36 (1987) 411

\* Institute of Atomic Energy, Academia Sinica, Beijing, Peoples Republic of China

#### 1.1.16 BETA-DECAY RATES OF HIGHLY IONIZED HEAVY ATOMS IN STELLAR INTERIORS

K. Takahashi\*, K. Yokoi\*\* (1)

Beta-decay rates are computed for heavy nuclides ( $26 \leq Z \leq 83$ ,  $59 \leq A \leq 210$ ) at stellar temperatures of  $5 \times 10^7 \leq T \leq 5 \times 10^8$  K and electron number densities of  $10^{26} \leq n_e \leq 3 \times 10^{27} \text{ cm}^{-3}$ . The  $\beta$ -decay processes considered are: (i) electron emission ( $\beta^-$ -decay) into the continuum as well as into bound states, (ii) positron emission ( $\beta^+$ -decay); and (iii) capture of orbital and free electrons. The degree of ionization is determined by solving the Saha equation corrected for the continuum depression within a finite-temperature Thomas-Fermi model. The adopted input atomic data are

based on a self-consistent mean-field method. The  $ft$  values for unknown  $\beta$  transitions are estimated from systematics. The result will be most useful for  $s$ -process nucleosynthesis studies.

(1) Atomic Data and Nuclear Data Tables 36 (1987) 375

\* present address: Physics Department, Ohio State Univ., Columbus, Ohio 43210

\*\* present address: Science and Engineering Research Laboratory, Waseda University, Tokyo, Japan

## 1.2 NEUTRON SCATTERING

### 1.2.1 MEASUREMENT OF THE n-p SPIN CORRELATION PARAMETER $A_{yy}$ AT FORWARD ANGLES

P.Doll, V.Eberhard, G.Fink, R.W.Finlay\*, T.D.Ford, W.Heeringa,  
H.O.Klages, H.Krupp, Chr.Wölfel

The measurement of the n-p spin correlation parameter  $A_{yy}$  at backward angles ( $\theta_{CM} = 90^\circ, 105^\circ, 120^\circ$ ) in the energy range from 20 to 50 MeV was described in the 1985/86 annual report (1). Since then a new experiment was carried out to determine  $A_{yy}$  at forward angles ( $\theta_{CM} = 45^\circ, 60^\circ, 75^\circ$ ) and simultaneously repeating the previous angles with less detectors.

Polarized neutrons were produced in the facility POLKA (2) at the Karlsruhe cyclotron. They were scattered by the polarized protons of a  $TiH_2$  sample in the polarization facility KRYPTA (3). Both the neutron and the proton polarization were around 50%. The scattered neutrons were detected by 10 cm diameter x 10 cm length NE213 detectors with gain monitoring by LED pulses (4).

The background of neutrons scattered from Ti was determined in measurements using a Ti sample instead of the  $TiH_2$  probe. These samples were exchanged at full magnetic field and at low temperature. The neutron flux in front of the polarized target was monitored by a set of four recoil proton telescopes (5). Multiparameter data were taken with a Camac-LSI 11 system.

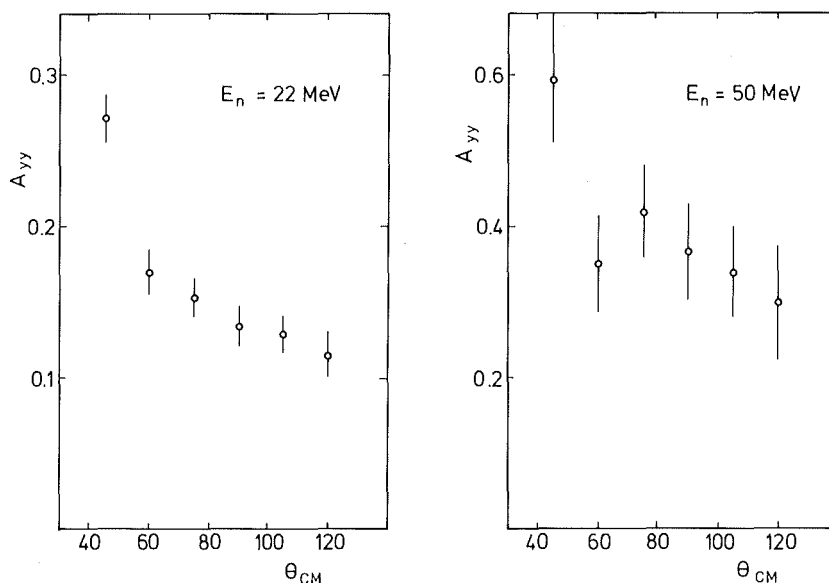


Fig.1: Preliminary  $A_{yy}$  results for n-p scattering at 22 and 50 MeV.

The off-line analysis is presently carried out. Basically, the results are obtained by subtracting the normalized Ti events from the TiH<sub>2</sub> events. Several corrections have to be applied. For example, for spin-dependent flux attenuation in the TiH<sub>2</sub> sample and for multiple scattering. With this new experiment the data base of A<sub>yy</sub> in the n-p system is enlarged by thirty new data points at forward angles and is improved in the backward angle range.

The figure shows some preliminary results of the angular distribution of A<sub>yy</sub> at 22 and 50 MeV. With these data a new phase shift analyses for the n-p system will be done.

- (1) H.Krupp et al., KfK report 4159 (1986), 19
- (2) H.O.Klages et al., Nucl.Instr.Meth., 219 (1984) 269
- (3) R.Aures et al., Nucl.Instr.Meth. 224 (1984) 347
- (4) V.Eberhard et al., KfK report 3969 (1985) 157
- (5) P.Doll et al., Nucl.Instr.Meth. A250 (1986) 526

\*Ohio State University, Athens, USA

#### 1.2.2 RESULTS FROM np ANALYZING POWER MEASUREMENTS AT BACKWARD ANGLES

V.Eberhard, P.Doll, G.Fink, R.W.Finlay\*, T.D.Ford, W.Heeringa,  
H.O.Klages, H.Krupp, Chr.Wölfel

In the last few years, several groups (1) have contributed high accuracy np analyzing power data in the energy range up to 50 MeV. Phase shift analyses and sensitivity calculations reveal, that these data have strong impact on the <sup>3</sup>D<sub>J</sub>- and <sup>3</sup>P<sub>J</sub>-phase shifts.

Especially the backward angle results for A<sub>y</sub> have gained new attention due to severe disagreements between some data sets (3). Neutron detection at far backward angles is difficult. Detection of recoil protons with ΔE-E telescopes at forward angles yields much cleaner spectra and more reliable results.

We used four of such ΔE-E telescopes as flux monitors for polarized neutrons in several experiments and simultaneously for analyzing power measurement at  $\theta_{lab} = 10^\circ, 17.5^\circ$  and  $25^\circ$ . In an other experiment, we used four symmetric pairs of ΔE-E telescopes in an evacuated scattering chamber at  $\theta_{lab} = 10^\circ, 17.5^\circ, 25^\circ$  and  $32.5^\circ$  to measure the same observable. As targets we used 2 mm and 3 mm polyethylene in both experimental set-ups (for details see ref.4). The measurements were carried out with the continuous energy ('white') neutron beam from POLKA (5).

The data analysis has been finished. Background from neutron-carbon scattering in the PE-targets was subtracted. Precise n-p analyzing power data

were obtained, which will enable us to put sharper constraints on the  $^3D_J$  phase shifts. The phase-shift analysis is presently carried out. Fig.1 shows all new  $A_y$  data from our experiments. A great number of data with high accuracy are obtained, especially for smaller scattering angles. Negative  $A_y$  values are excluded. The new data are in good agreement with other data, see fig.2.

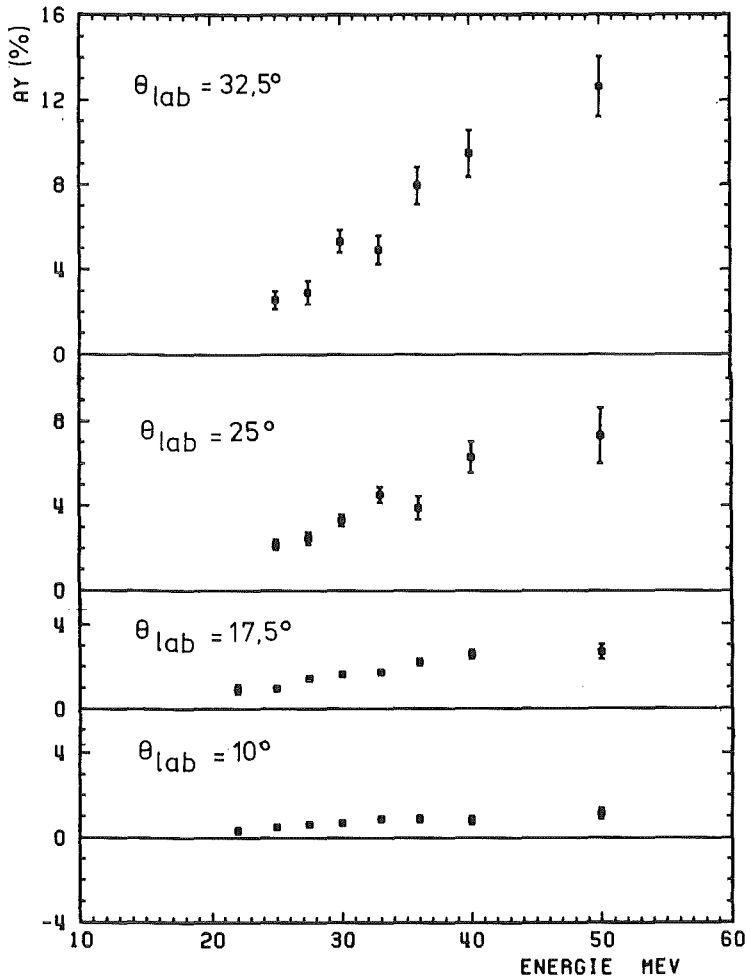


Fig.1: Averaged n-p  $A_y$  data from all measurements from  $\theta_{lab} = 10^\circ$  to  $32.5^\circ$  at neutron energies from 20 MeV to 50 MeV.

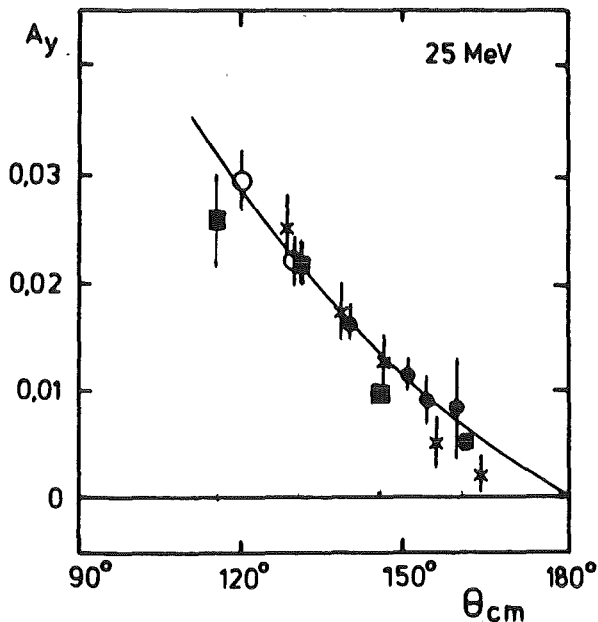


Fig.2: Backward angle distribution of the np analyzing power  $A_y$ . The new data (squares) are compared to older Karlsruhe data (2) (full dots) and results from the Madison group (3). Circles: neutron detected, crosses: protons detected. Solid line: phase shift analysis (2).

- (1) J.Wilczynski et al., Nucl.Phys. A425 (1984) 458  
W.Tornow et al., Nucl.Phys. A340 (1980) 34  
M.D.Barker et al., Proc.Few Body X, Karlsruhe (1983) IIp.31
- (2) H.Krupp, Ph.D.thesis, Univ. Karlsruhe (1986)
- (3) J.Sromicki et al., Proc.Few Body XI, Sendai (1986) IIp.394
- (4) P.Doll et al., Nucl.Instr.Meth. A250 (1986) 526
- (5) H.O.Klages et al., Nucl.Instr.Meth. 219 (1984) 269

\*Ohio State University, Athens, USA

### 1.2.3 MODEL CALCULATIONS FOR THE NEUTRON-PROTON SYSTEM

P.Doll

Besides the efforts to understand our large bulk of neutron-proton scattering data by means of phase-shift analyses, we started (1) to perform simple nucleon-nucleon interaction model calculations. The calculations are carried out in the N-matrix formalism, where the T-matrix elements are taken in the first Bonn approximation. It is the goal of the model calculations to find the components of the nucleon-nucleon interaction which are relevant for specific dynamical regions for our precise neutron-proton scattering data (2). So far the calculations are in a preliminary form, however, revealing already the energy variation of the total elastic scattering cross section within 5% on the average in the

energy range as indicated in the figure 1. This figure shows a comparison between our own data given by dots and older data at 25.8 MeV (3), 50 MeV (3) and 63.1 MeV (4) and the model calculations (dashed curves). During the course of the calculations the partial wave interaction strength which is associated with the corresponding Legendre function of the second kind was slightly varied with energy. This is of course not a justified procedure but better higher partial waves  $l \geq 2$  and off-shell effects are incorporated in the calculations. Higher order observables like the vector and tensor analyzing

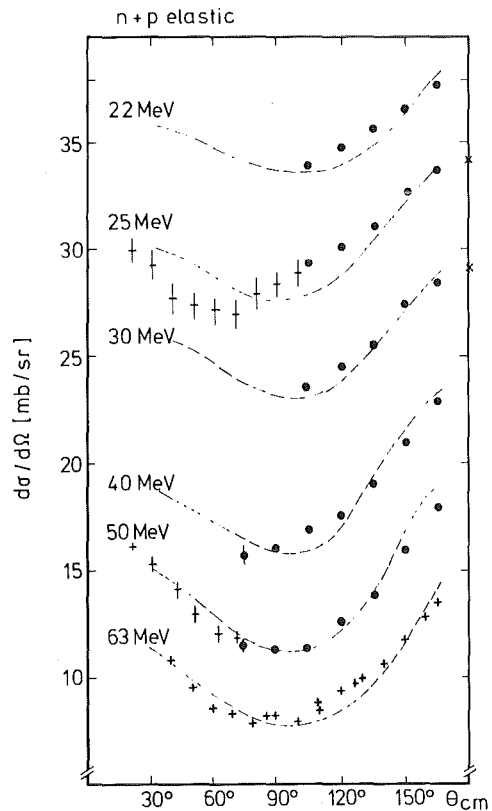


Fig.1: Neutron-Proton differential cross section.

power represent a further testing ground for the model calculations.(2)

- (1) P.Doll, Annual report KfK 4159 (1986) p.54
- (2) G.Fink, P.Doll, T.D.Ford, W.Heeringa, H.O.Klages, H.Krupp to be published
- (3) T.C.Montgomery, B.E.Bonner, F.P.Brady, W.B.Broste, N.W.McNaughton, Phys.Rev. 16C (1977) 499
- (4) N.S.P.King, J.D.Reber, J.L.Romero, D.H.Fitzgerald, J.L.Ullmann, T.S.Subramanian, F.P.Brady, Phys.Rev. 21C (1980) 1185

### 1.3 NEUTRON INDUCED REACTIONS

#### 1.3.1 NEUTRON SPIN-SPIN CROSS SECTIONS OF $^{27}\text{Al}$ AND $^{93}\text{Nb}$

Chr.Wölfl, D.Reppenhagen, P.Doll, R.W.Finlay\*, W.Heeringa, H.O.Klages, H.Skacel, T.D.Ford

Spin-spin cross section measurements have been carried out at the polarized neutron beam POLKA of the Karlsruhe cyclotron for the nuclides  $^{27}\text{Al}$  and  $^{93}\text{Nb}$ . The target samples were 40 mm long and had a diameter of about 30 mm. They were polarized in the cryostat KRYPTA by a 9 T magnetic field at temperatures around 10 - 15 mK. During the measurements the average polarization of the samples was 45% for aluminium and 55% for niobium.

For the neutron flux measurement in front of and behind the target three different types of detectors were employed: thin scintillation detectors, converter- $\Delta E$  arrangements and converter- $\Delta E$ - $\Delta E$  arrays. The data were

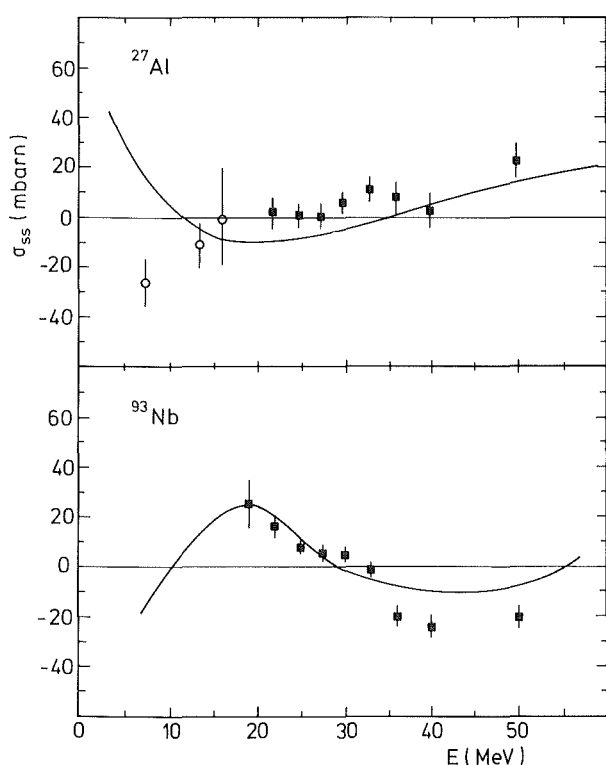


Fig.1: Results of our  $\sigma_{ss}$  measurements (squares) compared with data from TUNL (open circles) and microscopic calculations (full curve).

analyzed in energy bins from 21-50 MeV for  $^{27}\text{Al}$  and 19-50 MeV for  $^{93}\text{Nb}$ .

The results are shown in fig.1 as full squares. Also shown are data from TUNL on  $^{27}\text{Al}$  as open dots (1). The only other  $\sigma_{\text{SS}}$  data above 10 MeV have been measured for  $^{59}\text{Co}$  up to 30 MeV (2) with uncertainties of about 25 mb. Hence our results are the first above 30 MeV and they have a considerably increased accuracy. The curves are predictions by McAbee (3) using microscopic calculations. The agreement is quite good, considering the fact that there are no free parameters. Presently we are carrying out calculations with optical model spin-spin potentials.

- (1) C.R.Gould et al., Phys.Rev.Lett.
- (2) W.Heeringa et al., Phys.Rev.Lett. C16 (1977)
- (3) T.McAbee, Ph.D.Thesis, Chapel Hill, 1986

\*Ohio State University, Athens, USA

### 1.3.2 MEASUREMENT OF THE ANALYZING POWER OF THE REACTIONS

$^3\text{He}(\vec{n},p)t$  AND  $^3\text{He}(\vec{n},d)d$

A.Vollmer, P.Doll, G.Fink, R.W.Finlay\*, T.D.Ford, W.Heeringa,  
H.O.Klages

The investigation of the  $A=4$  system was extended continuing the systematic study of the  $\vec{n}+^3\text{He}$  entrance channel. In this framework the analyzing power of the reactions  $\vec{n}+^3\text{He} \rightarrow p+t$  and  $\vec{n}+^3\text{He} \rightarrow d+d$  has been measured in the energy range from 20 to 50 MeV.

The experiment was carried out using the polarized continuous energy neutron beam from POLKA (1), a  $^3\text{He}$  gas target and 8  $\Delta E/E$  telescopes (2) in an evacuated scattering chamber for the charged reaction products. The detectors covered an angular range from  $15.5^\circ$  to  $77.5^\circ$  (lab.).

At forward angles, also tritons are detected to overcome the problem of detecting protons at far backward angles. Together with the recoiled protons we obtained an angular distribution from  $16.5^\circ$  to  $155.1^\circ$  (CM) for the reaction  $^3\text{He}(\vec{n},p)t$ . An important requirement was the use of rather thin gas target windows and  $\Delta E$  detectors. The gas target was kept at a temperature of 18K and at a pressure of 2 bar during the experiment. For the  $\Delta E/E$  telescopes at forward angles 150  $\mu\text{m}$  Si detectors were used. At larger angles, where only protons are detected, the thickness of the  $\Delta E$  detectors was 500  $\mu\text{m}$ .

Multiparameter data acquisition was performed to separate the detected charged particles. During the analyzing procedure the continuous neutron energy spectrum was divided into 11 energy bins. Preliminary data are presented in Figure 1.



- (1) H.O.Klages et al., Nucl.Instr.Meth. 219 (1984) 269
- (2) P.Doll et al., Nucl.Instr.Meth. A250 (1986) 526

\*Ohio Univ. Athens, Ohio, USA

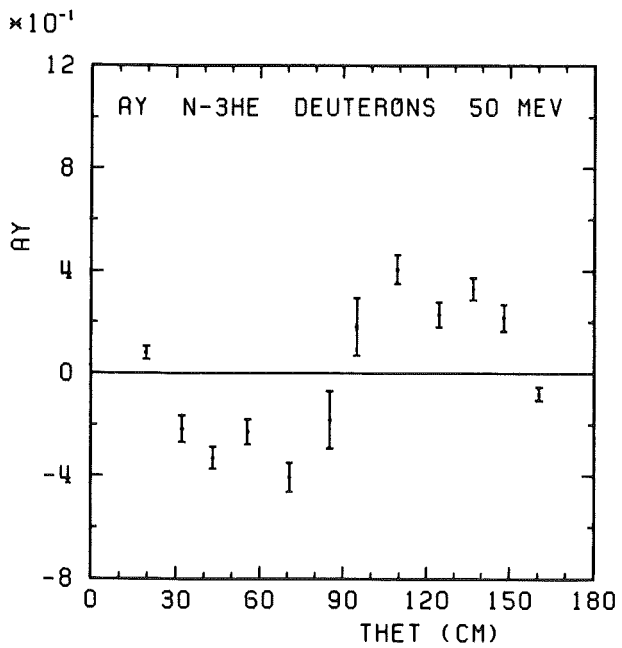
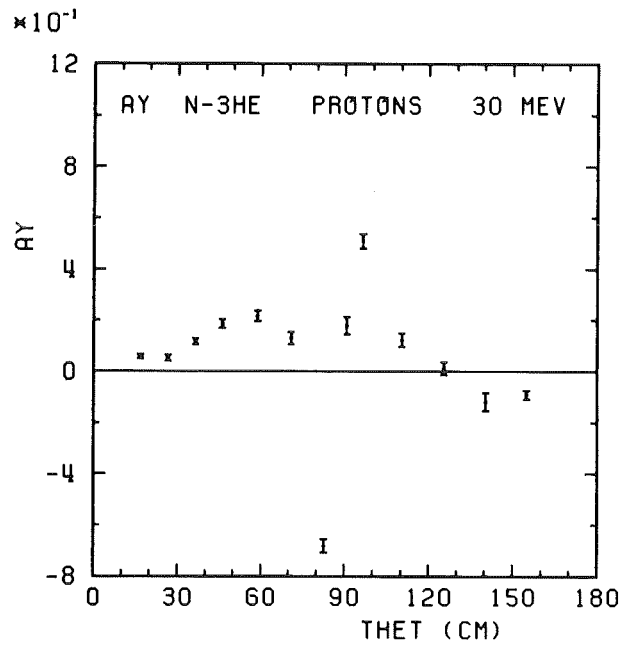
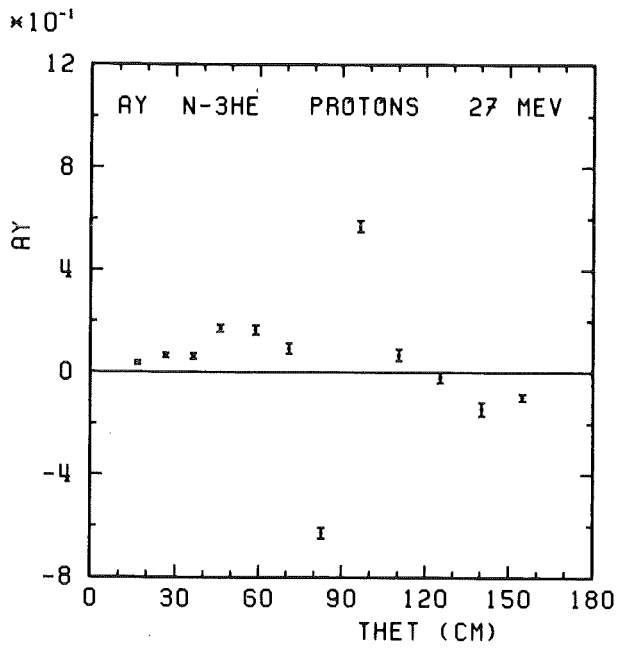


Fig.1: Preliminary results of the Analyzing power of the reaction:  
a)  ${}^3\text{He}(\vec{n},p)t$  at 27 MeV  
b)  ${}^3\text{He}(\vec{n},p)t$  at 30 MeV  
c)  ${}^3\text{He}(\vec{n},d)d$  at 50 MeV

1.3.3 PRELIMINARY RESULTS OF NEUTRON CAPTURE ON  $^1\text{H}$  AND  $^{12}\text{C}$  IN THE ENERGY RANGE FROM 18 MeV TO 50 MeV

M.Hauptenthal, P.Doll, G.Fink, S.Hauber, H.O.Klages, H.Schieler  
F.Smend\*, G.Wicke\*

Our aim is to study  $(n,\gamma)$ -processes on light nuclei (see 1.3.5). Therefore, we started to use our polarized continuous neutron beam at the Karlsruhe cyclotron (1) to study capture reactions in a scintillating target (NE110). The experimental set-up consists of three NaI-crystals ( $16 \times 16 \times 24 \text{ cm}^3$  each) passively and actively shielded and mounted at  $55^\circ$ ,  $90^\circ$  and  $125^\circ$  in the laboratory system.

Because the background of scattered neutrons is about three orders of magnitude higher than the capture gamma rate produced in the target, we use the pulse-shape-information in the NaI to discriminate neutrons and gammas (2). Fig.1 shows a pulse-shape (PS) versus pulse-height ( $E_{\text{NaI}}$ ) event matrix.. The separation between photons and charged particles (c.p.) in the NaI-detectors is possible above 10 MeV. But it is not possible to separate capture- $\gamma$ 's from the target from those produced in the crystal. Therefore we additionally measured the time-of-flight (TOF2) between target and detector. The combination of TOF2 and PS allows the separation of capture events  $^{12}\text{C}(n,\gamma)^{13}\text{C}$  or  $^1\text{H}(n,\gamma)\text{d}$  from other types of reactions as shown in Fig.2. Additionally we used the recoil energy information in the target, discriminating between  $^{13}\text{C}$  and deuterium over a large dynamic range.

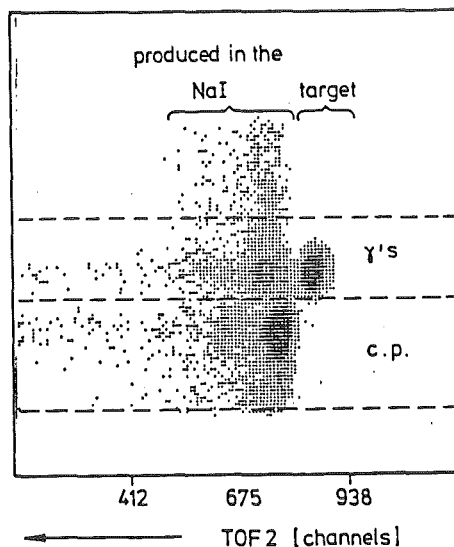
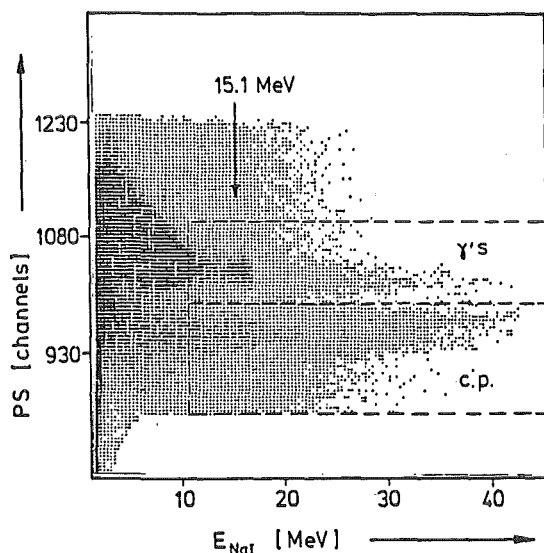


Fig.1:  $E_{\text{NaI}}$  versus PS. The PS exhibits a ridge from photon interactions in the crystal and a ridge from neutron interactions in the crystal.

Fig.2: TOF2 versus PS with  $E_{\text{NaI}} \geq 10 \text{ MeV}$ . The matrix allows the separation between capture events  $^{12}\text{C}(n,\gamma)^{13}\text{C}$  or  $^1\text{H}(n,\gamma)\text{d}$  from other types of reactions.

(1) H.O.Klages et al., NIM 219 (1984) 269  
(2) KfK 4159 (1986) 177  
\* University Göttingen, W.-Germany

#### 1.3.4 TEST RUN FOR CALIBRATING NaI DETECTORS AT 14.24 MeV

H.Schieler, P.Doll, G.Fink, S.Hauber, M.Haupenthal, H.O.Klages

For our neutron capture studies (1) the efficiencies of the employed 16x16x24 cm NaI detectors have to be known at high  $\gamma$ -energies. To measure such efficiencies high energy  $\gamma$ 's with a well known source strength are needed. Such a source can be obtained e.g. by capture reactions of protons on nuclei. Two possible reactions that are known with high accuracy are:

1. at  $E_p = 14.24$  MeV the reaction  $^{12}\text{C}(p,\gamma)^{13}\text{N}$  for which the yield has been measured with an accuracy of 3% (2)
2. at  $E_p = 14$  MeV the reaction  $^{11}\text{B}(p,\gamma)^{12}\text{C}$  with an accuracy of 10% (3).

We choose the first one for our calibration experiment with the 26 MeV proton beam from the Karlsruhe cyclotron (KIZ).

The 26 MeV protons were slowed down by a 3 mm Be foil. The momentum selection was achieved by a monochromator magnet with a current supply stable to  $10^{-5}$ . This magnet has a  $dE/E$  of  $2.37 \times 10^{-4}$ . With entrance and exit slits of 0.5 mm and a proton beam energie of about 14.2 MeV, the beam has an energy spread of 3.5 keV. The beam was scattered by a 30  $\mu\text{m}$  polyethylene target in a 1.2 m diameter scattering chamber. The NaI detector was positioned at  $90^\circ$  in the laboratory system. Scattered protons were detected at angles of  $\pm 20^\circ$ ,  $\pm 30^\circ$ , and  $\pm 40^\circ$  in the chamber by a 2 mm-Si detector. The symmetrical measurement allowed us to find an experimental asymmetry of about  $0.5^\circ$  in the scattering chamber.

The energy spectra contain peaks due to elastic and inelastic  $p\text{-}^{12}\text{C}$  scattering and to  $p\text{-}p$  scattering. These spectra were used to determine the energy of the incident proton beam by a kinematic variation method. This method allows to determine the proton energy with an accuracy of 30 keV, which is mainly due to the thickness of the polyethylene target. The result can be verified by the capture data, which should show the resonance peaking at 14.24 MeV proton energy for this reaction. The capture data are analyzed at present.

- (1) P.Doll et al., KfK report 4159 (1986) 25 and 177, see also contr. 1.3.3 and 1.3.5 of the present report.
- (2) R.E.Marrs et al., Phys.Rev.Lett. 35 (1975) 202
- (3) M.T.Collins et al., Phys.Rev. C26 (1982) 332

### 1.3.5 STUDY OF NEUTRON CAPTURE REACTIONS AT LIGHT NUCLEI

G.Fink, P.Doll, S.Hauber, M.Haupenthal, H.O.Klages, H.Schieler,  
F.Smend\*, G.Wicke\*

With our experimental set-up at the Karlsruhe cyclotron (Fig.1) for studying neutron capture reactions it is possible to measure angular distributions and analyzing powers for light nuclei.

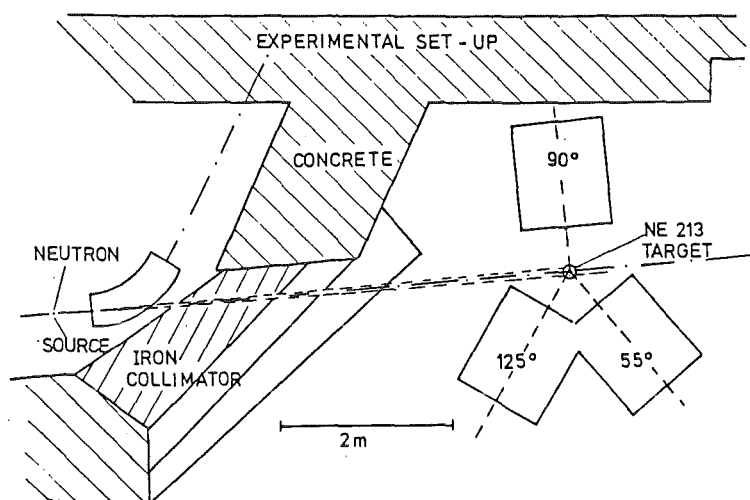


Fig.1: Detector set-up

Capture reactions at  $^{12}\text{C}$  are measured to compare with high flux proton experiments (1), which can be analyzed in terms of direct and semi-direct processes, studying the electromagnetic interaction beyond giant resonances. Furtheron capture reaction on  $^1\text{H}$ ,  $^2\text{H}$  and  $^3\text{He}$  will be examined to get more information in outstanding problems.

In the case of n-p capture measurements of the analyzing power at a lab. angle of  $90^\circ$  are sensitive to the presence of mesonic exchange currents (MEC) and are so far in disagreement with theoretical predictions (2). It is also possible to test different nucleon-nucleon potentials in this reaction. Angular distribution measurements are tests of the multipole decomposition of the electromagnetic excitation. There are indications in experimental data (3), that the E2 excitations are not adequately described in theoretical calculations. Probably MEC-corrections in the E2 operator are necessary. This would also contribute to the questions of D-state probability in the deuteron, because the E2 strength reflects the admixture of nonspherical components (4).

Neutron-deuteron capture is good for testing the small D-state component in the  $^3\text{H}$  wave function, if MEC corrections are the same as in np capture. By this means it is possible to investigate the role of three-body forces in the three-body system (5)

\*University Göttingen

Analyzing the D-state admixture is furtheron interesting in the  $^4\text{He}$  ground state. Capture reactions of  $^3\text{He}(n,\gamma)^4\text{He}$  give complementary information to existing  $^2\text{H}(d,\gamma)^4\text{He}$  data (6).

Data for  $^{12}\text{C}(n,\gamma)^{13}\text{C}$  and  $^1\text{H}(n,\gamma)d$  reactions are presently taken,  $^3\text{He}(n,\gamma)^4\text{He}$  and  $^2\text{H}(n,\gamma)^3\text{H}$  experiments are scheduled for 1988.

- (1) H.Ejiri et al., AIP Conf.Proc.Int.Conf. Capture Gamma Ray Spectroscopy, Knoxville USA, 125 (1984) 582
- (2) J.Soderstrum, L.Knutson, Phys.Rev. 35C (1987) 1246
- (3) K.Stephenson et al., Phys.Rev. 35C (1987) 2023
- (4) E.Hadjimichael et al., Phys.Rev. 36C (1987) 44
- (5) J.F.Mathiot, priv.communication
- (6) H.Assenbaum, K.Langanke, Phys.Rev. 36C (1987) 17

## 1.4 NUCLEAR REACTIONS BY CHARGED PARTICLES

### 1.4.1 EXPERIMENTAL METHODS FOR STUDYING NUCLEAR DENSITY DISTRIBUTIONS

C.J. Batty\*, E. Friedman\*\*, H.J. Gils , H. Rebel (1)

The present experimental state-of-the-art and the advanced methods of data analysis for determining nuclear density distributions were reviewed. Emphasis was put on studies of nuclear matter and neutron distributions using hadronic probes. Studies of nuclear charge distributions were only briefly included for completeness, since other reviews are available on this particular subject.

One of the dominant questions in such studies with hadronic probes is the way how the experimental observables  $Obs(y)$  are connected with the distribution of interest  $\rho(x)$  through a mapping function  $K(x,y)$

$$Obs(y) = \int K(x,y)\rho(x)d^3x .$$

The role of this function and the approximations in determining it were discussed in detail for the various probes.

In organising the article, we adopted the unconventional approach of classifying the technique by the nuclear density regions they probe, rather than by the type of particle used. For pedagogical reasons the scattering of alpha-particles was discussed more extensively since it exhibits a logical development of ideas and techniques which are relevant to the determination of nuclear density distributions with other probes.

The hadronic probes and methods for nuclear density distributions are compiled in Table 1. Additional information on specific orbitals also covered by the article is available through

*Coulomb displacement energies*

*Nuclear transfer reactions*

*Charge-exchange reactions to analog states*

*Magnetic scattering of electrons.*

Table 2 gives an example of proton and neutron density distributions of various isotopes from 800 MeV polarised proton scattering.

Table 1  
Hadronic methods for determination of nuclear matter distributions

Method	Localisation	Analysis
Scattering of strongly absorbed projectiles ( $\alpha$ , $^{16}\text{O}...$ ) near the Coulomb barrier	Tail region of $\rho_m$ outside the Coulomb barrier $\rho_m \approx 10^{-2} \rho_0$	Phenomenological optical potential analysis $\rightarrow$ Rutherford radius. "Constant fraction" radius $R_\epsilon$ at $U_{\text{real}}^{\text{opt}} = \epsilon$
Hadronic ( $K^-, \bar{p}, \pi^-$ ) atoms	————— Nuclear periphery	$(K^-, \bar{p}, \pi^-)$ -nucleus potential in terms of scattering lengths and $\rho_n, \rho_p$
$K^-$ and $\bar{p}$ reactions		Proton-neutron ratios in the outermost region of $\rho_m$ sampled by the $(K, \bar{p})$ -nucleon cross section and the $(K, \bar{p})$ -wave function
Low and medium-energy proton scattering		Folding models including exchange
Diffraction scattering - of low and medium energy alpha-particles - of pions near the (3,3) resonance - of low energy antiprotons	————— Nuclear surface	Diffraction models $\rightarrow$ Fraunhofer radius Strong absorption radii Folding models (ms radii differences) Microscopic $(\pi, \bar{p})$ -nucleus potentials
High-energy total and reaction cross-sections		$R_{\text{eff}}^2 = \sigma_R / \pi$ Glauber approximation. Isotopic differences
Intermediate energy alpha-particle scattering including large angles		Folding models with density dependent forces - phenomenological adjustments by calibrating with benchmark nuclei - Model independent densities
Intermediate energy (polarised) proton scattering	————— Nuclear surface and interior	Glauber approach. KMT multiple scattering theory with free NN amplitudes Model independent densities Relativistic wave equation
Low-energy pion scattering		Microscopic $\pi$ -nucleus potential Isotopic differences $\Delta \langle r^2 \rangle_n$
$K^+$ scattering		Multiple scattering theory in terms of KN amplitudes

Table 2

Root mean-square radii of neutron density distributions from 800 MeV polarised proton scattering. Proton and charge density rms radii are from other sources. Numbers in brackets are the errors in the last digits.

Target	KMT order	Neutron density	$\langle r_n^2 \rangle^{1/2}$ (fm)	$\langle r_p^2 \rangle^{1/2}$ (fm)	$\Delta r_{np}$ (fm)	$\langle r_{ch}^2 \rangle^{1/2}$ (fm)
<sup>12</sup> C	1	F3	2.393	2.319	+ 0.07(7)	2.453
<sup>40</sup> Ca	2	F3	3.491	3.392	+ 0.10(5)	3.482
<sup>48</sup> Ca	2	F3	3.625	3.396	+ 0.23(5)	3.470
<sup>46</sup> Ti	2	F3	3.435	3.513	- 0.08(7)	3.5976
<sup>48</sup> Ti	2	F3	3.448	3.505	- 0.06(7)	3.5843
<sup>58</sup> Ni	2	F3	3.700	3.686	+ 0.01(5)	3.772
<sup>64</sup> Ni	2	F3	3.912	3.745	+ 0.17(5)	3.845
<sup>90</sup> Zr	1	G3	4.289	4.204	+ 0.09(7)	4.280
<sup>116</sup> Sn	2	G3	4.692	4.546	+ 0.15(5)	4.619
<sup>124</sup> Sn	2	G3	4.851	4.599	+ 0.25(5)	4.670
<sup>208</sup> Pb	2	G3	5.593	5.453	+ 0.14(4)	5.503

Some apparently conflicting results of the large variety of probes and methods were revealed as providing complementary information.

(1) Advances in Nuclear Physics, to be published

\* Rutherford Appleton Laboratory, Chilton Didcot, U.K.

\*\* Racah Institute of Physics, Hebrew University of Jerusalem, Israel



#### 1.4.2 DENSITY DEPENDENT EFFECTIVE INTERACTIONS IN ANALYSES OF ELASTIC ALPHA-PARTICLE SCATTERING

H.J. Gils

Folding models of the real optical potential using two-body effective interactions provide a realistic microscopic interpretation of nuclear scattering experiments at low and medium energies (1). For the scattering of alpha-particles at energies high enough ( $E_\alpha > 80$  MeV) for refractive rainbow scattering to appear at large angles the effective interaction is density dependent (2).

Various analytical parametrisations have previously been used for this density dependence and new forms of density dependence have recently been proposed (3,4). The validity of these forms for very accurate elastic alpha-particle scattering data for  $^{40}\text{Ca}$ ,  $^{50}\text{Ti}$  and  $^{52}\text{Cr}$  at  $E_\alpha = 104$  MeV and for  $^{40}\text{Ca}$  and  $^{50}\text{Ti}$  at  $E_\alpha = 140$  MeV was carefully compared.

Another question, which generally appears in density dependent double-folding calculations of composite projectile scattering is the way how to take the dependence of the effective interaction on the *projectile* and *target* densities appropriately into account. This problem was empirically studied by introducing separate terms of different relative weight  $0 \leq w \leq 1$  for the projectile and target density dependence.

In most of the present double-folding model calculations the radial part of the effective interaction was assumed to have the widely used M3Y-form (1). The parametrisations for the density dependence are given in Fig. 1 with adjustable parameters  $\lambda, \beta, \gamma$ . The resulting parameter values are plotted as function of the weight parameter  $w$ . The representation of the experimental data ( $^{40}\text{Ca}$  at  $E_\alpha = 104$  MeV) is characterised by the value of  $\chi^2/F$  showing clear evidence that a *different* weight for the target and projectile density dependence is required by the experimental data for all parametrisations. The average best value of the weight parameter  $w \approx 0.8$  has the most plausible meaning in that the alpha-particle is more inert than the target nucleus in the scattering process.

In Fig. 2 the density dependence of the effective interaction is shown as function of the nuclear density. The three curves for the different parametrisations meet closely over a wide range of densities and the characteristic crossing points correspond to those radial parts of the optical potential which are best determined by the experimental data (5).

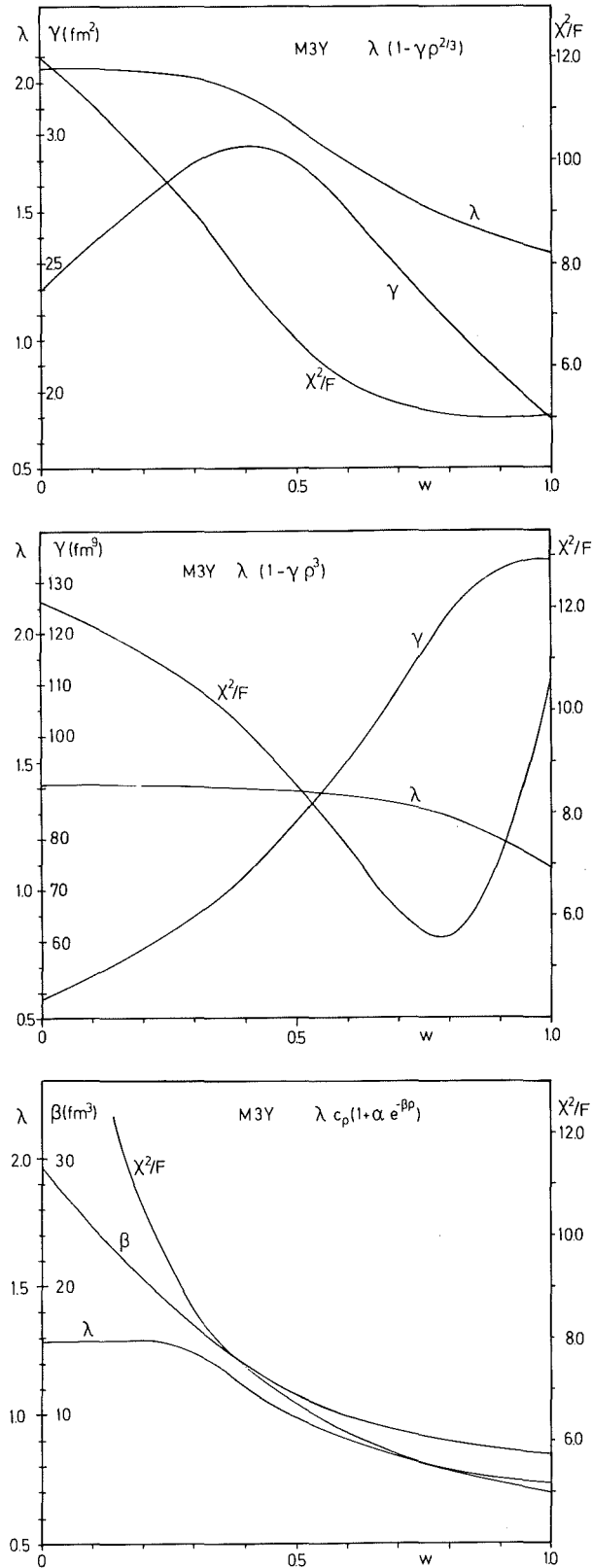


Fig. 1 Dependence of parameters  $\lambda, \beta$  and  $\gamma$  on the weights  $w$  of the density dependent terms and corresponding values of  $\chi^2/F$

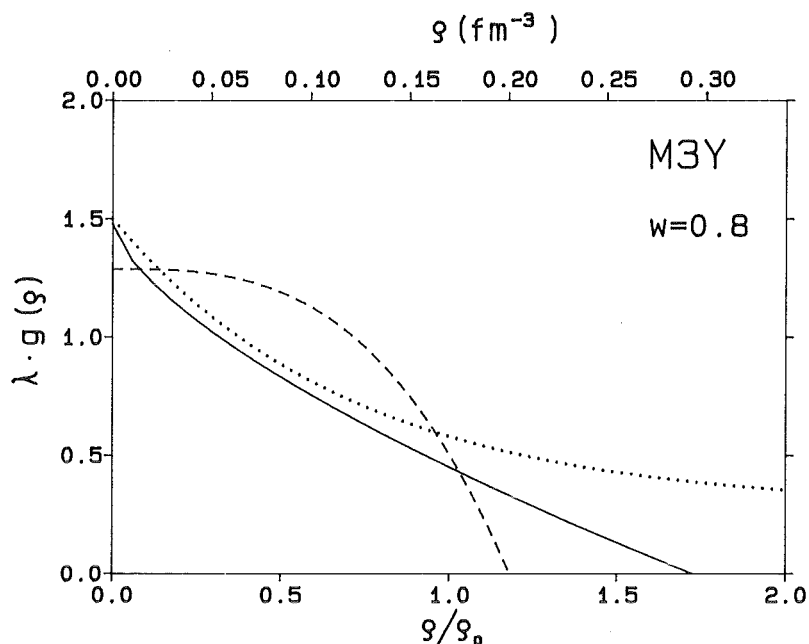


Fig. 2 Density dependence of the M3Y-interaction ,  
solid:  $\rho^{2/3}$ , dashed:  $\rho^3$ , dotted: exponential

Inferring the results from the studies of the density dependence into the question of how to determine nuclear density distributions from elastic alpha-particle scattering it was shown that an equivalent degree of phenomenology is necessary in both *double-* and *single-*folding model studies. Previous results of single-folding model analyses (5,6) were fully confirmed and hence it was concluded that the expenditure of double-folding is not justified for such analyses.

- (1) G.R. Satchler, W.G. Love, Phys. Rep. 55 (1979) 183
- (2) E. Friedman, H.J. Gils, H. Rebel, Z. Majka, Phys. Rev. Lett. 41 (1978) 1220
- (3) W.J. Thompson, T.L. McAbee, R.L. Varner, Phys. Letter 182 B (1986) 247
- (4) R. Schiavilla, V.R. Pandharipande, R.B. Wiringa, Nucl. Phys. A449 (1986) 219
- (5) H.J. Gils, Report KfK 3765, Kernforschungszentrum Karlsruhe (1984)
- (6) H.J. Gils, H. Rebel, E. Friedman, Phys. Rev. C29 (1984) 1295

1.4.3 INCLUSIVE ENERGY SPECTRA AND ANGULAR DISTRIBUTIONS OF  
 ${}^6\text{Li}$ -PROJECTILE BREAK-UP FRAGMENTS AND THE SERBER MODEL

H. Jelitto, V. Corcalciuc\*, H.J. Gils, N. Heide, J. Kiener,  
 H. Rebel, S. Zagromski

The break-up of  ${}^6\text{Li}$ -projectiles with an energy  $E_{\text{Li}} = 156$  MeV was studied at very small reaction angles using  ${}^{12}\text{C}$  and  ${}^{208}\text{Pb}$  targets (1). The results were compared with a simple spectator model introduced by Serber (2). Some experimental data and the corresponding theoretical curves are shown in Fig. 1 and Fig. 2.

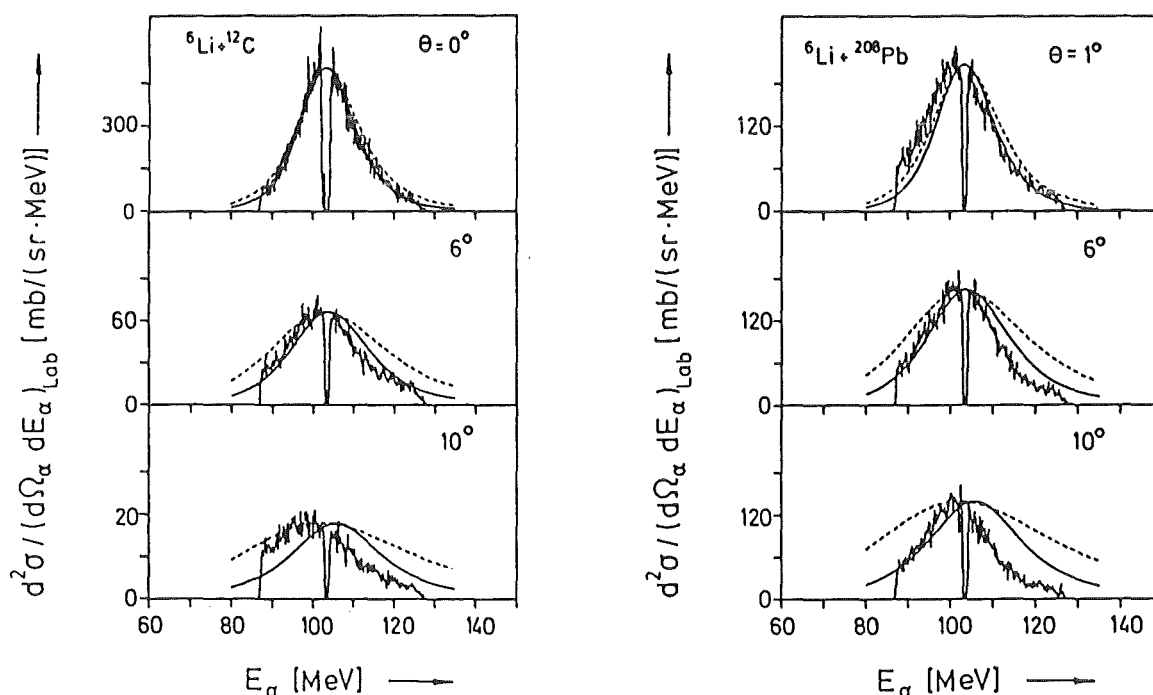


Fig.1 Measured and calculated inclusive alpha-particle spectra of the reactions  ${}^{12}\text{C}({}^6\text{Li}, \alpha X)$  and  ${}^{208}\text{Pb}({}^6\text{Li}, \alpha X)$  for emission angles (laboratory system) between  $0^\circ$  and  $10^\circ$ . --- transparent, — opaque Serber model.

The energy spectra in Fig. 1 indicate that the opaque model including nuclear absorption yields good results especially in the  $0^\circ$ -range. For the angular distributions of break-up alpha-particles and deuterons from the reaction  ${}^6\text{Li} + {}^{12}\text{C}$  only one common normalisation parameter had to be adjusted. The relative abundances of alpha-particles and deuterons and the different shapes of the angular distributions are given by the model (Fig. 2 I), where the latter is simply a consequence of the different masses of both fragments. As can be seen in Fig. 2 II the

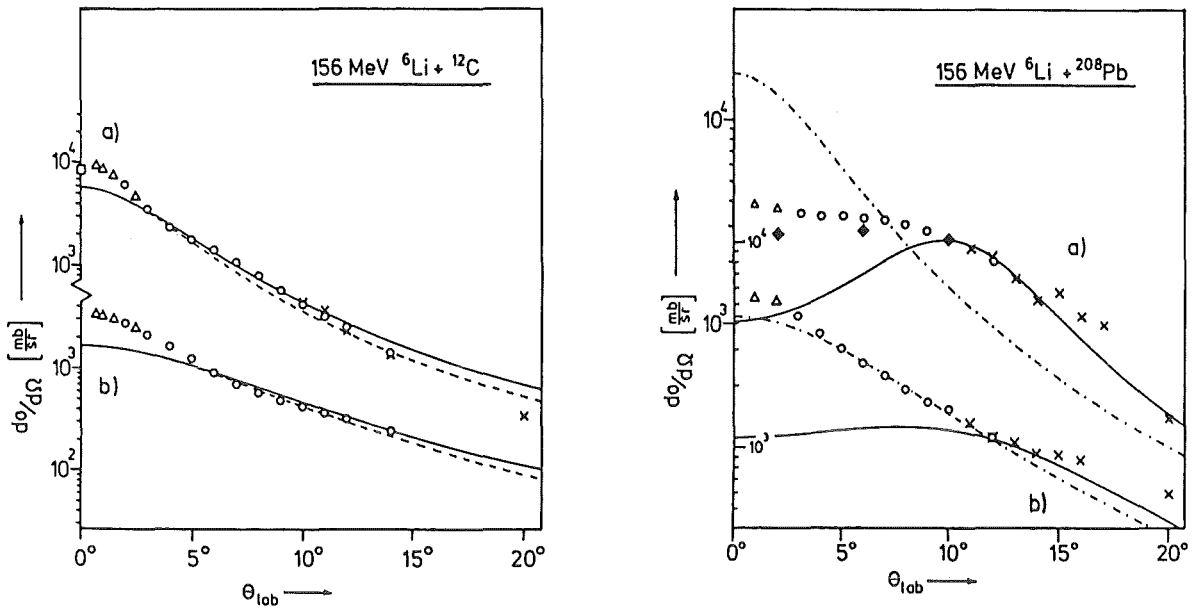


Fig.2 Measured and calculated angular distributions a) inclusive break-up alpha-particles, b) deuterons.  
 --- transparent, — opaque Serber model, - · - · - opaque model without Coulomb correction, ◆ DWBA-theory.

angular distribution of alpha-particles from the reaction  ${}^6\text{Li} + {}^{208}\text{Pb}$  has a clear change of slope around  $10^\circ$ . This effect can be understood qualitatively as being due to the deflection of the projectile in the Coulomb field of the target nucleus (2). For more detailed information see ref. (1).

In this spectator model the wave function of the relative motion between the alpha particle and the deuteron-cluster in the  ${}^6\text{Li}$ -projectile is assumed to be of a Yukawa type  $\Phi_{\alpha d} = Ne^{-\alpha r}/r$ , where  $N$  and  $\alpha$  are constants. It is a nodeless 1S-wave function implying a Lorentzian shape for the relative momentum distribution, which is one of the assumptions in the model. Studies in the framework of the model with a 2S-wave function resulting from a Woods-Saxon potential were started in order to examine, whether the 2S-wave function leads to a better agreement between experimental and theoretical data.

In the spirit of the Serber model the resonant break-up (3) via excited states of the  ${}^6\text{Li}$ -projectile is not taken into account. Information from  $\alpha$ -d-coincidence measurements and a Monte-Carlo type calculation demonstrate that in the considered energy and angular range the contribution from the resonant break-up is about one order of magnitude smaller than the total amount of the observed break-up

contributions. It can be concluded that the resonant break-up mode is not capable to explain the inclusive break-up spectra significantly.

- (1) H. Jelitto, Ph. D. thesis, Univ. of Heidelberg and Report KfK 4259, Kernforschungszentrum Karlsruhe (1987)
- (2) R. Serber, Phys. Rev. 72 (1947) 1008
- (3) H. Gemmeke, B. Deluigi, L. Lassen, D. Scholz, Z. Physik A286 (1978) 73

\* Central Institute of Physics, IFIN, Bucharest, Romania

#### 1.4.4 BREAK-UP OF 29.6 MeV ${}^7\text{Li}$ -PROJECTILES ON ${}^{27}\text{Al}$ AND ${}^{59}\text{Co}$

V. Corcalciuc\*, D. Galeriu\*, R. Dumitrescu\*, H. Rebel,  
H.J. Gils, N. Heide

The projectile break-up of  ${}^6\text{Li}$  and  ${}^7\text{Li}$  was experimentally demonstrated and studied for a variety of targets and energies of several tens of MeV/amu (1,2,3). Much attention has been devoted to these projectiles due to their small binding energies and transitional character between light and heavy ions. Using the facilities of the FN-Tandem Lab. at IFIN, Bucharest continuum spectra resulting from the bombardement of self-supporting  ${}^{27}\text{Al}$  and  ${}^{59}\text{Co}$  targets with 29.6 MeV  ${}^7\text{Li}$  were obtained. Data registered event-by-event, using E- $\Delta$ E identification techniques from measurements at 20°, 30° and 35° in the lab-system have been analysed off-line. We obtained characteristic inclusive alpha particle and triton spectra centered around the beam velocity energy with FWHM of about 7 MeV. The cross sections decrease rapidly with the observation angles.

Fig. 1a shows the alpha particle spectra at 20° and 30° from  ${}^7\text{Li} + {}^{27}\text{Al}$ . The experimental points are mean values averaged over 1.2 MeV intervals. Fig 2b shows the spectra from  ${}^7\text{Li} + {}^{59}\text{Co}$  at 35°. Continuous lines are results of calculations in the framework of the opaque Serber model (4) with corrections for Coulomb energy differences and using a two-body phase space normalised to the experimental data. When using the transparent Serber model or a three body phase space the theoretical predictions are too broad compared with the experimental data. From  ${}^{27}\text{Al}$  to  ${}^{59}\text{Co}$  the energy integrated cross-sections appear to be proportional to  $A^{1/3}$  i.e. to nuclear radius.

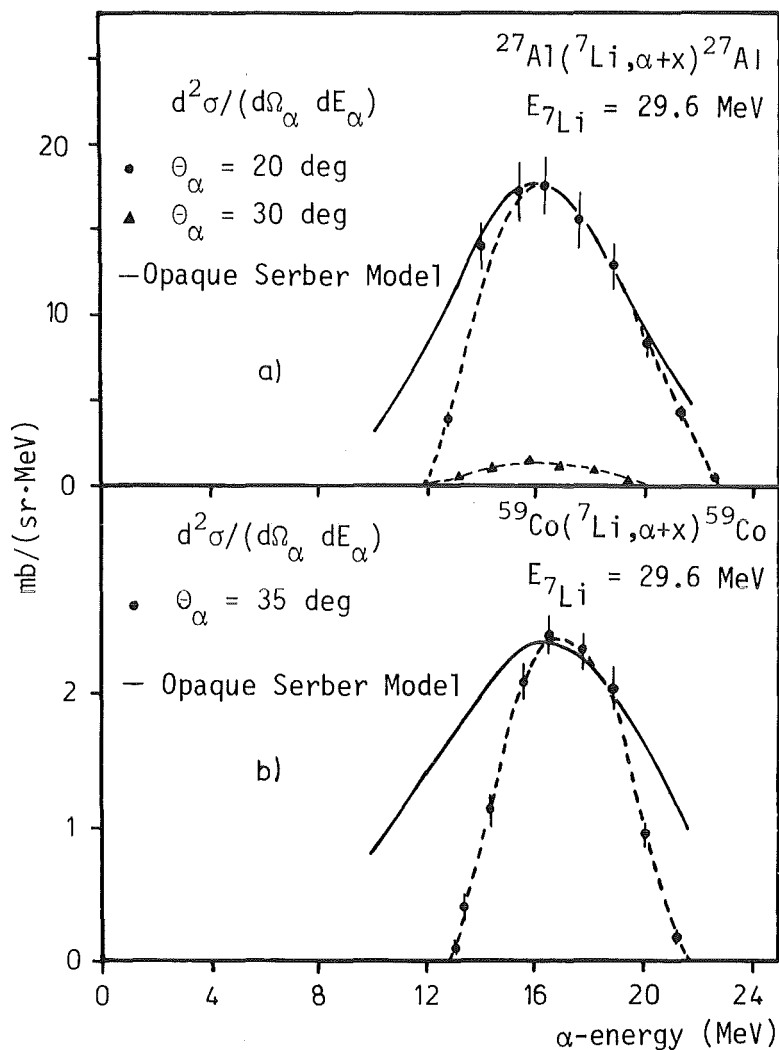


Fig.1 Inclusive energy spectra of alpha-particles from  $^7\text{Li}$  collisions on  $^{27}\text{Al}$  (a) and  $^{59}\text{Co}$  (b) at various lab. angles. The dashed curves are to guide the eyes. Solid lines are results of the calculations in the framework of the opaque Serber model normalised to the peak cross sections.

- (1) C.M. Castaneda, H.A. Smith, jr., P.P. Singh, H. Karwowski, Phys. Rev. C21 (1980) 179
- (2) B. Neumann, H. Rebel, J. Buschmann, H.J. Gils, H. Klewe-Nebenius, S. Zagromski, Z. Phys. A296 (1980) 113
- (3) A.C. Shotter, W. Rapp, T. Davidson, D. Branford, M.S. Sanderson, M.A. Nagarajan, Phys. Rev. Lett. 53 (1984) 1539
- (4) R. Serber, Phys. Rev. 72 (1947) 1008

\* Central Institute of Physics, IFIN, Bucharest, Romania

#### 1.4.5 ENERGY DEPENDENCE OF THE SEQUENTIAL AND DIRECT COULOMB BREAK-UP OF LIGHT IONS

D.K. Srivastava\*, D.N. Basu\*, Bikash Sinha\*, H. Rebel

The Coulomb contribution to the direct and sequential break-up of light ions proves to be substantial at all energies since at sub-Coulomb energies the projectile does not experience the nuclear interaction and at high energies the break-up is limited to grazing partial waves and beyond, for which the Coulomb contribution is dominant. The situation at higher energy differs substantially from the low energy cases because of the relaxation of the adiabaticity condition which allows excitation of high lying states. The direct break-up processes benefit immensely from this relaxation and the break-up of light ions via the nonresonant continuum states may become sizable.

We have calculated the Coulomb contribution of the  $L = 2$  resonant and nonresonant states for the break-up of  ${}^6\text{Li} \rightarrow \alpha + d$  in the field of  ${}^{208}\text{Pb}$  as a function of projectile energy. For the resonant states  $3_1^+$ ,  $2_1^+$  and  $1_1^+$  we follow Alder et. al (1)

$$\sigma_{E\lambda} = \left( \frac{Z_T e}{\hbar v} \right)^2 a^{-2\lambda+2} B(E\lambda) f_{E\lambda}^N(\xi) \quad (1)$$

where we have taken  $B(E2, 1^+ \rightarrow 3^+) = 45 \cdot e^2 \cdot \text{fm}^4$  and the  $B(E2)$  values for the  $2^+$  and  $1^+$  states are taken in proportion to the spin statistics, implied by an assumption that the radial wave functions for the three states are similar.

For the continuum states with the excitation energy  $\varepsilon$  the energy differential cross section is written as

$$\sigma(\varepsilon) = \left( \frac{Z_T e}{\hbar v} \right)^2 a^{-2\lambda+2} b(E\lambda, \varepsilon) f_{E\lambda}^N(\xi, \varepsilon) \quad (2)$$

We have calculated the reduced transition strength per unit energy  $b(E2, \varepsilon)$  using continuum wave functions calculated with the same nuclear potential which generates the ground state ( $\alpha + d$ ) wave function. The spin-orbit interaction has been neglected to obtain the same radial wave functions for the  $3^+$ ,  $2^+$  and  $1^+$  continuum states as before. The total break-up via the continuum states having  $L = 2$  is obtained by integrating (2).

In Fig. 1 we present the energy variation of the Coulomb break-up cross section of the individual resonant levels as well as that for the continuum levels. We see that at lower energies the resonant break-up of  ${}^6\text{Li}$  proceeds mainly via the  $3^+$  level at 2.18 MeV. However at higher energies the contributions of the  $2^+$  level at 4.52 MeV and the  $1^+$  level at



5.50 Mev are of the same order of magnitude. This is an important result since the dominance of the break-up via  $3_1^+$  state at lower energies is often used as an argument to completely neglect the contribution of other levels to break-up at high energies.

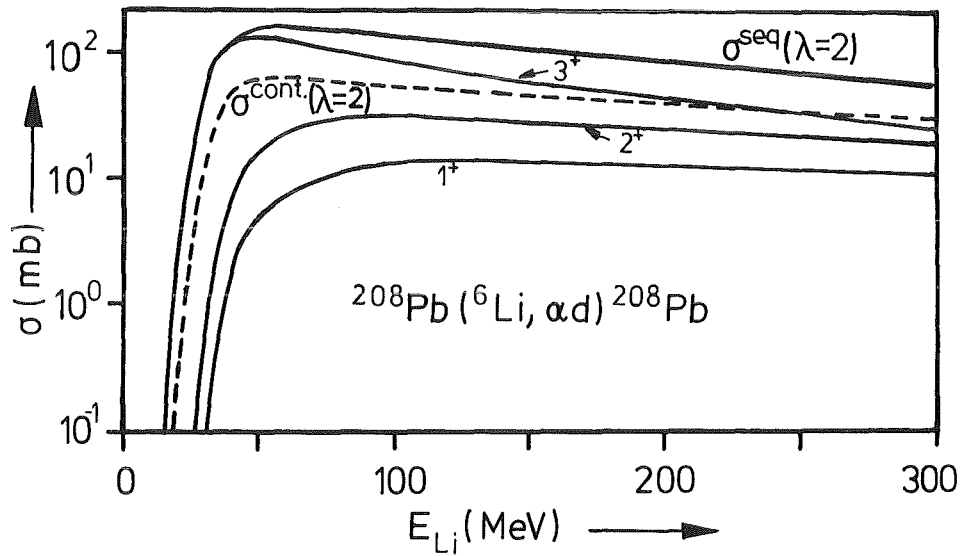


Fig. 1 Energy variation of the Coulomb break-up cross section

The total contribution of the continuum states is found to be substantial at all energies and even exceeds that for the generally believed to be dominating  $3_1^+$  state.

- (1) K. Alder, A. Bohr, T. Huns, B. Mottelson, A. Winther, Rev. Mod. Phys. 28 (1956) 432

\* Variable Energy Cyclotron Centre, Bhabha Atomic Research Centre, Calcutta, India

1.4.6 LOOKING FOR NONRESONANT COULOMB BREAK-UP OF 156 MEV  
 ${}^6\text{Li}$ -PROJECTILES

J. Kiener, H.J. Gils, N. Heide, H. Jelitto, H. Rebel,  
S. Zagromski

It has been pointed out (1) that nonresonant Coulomb break-up reactions offer a promising way for the indirect determination of capture cross sections at very low energies, which are needed for the understanding of nucleosynthesis of chemical elements in stars. One example is the break-up reaction of  ${}^6\text{Li} + \gamma \rightarrow \alpha + d$ , where the astrophysically relevant relative energies of the fragments are of the order of 100 keV. This corresponds to very small relative emission angles ( $<3^\circ$ ) of the break-up fragments for 156 MeV  ${}^6\text{Li}$  projectiles. Therefore, a special detection system for the magnetic spectrograph "Little John" was constructed, so that both particles can be detected in coincidence in the spectrograph, penetrating through the same acceptance slit.

We started to measure the break-up reaction  ${}^6\text{Li} + \gamma \rightarrow \alpha + d$  at 156 MeV using a  ${}^{208}\text{Pb}$  target, the Coulomb field of which serves as a source of virtual photons. The mean break-up reaction angle was  $3^\circ$ , which is considerably smaller than the grazing angle (ca.  $6^\circ$ ), assuring the dominance of Coulomb break-up. An important point for the measurements of these continuous energy spectra is a careful energy calibration. For that purpose we used alpha-particles and deuterons at 104 MeV and 52 MeV, respectively, which were detected after elastic scattering from a  ${}^{208}\text{Pb}$  target with 10 different settings of the magnetic field strength of the spectrograph covering the whole energy region measured. The energy resolution was better than 200 keV for deuterons and better than 350 keV for alpha-particles.

As the coincidence rate is very low, the full angular acceptance of the spectrograph,  $1.14^\circ \times 2.85^\circ$ , should be used. This requires the determination of the emission angles of the fragments for a kinematically complete measurement of the three body reaction. In our first experiments we reduced the horizontal acceptance to  $0.3^\circ$  and determined only the vertical emission angles with the focal plane detector via an approximately parallel-to-point imaging condition. The overall resolution for the relative angle in this system is about  $0.4^\circ$ . For the future a position sensitive acceptance detector (2) is to detect the emission angles of both particles before the magnetic system, thus allowing the use of the full acceptance.

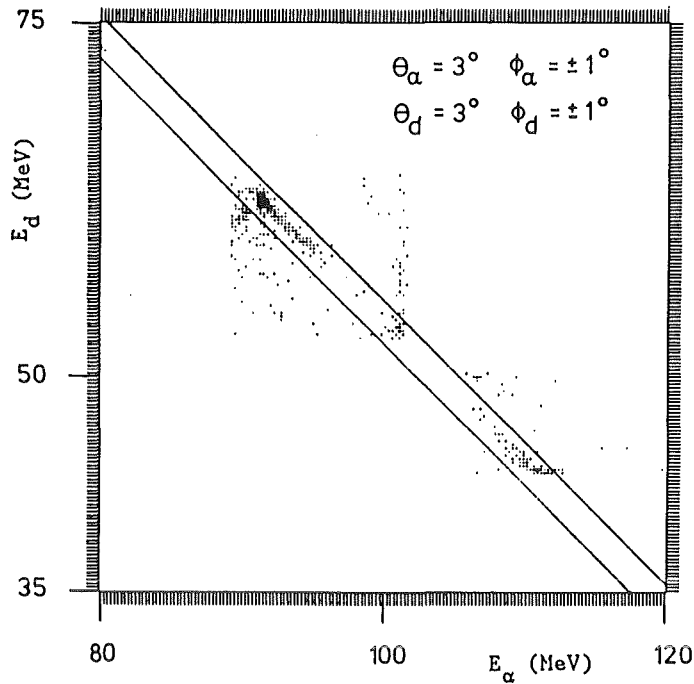


Fig. 1  
Kinematical plot for the  
reaction  $^{208}\text{Pb}(^6\text{Li},\text{ad})$ .  
The solid lines show the  
window for the  
kinematical cut for  
elastic break-up

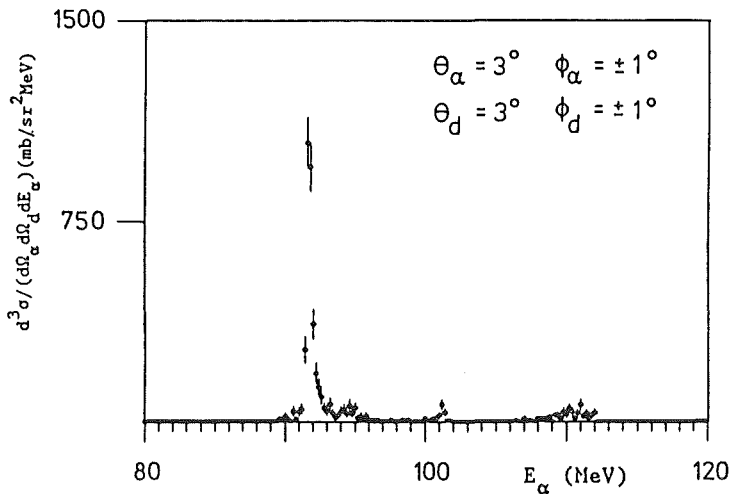


Fig. 2  
Alpha-particle energy  
spectrum from the  
reaction  
 $^{208}\text{Pb}(^6\text{Li},\text{ad})^{208}\text{Pbg.s.}$

Preliminary results are shown in Fig. 1 and Fig. 2. In the energy spectrum only events are considered which are inside the kinematical window indicated in Fig. 1. In this way background events are considerably reduced. The sharp peak from the resonant break-up via the 2.18 MeV  $3^+$  state in  $^6\text{Li}$  clearly dominates the cross section. Although there is some indication for nonresonant break-up, the present statistical accuracy does not allow definite conclusions.

- (1) G. Baur, C.A. Bertulani, H. Rebel, Nucl. Phys. **A458** (1986) 188
- (2) G. Gantenbein, J. Kiener, H.J. Gils, S. Zagromski, this report, contrib. 5.1.4

1.4.7 A REALISTIC SIGNATURE OF FINAL STATE INTERACTION IN DIRECT COULOMB BREAK-UP

D.N. Basu\*, D.K. Srivastava\*, Bikash Sinha\*, H. Rebel

Break-up of light ions at high energies is characterised by broad and pronounced bumps around the beam velocity energies in the singles or the coincidence fragment spectra. This can be understood in terms of a spectator-participant model where the final state interaction between the break-up fragments is neglected. This description is expected to be valid when the relative energy is large. However at small relative energies final state interactions should be explicitly accounted for, in particular in the case of the break-up by the Coulomb field which especially favours low relative energies due to the adiabaticity condition.

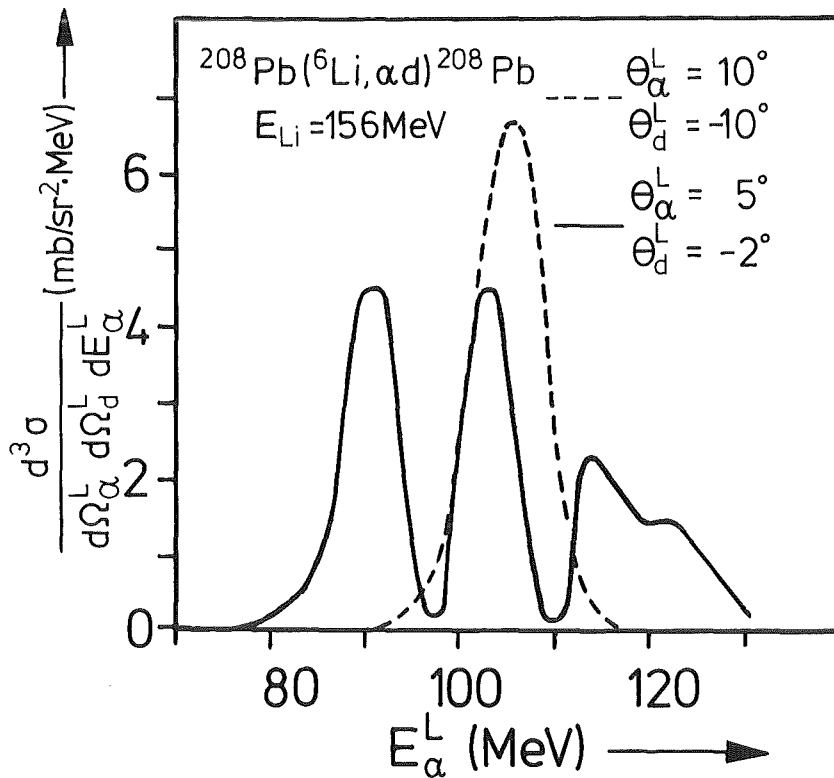


Fig. 1 Quadrupole contribution to the triple differential cross section of  ${}^6\text{Li}$  break-up at different kinematical conditions

We use a strong absorption model in the prior form of DWBA theory to evaluate the Coulomb contribution to the direct break-up of  ${}^6\text{Li}$  ions colliding with  ${}^{208}\text{Pb}$ . Here the T-matrix for the process

$$a + A \rightarrow b + x + A \quad (1)$$

is given by

$$T_{fi} = \langle \phi_f \chi_f^{(-)} | V_{res} | \chi_i^{(+)} \phi_0 \rangle \quad (2)$$

where the symbols have their usual meaning. In Fig. 1 we show the dominant  $L=2$  contribution of the direct Coulomb break-up to the triple differential cross section for 156 MeV  ${}^6\text{Li}$  ions calculated in the above mentioned model for two kinematical conditions. For the in-plane geometry with  $\theta_a = 10^\circ$  and  $\theta_d = -10^\circ$ . The relative energy is relatively large and the theory predicts a single peaked distribution having a maximum around the beam velocity alpha-particles similar to the predictions of a simple spectator-participant model.

However the case for  $\theta_a = 5^\circ$  and  $\theta_d = -2^\circ$ , involving rather small relative energies provides a dramatically different multiple peak structure which can be understood by the specific structure of the transition amplitude.

We conclude that coincidence measurements in break-up experiments are able to test post and prior form of theories if close geometries are chosen, which are predicted to provide for a distinct signature of final state interaction.

\* Variable Energy Cyclotron Centre, Bhabha Atomic Research Centre, Calcutta, India

#### 1.4.8 MANIFESTATION OF THE INTERNAL MOMENTUM DISTRIBUTION IN ${}^6\text{Li}$ BREAK-UP REACTIONS ?

N. Heide, V. Corcalciuc\*, H.J. Gils, J. Kiener, H. Rebel,  
S. Zagromski, D.K. Srivastava\*\*, C. Samanta\*\*\*

The coincidence cross section for the break-up reaction  ${}^6\text{Li} \rightarrow \alpha + d$  in the field of a heavy target nucleus at medium high energies can furnish information about the intrinsic momentum distribution of  $\alpha$ - and  $d$ -fragments in  ${}^6\text{Li}$  (1). Various descriptions have recently been used in the literature for the  $\alpha$ - $d$  relative motion wave function in the ground state of  ${}^6\text{Li}$ . Generally these wave functions are either 2S functions, with one internal node in addition to the node at the origin, or nodeless 1S functions. It is possible to investigate selectively the region of  $\alpha$ - $d$  relative momenta where the 2S and 1S relative wave functions are essentially different by choosing an appropriate kinematical situation and measuring

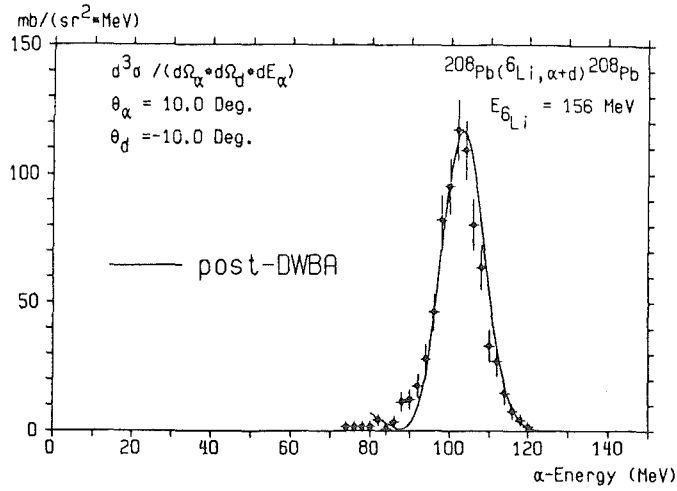


Fig. 1 The triple differential cross section for direct elastic break-up of  ${}^6\text{Li}$  in  ${}^6\text{Li}+{}^{208}\text{Pb}$  collisions at 156 MeV

the  $\alpha$ -d coincidence cross section. We measured the triple differential cross section  $d^3\sigma/(d\Omega_\alpha d\Omega_d dE_\alpha)$  for the direct elastic break-up reaction  ${}^{208}\text{Pb}({}^6\text{Li}, \alpha d){}^{208}\text{Pb}$  at 156 MeV,  $\theta_\alpha = 10^\circ$ ,  $\theta_d = -10^\circ$  in an in-plane geometry (1). The data have been taken at the Karlsruhe Isochronous Cyclotron using two  $\Delta E$ -E semiconductor telescopes, with 2 mm Si  $\Delta E$ -detectors each and two 15 mm or 21 mm, respectively, intrinsic Ge E-detectors cooled by liquid nitrogen. Fig. 1 compares the experimental coincidence cross section with theoretical predictions of the post-DWBA approach according to Baur et al. (2). The post-DWBA gives a good description of the experimental data. Both the position and the width of the peak are well reproduced. Due to the kinematical situation the observed alpha-particle energies correspond to asymptotic relative momenta around  $k \approx 0.5 \text{ fm}^{-1}$ . The implicit assumption of a Lorentzian momentum distribution corresponding to a 1S relative motion wave function is not essential for the present case since the 2S and 1S momentum distributions do not differ very much for relative momenta of  $k \approx 0.5 \text{ fm}^{-1}$ .

Due to the low coincidence counting rate we used a modified experimental arrangement for our measurements at larger relative angles involving higher relative momenta. The 2 mm  $\Delta E$  Si detectors were replaced by position sensitive 500  $\mu\text{m}$  Si detectors allowing simultaneous detection for angular ranges  $\theta_\alpha = +11^\circ, \dots, +14^\circ$  and  $\theta_d = -11^\circ, \dots, -14^\circ$  corresponding

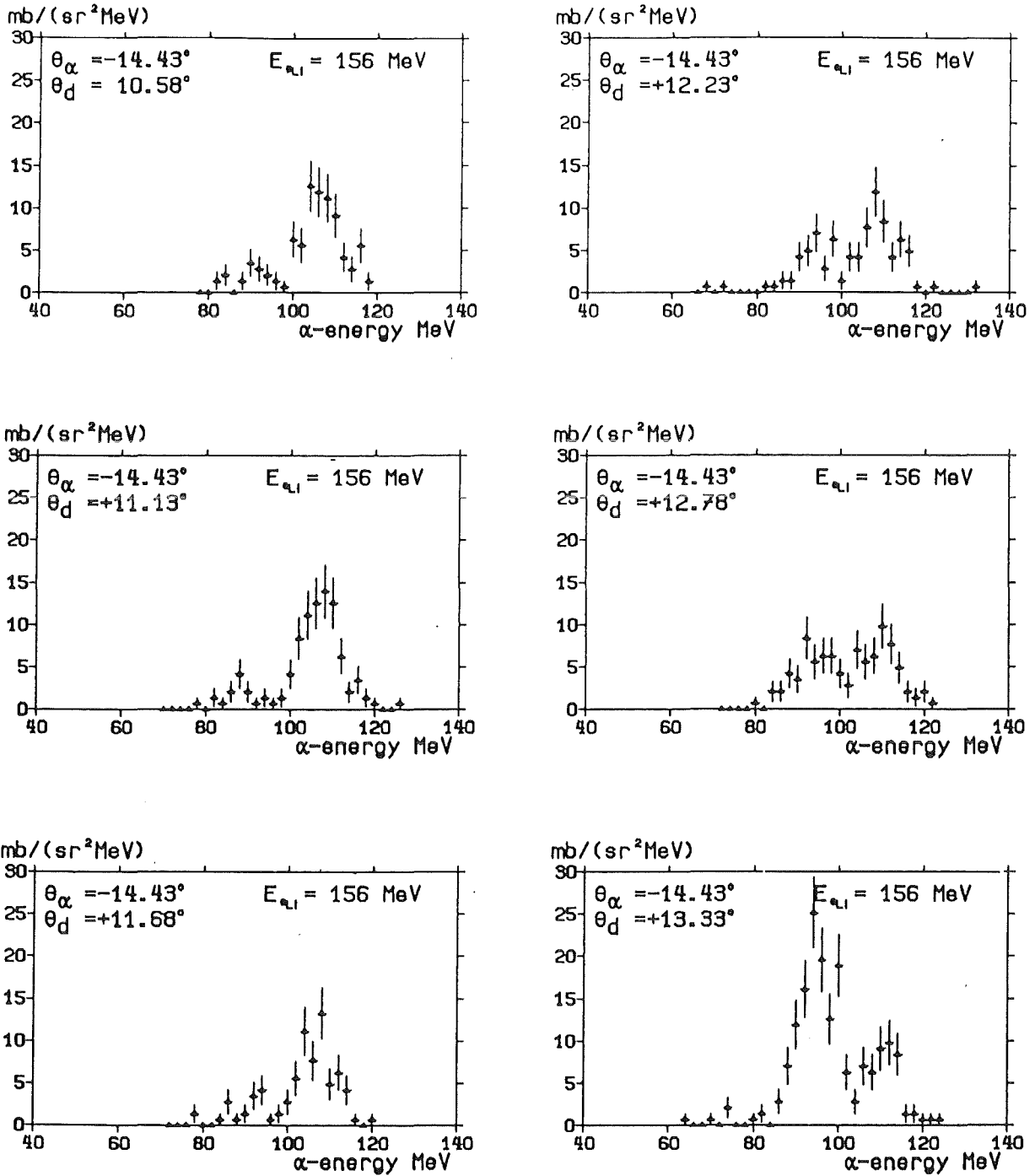


Fig. 2 Preliminary triple differential cross sections  $d^3\sigma / (d\Omega_\alpha d\Omega_d dE_\alpha)$  at large relative momenta of the fragments for direct elastic break-up of  ${}^6\text{Li}$  in  ${}^6\text{Li} + {}^{208}\text{Pb}$  collisions at 156 MeV

to asymptotic relative momenta  $k = 0.55 - 0.75 \text{ fm}^{-1}$ . Fig. 2 presents preliminary coincidence cross sections at large scattering angles.

- (1) N. Heide, V. Corcalciuc, H.J. Gils, H. Rebel, D.K. Srivastava, C. Samanta, S. Zagromski, Proceedings of the XXV International Winter Meeting on Nuclear Physics, Bormio, Italy, 1985, ed. by I. Iori, Ricerca Scientifica ed Educazione Permanente, University of Milano, Suppl.No. 46
- (2) G. Baur, D. Trautmann, Phys. Rep. C25 (1976) 293;  
G. Baur, F. Rösler, D. Trautmann, R. Shyam, *ibid.* C111 (1984) 333
- \* Central Institute of Physics, IFIN, Bucharest, Romania  
\*\* Bhabha Atomic Research Centre, Calcutta, India  
\*\*\* Saha Institute for Nuclear Physics, Calcutta, India

#### 1.4.9 INTERMEDIATE MASS FRAGMENTS IN THE REACTION ${}^6\text{Li} + {}^{46}\text{Ti}$ AT $E/A = 26 \text{ MeV}$

T. Kozik\*, J. Buschmann, K. Grotowski\*, H.J. Gils, N. Heide,  
J. Kiener, H. Klewe-Nebenius\*\*\*, H. Rebel, S. Zagromski,  
A.J. Cole\*\*, S. Micek\* (1)

Intermediate mass fragment cross-sections  $\sigma(E, \theta, 4 \leq Z \leq 11)$  have been measured in the reaction  ${}^6\text{Li} + {}^{46}\text{Ti}$  at 156 MeV incident energy. A simple sequential binary decay model describes most of the  $Z > 8$  data as evaporation from the compound nucleus. The complete fusion cross section is also well reproduced. An intermediate velocity source model ( $\beta=2\beta_{\text{CN}}$ ,  $T=7 \text{ MeV}$ ) has been used in order to explain the small angle and  $Z \leq 8$  data which indicate a  $Z^{-4.1}$  dependence.

- (1) Z. Phys. A 326 (1987) 421

\* Institute of Physics, Jagellonian University, Cracow, Poland  
\*\* Institut des Sciences Nucléaires, Grenoble, France  
\*\*\* Institut für Radiochemie, Kernforschungszentrum Karlsruhe

#### 1.4.10 INTERMEDIATE MASS FRAGMENTS FROM THE REACTIONS ${}^6\text{Li} + \text{natCu}$ AND ${}^6\text{Li} + \text{natAg}$ AT $E/A = 26 \text{ MeV}$

J. Brzychczyk\*, K. Grotowski\*, H.J. Gils, N. Heide, H. Jelitto,  
J. Kiener, T. Kozik\*, S. Micek\*, R. Rebel, Z. Sosin\*, S. Zagromski

The reaction mechanism of intermediate mass fragment emission in  ${}^6\text{Li}$  induced reactions with  $\text{natCu}$  and  $\text{natAg}$  target nuclei at  $E/A = 26 \text{ MeV}$  has been investigated by experiments at the Karlsruhe Isochronous Cyclotron.



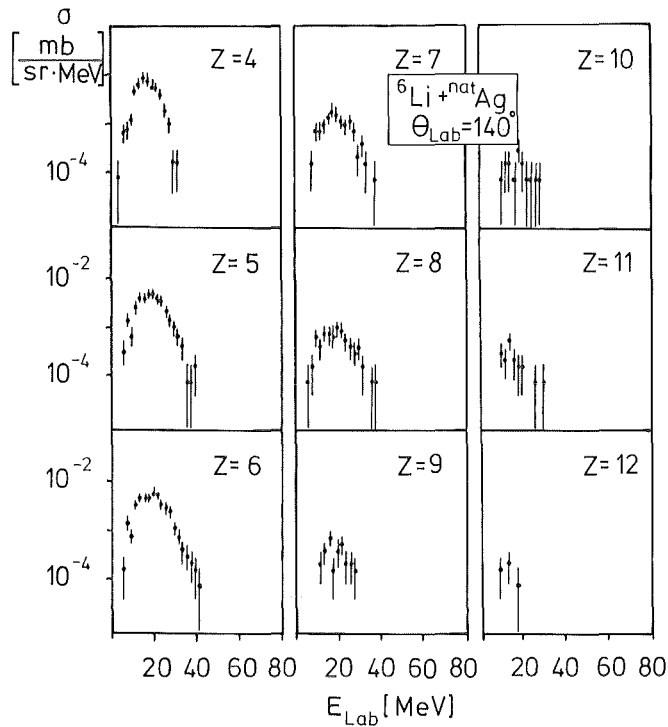


Fig. 1 Energy distributions of different ejectiles (Z) in the  ${}^6\text{Li} + \text{natAg}$  reaction

The work continues the studies of the  ${}^6\text{Li} + {}^{46}\text{Ti}$  reaction (1). The measured data have been evaluated at the computer centre of the Institute of Physics of the Jagellonian University Cracow, extracting energy spectra, angular and element distributions. Some examples are presented in Figs. 1 - 3. The element distribution shown in Fig. 3 exhibits an interesting dependence of the cross section upon the targets mass number, which follows the excitation energy per nucleon (apparent temperature) of the compound nucleus. This observation suggests a thermal character of the observed intermediate mass fragment emission.

More recently additional measurements at very large emission angles have been performed in order to explore more details of the compound nucleus evaporation contributing to the measured angular distributions. For this purpose a system of 21 detector telescopes (developed in Cracow and installed at the Karlsruhe Cyclotron) has been used (see Fig. 4). Each telescope is a combination of a gas proportional counter and a Si(Li) detector.

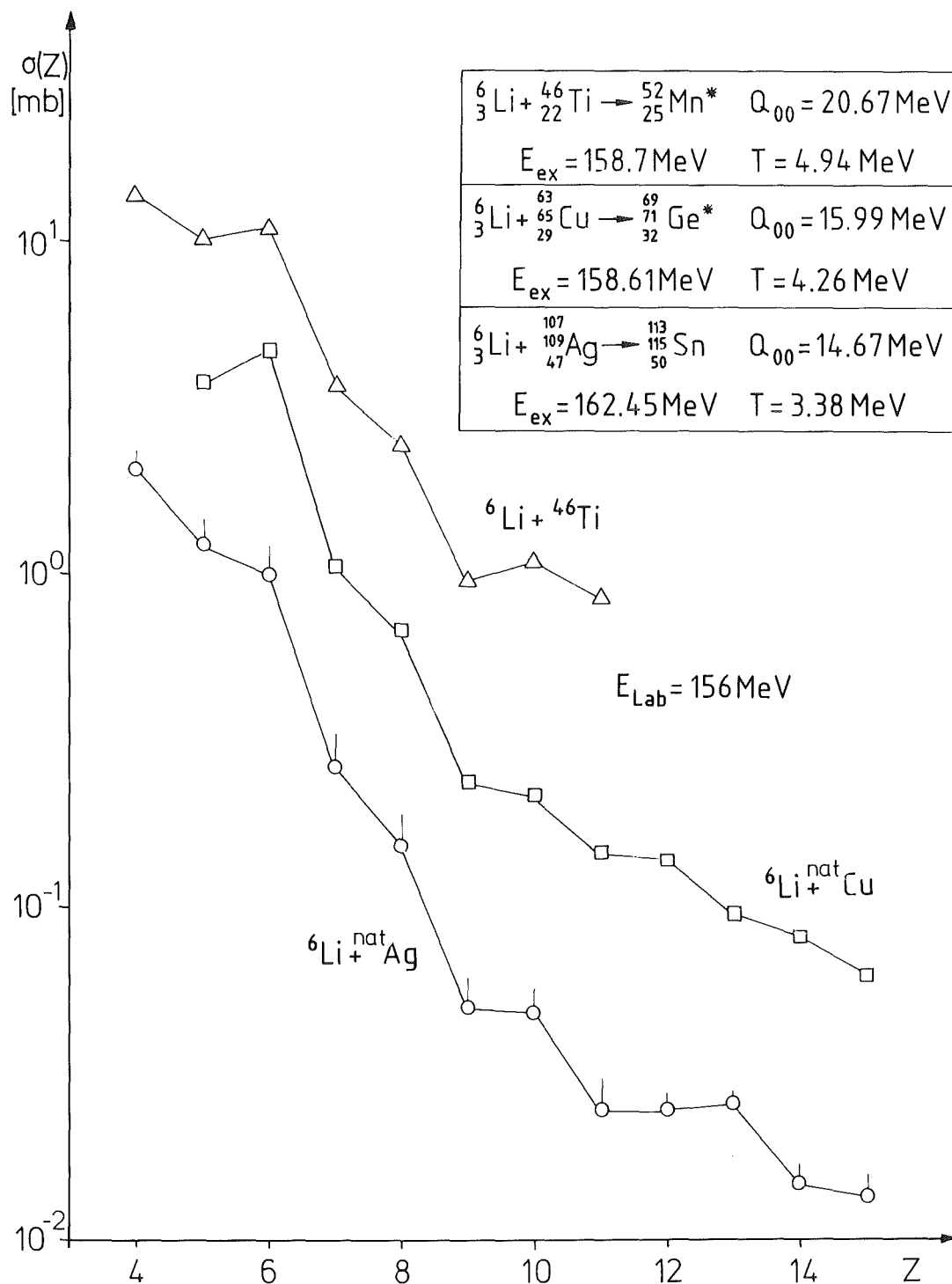


Fig. 2 Z-distribution of ejectiles emitted in  ${}^6\text{Li}$  induced nuclear reactions at 156 MeV

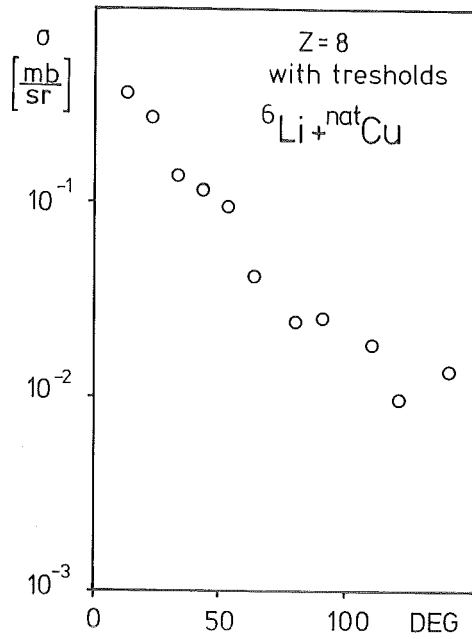


Fig. 3  
Angular distribution of  
160 ejectiles in the  
 ${}^6\text{Li} + \text{natCu}$  reaction at  
 $E_{\text{Li}} = 156 \text{ MeV}$

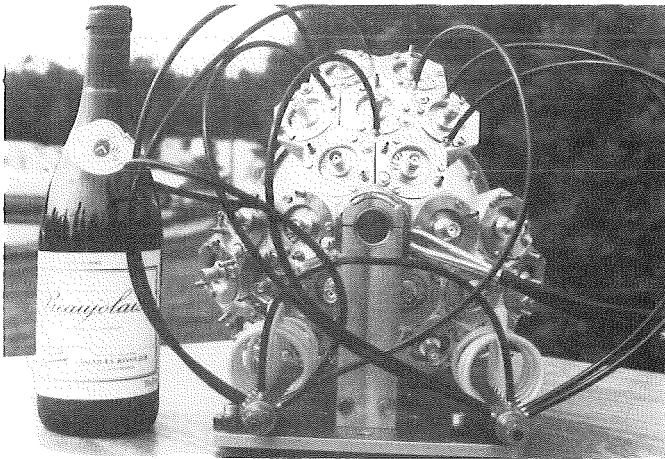
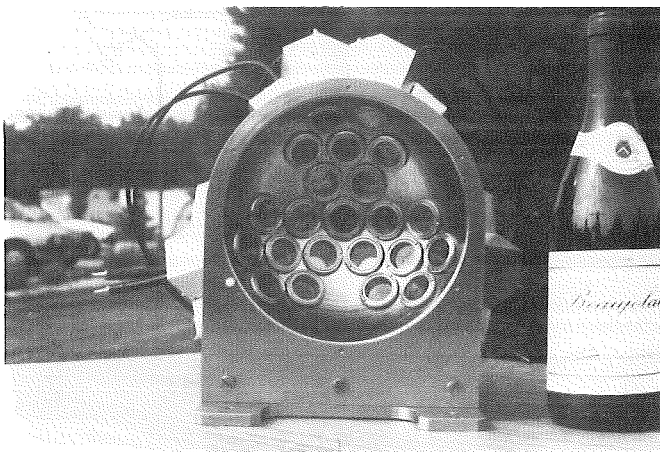


Fig. 4  
Gas proportional  
counter - Si(Li)  
multidetector telescope



- (1) T. Kozik, J. Buschmann, K. Grotowski, H.J. Gils, N. Heide, J. Kiener, H. Klewe-Nebenius, H. Rebel, S. Zagromski, A.J. Cole, S. Micek, *Z.Phys. A326* (1987) 421

\* Institute of Physics, Jagellonian University, Cracow, Poland

1.4.11 A SEMICLASSICAL MULTISTEP EVAPORATION MODEL OF INTERMEDIATE MASS FRAGMENT EMISSION.

J. Brzychozyk\*, A.J. Cole\*\*, H.J. Gils, K. Grotowski\*, T. Kozik\*, S. Micek\*, H. Rebel, Z. Sosin\*

Various experimental investigations have suggested that intermediate mass fragment emission originates from sources with velocities intermediate between the incident projectile velocity and the compound nucleus velocity as well as from the compound nucleus itself (1). Such intermediate velocity sources have been associated with nonequilibrium emission via more or less exotic models. The aim of our work is to try to explain the observed data on the basis of conventional compound nucleus emission.

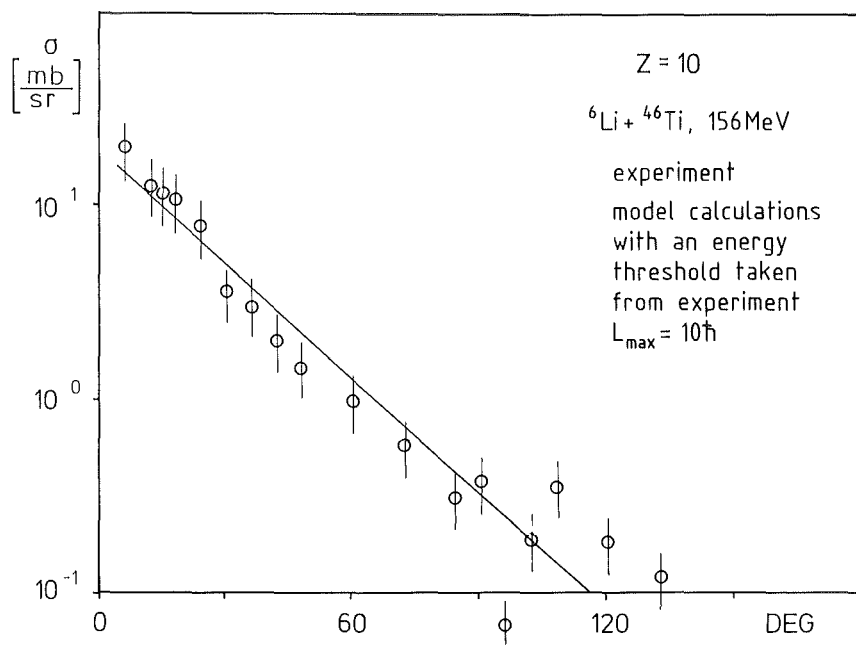


Fig. 1 Differential cross sections of  ${}^{20}\text{Ne}$  emission in the reaction  ${}^6\text{Li} + {}^{46}\text{Ti}$

We propose a simple semiclassical model of multistep evaporation with binary splittings along all the evaporation chains. The  $L = 0$  version of the model is described elsewhere (1). In a more refined version angular momentum effects have been included. We assume an isotropic CM angular distribution in each reaction plane and sum contributions from all reaction planes. For each splitting the disintegration energy consists of the Coulomb and rotational contribution with the nuclear shape at the scission point taken from the liquid drop model (2). Energy spectra after each

splitting are calculated according to the procedure of Moretto (3). Fig. 1 displays predictions of the model, applied to the case of  $^{46}\text{Ti}(^6\text{Li}, ^{20}\text{Ne})$  at 156 MeV and compared to experimental data. These preliminary results are encouraging.

- (1) T. Kozik, J. Buschmann, K. Grotowski, H.J. Gils, N. Heide, J. Kiener, H. Klewe-Nebenius, H. Rebel, S. Zagromski, Z. Phys. A326 (1987) 421
- (2) J. Blocki, K. Grotowski, R. Planeta, W.J. Świątecki, Nucl. Phys. A445 (1985) 367
- (3) L.G. Moretto, Nucl. Phys. A247 (1975) 211

\* Institute of Physics, Jagellonian University, Cracow, Poland

\*\* Institut des Sciences Nucléaires, Grenoble, France

#### 1.4.12 EO STRENGTH IN $^{12}\text{C}$ FROM $^6\text{Li}$ -SCATTERING

W. Eyrich\*, A. Hofmann\*, A. Lehmann\*, B. Mühldorfer\*, H.

Schlösser\*, H. Wirth\*, H.J. Gils, H. Rebel, S. Zagromski (1)

The ( $^6\text{Li}, ^6\text{Li}'$ ) reaction was studied on  $^{12}\text{C}$  at  $E_{\text{Li}} = 156$  MeV at extrem forward angles including  $\theta = 0^\circ$ . Spectra were taken in the excitation energies  $E_x < 30$  MeV. EO strength was deduced at  $E_x = 7.65$  MeV (9.5% EWSR), around  $E_x = 10.2$  MeV ( $5\% \pm 1\%$  EWSR) and in the region  $19 \text{ MeV} \leq E_x \leq 21.5$  MeV ( $5\% \pm 2\%$  EWSR).

- (1) Phys. Rev. C36 (1987) 416

\* Physikalisches Institut der Universität Erlangen-Nürnberg

#### 1.4.13 ISOSCALAR GIANT MONOPOLE RESONANCES IN Sn-ISOTOPES FROM $^6\text{Li}$ SCATTERING

R. Dietzel\*, W. Eyrich\*, A. Hofmann\*, A. Lehmann\*,

M. Moosburger\*, R. Rudeloff\*, H. Schlösser\*, H. Wirth\*,

H.J. Gils, H. Rebel, S. Zagromski

One of the fundamental quantities to describe nuclei and nuclear matter is the compression modulus which is also interesting in connection with astrophysical problems like the dynamics of supernova explosions and neutron stars. One of the most direct sources of information on the nuclear compressibility  $K_A$  is the excitation energy  $E_x$  of the isoscalar giant monopole resonance. In the hydrodynamical model one obtains

$E_x = \text{const} \cdot \sqrt{K_A} / (r_0^2)$  where  $r_0$  is the radius of the nucleus. The quantity  $K_A$  is related to the compressibility of nuclear matter  $K_\infty$  according to the semi-empirical mass formula:

$$K_A = K_\infty + K_S \cdot A^{-1/3} + K_t \cdot [(N-Z)/A]^2 + K_C \cdot Z^2 \cdot A^{-4/3}$$

The parameters  $K_S$ ,  $K_t$  and  $K_C$  can be fitted using the experimental excitation energies  $E_x$  of the giant monopole resonance (EO-GR) over a wide range of nuclei. The currently "accepted" experimental value from such kind of analysis is  $K_\infty = (210 \pm 30)$  MeV (1).

From a more recent study using small angle alpha-particle scattering a significantly higher value of 290 MeV was extracted (2). In

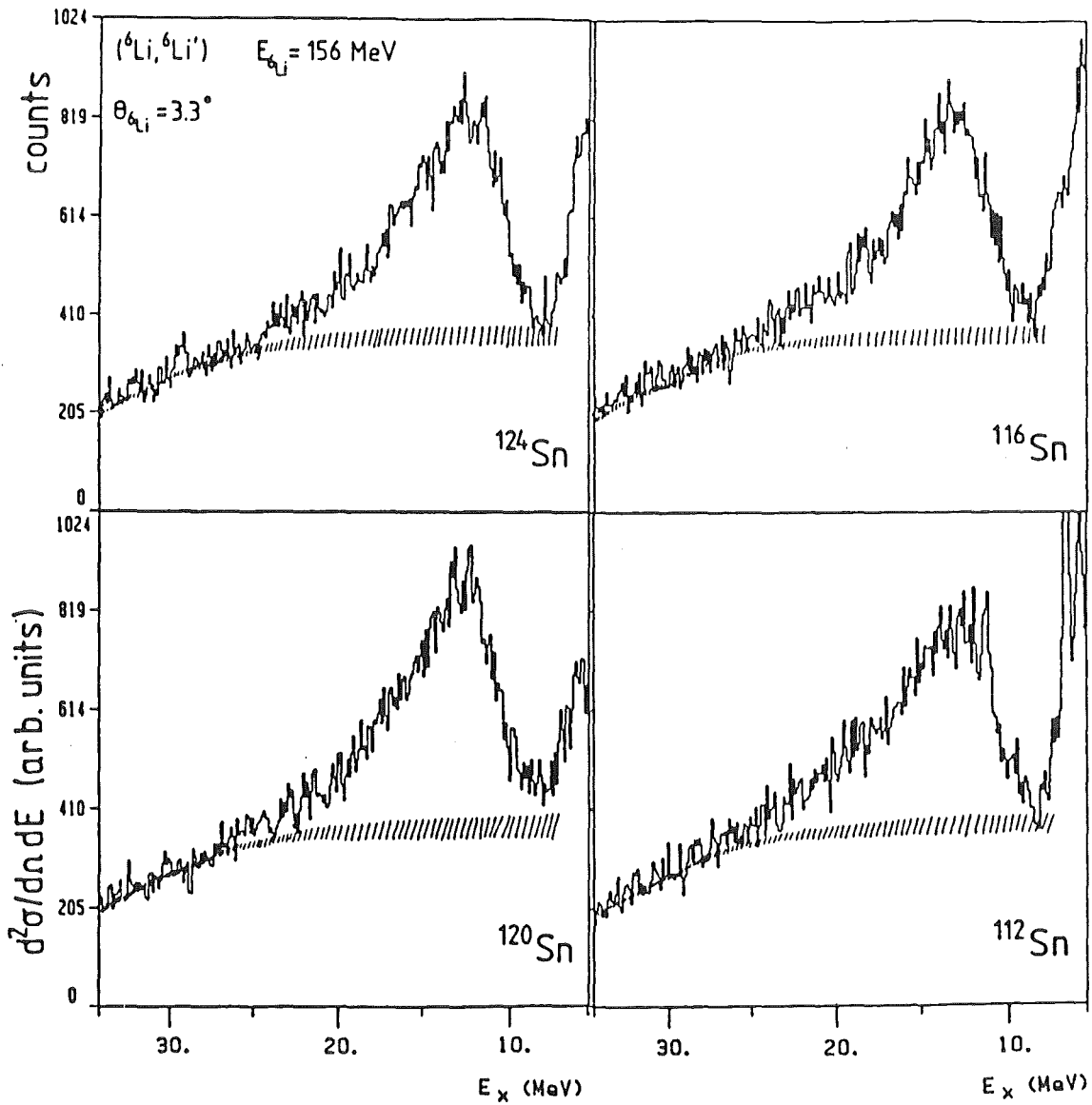


Fig. 1  $(^6\text{Li}, ^6\text{Li}')$  spectra on  $^{112}, ^{116}, ^{120}, ^{124}\text{Sn}$  in a maximum of the EO-GR

this work especially the shift of the EO-GR in the Sn-isotopes from  $^{112}\text{Sn}$  to  $^{124}\text{Sn}$ , which is important for the asymmetry parameter  $K_1$ , was deduced to be about 0.5 MeV in contrast to the previous value of about 1.3 MeV. This can be proved from our study of the isoscalar giant resonances in the isotopes  $^{112}, ^{116}, ^{120}, ^{124}\text{Sn}$  using  $^6\text{Li}$  scattering at small angles. The decisive advantage of the  $(^6\text{Li}, ^6\text{Li}')$  reaction in comparison to the usually used alpha-particle scattering is the relatively low background in the Li-spectra especially in the region of the EO-GR due to the low binding energy of the  $^6\text{Li}$ -projectile.

In Fig. 1  $^6\text{Li}$ -spectra at a maximum of the EO-GR angular distribution are shown. One clearly recognizes the favourable resonance to background ratio. In Fig. 2 the difference of the spectra between a maximum ( $\theta=3.5^\circ$ ) and the first minimum ( $\theta=2.3^\circ$ ) of the EO angular distribution is shown for  $^{120}\text{Sn}$  (upper part) together with a fit of the EO and E2-GRs to the resonance part of the spectrum of Fig. 1 (lower part). Due to the fact that the E2-GR strength and strengths with higher multipolarities are nearly constant in this angular region the difference spectrum allows to extract the parameters of the EO-GR. From our preliminary analysis we extract a shift of the excitation energy of the EO-GR from  $^{124}\text{Sn}$  to  $^{112}\text{Sn}$  of about  $(0.5 \pm 0.2)$  MeV which is in agreement with the results of ref.2.

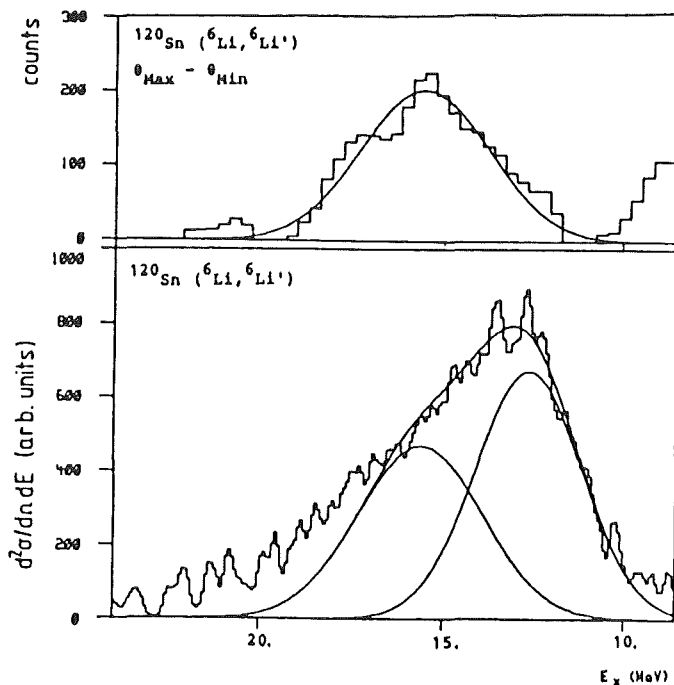


Fig. 2

Upper part: Difference of the spectra of a maximum and the first minimum of the EO-GR in  $^{120}\text{Sn}$

Lower part: Fit of the EO and E2 GR to the resonance part of the  $^{120}\text{Sn}$  spectrum shown in Fig. 1

- (1) J.P. Blaizot, Phys. Rep. 64 (1980) 171
- (2) M.M. Sharma et al., Int. Symp. on Collective Phenomena, Bad Honnef, 1987

\* Physikalisches Institut, Universität Erlangen-Nürnberg

1.4.14 THE ( ${}^6\text{Li}, {}^6\text{He}$ ) REACTION AT SMALL ANGLES TO STUDY SPIN-ISOSPIN STRENGTH

M. Moosburger\*, R. Dietzel\*, W. Eyrich\*, A. Hofmann\*,  
A. Lehmann\*, R. Rudeloff\*, H. Schlösser\*, H. Wirth\*,  
H.J. Gils, H. Rebel, S. Zagromski

Most studies of spin-isospin excitations in nuclei have employed so far the (p,n) and the ( ${}^3\text{He}, t$ ) reaction (1).

An alternative choice to study these excitations is the ( ${}^6\text{Li}, {}^6\text{He}$ ) reaction. Its main advantage is the selective sensitivity for  $\Delta S = \Delta T = 1$  transitions, which causes the isobaric analog state (IAS) to vanish and leads to a strong reduction of the  $\Delta S = 0$  background that contributes to the (p,n) and ( ${}^3\text{He}, t$ ) spectra. Therefore, the ( ${}^6\text{Li}, {}^6\text{He}$ ) reaction should be in particular suitable to search for Gamow-Teller (GT) strength and to extract spin-isospin strengths with higher multiplicities ( $L > 0$ ).

We measured the ( ${}^6\text{Li}, {}^6\text{He}$ ) reaction on various target nuclei using the 156 MeV  ${}^6\text{Li}^{3+}$  beam of the Karlsruhe Isochronous Cyclotron and the magnetic spectrograph "Little John" in an angular region  $0^\circ \leq \theta_{\text{He, Lab}} \leq 10^\circ$ . Thus we started for the first time a systematic investigation of the ( ${}^6\text{Li}, {}^6\text{He}$ ) reaction at zero degree.

In this contribution we present first results of our measurements on the target nuclei  ${}^{12}\text{C}$ ,  ${}^{18}\text{O}$ , and  ${}^{58}\text{Ni}$ .

In Fig. 1  ${}^{12}\text{C} \rightarrow {}^{12}\text{N}$  transfer spectra are shown. The  $0^\circ$  spectrum (upper part) shows a maximum for the  $1^+$  GT state at 0.0 MeV, whereas the  $2^+$  state at 0.96 MeV is small. Coming to  $5^\circ$  (middle part), both states have approximately equal strength. The broad peak at  $E_x \approx 4$  MeV obviously consists of several components with different multiplicities. This can be seen by comparing the  $8^\circ$  spectrum (lower part) with that obtained at  $0^\circ$ .

The reaction  ${}^{18}\text{O}({}^6\text{Li}, {}^6\text{He}){}^{18}\text{F}$  has been studied using a gas target. Fig. 2a) shows a spectrum of this reaction at  $\theta = 0^\circ$ . It is dominated by the strong ground state transition, which represents most of the GT strength in this system. Moreover, additional transitions with small strengths were found, corresponding to different multiplicities.

In Fig. 2b) a zero degree spectrum of the transition  ${}^{58}\text{Ni} \rightarrow {}^{58}\text{Cu}$  is displayed, which shows a variety of states, including strong GT excitations.



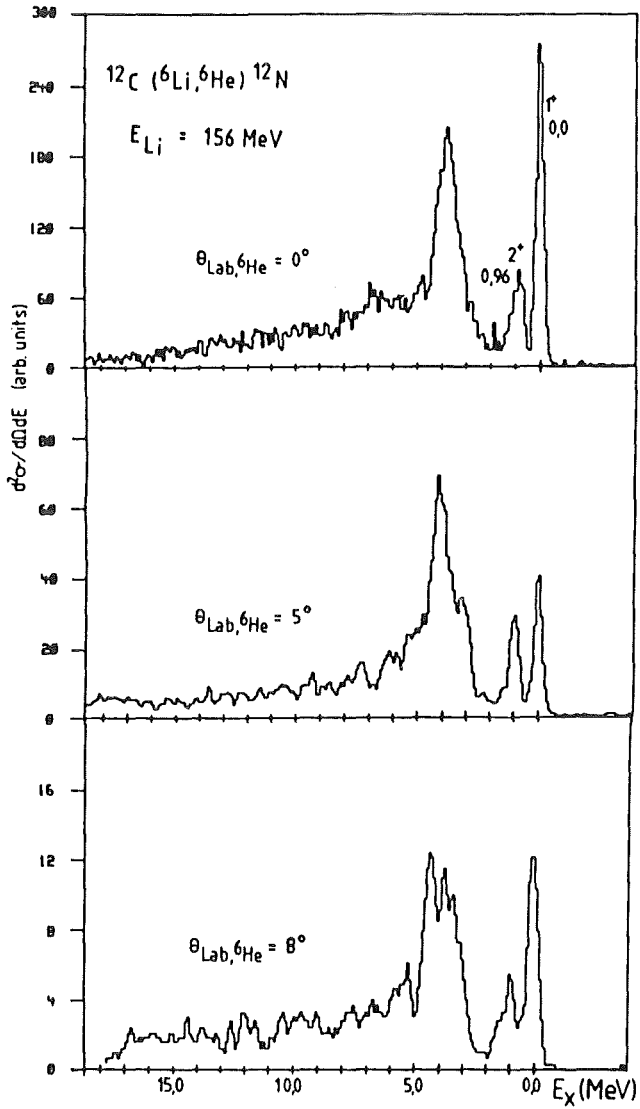


Fig. 1 Spectra of the reaction  $^{12}\text{C}(^6\text{Li},^6\text{He})^{12}\text{N}$  taken at  $\theta = 0^\circ$ ,  $5^\circ$  and  $8^\circ$

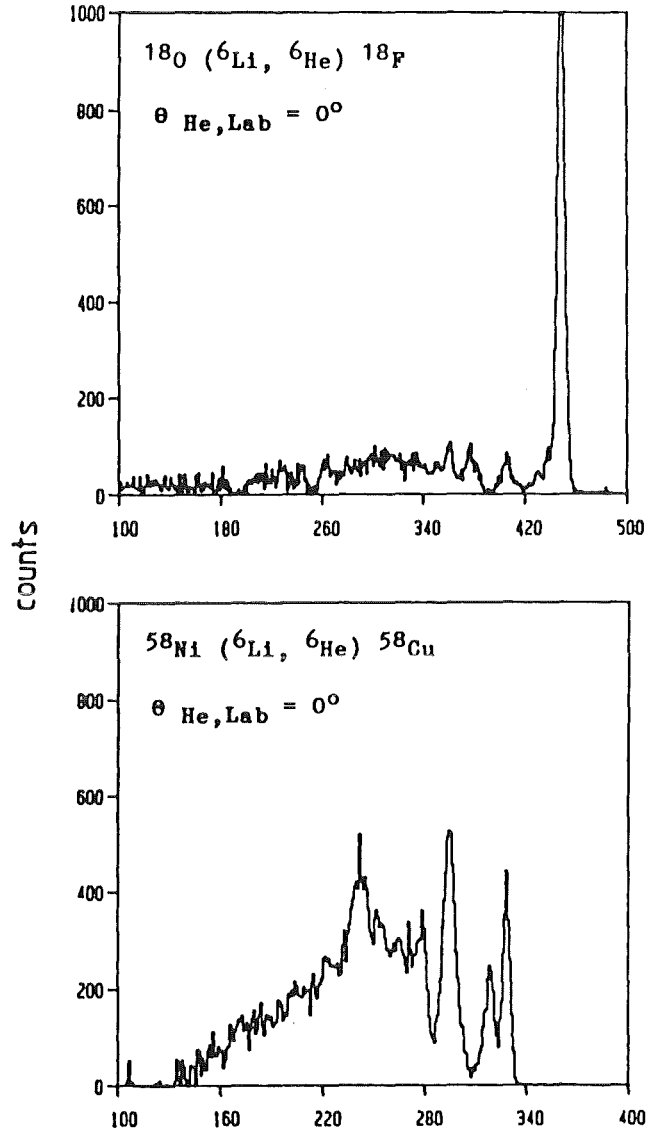


Fig. 2 Zero degree spectra of the  $(^6\text{Li},^6\text{He})$  reaction on  $^{18}\text{O}$  (upper part) and  $^{58}\text{Ni}$  (lower part)

(1) C. Gaarde, Proc. Int. Nucl. Phys. Conf. Harrogate 1986, Vol. 2, p. 173, and references given therein

\* Physikalisches Institut der Universität Erlangen-Nürnberg

1.4.15 GAMOW-TELLER STRENGTH AND OTHER SPIN-ISOSPIN MODES IN THE REACTION  $^{90}\text{Zr}(^6\text{Li},^6\text{He})^{90}\text{Nb}$

H. Wirth\*, R. Dietzel\*, W. Eyrich\*, A. Hofmann\*, A. Lehmann\*,  
M. Moosburger\*, R. Rudeloff\*, H. Schlösser\*, H.J. Gils, H. Rebel,  
S. Zagromski, A. Schulte\*\*, F. Osterfeld\*\*, T. Udagawa\*\*

One of the most interesting nuclei to study spin-isospin flip modes, especially Gamow-Teller (GT) transitions, is  $^{90}\text{Zr}$ . In addition to the strong experimental signal due to the large neutron excess, sophisticated microscopic model calculations are available for this system. In our program to investigate  $(^6\text{Li},^6\text{He})$  transitions, we therefore measured the  $^{90}\text{Zr}\rightarrow^{90}\text{Nb}$  reaction in an angular region  $0^\circ \leq \theta_{\text{He,Lab}} \leq 10^\circ$  for excitation energies up to ca. 30 MeV.

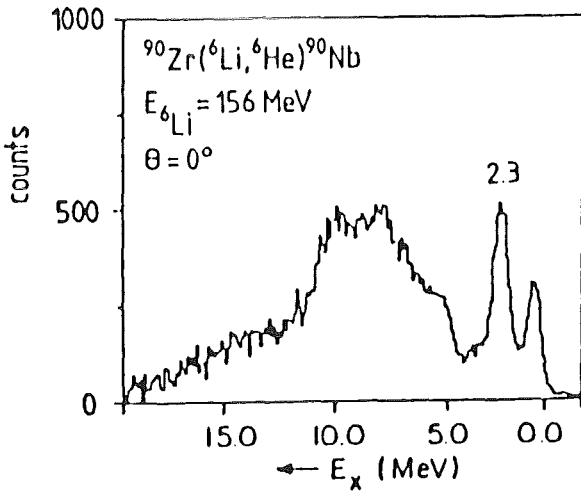


Fig. 1

Comparison of energy spectra  
taken at  $0^\circ$  from the reactions  
a)  $^{90}\text{Zr}(^6\text{Li},^6\text{He})$  and  
b)  $^{90}\text{Zr}(p,n)$  (1)

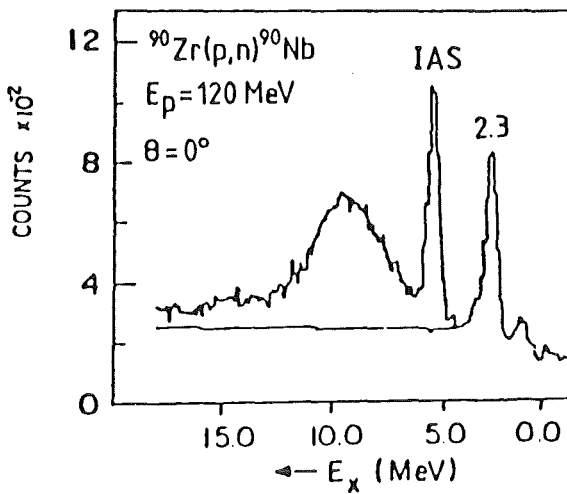


Fig. 1a) shows a zero degree spectrum after subtraction of the continuum "background", which was fixed at a minimum of the GT strength. In the spectrum one clearly recognizes the peak at 2.3 MeV and the bump around 9 MeV with a shoulder towards higher excitation energies. These strengths represent the GT mode. The additional peak at 1.0 MeV exhibits different angular behaviour corresponding to  $L > 0$ . This is also known from (p,n) work (1). For comparison in Fig. 1b) a (p,n) spectrum at  $0^\circ$  taken from ref. 1 is shown. There is good agreement between both spectra concerning the GT strength. The isobaric analogue state (IAS in Fig. 1b) is absent in the ( ${}^6\text{Li}, {}^6\text{He}$ ) case proving the high selectivity of the ( ${}^6\text{Li}, {}^6\text{He}$ ) reaction for  $\Delta S = 1$  transitions.

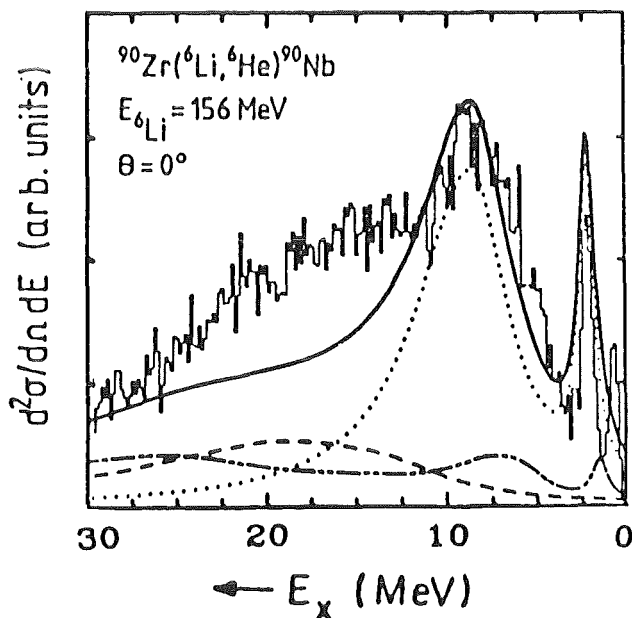


Fig. 2  
Comparison between experimental data and a microscopic model calculation for  ${}^{90}\text{Zr}({}^6\text{Li}, {}^6\text{He}){}^{90}\text{Nb}$  at  $0^\circ$  (solid line: full calculation, dotted: GT distribution, dashed: negative parity states, dashed-double dotted: positive parity states)

In Fig. 2 a full ( ${}^6\text{Li}, {}^6\text{He}$ ) zero degree spectrum is displayed together with a spectrum obtained by microscopic RPA model calculations for the GT mode and spin-isospin transitions with higher multipolarities. The calculation is in good agreement with the experimental strength distribution showing that most of the continuum "background" is due to excitations of strength with higher multipolarities and "hidden" GT strength. It can also be concluded that for the given experimental parameters the contribution of multistep processes does not play an important role.

(1) D.E. Bainum et al., Phys. Rev. Lett. 44 (1980) 1751

\* Physikalisches Institut der Universität Erlangen-Nürnberg.

\*\* Kernforschungsanlage Jülich, Institut für Kernphysik

1.4.16 EMPIRICAL RELATIONSHIPS BETWEEN LOW ENERGY ANTIPROTON-NUCLEON AND ANTIPROTON-NUCLEUS INTERACTIONS

C.J. Batty\*, E. Friedman\*\*, H.J. Gils

The recent high-quality data for the scattering of 300 and 600 MeV/c antiprotons by nuclei has been analysed previously (1). Because of the very strong absorption of antiprotons in nuclei the data give information on just three parameters. In a folding model approach one can get a range and a complex strength for the antiproton-nucleon effective interaction. Table 1 summarises the results of an analysis of all available antiproton-nucleus scattering data. It is seen that excellent fits are obtained. An interesting feature is the rather strong dependence on energy of the range

Table 1  
Range and strength parameters  
for antiproton-nucleus scattering

E (MeV)	47	47	180	180	180	180
Target	C	Ca	C	<sup>16</sup> O	<sup>18</sup> O	Ca
a <sub>G</sub> (fm)	1.281 (.054)	1.364 (.084)	0.970 (.020)	1.015 (.021)	1.040 (.019)	1.134 (.039)
V <sub>RA</sub> G <sup>3</sup> (MeV fm <sup>3</sup> )	52.3 (3.3)	27.4 (4.1)	60.6 (1.6)	58.1 (2.2)	47.8 (1.6)	52.2 (2.2)
V <sub>IA</sub> G <sup>3</sup> (MeV fm <sup>3</sup> )	103.5 (4.1)	100.9 (6.3)	165.4 (2.8)	153.3 (3.3)	137.1 (2.5)	133.2 (5.1)
χ <sup>2</sup> /F	1.1	1.6	1.2	1.4	1.1	2.5

Numbers in bracket are the parameter errors obtained from the fits

parameter, which is at first surprising when compared to the corresponding proton-nucleus interaction.

Very recent results (2) for antiproton-proton small angle scattering show a surprisingly strong dependence of the slope parameter on energy. When interpreted in terms of a Gaussian interaction it is found

Table 2  
Slope and range parameters  
for antiproton-proton scattering

p (MeV/c)	600	300	272	233
E (MeV)	180	47	39	29
slope (GeV/c) <sup>-2</sup>	20	40	48	72
a <sub>G</sub> (fm)	1.25	1.76	1.92	2.36

(see Table 2) that the ranges are somewhat larger than those obtained from antiproton-nucleus scattering but the same strong dependence on the energy is observed.

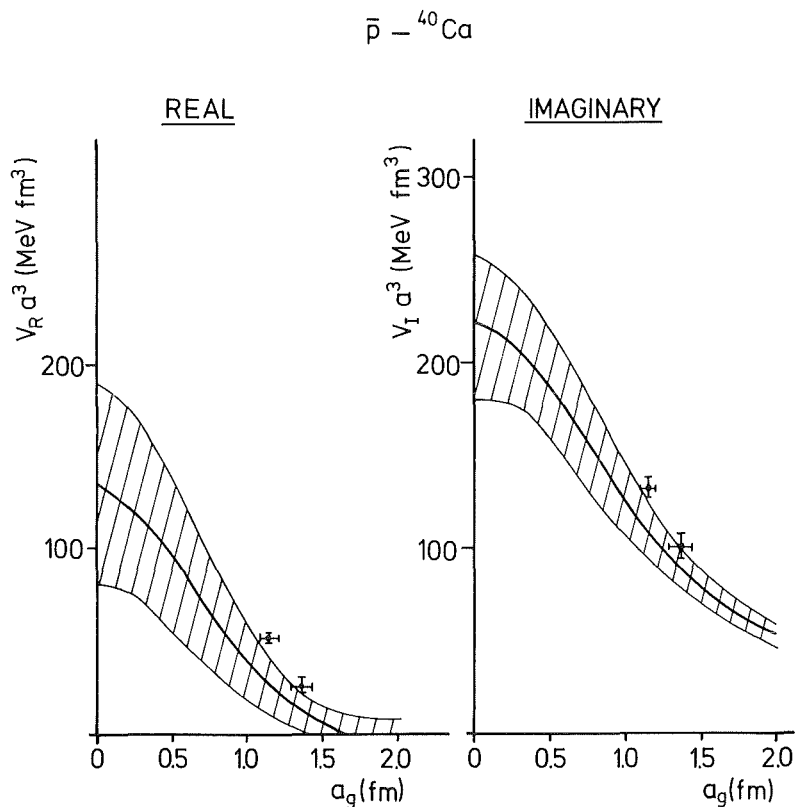


Fig.1 Strength-range ambiguity for the antiproton- ${}^{40}\text{Ca}$  interaction from antiprotonic atoms and results from antiproton scattering (points with error bars).

Studies of antiprotonic atoms give information on the antiproton-nucleus interaction at zero energy but since only two or three experimental values are available for each target nucleus the range of the interaction is not well determined by the data. Figure 1 shows an example of the strength-range ambiguity. Also shown are single points from the analysis of scattering data mentioned above. Considering Fermi motion in nuclei, one might expect the 47 MeV (300 MeV/c) results to agree with those for atoms, as is indeed observed. The potential parameters are not determined with sufficient accuracy to enable further conclusions to be drawn from comparisons of scattering and atom data.

The effects of Fermi motion should be absent from the antiproton-proton interaction. Analysing antiproton-H X-ray data, we indeed find a larger range parameter of about 1.5 - 2.5 fm, consistent with the slope

parameters mentioned above. The values of  $V \cdot a^3$ , however, deviate considerably from those of Fig. 1, as is to be expected.

To summarise, we have observed a semi-quantitative relationship between antiproton-nucleus and antiproton-nucleon effective interactions. In particular, effects due to Fermi motion seem to be observed and the strong dependence of the range parameter on energy is traced to originate from the antiproton-proton interaction. More accurate data may enable further studies to be made along these lines.

- (1) See for example E. Friedman, J. Lichtenstadt, Nucl. Phys. A455 (1986) 573
  - (2) L. Linssen et al., Nucl. Phys. A469 (1987) 726
- \* Rutherford Appleton Laboratory, Chilton Didcot, U.K.  
\*\* Racah Institute of Physics, Hebrew University of Jerusalem, Israel

## 2. LASER SPECTROSCOPY

### 2.1 CHARGE RADII AND MOMENTS OF STRONTIUM NUCLEI BY LASER SPECTROSCOPY

M. Anselment\*, K. Bekk, S. Chongkum, S. Göring, A. Hanser,  
H. Hoeffgen\*\*, W. Kälber, G. Meisel, H. Rebel (1)

The isotope shifts and hyperfine splittings for eleven strontium isotopes ( $A=80-90$ ) and two isomers for the optical transition  $\lambda = 293.2$  nm were measured. The magnetic dipole and electric quadrupole moments and the changes of the mean square charge radii are derived. The results are discussed with respect to the increasing nuclear deformation and the anomalous coupling scheme of light Sr nuclei.

(1) Z. Phys. A - Atomic Nuclei 326 (1987) 493

\* Department of Physics and Astronomy, Louisiana State University,  
Baton Rouge, USA

\*\* Batelle-Institut e.V., Frankfurt/Main

### 2.2 HYPERFINE SPLITTING OF THE $^{242m}\text{Am}$ GROUND STATE FROM ATOMIC BEAM LASER SPECTROSCOPY

K. Bekk, S. Göring, W. Kälber, G. Meisel, A. Sameh\*

Our previous measurements (1) of isotope shifts and hyperfine splittings of americium were done employing the method of optogalvanic laser spectroscopy. In this technique the spectral lines are Doppler broadened. The samples for those experiments with  $^{242m}\text{Am}$  contained mainly  $^{241}\text{Am}$  with only 1% of  $^{242m}\text{Am}$  and  $^{243}\text{Am}$  each; therefore many components of  $^{242m}\text{Am}$  were unresolved and invisible and the interpretation of the observed components was difficult leaving some doubt on their assignment. The ground state hyperfine splitting was completely unresolved.

The method applied to overcome these problems was laser induced resonance fluorescence with a collimated atomic beam (2,3). For safety reasons only selected experiments were done with few samples of 20 ng Am which consequently contained only 200 pg of  $^{242m}\text{Am}$  dissolved in 5n  $\text{HNO}_3$ .

The Am atoms were excited at  $\lambda=605.438\text{nm}$  from the  $5f^7 7s^2 8s_{7/2}$  ground state to the  $5f^7 7s 7p 10p_{9/2}$  state. The resonance detection was by the spontaneous reemission to the ground state. Records of the hyper-

fine components of  $^{242m}\text{Am}$  are given in Fig. 1; they illustrate the 107 fold increase of the sensitivity as compared to earlier atomic beam experiments which were done with gigantic mg amounts of Am in the samples (4).

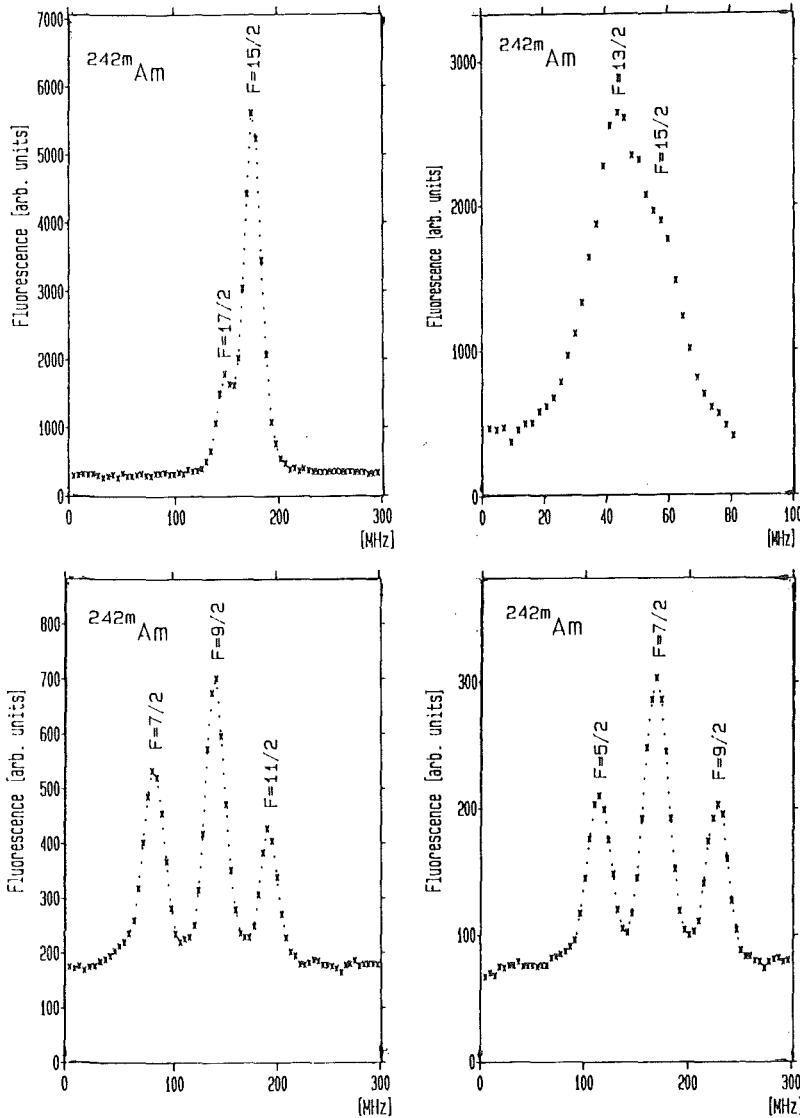


Fig. 1  
Spectra of the  
 $^{242m}\text{Am}$  ground state  
splitting

The records were evaluated with respect to the hyperfine splitting factors A and B of the Am ground state. This requires to assign total angular momentum quantum numbers F to the observed components. Our assignment is based on a combined analysis of the number, the spacings and the relative intensities of the components. The observed intensity ratios are not the same as obtained from the transition matrix elements because of slight saturation. However, they are not modified to such an extent that



the ratios are inverted. Thus it was possible to assign unambiguous F values resulting in  $F'=17/2$ ,  $15/2$ ,  $9/2$ , and  $7/2$  (Fig. 1) for the upper state of the transition investigated. This confirms independently the findings of the optogalvanic measurements (1), where only the  $F'=17/2$ ,  $11/2$  and  $7/2$  components were observed.

The hyperfine splitting constants for the ground state of  $^{242}\text{mAm}$  were found to be  $A = -5,3(6)$  MHz and  $B = 198(17)$  MHz.

- (1) W. Liewehr, K. Bekk, W. Kälber, G. Meisel, H. Rebel, Ali Sameh, Report KfK 4159, Kernforschungszentrum Karlsruhe (1986) 61
- (2) M. Anselment, K. Bekk, S. Chongkum, S. Göring, A. Hanser, H. Hoeffgen, W. Kälber, G. Meisel, H. Rebel, Z. Phys. A326 (1987) 493
- (3) M. Anselment, K. Bekk, A. Hanser, H. Hoeffgen, G. Meisel, S. Göring, H. Rebel, G. Schatz, Phys. Rev. C34 (1986) 1052
- (4) B. Le Garrec, A. Petit, J. Less. Comm. Met. 122 (1986) 55
- \*) Institut für Radiochemie, Kernforschungszentrum Karlsruhe

### 2.3 NUCLEAR QUADRUPOLE MOMENT OF $^{243}\text{Am}$ FROM A HYPERFINE STRUCTURE ANALYSIS OF THE Am I LEVEL SPECTRUM

J. Dembczyński\*, M. Elantkowska\*, K. Bekk, H. Rebel

The results of recent laserspectroscopic measurements of the hyperfine structure (hfs) and isotope shifts of various atomic transitions in  $^{241}, ^{243}, ^{242}\text{mAm}$  (1) provide a basis for an improved analysis of the Am I structure. In particular, the data allow a semiempirical determination of the one-electron hfs parameters  $a_{nl}^{kk}$  and  $b_{nl}^{kk}$  for the  $5f^7(8s)7s7p$  configuration. These parameters relate the observed B factor to the value of the nuclear quadrupole moment Q.

Following Sandars and Beck (2) the hfs constants A and B are given by the intermediate coupling expressions:

$$A(8P_{5/2}) = 1.28171a_{5f}^{10} - 0.19499a_{7p}^{01} - 0.15012a_{7p}^{12} - 0.00124a_{7p}^{10} - 0.08548a_{7s}^{10}$$

$$B(8P_{5/2}) = 0.00677b_{7p}^{02} + 0.01343b_{7p}^{11}$$

$$A(10P_{7/2}) = 0.98192a_{5f}^{10} - 0.17768a_{7p}^{07} - 0.10342a_p^{12} + 0.08226a_{7p}^{10} + 0.11350a_{7s}^{10}$$

$$B(10P_{7/2}) = 0.08946b_{7p}^{02} - 0.02442b_{7p}^{11}$$

$$A( 6 P_{7/2} ) = 0.95028a_{5f}^{10} + 0.16256a_{7p}^{01} + 0.15651a_{7p}^{12} - 0.04453a_{7p}^{10} - 0.068317a_{7s}^{10}$$

$$B( 8 P_{5/2} ) = 0.03825b_{7p}^{02} - 0.03479b_{7p}^{11}$$

$$A( 10 P_{9/2} ) = 0.77592a_{5f}^{10} + 0.09188a_{7p}^{01} + 0.14763a_{7p}^{12} + 0.036138a_{7p}^{10} + 0.096069a_{7s}^{10}$$

$$B( 10 P_{9/2} ) = -0.30387b_{7p}^{02} + 0.05483b_{7p}^{11}$$

The numerical coefficients have been calculated by use of the HFSZM computer code (6) and the one-electron parameters have been fitted to the experimental data by a least-squares fit procedure. Introducing additional information the number of the free parameters could be reduced. For example, the parameters  $a_{7s}^{10}$  and  $b_{7p}^{02}$  are required to give the main contributions to A and B, respectively. The value of the  $a_{7p}^{10}$  parameter has been estimated from the Am II spectrum (as given by Fred and Tomkins (3)) by the procedure described in Ref.(4). In addition, the relations between  $a_{7p}^{01}$ ,  $a_{7p}^{12}$  and  $a_{7p}^{10}$  and between  $b_{7p}^{02}$  and  $b_{7p}^{11}$ , respectively, as derived on the basis of the relativistic theory and with relativistic correction factors (5) have been exploited. Thus, we find

$$a_{7p}^{10} = -150\text{MHz (from Am II)}$$

and

$$\begin{aligned} a_{7p}^{12}/a_{7p}^{01} &= 2.0011 & a_{7p}^{10}/a_{7p}^{01} &= -0.2894 \\ b_{7p}^{11}/b_{7p}^{02} &= -0.5670 \end{aligned}$$

Tab. 1 compiles the results of the fitting procedure, whereas the A and B factors of the  $8P_{5/2}$  level have not been included in the least-square-fit-procedure.

The resulting values of the one-electron hfs parameters of  $^{243}\text{Am}$  are

$$\begin{aligned} a_{7p}^{01} &= 711(1) \text{ MHz} & a_{7s}^{10} &= 16462(100) \text{ MHz} \\ b_{7p}^{023} &= 10152(248) \text{ MHz} \end{aligned}$$

With these results we can give the spectroscopic quadrupole moment via

$$Q = 0.40606 \cdot g_I \frac{b_{7p}^{02}}{a_{7p}^{01}} \cdot \frac{F_{7p}^{01}(Z_i)}{R_{7p}^{02}(Z_i)}$$

Here the g-factor  $g_I = 0.632$ . The factors  $F_{7p}^{01}$  and  $R_{7p}^{02}$  are relativistic correction factors calculated for an effective atomic number  $Z_i = Z - \Delta Z$  ( $\Delta Z = 4$  for p electrons (4,5)). The result is

$$Q(243Am) = 4.21 \text{ b}$$

which is in excellent agreement with Coulomb excitation results. However, the result is strongly dependent from the  $a_{7p}^{01}$  value deduced for the magnetic dipole interaction. Using alternatively an  $a_{7p}^{01}$  value resulting from ab-initio theoretical calculations (6) would increase the Q-value to  $Q(243Am) = 6.2 \text{ b}$ .

Tab. 1 Results of the hfs analysis

Level [cm <sup>-1</sup> ]	A <sub>exp</sub> [MHz] B <sub>exp</sub> [MHz]	A <sub>calc</sub> [MHz] B <sub>calc</sub> [MHz]	Exp.-Calc. [MHz]
18429 <sup>8</sup> P <sub>5/2</sub>	-1240.15(8) <sup>+</sup> -133.4(1.0) <sup>+</sup>	-1759. -9.	733. -124.
15608 <sup>10</sup> P <sub>7/2</sub>	1414.7(3) 1037.(7.)	1415. 1049.	0. -11.
18504 <sup>6</sup> P <sub>7/2</sub>	-935.6(2) 762.6(3.0)	-936. 589.	0. 144.
16512 <sup>10</sup> P <sub>9/2</sub>	1714.2(8) -3374.(32.)	1714. -3400.	0. 26.

+ The observed values for the <sup>8</sup>P<sub>5/2</sub> level are not included in the fitting procedure as a strong configuration mixing is suggested by the isotope shift measurements.

- (1) W. Liewehr, K. Bekk, W. Kälber, G. Meisel, H. Rebel, Ali Sameh, Report KfK 4159, Kernforschungszentrum Karlsruhe (1986) 61
- (2) P.G.H. Sandars, J. Beck, Proc. R. Soc. A289 (1965) 97
- (3) M. Fred, Tomkins, J. Opt. Soc. Am. 47 (1957) 1076
- (4) Y. Bordarier, B.R. Judd, M. Klapisch, Proc. R. Soc. A289 (1965) 81
- (5) H. Kopfermann, Nuclear Moments, New York, Academic Press 1958
- (6) J. Dembczyński, private communication

\* Politechnika Poznańska, Instytut Fizyki, Poznań, Poland

## 2.4 LASER SPECTROSCOPIC INVESTIGATIONS OF ISOTOPE SHIFTS AND HYPERFINE STRUCTURE OF THORIUM ISOTOPES IN AN RF ION TRAP

K. Bekk, W. Faubel\*, S. Göring, W. Kälber, G. Meisel, H. Rebel,  
J. Rink, G. Schatz, R.C. Thompson\*\*

In our recent studies of thorium isotopes we have measured isotope shifts and the hyperfine structure of an optical transition of singly ionized thorium in order to get information on changes of mean square charge radii and on electromagnetic moments of thorium nuclei. The experimental method used was laser spectroscopy of stored ions in an rf ion trap (1). This method is well suited for the study of radioactive atomic ions because of the long storage times of confined ions; spectroscopy with only a single ion has been reported (2).

An ion trap consists of conjugated hyperboloids of revolution as electrodes. An rf and a dc voltage supplied to the electrodes generate inside the electrode structure electric quadrupole fields by which charged particles are confined in a small volume. The ion trap is situated in a vacuum chamber evacuated by a turbomolecular pump. A residual gas pressure of  $10^{-10}$  mbar is obtained after the chamber is baked out at 300 °C for several hours. Ions are stored in the presence of a light buffer gas, as e.g. hydrogen or helium (pressure  $10^{-6}$  to  $10^{-2}$  mbar). The procedure of creating thorium ions is as follows: Thorium nitrate solution is deposited outside the trap on a tantalum wire and dried by heating. The prepared tantalum wire is placed about 1 mm deep into the trap volume through a hole in one of the electrodes. The wire is heated up to about 2000 K. Evaporation products are bombarded in flight by electrons emitted from the hot wire. In this way we obtain  $5 \cdot 10^4$  confined thorium ions from  $10^{12}$  sample atoms (i.e. 0.4 ng of thorium); they provide sufficient fluorescence light for optical spectroscopy. Reactions of stored ions with small impurities in the buffer gas have been a problem of particular interest: We observe an increase of the mass of the stored thorium ions by about 18 amu with the electronic ion detection (3); at the same time the fluorescence light from the ions decreases accordingly. By outgassing the ion trap at high temperatures (800-1000 °C) and by use of a titanium getter pump we were able to stretch the reaction time constant of the stored ions from 5 minutes up to 10 hours.

We have measured a series of thorium isotopes:  $A = 227-230, 232$ . The isotopes  $^{228}\text{Th} - ^{230}\text{Th}$  were commercially available as nitrate solutions in appropriate concentrations;  $^{227}\text{Th}$  was prepared from its parent

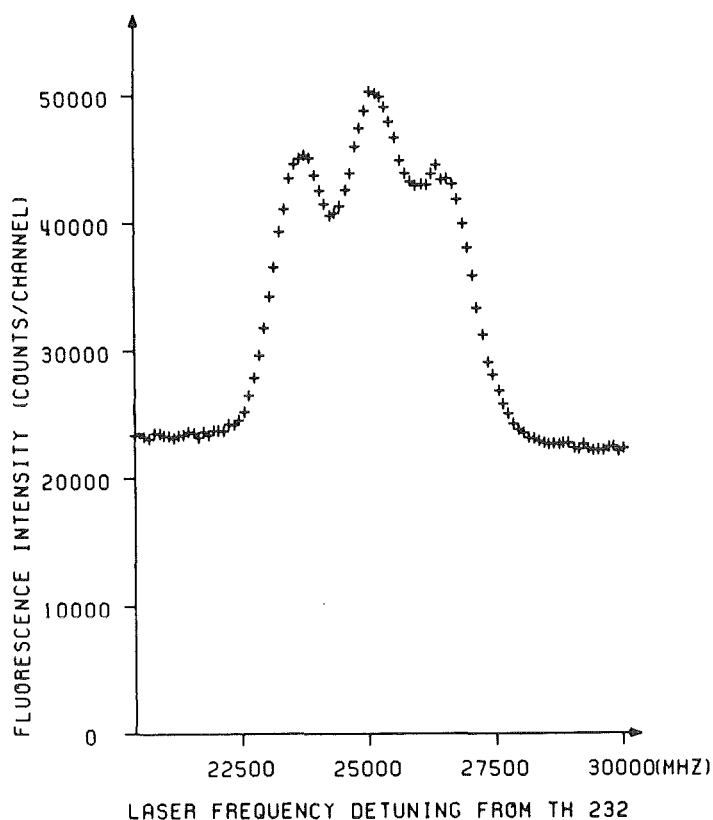


Fig. 1  
Spectrum of the  
583.9 nm transition  
of  $^{229}\text{Th}$

$^{227}\text{Ac}$  by radiochemical separation. For spectroscopy the transition Th II  $\lambda = 583.9$  nm from the ground state  $[6d^2 7s ({}^4F_{3/2})] + [6d 7s^2 ({}^2D_{3/2})] + [6d^2 7s ({}^2D_{3/2})]$  to the  $[5f 6d^2 ({}^2P_{3/2})] + [5f 6d 7s ({}^2P_{3/2})]$  state at  $17121.623 \text{ cm}^{-1}$  was excited with a tunable cw dye laser. The excitation was monitored by detection of the fluorescence light of the transition  $640.9$  nm into the  $[6d^2 7s ({}^4F_{5/2})]$  metastable state at  $1521.9 \text{ cm}^{-1}$ ; the ions are subsequently quenched back to the ground state by collisions with the buffer gas. A wavemeter (4) consisting of a grating spectrograph and three Fabry-Perot interferometers was used for the determination of the dye laser frequency. Fig. 1 shows a spectrum of the  $583.9$  nm transition of  $^{229}\text{Th}$ .

For the  $583.9$  nm transition the isotope shifts with respect to the natural  $^{232}\text{Th}$  were measured. The results of the measurements are summarized in Table 1. From the isotope shifts the changes of mean square charge radii multiplied by the electronic screening factor  $\beta$  were determined, using for calibration  $\beta\delta\langle r^2 \rangle_{232,230}$  given in (5). The results for  $\beta\delta\langle r^2 \rangle_{A,232}$  are plotted in Fig. 2 showing an increasing  $\beta\langle r^2 \rangle$  with increasing neutron number as expected from the liquid drop model. The results also show the normal odd-even staggering effect, i.e. the isotopes

### 3. NEUTRINO PHYSICS

KARMEN Collaboration

Karlsruhe Rutherford Medium Energy Neutrino Experiment KARMEN

G.Drexlin, H.Gemmeke, G.Giorginis, W.Grandegger, A.Grimm,

R.Gumbsheimer, J.Hesselbarth, H.Hucker, L.Husson, J.Kleinfeller

D.Mann, R.Maschuw, P.Plischke, F.Raupp, F.K.Schmidt, G.Spoehrer

P.Wild, S.Wölfle, J.Wochele, B.Zeitnitz

Kernforschungszentrum Karlsruhe, IK I and University of

Karlsruhe

E.Finck, W.Kretschmer, K.Stauber, D.Vötisch, J.Böttcher

University of Erlangen

N.E.Booth

Oxford University

J.A.Edgington, T.Gorringe

Queen Mary College, London

A.Dodd, A.G.D.Payne

Rutherford Appleton Laboratory, Chilton

KARMEN denotes a program of neutrino physics to be performed at the pulsed spallation neutron source ISIS of the Rutherford Appleton Laboratory (RAL). It is based on the beam dump neutrino source of the ISIS facility providing bursts of  $\nu_\mu$ ,  $\nu_e$  and  $\bar{\nu}_\mu$  from  $\pi^+$ -decay at rest. The main purpose of the experiment is to contribute to the questions of neutrino oscillations, neutrino nuclear excitation and neutrino electron scattering in the energy range from 5 to 50 MeV (1,2).

#### 3.1 STATUS OF THE PROJECT

##### 3.1.1 NEUTRINO AREA

The KARMEN experimental area is shown in fig.1. It consists of a 6000 t shielding bunker (inner dimensions 10x4x7 m) with 2 m thick steel walls and a 3 m thick steel roof. A 500 t rolling door opens into a 200 m<sup>2</sup> experimental hall for detector assembly and service as well as to house the electronics.

The detector has been assembled in its main mechanical components weighting about 230 tonnes. It was successfully moved into the bunker and out again on its air pad system where each of the six air cushions was loaded with 3.1 bar pressure.

Brewster's angle. The crystal introduces only very little loss causing an output power reduction of about 7%. The frequency control system has a unity-gain frequency of 1 MHz.

- (1) H. Kriz, Diplomarbeit (Universität Bonn 1980, unpublished)
- (2) D. Knauß, Diplomarbeit (Universität Karlsruhe 1987, unpublished)
- (3) F. Biraben, Opt. Comm. 29 (1979) 353
- (4) A.L. Bloom, J. Opt. Soc. Am. 64 (1974) 447
- (5) G. Holtom, O. Teschke, IEEE-QE 10 (1974) 577
- (6) W.R. Leeb, Appl. Phys. 6 (1975) 267

dispersion etalon of 1 mm thickness is used for the fine mode selection.

Because of the well developed mode competition in a traveling wave dye laser, it is possible to obtain dependable single mode operation in this way (1). Experience has shown that the power output of such lasers drops to about 50% when the normally used high dispersion etalons are inserted into the cavity. Our 1 mm etalon, though, avoids the losses due to the coating, and the tilting loss is negligible (6). This approach, however, has the disadvantage that the laser can oscillate on 3 - 4 neighboring longitudinal modes. Thus while the laser operates in only one mode at a time, the mode can change each time the laser experiences a sufficiently strong perturbation. The occurrence of such mode jumps depends mainly on the quality of the jet stream; therefore bubbles and particles in the dye solution are carefully removed since they can interrupt the laser oscillation causing mode jumps. Figure 2 is a diagram of the waiting time for the next jump; it shows that about 2/3 of all jumps had a waiting time longer than 5 minutes which is sufficient for the planned experiments since the laser will be locked to another frequency every few minutes.

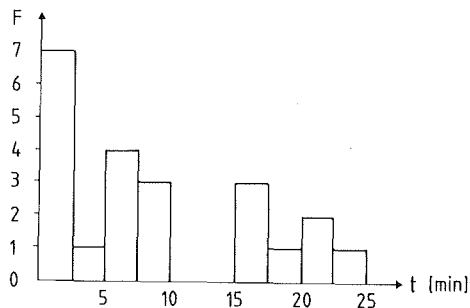


Fig. 2  
Frequency F of waiting  
times t for the next mode  
jump. The actual waiting  
times were grouped in 2.5  
minute intervals

The frequency of the laser is continuously checked by confocal interferometers and a wavemeter. If a mode jump occurs, the laser is reset to the correct frequency by an online computer. Thus the experiment is interrupted only for a few seconds.

The laser is frequency stabilized by a feedback system. The frequency error signal is split into slow and fast components which are fed to two transducers. The slow and wide frequency excursions are compensated by piezoelectric movements of mirror M4. The fast but small corrections are achieved by an intracavity electro-optic crystal made of ADP (ammonium dihydrogen phosphate) with entrance and exit windows under



thus the signal-to-noise ratio is expected to increase beyond the 50dB level reached so far.

- (1) B. Burghardt, H. Hoeffgen, G. Meisel, W. Reinert, B. Vowinkel, Precision Measurement and Fundamental Constants II, B.N. Taylor and W.D. Phillips, Eds., Natl. Bur. Stand. (U.S.), Spec. Publ. 617 (1984) p. 49
- (2) B. Burghardt, H. Hoeffgen, G. Meisel, W. Reinert, B. Vowinkel, Appl. Phys. Lett. 35 (1979) 498
- (3) H. Hoeffgen, Thesis (Universität Bonn 1982, unpublished)

## 2.8 A FREQUENCY STABILIZED cw RING DYE LASER WITH HIGH EFFICIENCY

D. Knauß, G. Meisel

For precise measurements of optical frequencies, well controlled frequency stabilized laser oscillators are required. A cw dye laser oscillator has been built for this purpose since dye lasers can be tuned to any frequency within a band of about 50 nm width. The laser cavity is of the ring type, and the number of intracavity optical elements is minimized to reduce the internal power losses (1) so that two lasers of this type can be pumped from one argon ion laser. Fig. 1 is a schematic diagram of the optical setup (2).

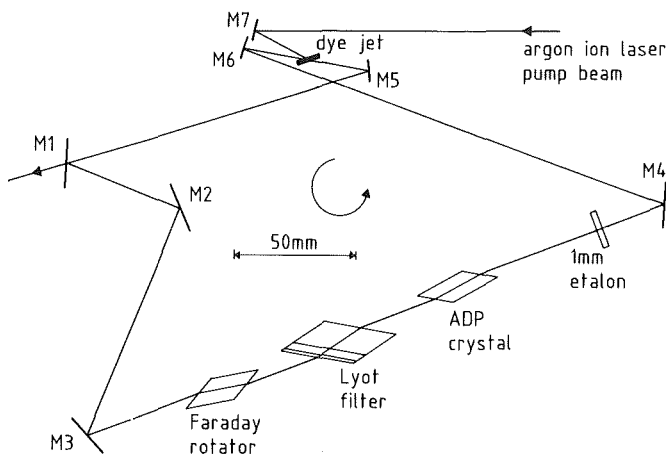


Fig. 1  
Schematic diagram of the ring dye laser. M1 is the output coupler. M2 is out-of-plane to compensate the Faraday rotation. M4 is mounted on a piezo drive. M5 to M7 have a focal length of 25 mm.

The Faraday rotator ensures one-way operation; the polarization rotation that compensates the Faraday rotation for the desired direction is achieved by rising the beam by mirrors M1, M2 and M3 above the main plane (3).

The coarse mode selection is by a three element Lyot filter (1,4,5). It is a special feature of this laser that only one uncoated low

## 2.7 SYSTEM FOR THE DETECTION AND DETERMINATION OF LASER BEAT FREQUENCIES IN THE E-BAND RANGE

M. Eichenlaub, G. Meisel

The precise measurement of optical laser frequencies requires to determine large frequency differences between two laser oscillators (1). A beat oscillation between two dye lasers is generated in an E-band diode detector of special design (2). Its key element is a fast GaAs Schottky barrier diode which shows photo effect. The output of this detector is guided to an E-band downconverter which is driven by a phase locked Gunn oscillator operating at 77.6 GHz (3). The output of the downconverter is in the 2-4 GHz band; it is amplified and fed to a microwave frequency counter. Thus optical frequency differences from 79.6 to 81.6 GHz and from 73.6 to 75.6 GHz can be processed with the present setup. Figure 1 shows the components of the full system. Its reference frequency is 10 MHz which is to be supplied by an appropriate oscillator.

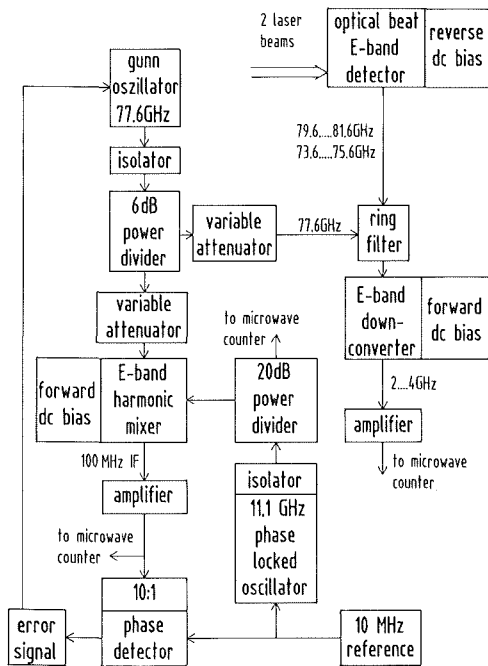


Fig. 1

Block diagram of the E-band system. The ring filter combines the two input oscillations. The E-band harmonic mixer generates the 100 MHz difference frequency between the 77.6 GHz Gunn oscillator and the 7th harmonic of the 11.1 GHz oscillator.

To test the system, a HeNe laser and a cw dye laser were tuned to a frequency difference in the receiver band and focussed onto the detector diode. The noise from the optical detector as seen at the input of the microwave counter was -70 dBm. In comparison, the beat signal was -10 to -20 dBm for a HeNe laser power of 0.5 mW and a dye laser power between 15 and 50 mW. If two dye lasers of 50 mW each are irradiated, the signal and

## 2.5 ATTEMPTS TO PRODUCE A BEAM OF RADIOACTIVE PLATINUM ATOMS

P. Pietruk, K. Bekk, A. Hanser, G. Meisel

It is interesting to study the isotope shift of neutron deficient platinum atoms since some peculiarities of the square charge radii are expected to begin between  $A = 188$  and  $187$ . To perform the respective laser spectroscopic experiments, an atomic beam of Pt atoms is needed. This requires to evaporate small amounts of Pt which are produced by  $\text{Os}(\alpha, \text{xn})\text{Pt}$  reactions. To separate the Pt from the Os after irradiation, a dry and a wet chemical process are being investigated.

The dry process works by oxidation of Os in an  $\text{O}_2$  atmosphere. It was found that Os can be converted into volatile  $\text{OsO}_4$  at  $600^\circ \text{C}$ , and that the radioactive Pt atoms remain in the ash. The next step is to transfer the ash into a graphite crucible to evaporate the Pt atoms.

The wet process (1) starts from Os powder which we dissolved in aqua regia at boiling temperature. When the solution is dried in a crucible, the Os is evaporated as  $\text{OsO}_4$  whereas the Pt stays in the remaining precipitate from which it will be vaporized.

- (1) J.D. Gile, W.M. Garrison, J.G. Hamilton, Chem. Phys. 19 (1951)  
1426

## 2.6 A TEST OF THE ACCURACY OF ATOMIC BEAM LASER SPECTROSCOPY

M. Anselment, S. Göring, G. Meisel (1)

To determine the accuracy to which hyperfine splittings can be measured using a cw dye laser with rf sideband tuning, a series of atomic beam experiments with  $^{59}\text{Co}$  was performed. One hyperfine splitting of the first excited metastable atomic state was measured and compared with the results for the same splitting from magnetic rf resonance experiments. The uncertainty with the methods applied was found to be about 0.05 to 1% of the experimental linewidth in general; it is  $\pm 20$  kHz or  $\pm 0.05\%$  of the linewidth in the present Co experiment. The hyperfine splitting constants of the  $3d^8 4p \ ^2F_{1/2}$  state were found to be  $A = 419.3(9)$  MHz,  $B = -77(17)$  MHz.

- (1) Z. Phys. D 7 (1987) 113

Table 2: A and B factors for  $^{229}\text{Th}$  for the ground state and the  $17122\text{ cm}^{-1}$  state, electromagnetic moments for  $^{229}\text{Th}$

State [ $\text{cm}^{-1}$ ]	A [MHz]	B [MHz]
0	-450(30) +)	420(150) +)
17121.623	-440(40)	420(190)

Magnetic dipole moment  $\mu(^{229}\text{Th}) = + 0.45(4) \text{ n.m. } +)$

Electric quadrupole moment  $Q(^{229}\text{Th}) = + 4.3(9) \text{ b } +)$

+ )values from ref. (6)

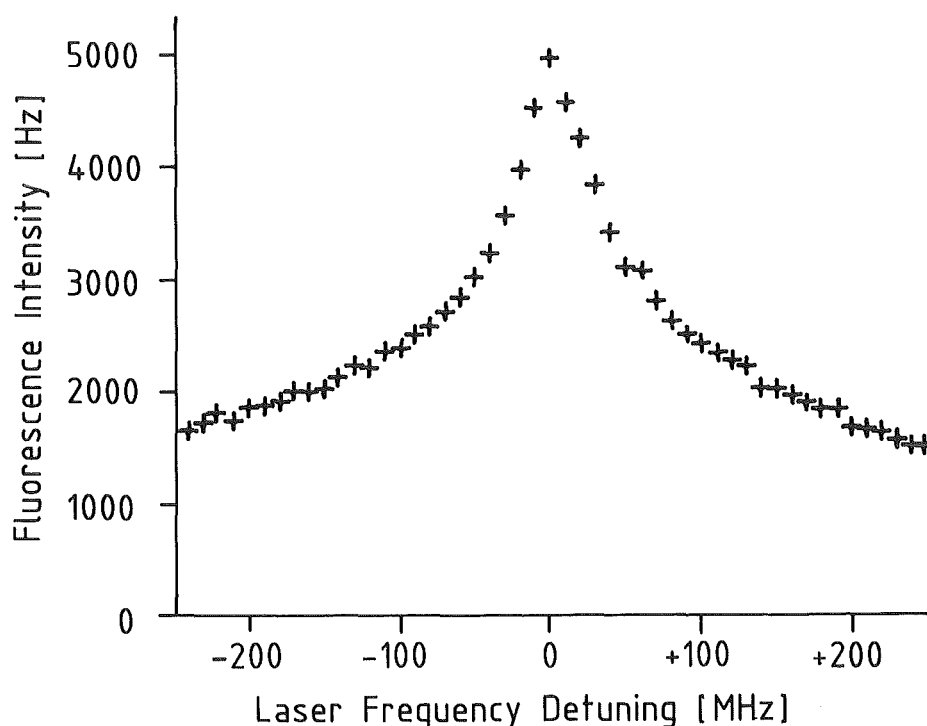


Fig. 3 Doppler reduced two-step excitation of  $^{232}\text{Th}$

- (1) E. Fischer, Z. Phys. 156 (1959) 1;  
G. Werth, Progr. At. Spectr. Part C (H.J. Beyer and  
H. Kleinpoppen Ed.) (1984) 151
  - (2) P.E. Toschek, W. Neuhauser, Phys. Bl. 36 (Nr. 7) (1980) 198
  - (3) H.G. Dehmelt, Adv. At. Mol. Phys. 5 (1969) 109
  - (4) A. Steiger, Report KfK 3820, Kernforschungszentrum Karlsruhe  
(1984)
  - (5) K. Heilig, A. Steudel, At. Data Nucl. Data Tabl. 14 (1974) 613
  - (6) S. Gerstenkorn et al., Journal de Physique 35 (1974) 483
- \* Institut für Radiochemie, Kernforschungszentrum Karlsruhe  
\*\* Optics section, Blackett Laboratory, Imperial College, London

Table 1: Isotope shifts for the Th II 583,9 nm transition and mean square charge radius changes  $\delta\langle r^2 \rangle$  multiplied by the electronic screening factor  $\beta$

A	isotope shifts $\nu_0(A) - \nu_0(232)$ [MHz]	$\beta(\langle r^2 \rangle^A - \langle r^2 \rangle^{232})$ [fm <sup>2</sup> ]
230	15361(32)	-0.205(33) +)
229	25009(93)	-0.333(54)
228	30953(81)	-0.412(67)
227	38090(210)	-0.509(82)

+) from ref. (5)

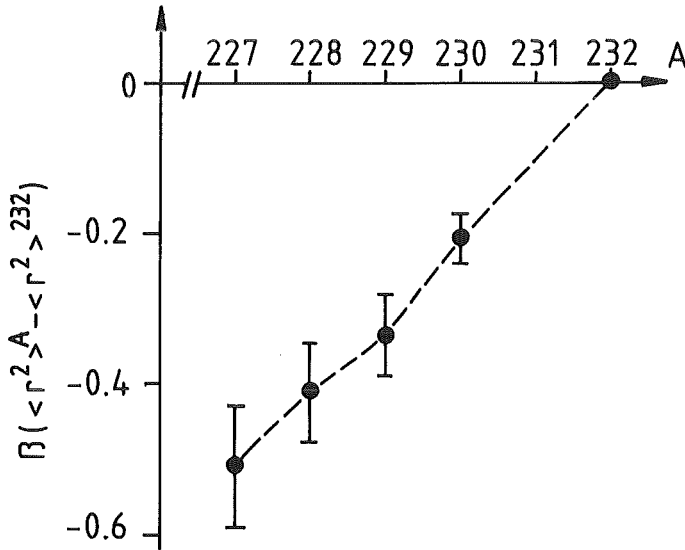


Fig. 2

Plot of the mean square charge radius changes multiplied by the electronic screening factor  $\beta$  against mass number A. The error bars are due to uncertainties in calibration

with odd neutron numbers are somewhat smaller than the average of the neighbouring even isotopes. For the odd isotope <sup>229</sup>Th we have determined the A and B factors of the upper level. The results are given in Table 2. As can be seen from Fig. 1 and Table 2, the hyperfine splitting is small compared to the Doppler broadening of the transition, so that the hyperfine interaction constants cannot be determined accurately.

To improve the resolution, we have tested the Doppler reduced two-step excitation of Th II. A spectrum of <sup>232</sup>Th is shown in Fig. 3. The thorium ions are excited by two counter propagating laser beams exciting the transitions Th II 0-17122 cm<sup>-1</sup> and 17122-34544 cm<sup>-1</sup>, respectively. The excitation is detected by the fluorescence light at 332.6 nm, 358.9 nm, and 367.3 nm.

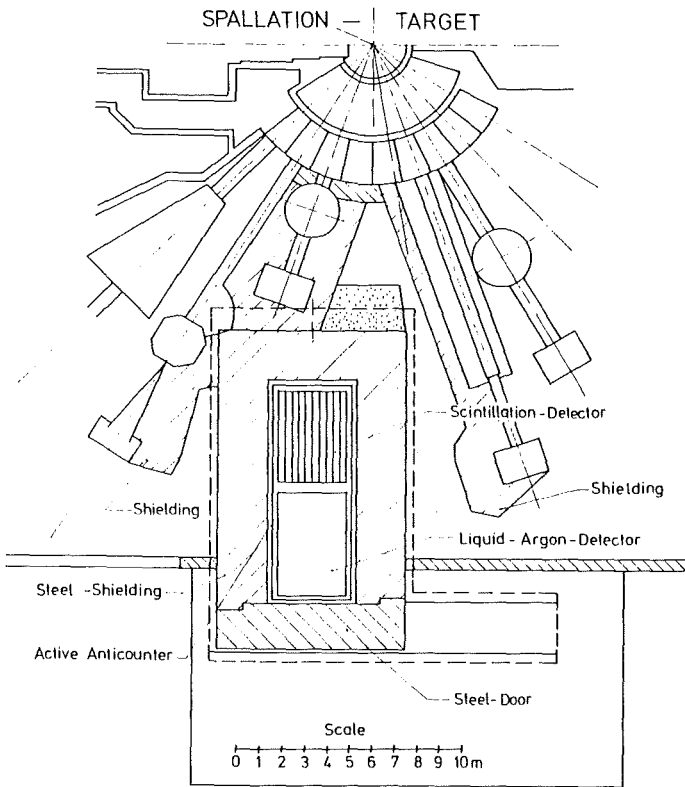


Fig.1: The KARMEN experimental area at ISIS.

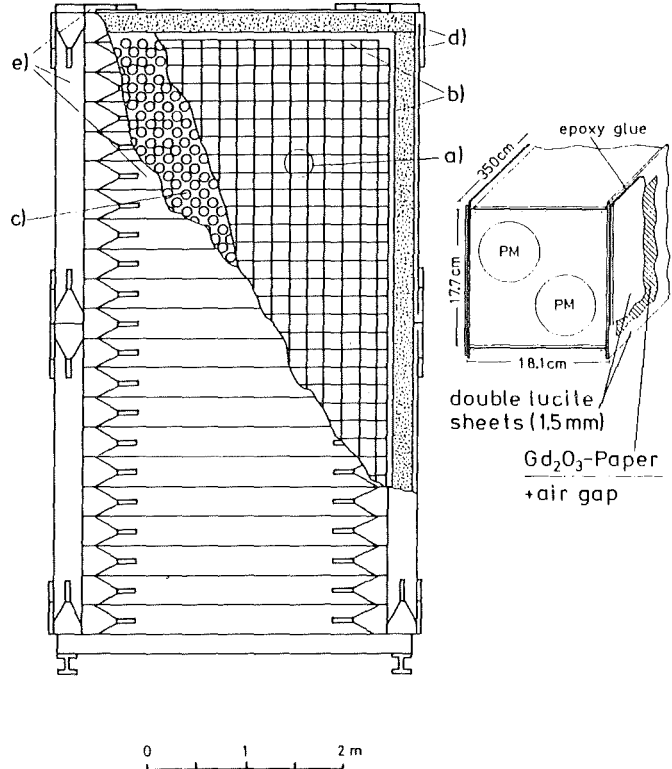


Fig.2: The KARMEN neutrino detector. a) 512 central modules 17.7x18.1x350cm, b) inner active shield, 96 half width modules, c) 2240 PM 3", VALVO XP3462, d) passive inner shield, 20 cm steel, e) outer active shield, 3 cm NE110 plastic scintillator.

### 3.2 THE SCINTILLATOR CALORIMETER KARMEN

The KARMEN detector is a 56 t liquid scintillation calorimeter dedicated to detect neutrino reactions with  $^1\text{H}$ - and  $^{12}\text{C}$ -nuclei with high precision. A schematic view of the detector is shown in fig.2. The mineral oil based scintillator PPP (PPP-scintillator: 75% Paraffin, 25% Pseudocumene, 2g/l PMP-fluor) is contained in one single tank with dimensions 3.2x3.5x6 m. A totally reflecting lucite structure divides the central detector into 512 optically isolated modules (17.7x18.1x350 cm) each viewed by two 3" photomultipliers

from either end. A half width layer of modules serves as inner anticounter to define a "contained" event. A passive inner shield of 20 cm of steel is followed by an active outer anticounter of 3 cm NE110 plastic scintillator.

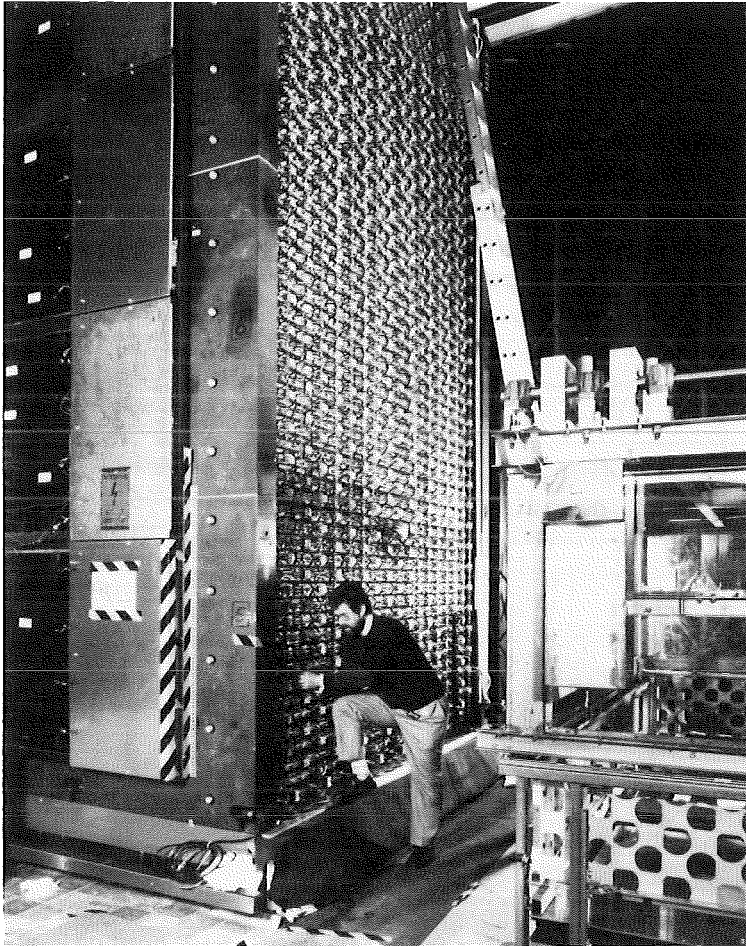


Fig.3: Current status of detector assembly.

Fig.3 shows the current status of detector assembly. 200 phototubes after being tested and matched to pairs (3) have been attached to the detector head walls. Each pair of tubes is equipped with an optical fibre for calibration and monitoring of the detector modules. The fibres are fed by four light splitters where pulses of ultraviolet light from a N<sub>2</sub>-Laser are shifted into "blue" scintillation light (see fig.4).

The side walls of the detector (see left side of fig.3) have already been covered with anticounter modules providing the first signals from cosmic rays as well as from ISIS correlated background radiation.

Currently the delicate optical structure consisting of 1800 3 mm thick lucite double sheets is assembled. Nine submodules of 3.2x3.5 m size will sub

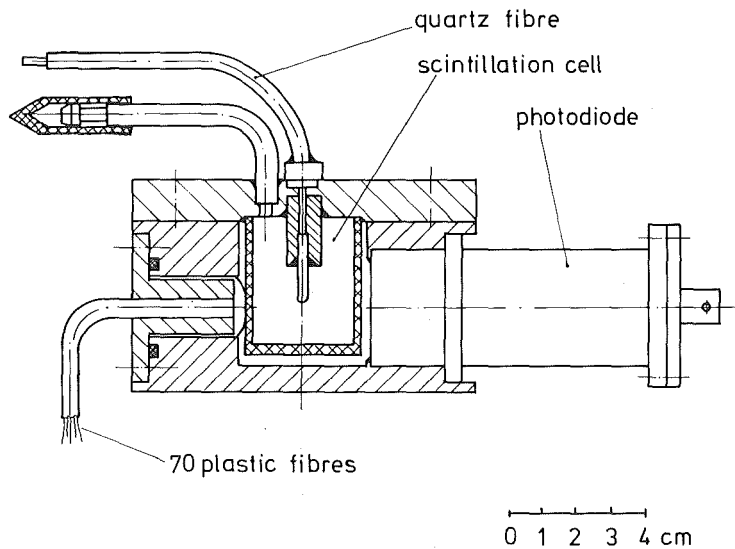


Fig.4: Light splitter for UV N<sub>2</sub>-Laser pulses.

sequently be inserted into the detector vessel after carefully being mounted and adjusted outside the calorimeter. Each subunit is picked up by a large bell shaped insertion structure (see bottom right of fig.3) to be located on top of the detector vessel flange. Hanging from chains the optical structure is then lowered into the liquid, the top rows of photomultiplier holes allowing visual inspection of the tightness of the optical segmentation.

Assembly of the bottom submodule has been completed and insertion into the filled detector vessel is just about to happen. Further installation of the optical structure is going on during the shut down period of ISIS before first neutrino correlated events can be looked for in May 1988.



### 3.3 ELECTRONICS AND DATA HANDLING

The electronics trailer to supply and handle the overall 1500 data channels has been shipped to RAL and installed at KARMEN. Data from the outer anti-counter modules are used for debugging the different hardware modules as well as the data acquisition programs.

The detector is self triggering by a coincidence between the downstream and upstream end of any module with deposited energy above 0.7 MeV. Within an "event time" of 70 nsec, 186 front end boards are collecting the analog information of deposited energy and time for four detector modules each. A "valid event" decision is made by a timing logic and a programmable trigger processor within 400 nsec before this information is multiplexed into fast converting ADC's with 8 word deep buffer. After about 10  $\mu$ sec the same detector module is ready for analysis again which is of great importance with respect to the delayed coincidence signatures of neutrino induced reactions. Absolute timing is recorded in a multi-hit TDC with 16 msec range. Readout of all data is done during the last 4 msec of the 20 msec beam period.

A software controlled event pattern unit can test any electronic channel individually. A pulsed UV N<sub>2</sub>-Laser system is calibrating and monitoring all modules including the anticounter bars simultaneously.

All electronic modules - 186 frontend boards, 12 CAMAC ADC boards, the timing logic and trigger processor, all driver and interface boards as well as numerous standard NIM and CAMAC devices do exist and are currently under test. The data acquisition system consisting of a front end processor (ACC 2180 auxiliary crate controller with DEC-J-11 processor) backed by a LSI-11/73 system and linked to a VAX-11/750 computer has been described in last years annual report. Programming of the ACC has been completed. Further effort has concentrated on programming the LSI host computer particularly the handshake operation between ACC and host for experiment control, data readout and appropriate display of data. For on-line evaluation on the VAX-11/750 computer allowing complex operation and display of data, a software package LISA (4) is adapted to our experiment.

### 3.4 PROTOTYPE RESULTS

With the operation of the 7000 l Prototype III detector we have completed our prototype detector program comprising an earlier 200 l and 1000 l detector. Prototype III was identical to the KARMEN detector in all relevant dimensions and components including phototubes and scintillator. The prototype results can be summarized as follows:

- i. The position dependent light output of a detector module can be reproduced by an appropriate Monte-Carlo light transport program.
- ii. The summed light output from both ends of the 350 cm long module is fairly constant over a central range of 250 cm yielding about 75 photoelectrons per 1 MeV absorbed energy.
- iii. The light output is a linear function of the deposited energy measured by different muon track lengths in one module.
- iv. The energy resolution at the centre of a module was determined to be  $\sigma(E)/E = (11.5 \pm 0.6)\%/\sqrt{E(\text{MeV})}$ , measured with cosmic muons as well as with the UV-Laser system.
- v. The time difference for the scintillation light to arrive at the ends of a module is a linear function of the location of light emission; the time resolution of  $\Delta t = 0.8 \pm 0.1$  nsec represents a spatial resolution of  $\Delta x = 7 \pm 1$  cm along the module axis.
- vi. From a mock up experiment with the 1000 l detector using a tagged neutron source the KARMEN efficiency for the reaction  $\bar{\nu}_e + p \rightarrow n + e^+$  could be deduced to be 30% (5).

- (1) B.Zeitnitz, Progress in Particle and Nuclear Physics 13 (1985) 445
- (2) R.Maschuw, B.Zeitnitz, KfK 3362 (1982)
- (3) H.Gemmeke, A.Grimm, J.A.Edgington, J.Kleinfeller, R.Maschuw, B.Zeitnitz; to be published in IEEE Trans.of Nucl. Sci. NS 35, Vol.1 (1987)
- (4) LISA general purpose data analysis program adapted from WA80 CERN experiment
- (5) H.Gemmeke, W.Grandegger, R.Maschuw, P.Plischke, B.Zeitnitz; to be published in IEEE Trans. of Nucl. Sci. NS 35, Vol.1 (1987)

4. HIGH ENERGY PHYSICS

CELLO Collaboration

H.-J.Behrend, J.Bürger, L.Criegee, J.B.Dainton, H.Fenner, J.H.Field,  
G.Franke, J.Fuster, Y.Holler, J.Meyer, V.Schröder, H.Sindt, U.Timm,  
G.G.Winter, W.Zimmermann

Deutsches Elektronen-Synchrotron, DESY, Hamburg, Germany

P.J.Bussey, C.Buttar, A.J.Campbell, D.Hendry, G.McCurrach, J.M.Scarr,  
I.O.Skillicorn, K.M.Smith

University of Glasgow, United Kingdom

J.Ahme, V.Blobel, M.Feindt, J.Harjes, M.Poppe, H.Spitzer,

II. Institut für Experimentalphysik, Universität Hamburg, Germany

W.-D.Apel, A.Böhrer, J.Engler, D.C.Fries, K.Gamerdinger, J.Hansmeyer,  
J.Jung, J.Knapp, H.Küster, P.Mayer, H.Müller, K.H.Ranitzsch,  
H.Schneider, J.Wolf

Kernforschungszentrum Karlsruhe and Universität Karlsruhe, Germany

W.de Boer, G.Buschhorn, G.Grindhammer, B.Gunderson, Ch.Kiesling,  
R.Kotthaus, H.Kroha, D.Lüers, H.Oberlack, B.Sack, P.Schacht,  
G.Shooshtari, W.Wiedenmann

Max-Planck-Institut für Physik und Astrophysik, München, Germany

A.Cordier, M.Davier, D.Fournier, M.Gaillard, J.F.Grivaz, J.Haissinski,  
P.Janot, V.Journé, F.Le Diberder, E.Ros, A.Spadafora, J.-J.Veillet

Laboratoire de l'Accélérateur Linéaire, Orsay, France

B.Fatah, R.George, M.Goldberg, O.Hamon, F.Kapusta, F.Kovacs,  
L.Poggioli, M.Rivoal

Laboratoire de Physique Nucléaire et Hautes Energies, Université de  
Paris, France

G.D'Agostini, F.Ferrarotto, M.Gasparo, B.Stella

University of Rome, Italy

R.Aleksan, G.Cozzika, Y.Ducros, Y.Lavagne, F.Ould Saada, J.Pamela,  
F.Pierre, J.Zacek

Centre d'Etudes Nucléaires, Saclay, France

G.Alexander, G.Bella, Y.Gnat, J.Grunhaus, A.Levy

Tel Aviv University, Israel

#### 4.1 HARDWARE ACTIVITIES

##### 4.1.1 DEVELOPMENT AND TESTS OF TRIGGERCOUNTERS FOR THE ELECTROMAGNETIC CALORIMETER OF THE DELPHI DETECTOR (CERN/LEP)

For the generation of a prompt neutral trigger in the electro-magnetic calorimeter (HPC) of the DELPHI detector a plane of scintillators (820×166×8mm) will be installed in each of the 144 HPC modules.

The scintillator signals are to be read out using wavelength-shifting optical fibers (fluorescent Polystyrene fibers of 1 mm diameter, doped with the wave length shifting material K27 which emits in the 'green' spectral region). The green fibers were attached - alternatively - either to one or to both long small sides of the scintillator plate. Optical clear fibers (Polyacryl), coupled to the green fibers, have been used for the transport of the light signal to a photomultiplier.

Prototypes of those counters have been developed and tested. A counter with 4 green fibers on both sides of the scintillator appeared to be suited best for our purpose. The optical coupling between the green and clear fibers consists of a Lucite blocklet with 4 tubular holes, in which the green and clear fibers are joined by glueing.

The performance of the counters have been tested with gammas and charged particles from various sources. We used as well cosmic radiation and a gamma source ( $^{22}\text{Na}$ ) as electrons and pions from accelerators (KfK, DESY and CERN).

Analyzing the pulse-height distributions obtained in the test measurements the average yield of photoelectrons per minimum ionizing particle was evaluated. As a test function we choose a Poisson distribution folded with a Gaussian and a noise-background term. From a great number of measurements with different counters we concluded that minimum ionizing particles yield about  $4 \pm 1$  photoelectrons in a set-up where the 8 green fibers were coupled to 8 Polyacryl fibers of 10 m length. (The errors are estimated, since the fit results are subject to systematic errors due to the oversimplifying assumption concerning the test function.) Fig.1 a,b show the pulse-height distribution due to cosmic and pions of 15 GeV.

Tests have also been performed in a high energy electron shower. The intended location of the trigger counter in the HPC detector was simulated by measuring the counter in an electron beam behind  $5 X_0$  (radiation length) of lead (CERN). The pulse-height spectra for 6 and 15 GeV electrons (with some visible pion content in the electron beam) are shown in Fig.2 a,b.

The trigger efficiency for electrons (gammas) above 3 GeV appears to be satisfactory. The trigger efficiency for lower energy electrons depending on the general noise background in the HPC modules and on the trigger logic chosen, will be studied.

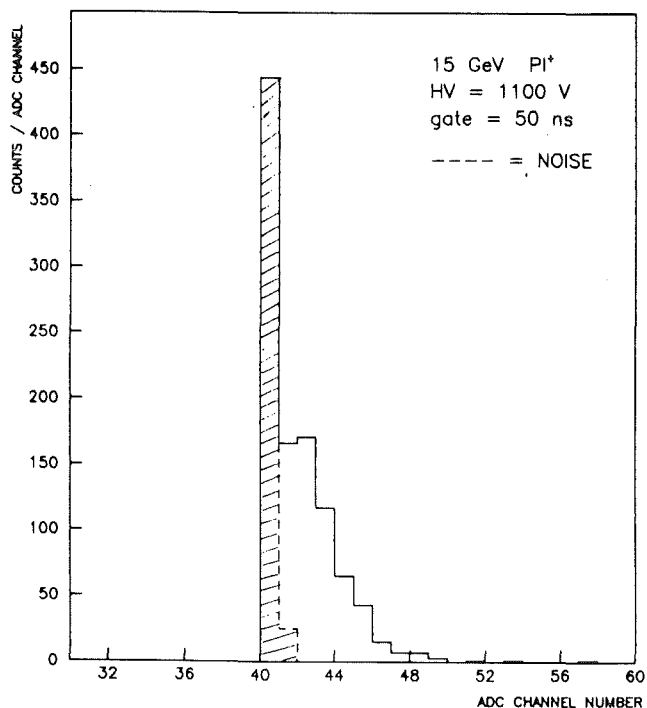


Fig.1a: Energy deposition (pulse height distribution) of 15 GeV pions in a fiber-read scintillation counter (8mm thickness, 2x4 fibers)

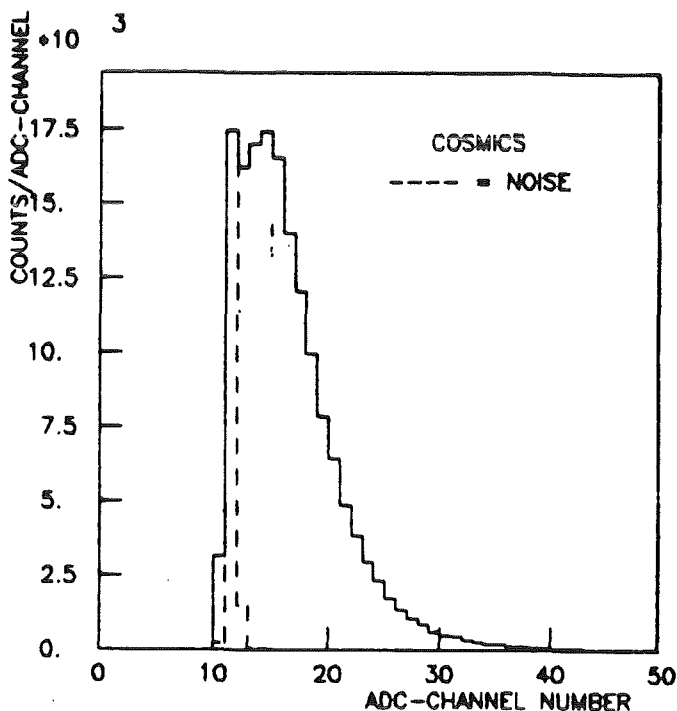


Fig.1b: Energy depositon (pulse height distribution) of cosmic radiation in a fiber-read scintillation counter.

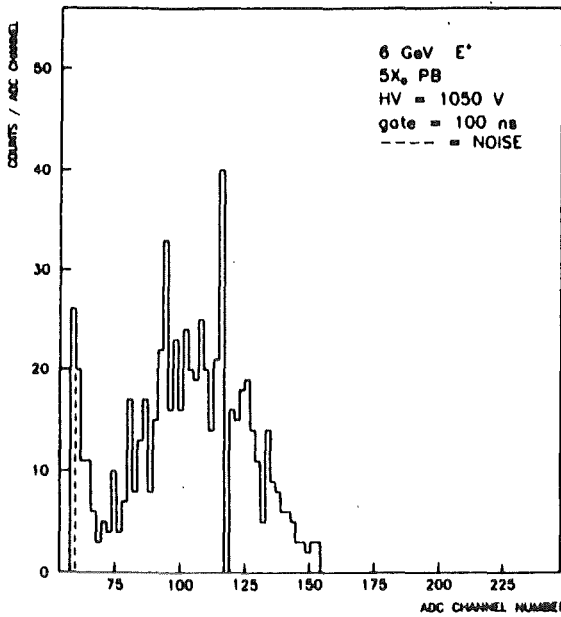


Fig.2a: Energy deposition (pulse height distribution) of showering electrons of 6 GeV after 5 X<sub>0</sub> in a fiber-read scintillation counter

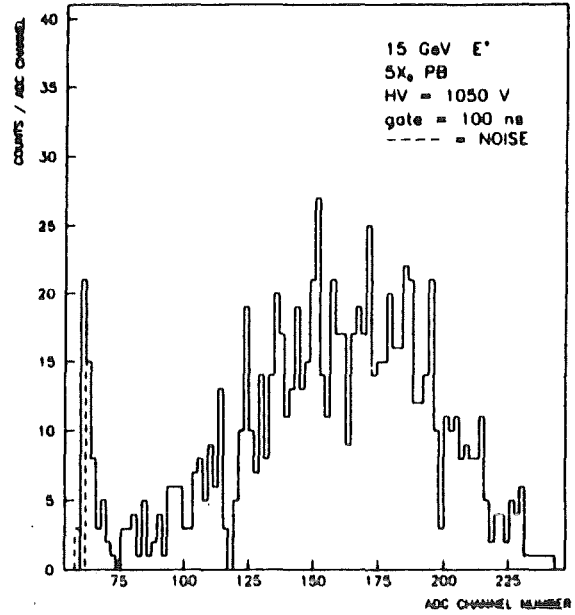


Fig.2b: Energy deposition (pulse height distribution) of showering electrons of 15 GeV after 5 X<sub>0</sub> in a fiber-read scintillation counter.

## 4.2 ANALYSIS OF HADRONIC FINAL STATES AND TEST OF QCD

### 4.2.1 MODEL INDEPENDENT LIMITS OF THE QCD SCALE PARAMETER $\Lambda_{MS}$ FROM $e^+e^-$ ANNIHILATION DATA IN THE ENERGY RANGE FROM 14 TO 46 GeV

It is well known, that measurements of the strong coupling constant  $\alpha_s$  depend strongly on the fragmentation model if a Monte-Carlo simulation of the hadronic final states is used in the analysis (1,2).

Therefore it was suggested (3,4) to compare the data directly to jet measures, which are insensitive to infrared and collinear divergences of the QCD matrix element and therefore calculable in perturbative QCD. In this work four quantities, calculated up to 2nd order in  $\alpha_s$  have been studied:

1-T The thrust is defined by  $T = \max \frac{\sum |p_{1i}|}{\sum |p_i|}$

$M_H^2/s$  The heavy ( $M_H$ ) and light ( $M_L$ ) jet mass (4,5) of an event are calculated by dividing it in two hemispheres, such that  $M_H^2 + M_L^2$  is minimal.

$(M_H^2 - M_L^2)/s$ . The difference of the jet masses is of special interest, since the 2nd order corrections are small.

$\int AEEC(X)dX$  The asymmetry of the energy-energy correlations (6) is integrated from  $X = 30^\circ$  to  $82.3^\circ$ .

To describe the data, it is necessary to add a fragmentation term to the QCD calculation. Four different fragmentation models have been studied, the Ali (7) and Hoyer (8) model with independent jet fragmentation, the LUND string and the LUND parton shower model (9,10). In all of them the fragmentation term falls approximately like  $C/\sqrt{s}$  for  $1-T$ ,  $M_H^2/s$  and  $\int AEEC(X)dX$  and is constant for  $(M_H^2-M_F^2)/s$ . It is negative for  $\int AEEC(X)dX$  and  $(M_H^2-M_F^2)/s$  positive for the other two.

Knowing the sign, it is possible to derive fragmentation independent limits for  $\Lambda_{\overline{MS}}$ , i.e. lower/upper limits in the case of negative/positive sign.

The energy dependence of the QCD terms is due to the running coupling constant

$$\sigma_s(Q^2) = \frac{12\pi}{28 \ln \frac{Q^2}{\Lambda^2} + 15.1 \ln \ln \frac{Q^2}{\Lambda^2}}$$

and is different from that of the fragmentation term. With data at different energies it can therefore be tried to separate QCD from fragmentation.

The data sample, taken with the CELLO detector (11) covers the energy range from 14 GeV to 46.8 GeV. Multihadronic events are selected by standard cuts and the event axis has to be inside the fiducial volume. The measured distributions have to be corrected for the effects of initial state radiation, detector acceptance, detector resolution and event selection. This is done with an unfolding procedure, by solving the convolution integral:

$$g(y) = \int A(y,x)f(x)dx$$

$g(y)$  measured distribution  
 $f(x)$  corrected distribution  
 $A(y,x)$  resolution function.

The distribution used here are discrete histograms, the integral equation transforms in this case to

$$g_i = \sum_j A_{ji} f_j$$

A very detailed detector simulation is used to determine the resolution matrix  $A_{ji}$  with a minimization procedure. To obtain stable solutions (no oscillations) two conditions have to be fulfilled:

- (1)  $f_i \geq 0$
- (2) limited curvature of  $f(x)$ .

The corrected distribution should not depend on the fragmentation model, which was used to produce the Monte-Carlo events for the detector simulation. Due to the definition of the energy-energy correlations, it is difficult to apply this unfolding procedure. Therefore binwise correction factors are used in this case.

Results:

The solution of the pure QCD terms for the corrected data gives limits on  $\Lambda_{\overline{MS}}$  depending on the sign of the fragmentation term.

Figure 1 shows these limits for the variables  $M_H^2/s$  and  $A_{EEC} = \int AEEC(x)dX$ . At the 95% confidence level one finds:

$$\Lambda_{\overline{MS}} < 450 \text{ MeV}, \alpha_s(35 \text{ GeV}) < 0.162$$

$$\Lambda_{\overline{MS}} > 55 \text{ MeV}, \alpha_s(35 \text{ GeV}) > 0.112$$

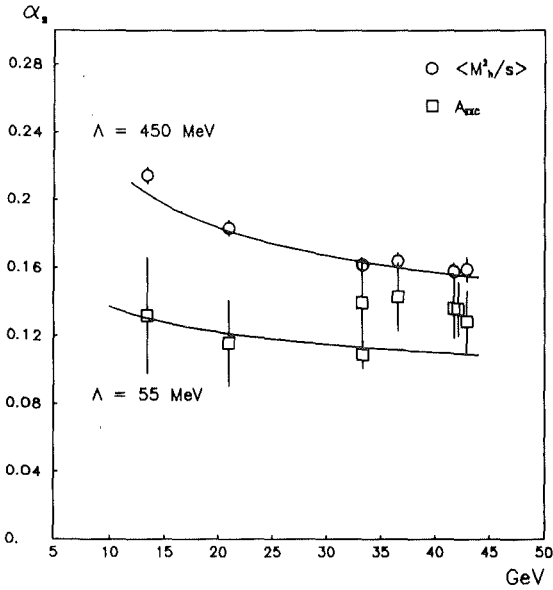


Fig.1: Model independent limits of the QCD scale parameter  $\Lambda_{\overline{MS}}$ . The fit of  $\alpha_s$  to  $A_{EEC}$  as function of energy provides the lower limit, to  $\langle M_H^2/s \rangle$  the upper limit.

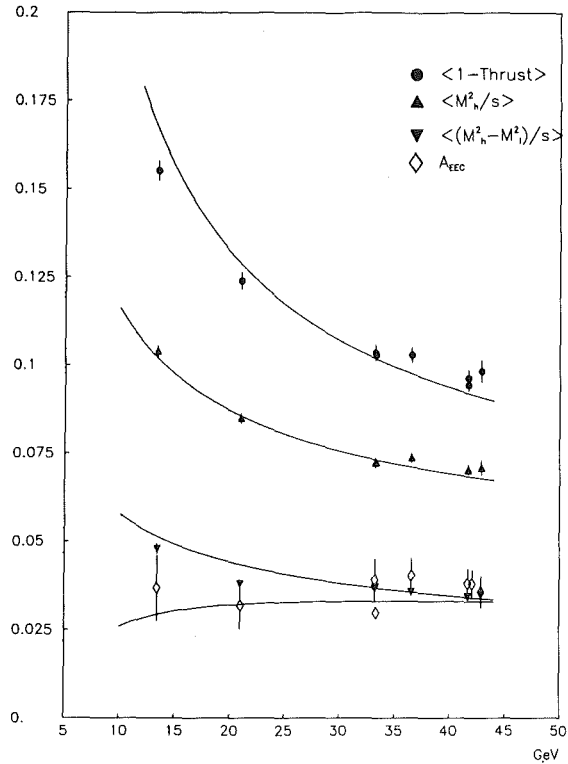


Fig.2: Simultaneous fit of  $\alpha_s$  as a function of energy to four experimental variables. Fragmentation effects have been parametrized as described in the text.



The simultaneous fit of the four parameters of the parametrization of the fragmentation effects and  $\Lambda_{\overline{MS}}$  as free parameter of the QCD terms is shown in Figure 2. The result is:

$$\Lambda_{\overline{MS}} = 310 \pm 20 \text{ stat. } \begin{matrix} + 90 \\ - 60 \end{matrix} \text{ syst. [MeV]}$$

corresponding to  $\alpha_s$  at 35 GeV:

$$\alpha_s = 0.15 \pm 0.002 \text{ stat. } \begin{matrix} + 0.008 \\ - 0.006 \end{matrix} \text{ syst.}$$

The large systematical error is a result of the only coarse agreement of the fragmentation effects and the simple parametrization of the energy dependence.

- (1) CELLO Collab., Nucl.Phys. B218, 269 (1983)
- (2) CELLO Collab., Phys.Lett. 138B, 311 (1984)
- (3) PLUTO-Kollaboration; Ch.Berger et al., Z.Phys. C12, 297 (1981)
- (4) R.D.Field, Proc.Int. Symposium on Lepton and Photon Interactions at High Energies, Cornell, (1983)
- (5) L.Clavelli, Phys.Lett 85B, 111 (1979)
- (6) A.Ali und F.Barreiro, Nucl.Phys. B236, 269 (1984)
- (7) A.Ali et al., Phys.Lett. 93B, 349 (1979)
- (8) P:Hoyer et al., Nucl.Phys. B161, 349 (1979)
- (9) T:Sjöstrand, Computer Phys.Comm. 43, 367 (1987)
- (10) G.Marchesini und B.R.Webber, Nucl.Phys. B238, 1 (1984)
- (11) CELLO Collab., Phys. Scripta 23, 610 (1981).

#### 4.2.2 DETERMINATION OF $\alpha_S$ WITH ENERGY CORRELATIONS

The process  $e^+e^- \rightarrow$  hadrons was analyzed in the framework of the LUND 5.2 Monte Carlo program. The partons (quarks and gluons) are produced according to  $O(\alpha_S^2)$  and fragmented with the string model.

The QCD cross sections are divergent for small invariant masses between partons, and one has to introduce a cut-off to separate the finite from the divergent region. We used as cut-off  $Y = (p_i + p_j)^2/s$ , the scaled invariant mass between any two partons.

There are two calculations of the 3 jet cross section in  $O(\alpha_S^2)$  the so called ERT (1,2) and GKS (3,4), ERT gives a higher number of 3 jets. ERT is exact, whereas GKS neglects terms of  $O(y)$ . This difference may lead to systematic errors of 5 to 15% in the determination of  $\alpha_S$ , (5,6,7) depending on the variable used in the analysis. To look into this problem for the case of the Y-cut we determined  $\alpha_S$  with the energy-energy correlation asymmetry (AEEC) (9) and the planar triple energy correlation (PTEC) (10). Lund 5.2 (8) uses GKS in the standard version. The ERT calculation had been implemented by F.Csikor (11), using a parametrization of (12).

The energy correlation function EEC (9) is defined as:

$$F(\chi) = \frac{d\Sigma}{d\chi} = \frac{1}{N\Delta\chi} \sum_{k=1}^N \sum_{i,j} \frac{E_{k1} E_{kj}}{E_{k,tot}^2}$$

where the first sum runs over all events and the second sum over all possible pairs of particles in a given event, which have a relative angle in the range  $(\chi \rightarrow \chi/2, \chi + \Delta\chi/2)$ . Of particular interest is the asymmetry (AEEC),

$$\frac{d\Sigma_A}{d\chi} = F(\pi - \chi) - F(\chi)$$

which is sensitive to hard gluon radiation, whereas fragmentation effects from two jet events cancel, if one stays outside the small  $p_{\perp}$  region of jets, i.e.  $\chi > \delta$ , with  $\delta \approx 30^\circ$  at our energies.

The AEEC is not independent from the infrared cut-off.  $Y_{min}$ , as shown in Table 1 for Monte Carlo data.

The data prefers a very low value of  $Y_{min} \approx 0.01$ . Figure 1 shows several cross sections as a function of  $Y_{min}$ . ERT is a factor of 2.5 higher than GKS at  $Y = 0.02$ , decreasing to 1.4 at  $Y = 0.05$ . The total 3 jet cross section is changed by 16% and 8% respectively.

Surprisingly there is only a very small difference for the AEEC (Fig.2). This is, because GKS and ERT mainly differ in the soft gluons, which do not contribute to the AEEC in the considered angular region.

$\int AEEC$	$(\delta = 39.6^0) \quad * 10^{-3}$			
$Y_{min}$	total	2jet	3 jet	4 jet
0.0108	19.2	-0.03	9.6	9.6
0.015	19.7	-0.03	13.0	6.7
0.02	19.5	-0.04	15.1	4.4
0.03	21.0	-0.06	18.6	2.4
0.04	22.0	-0.09	20.7	1.4

Table 1

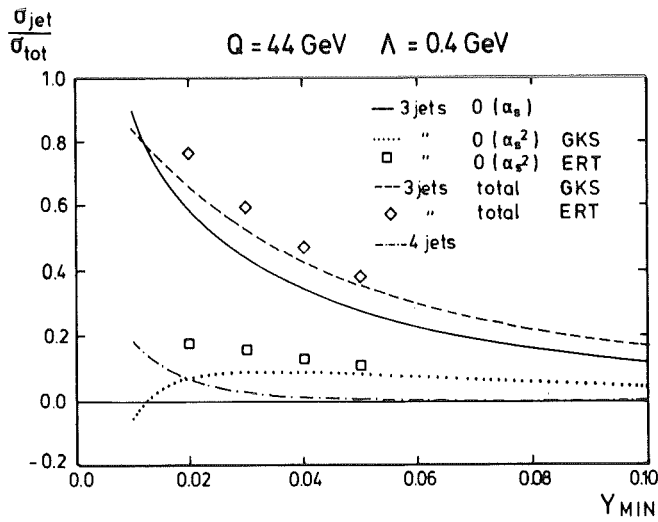


Fig.1: Cross sections for  $e^+e^- \rightarrow$  jets as a function of the infrared cutoff  $Y_{min}$ . The Lund Monte Carlo has been used at  $Q = 44$  GeV and  $\Lambda_{\overline{MS}} = 0.4$  GeV with two different parametrizations of the 3 jet cross section in  $O(\alpha_s^2)$ .

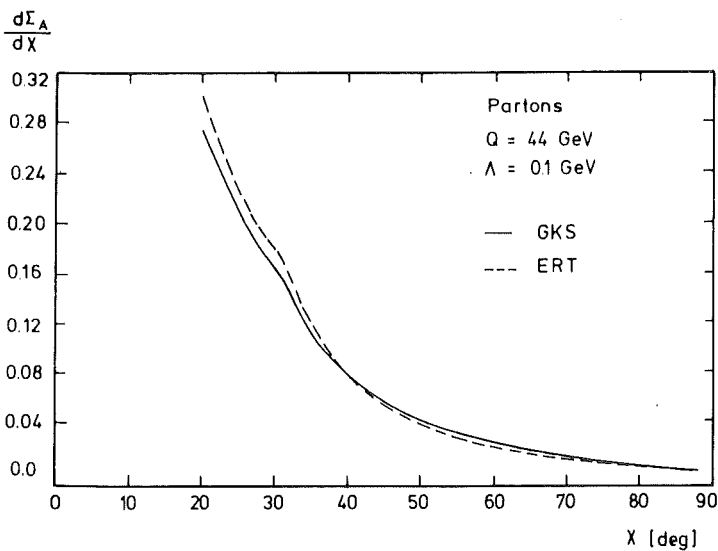


Fig.2: Energy correlation asymmetry (AEEC) for partons,  $Q=44$  GeV,  $\Lambda_{\overline{MS}} = 0.1$  GeV and  $Y_{min} = 0.02$ .

Triple energy correlation

The next step in the hierarchy is the triple energy correlation (TEC) (10.)

$$\frac{d^3\sigma}{d\chi_1 d\chi_2 d\chi_e} = \frac{1}{N\Delta\chi^3} \sum_{k=1}^N \sum_{i,j,l} \frac{E_{ki}E_{kj}E_{kl}}{E_{tot}^3}$$

with the same terminology as for the EEC.  $\chi_1, \chi_2, \chi_3$  are the angles between the three particles  $i,j,l$  in a given event  $k$ . The TEC has similar properties to the EEC, except that one now has triplets of particles. For simplicity one defines the planar triple energy correlation (PTEC) by integrating over the angle  $\chi_3$ , requiring that the triplets are planar, i.e.  $\chi_1 - \chi_2 - \chi_3 > 2\pi - \phi$ . The finite experimental resolution is taken into account by  $\phi = 0.1$  rad.

Table 2

$\int$ PTEC	$(\delta = 30^\circ)$				$* 10^{-3}$
$Y_{min}$	total	2 jet	3 jet	4 jet	
0.0108	11.17	0.014	6.70	4.40	
0.015	11.36	0.112	8.20	3.04	
0.02	11.18	0.193	9.02	1.96	
0.03	11.42	0.304	10.15	0.97	
0.04	11.45	0.380	10.58	0.49	

The central part, defined by  $\delta < \chi_1, \chi_2 < \pi - \delta, \chi_1 + \chi_2 > \pi + \delta$ , is expected not to be sensitive to 2 jets and fragmentation, but proportional to  $\alpha_s$  or the number of 3 jets. Table 2 shows the values of the integral as a function of  $\delta$  and  $Y_{min}$ . The PTEC is much more infrared stable and dominated by the 3 jets. 4 jets contribute less and 2 jets more than for the AEEC.

Determination of  $\alpha_s$

The AEEC and PTEC were calculated with multihadronic events, taken with CELLO at  $\sqrt{s} = 35, 38$  and  $44$  GeV. The measured distributions are corrected for detector effects and initial state radiation.

To determine  $\alpha_s$  we calculated the AEEC from the corrected EEC function and fitted the Monte Carlo inside the region  $\delta = 38^\circ$  to  $90^\circ$ . The fitted curves are in good agreement with the data for  $Q = 35$  GeV (Fig. 3). The results are summarized in table 3. As expected the difference between GKS and ERT is negligible.

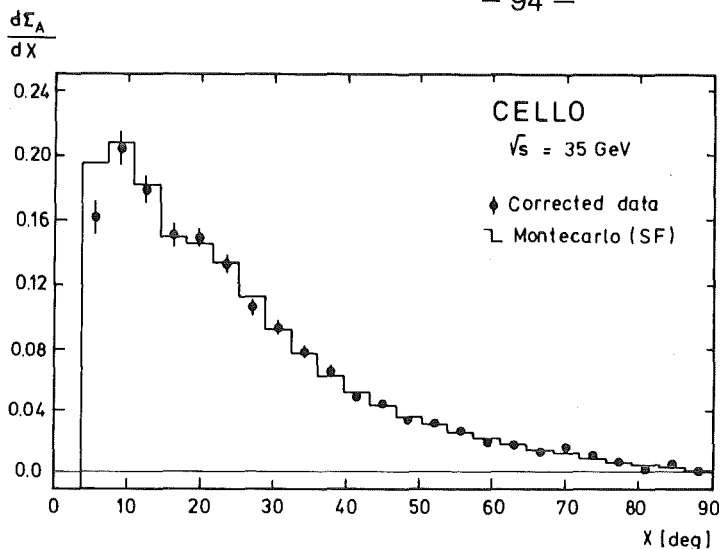


Fig.3: Asymmetry of the energy energy correlation (AEEC) for data and Monte Carlo. The data had been corrected for detector effects and initial state radiation. The Monte Carlo represents the fit of  $\alpha_s$  in the region  $\chi > \delta = 38^\circ$ .

The PTEC results are somewhat lower than the AEEC results, although still inside the systematical error. The reason may be the difference in infrared sensitivity or the contribution of 4 jets. The three data samples can be used for a combined fit to  $\Lambda_{\overline{MS}}$ .

$$\Lambda_{\overline{MS}} = 0.41 \pm 0.04^{+0.08}_{-0.09} \text{ GeV (AEEC)}$$

$$\Lambda_{\overline{MS}} = 0.32 \pm 0.03^{+0.06}_{-0.05} \text{ GeV (PTEC)}$$

with statistical and systematical errors.

$\alpha_s$  fit results for AEEC

Monte Carlo	35 GeV	38 GeV	44 GeV
GKS	0.157±0.004±0.005	0.163±0.009±0.008	0.152±0.006±0.008
ERT	0.157±0.004±0.005	0.162±0.009±0.008	0.154±0.006±0.010

$\alpha_s$  fit results for PTEC

GKS	0.151±0.003±0.003	0.148±0.008±0.006	0.145±0.004±0.006
ERT	0.148±0.003±0.003	0.146±0.008±0.006	0.143±0.004±0.006

Table 3

- (1) R.K.Ellis, D.A.Ross, A.E.Terrano, Nucl.Phys. B178, 421 (1981)
- (2) J.A.M.Vermaseren, K.J.F.Gaemers, S.J.Oldham, Nucl.Phys. B187, 301 (1981)
- (3) F.Fabricius, G.Kramer, G.Schierholz, I.Schmitt, Z.Phys. C11, 315 (1982)
- (4) F.Gutbrod, G.Kramer, G.Schierholz, Z.Phys. C21, 235 (1984)

- (5) B.Adeva et al., Phys.Rep. 109, 133 (1984) and Phys.Rev.Lett. 54, 1750 (1985)
- (6) M.Althoff et al., Z.Phys. C26, 157 (1984)
- (7) T.D.Gottschalk, M.P.Shatz, Phys.Lett. 150B, 451 (1985)
- (8) B.Andersson et al., Phys.Rep. 97, 31 (1983)  
T.Sjöstrand, Computer Phys.Comm. 27, 243 (1982)  
T.Sjöstrand, Computer Phys.Comm. 28, 229 (1983)
- (9) C.L.Basham, L.S.Brown, S.D.Ellis, S.T.Love, Phys.Rev. D19, 2018 (1979)
- (10) F.Csikor et al., Phys.Rev. D31, 1025 (1985)
- (11) F.Csikor, private communication
- (12) R.-Y.Zhu, Ph.D. Thesis, MIT Nov.1983

#### 4.2.3 A MODEL INDEPENDENT STUDY OF THE SHAPE OF THE THIRD JET IN $e^+e^-$ ANNIHILATION INTO MULTIHADRONS AT 35 GeV

Because of the higher colour charge and the self coupling of the gluons the gluon jet is expected to be broader than the quark jet. Monte Carlo simulations show that in 3-jet events the lowest energy jet originates preferentially from a gluon and therefore reflects properties of the gluon jet. We perform a phenomenological analysis of jet properties. From 2-jet events at 14 GeV we obtain reference jets at 7 GeV quark energy. We select 3-jet events from data at 35 GeV for which the energy of the third jet is around 7 GeV and compare the two samples.

Jets are established with a cluster algorithm. Models are used only to estimate systematic effects which might originate in the cluster algorithm and from efficiencies in our detector. The directions of the maxima of a generalized energy flow serve as initial jet axes. Particles are merged into the nearest jet if the angle to the proposed jet axis is below a preset half cone angle, typically  $45^\circ$ . After merging a new jet axis is determined by the sum of the momenta of the particles in the jet and the procedure is repeated with this new axis until a stable situation is reached.

The jet-energy  $E_j^q$  is calculated from the angles between the jets. 3-jet events are used in the range  $5 \text{ GeV} < E_j^q < 9 \text{ GeV}$ . To have well reconstructed jets we request that the dip angles of the 3rd jets and the reference jets stay below  $45^\circ$  and that the angles between the three jets are above  $60^\circ$ . 461 2-jet events at 14 GeV and 542 3-jet events at 35 GeV pass these cuts.

We present ratios of quantities from the lowest energy jet in three-jet events and the same quantities from the average jet in two-jet events.

$\langle p_\perp \rangle$  average transverse momentum of the particles with respect to the jet axis.

$\langle p_{\perp \text{in}} \rangle$   $p_{\perp}$  of each particle is split into two components.  $p_{\perp \text{in}}$  of the 3rd jet is taken in the plane which is defined by jet 1 and 2.

$\langle p_{\perp \text{out}} \rangle$  is orthogonal to both  $p_{\perp \text{in}}$  and  $p$ .

The influence of the limited acceptance and efficiency of the detector has been studied by detector simulations. It largely cancels when ratios of quantities are taken.

The  $p_{\perp}$ -distributions of the particles in the 3rd jet and the reference jet are similar (Fig.1). For the 3rd jet a 35 GeV we also compare  $\langle p_{\perp \text{in}} \rangle$  with  $\langle p_{\perp \text{out}} \rangle$  (Fig.2). We observe  $\langle p_{\perp} \rangle(\text{3rd jet}) / \langle p_{\perp} \rangle(\text{ref. jet}) = 1.03 \pm 0.03 \pm 0.04$ , i.e. we see no evidence for the jet broadening of the 'gluon jet'. The ratio  $\langle p_{\perp \text{in}} \rangle / \langle p_{\perp \text{out}} \rangle = 1.02 \pm 0.04 \pm 0.04$  shows that the 3rd jet is round within our experimental accuracy.

The half cone angle for particle merging has been varied from  $25^{\circ}$  to  $60^{\circ}$ . The changes of the results remain within the statistical errors. Thus the qualitative conclusions are independent from the opening of the cones used for the clusters.

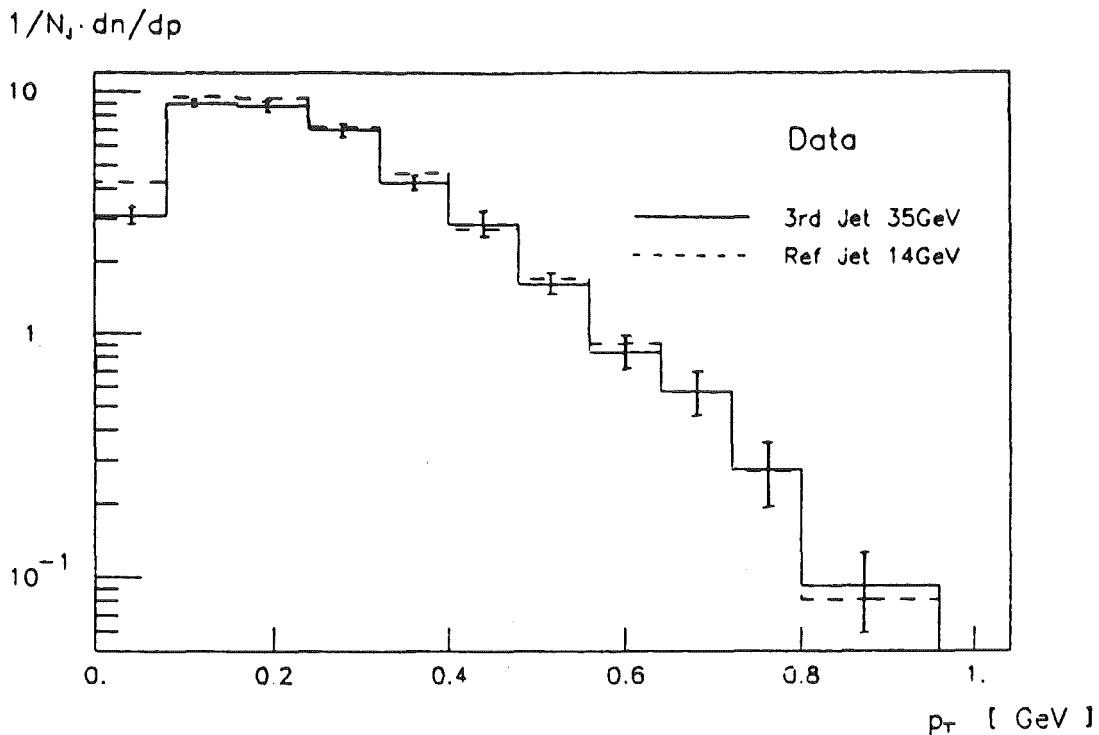


Fig.1: The distributions of transverse momentum  $p_{\perp}$  of charged particles within a jet relative to the jet-axis.  $N_J$  = Number of Jets. Solid line: third jet in 3-jet events at  $E_{\text{cm}} = 35$  GeV. Dashed line: average jet in 2-jet events at 14 GeV

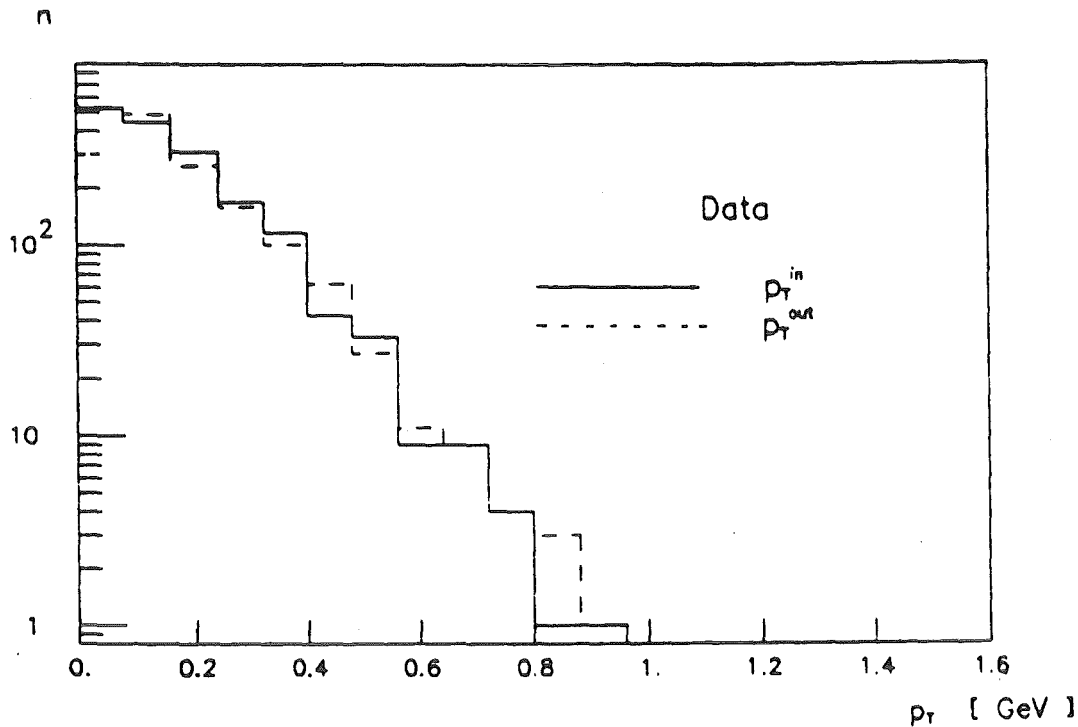


Fig.2: Comparison of  $p_{T,lin}$  and  $p_{T,out}$  for the 3rd jet at 35 GeV. Solid line:  $p_{T,lin}$  distribution. Dashed line:  $p_{T,out}$  distribution

#### 4.3 STUDY OF ELECTROWEAK INTERACTIONS

##### 4.3.1 STUDY OF INCLUSIVE LEPTONS FROM b-QUARK PRODUCTION IN $e^+e^-$ -ANNIHILATIONS

The study of inclusive leptons in multihadronic events in high energy  $e^+e^-$  annihilation yields information of the heavy charm and bottom quarks. The Cello measurement at  $\sqrt{S} = 35$  GeV permits determination of the semi leptonic branching ratios  $b \rightarrow l\nu X$  ( $l=e,\mu$ ) and  $c \rightarrow \mu\nu X$ . Using the electron and muon signal we also measured the electroweak induced charge asymmetry of the  $b\bar{b}$  and  $c\bar{c}$  production to test the standard model of Glashow, Weinberg and Salam.

Leptons from the weak decay of the b/c-quark are used to tag b-events and c-events. The simplest picture of this semi leptonic decay of B/C mesons is the spectator model. The b/c quark decays to a c/s-quark by emitting a virtual W boson. The light quark in the heavy meson acts only as a spectator. The expectation for branching ratio in a lepton is 10-15%.

Because of the heavy mass of the b quark, the lepton has on average a high momentum transverse to the quark direction. The shape of the events also



depends slightly on the mass of the parent quarks. Therefore, two obvious methods were used to separate b - enriched and c - enriched event samples: the first just splits the inclusive lepton events into those with  $p_T(\text{lepton}) \leq \text{cut}$  (cut = 0.8 GeV) and those with  $p_T(\text{lepton}) > \text{cut}$  ( $p_T$  measured with respect to the cluster axis, to which the lepton is attached). In Table 1 the contributions to the lepton yield for leptons with  $p > 1.6$  GeV,  $p_T > 0.8$  GeV together with backgrounds coming from other l-sources and misidentified hadrons are listed.

The second method uses the general event shape as a additional help to separate b - quark induced events from those which come from uds and c - quarks. Actually 4 measures are taken: the sphericity of the event, the average  $\langle p_T^n \rangle$  of all tracks in the plane of the event, the transverse mass  $\langle p_T^{\text{out}} \rangle \times N_{\text{tot}} \times E_{\text{CM}}/E_{\text{vis}}$  and the lepton  $p_T$ . For each measure we extract from Monte Carlo the probability distribution  $\rho(x)$  for light (= uds) and heavy b-quarks. Then we construct the ratio

$$P = \prod_i \rho_i^{\text{heavy}} / \rho_i^{\text{light}}$$

and cut at  $P = 1$ . Events at  $P < 1$  we call: C-tagged, at  $P > 1$ : B-tagged. The separation is shown in Fig.1. Then we repeat the analysis procedure of method 1 with the  $p_T(\text{lepton})$  cut at 0.6 GeV. The contributions to the lepton yield are listed in Tab.1.

Table 1: Composition of the inclusive lepton sample (in %).

Channel	Method 1			Method 2		
	l=e	l= $\mu$	l= $\mu$	l=e	l= $\mu$	l= $\mu$
$p_T$ :	>0.8	>0.8	<0.8	>0.6	>0.6	<0.6
b $\rightarrow$ l	57.4	47.6	10.5	56.7	48.9	5.7
b $\rightarrow$ c $\rightarrow$ l	7.6	5.6	5.1	10.2	7.8	2.9
c $\rightarrow$ l	15.5	23.5	41.9	15.6	22.3	46.7
uds $\rightarrow$ l	0.7	0.0	0.0	0.8	0.0	0.0
misident. l	17.9	23.4	42.4	15.9	21.0	44.7
deep inel.	0.9	0.0	0.1	0.9	0.0	0.1

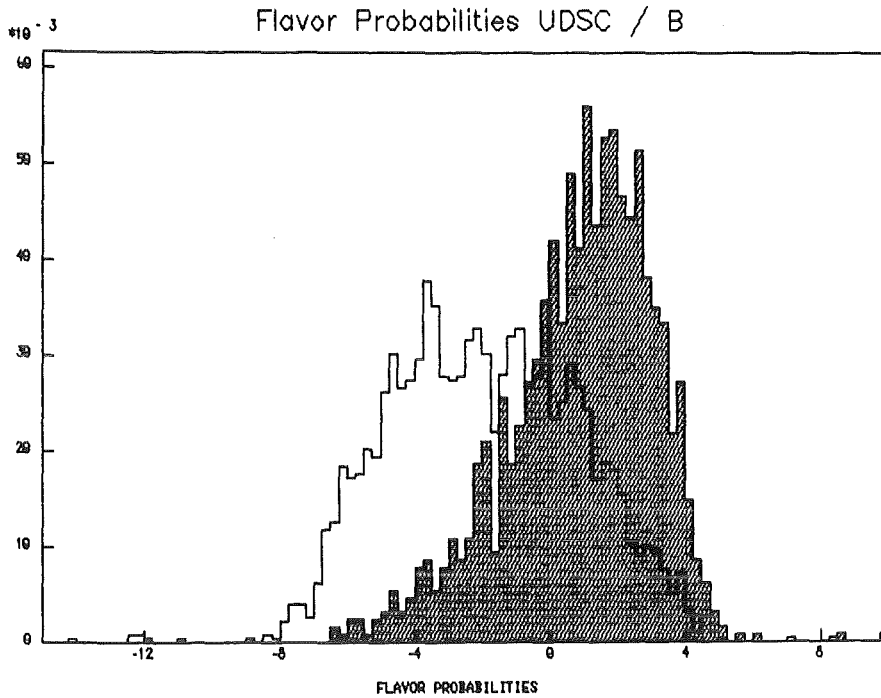


Fig.1: Flavour separation by means of shape variables.

Out of 21086 multihadron events we collect at high  $p_T$  in method 1/method 2 samples of 71/62 electron and 223/229 muon candidates. At low  $p_T$  we have 630/352 muon candidates. With these samples we determine the semileptonic branching ratios for b- and c-quarks.

	method 1	method 2
Br	$p_T > 0.8 \text{ GeV}$	$p_T > 0.6 \text{ GeV}$
$b \rightarrow e \nu X$	$10.6 \pm 2.3\%$	$10.8 \pm 2.5\%$
$b \rightarrow \mu \nu X$	$14.6 \pm 1.9\%$	$12.6 \pm 1.9\%$
$b \rightarrow l \nu X$	$13.4 \pm 1.5\%$	$12.1 \pm 1.6\%$
	$p_T < 0.8 \text{ GeV}$	$p_T < 0.6 \text{ GeV}$
$c \rightarrow \mu \nu X$	$11.2 \pm 0.9\%$	$10.4 \pm 1.0\%$

l stands for lepton and is the average of e and  $\mu$ . The errors quoted are statistical errors.

Asymmetries are determined in two ways: from the forward and backward integrals or by a likelihood fit to the angular distribution of the cluster axis to which the lepton is attached. The raw asymmetries are then corrected for backgrounds with the help of Monte Carlo.

Acceptance, resolution, initial state bremsstrahlung and gluons are taken into account by a factor derived from Monte Carlo. Finally we arrive with:

		method 1		method 2	
b-asymmetry	from	FB-integral	likelihood fit	FB-integral	likelihood fit
$A_b (e)$	=	$.27 \pm .28$	$.04 \pm .27$	$-.17 \pm .30$	$-.37 \pm .30$
$A_b (\mu)$	=	$-.09 \pm .19$	$-.15 \pm .20$	$.00 \pm .22$	$-.01 \pm .22$
$A_b (\text{lept.})$	=	$.01 \pm .16$	$-.09 \pm .16$	$-.05 \pm .18$	$-.13 \pm .18$
c-asymmetry					
$A_c (\mu)$	=	$.11 \pm .13$	$.01 \pm .12$	$-.06 \pm .15$	$-.18 \pm .15$

The standard model prediction with  $\sin^2 \theta_W = .22$  and no b-mixing would be:

$$A_b = -.26$$

$$A_c = -.13$$

The results are compatible with the expectation of the standard model.

#### 4.4 SEARCH FOR NEW PARTICLES IN $e^+e^-$ -ANNIHILATIONS

##### 4.4.1 SINGLE PHOTON SEARCH WITH THE CELLO DETECTOR

It was first suggested by Ma and Okada (1) to use the process  $e^+e^- \rightarrow \gamma \nu \bar{\nu}$  as a direct method for counting the number of neutrino families since the cross section for neutrino pair production is directly related to the number of neutrino species,  $N_\nu$ . As neutrinos interact only weakly with matter, they escape the detector unobserved and the signature for this process is a single photon and nothing else in the detector. In  $e^+e^-$  collisions neutrinos can be pair produced via  $Z_0$  exchange, and for electron neutrinos there is an additional component from W exchange. The cross section for  $e^+e^- \rightarrow \gamma \nu \bar{\nu}$  can be found in (2).

The photon spectrum is of the bremsstrahlung type, peaked at small angles and at low energies. Therefore large acceptance for photon tagging and low single photon trigger energy threshold are needed. In addition, to ensure that only weakly interacting particles are produced in association with the tagged photon, the veto capability of the detector must be extended to the largest solid angle. However, in  $e^+e^-$  storage rings it is unavoidable that a hole be left for the beam pipe. This causes the reaction  $e^+e^- \rightarrow \gamma e^+e^-$  to be

the major experimental background, when both electrons are scattered at small polar angles. If  $\theta_{\text{veto}}$  is the minimum veto angle, this background is kinematically totally eliminated as soon as  $\chi_t = \chi(1-y^2) \geq 2\theta_{\text{veto}}$ . For the CELLO detector (3) this minimum veto angle is  $\theta_{\text{veto}} = 50$  mrad.

The data used for this analysis were taken at the PETRA storage ring at DESY, at center of mass energies of  $46.57 > \sqrt{s} > 35.0$  GeV with a total integrated luminosity of  $\int L dt = 115.5 \text{ pb}^{-1}$ .

Single photon events were triggered by a total energy deposit of  $E_\gamma > 1.75$  GeV in one of the 16 modules of the barrel calorimeter. QED events were rejected by requiring essentially no energy in the calorimeters in the forward and backward regions down to  $\theta_{\text{veto}} = 50$  mrad.

Finally one event is kept as a candidate and has  $\chi = 0.18$  and  $|\cos(\theta)| = 0.23$ . Within our cuts and acceptance, with an average detection efficiency for single photon events of 44%, we expect 1.7 event from the three known neutrinos. With one observed event, we derive an upper limit of

$$N_\nu < 10 \quad \text{at the 90\% CL}$$

for the total number of neutrino species.

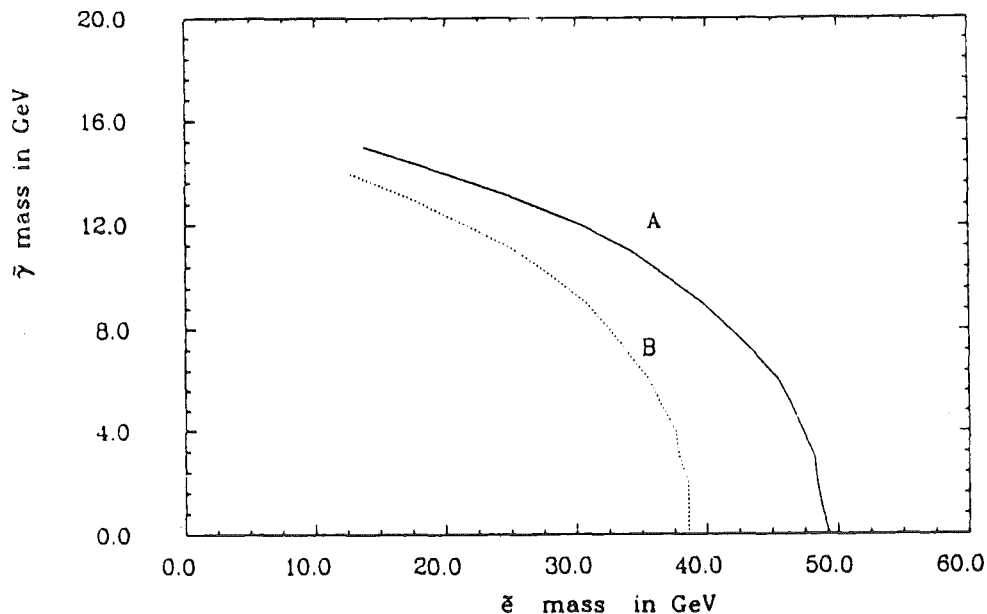


Fig.1: In the  $\tau - \tilde{e}$  mass plane, boundaries of the 90% CL domains excluded by this analysis for mass degenerate scalar electrons (A), and if one of the scalar electrons is very heavy (B).

This search for single photons can also be used to set limits on the radiative production of other kinds of weakly interacting particles. This is the case, for instance, for the photino of supersymmetric theories, commonly assumed to be the lightest supersymmetric particle (LSP). Its radiative pair production (4) by scalar electron t-channel exchange would lead to the same signature as  $e^+e^- \rightarrow \gamma\nu\bar{\nu}$ . In a way similar to the one used to obtain the limit for  $N_\nu$ , we get lower limits for the masses of the scalar electron ( $m_{\tilde{e}}$ ) and of the photino ( $m_\gamma$ ), but now using the expected contribution from  $e^+e^- \rightarrow \gamma\nu\bar{\nu}$  as background. With the cross section for the reaction  $e^+e^- \rightarrow \gamma\tilde{\gamma}\tilde{\gamma}$ , given in (5), we can limit the scalar electron mass  $m_{\tilde{e}}$  to

$$m_{\tilde{e}} \geq 49.0 \text{ GeV} \quad \text{at } 90\% \text{ CL for } m_{\tilde{e}_R} = m_{\tilde{e}_L} \text{ and } m_\gamma = 0.0 \text{ GeV}$$

- (1) E.Ma and J.Okada, Phys.Rev.Lett.41 (1978) 287
- (2) K.J.F.Gaemers, R.Gastmans and F.M.Renard, Phys.Rev. D19 (1979) 1605
- (3) CELLO Coll., H.-J.Behrend et al., Phys.Scr. 23 (1981) 610
- (4) P.Fayet, Phys.Lett. 117B (1982) 460  
J.Ellis, J.S.Hagelin, Phys.Lett. 122B (1983) 303
- (5) K.Grassie and P.N.Pandita, Phys.Rev. D30 (1984) 22

5. DEVELOPMENTS AND INSTRUMENTATION

5.1 DETECTORS

5.1.1 STATUS AND TESTS OF THE KARLSRUHE  $^{411}\text{BaF}_2$  DETECTOR

K. Wisshak, K. Guber, F. Käppeler

During the last two years 45 crystals for the Karlsruhe  $^{411}\text{BaF}_2$  detector have been tested, 38 of which were finally accepted. Four crystals had to be refused because of poor energy resolution while three showed too high alpha backgrounds from radium impurities. The measured energy resolution for  $^{137}\text{Cs}$  and the alpha background defined as the sum intensity of the four alpha lines are plotted in Fig. 1 for all crystals according to their production date. After some problems in the beginning a reproducible energy resolution has been achieved by the manufacturer (Firma Dr. Karl Korth, Kiel, FRG). The very good results of crystals 4 and 7 were obtained

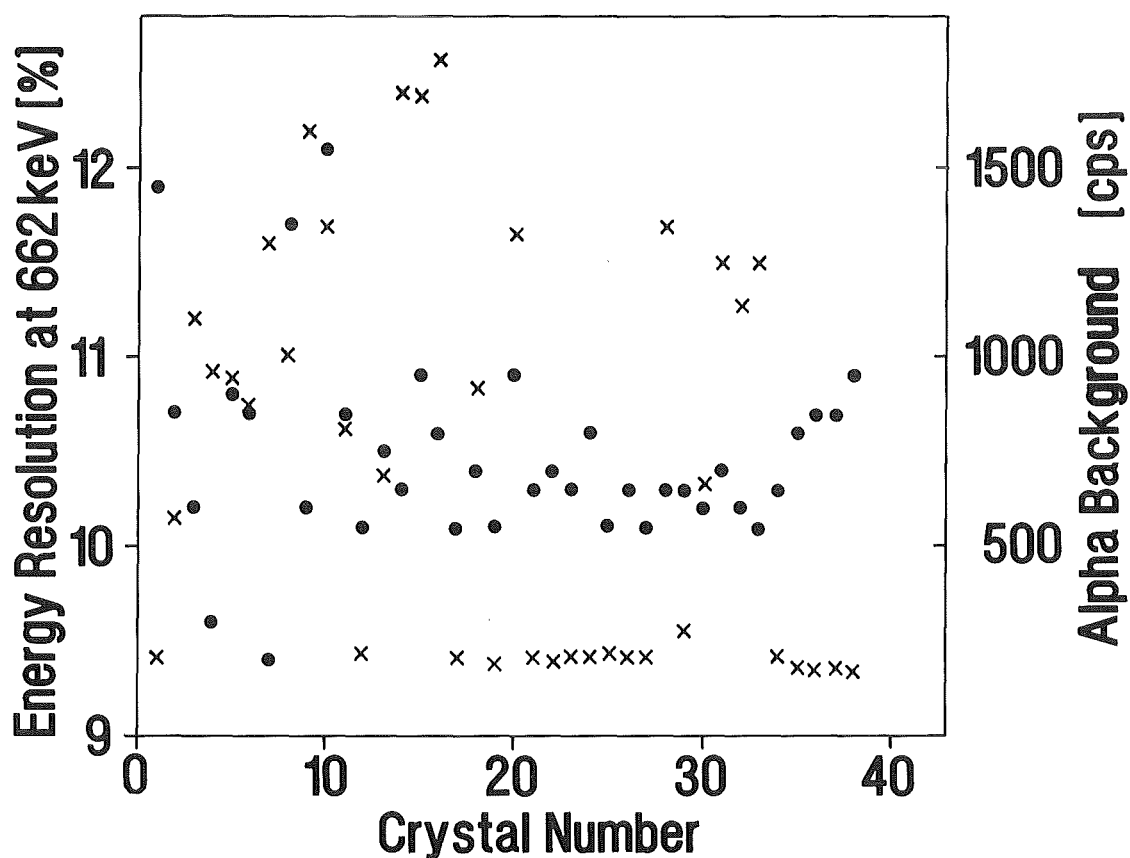


Fig. 1 Energy resolution for  $^{137}\text{Cs}$  (dots) and alpha background (crosses) of the 38 crystals accepted for the  $^{411}\text{BaF}_2$  detector

in careful measurements allowing detector and electronics to fully stabilize and taking care for a stable and low room temperature. All other tests were performed by a routine procedure; short running-in periods and room temperatures of 22 - 25 °C deteriorated the energy resolution by roughly 0.5 % absolute compared to the optimum results.

The scatter in the alpha background among the first crystals reflects the large differences in uranium and consequently radium content of barium minerals as obtained from different suppliers. After this problem has been recognized the raw material was analyzed and selected for crystal production. Unfortunately, unexpected inhomogeneities were found even within the same batch causing the high backgrounds around crystal # 30.

The final detector modules have been assembled and are tested for 35 crystals. In general, the energy resolution is worse by about 0.5 % absolute compared to the crystal tests, due to the lower average quality of the phototubes. Presently, the individual detector modules are being mounted in the experimental area of the Van de Graaff accelerator. The electronics have been assembled and tested in the laboratory and are ready for being shifted to the experimental area, too.

The computer software for detector handling and gain stabilization has been successfully used over long periods with a subassembly of 6 modules. It was found that detectors and electronics are operating sufficiently stable. The observed gain shifts can be explained by the day-night temperature differences causing changes in the light output of the BaF<sub>2</sub> crystals (see next contribution).

#### 5.1.2 GAMMA-RAY SPECTROSCOPY WITH A COOLED BARIUM-FLUORIDE CRYSTAL

K. Wisshak, K. Guber, F. Käppeler (1)

The increasing interest in BaF<sub>2</sub> crystals as scintillators for gamma-ray spectroscopy (2,3) is mainly caused by the very good timing characteristics and the high density of the material. The only drawback of BaF<sub>2</sub> is the gamma-ray energy resolution at room temperature which is about 20 to 30 % worse compared to NaI(Tl). While NaI(Tl) shows the maximum light output at room temperature (4), the light output of BaF<sub>2</sub> increases with decreasing temperature (5). Thus, the energy resolution of BaF<sub>2</sub> detectors can be improved significantly by cooling. In the following, we demonstrate

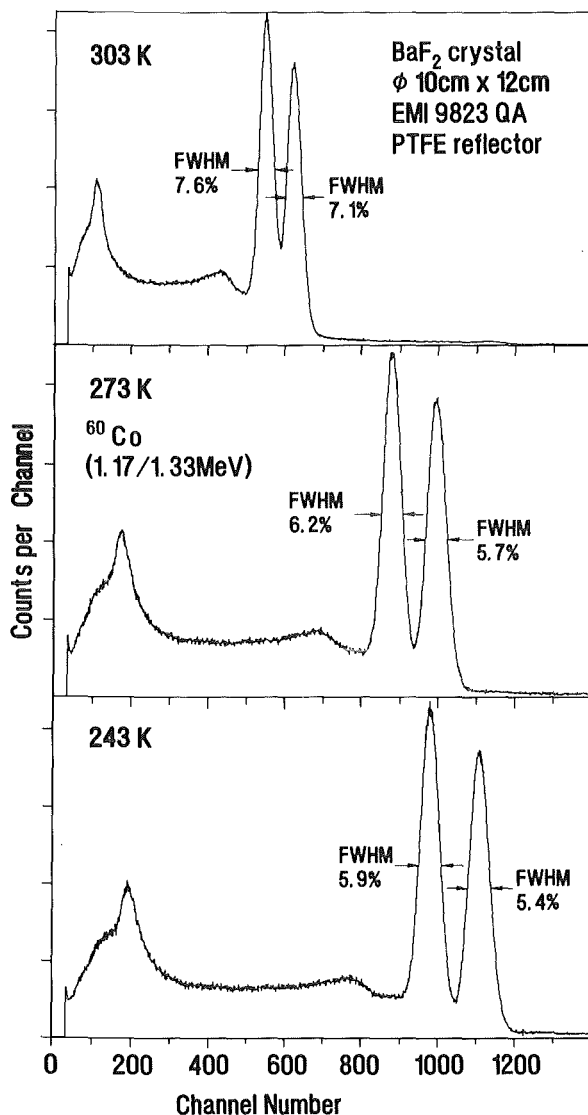


Fig. 1

Energy spectra of a <sup>60</sup>Co source as measured at 243, 273 and 303 K with a 1 l BaF<sub>2</sub> crystal. The improvement in energy resolution is to a good approximation proportional to the square root of the relative shift of the peak intensity.

that at temperatures of 243 - 253 K the energy resolution of a large BaF<sub>2</sub> crystal is comparable to or even better than for NaI(Tl) detectors with similar efficiency.

The measurements have been performed using a cylindrical BaF<sub>2</sub> crystal of 10 cm diameter and 12 cm length (Dr. Karl Korth, Kiel, Fed. Rep. of Germany). The crystal was carefully ground and covered by a PTFE reflector as described in refs. (2) and (6). An EMI 9823 QA phototube was connected to the crystal via silicon oil with a viscosity of 100000 cst. The voltage divider chain was the same as described in ref. (2) without any special gain stabilization system. A copper tube of 10 mm diameter was wound around the aluminum canning of the crystal covering the side as well as the front surface. For thermal insulation the whole detector except the voltage divider was embedded in a styropor block, and liquid from a ther-



mally stabilized reservoir was continuously pumped through the copper tube.

The energy resolution was determined in the range from 60 keV to 6.13 MeV using  $^{241}\text{Am}$ ,  $^{137}\text{Cs}$ ,  $^{88}\text{Y}$ ,  $^{60}\text{Co}$ ,  $^{228}\text{Th}$ , ( $^{241}\text{Am}+\text{Be}$ ) and ( $^{13}\text{C}+^{238}\text{Pu}$ ) sources. The results from the ( $^{241}\text{Am}+\text{Be}$ ) source have been corrected for the natural line width of 2.2% as determined with a germanium detector. The temperature was varied in the range from 243 to 303 K. The  $^{60}\text{Co}$  spectra measured under identical conditions at three different temperatures are displayed in Figure 1, illustrating the following observations:

- a) The energy resolution of the  $\text{BaF}_2$  crystal improves significantly with decreasing temperature.
- b) The energy resolution is always proportional to the square root of the peak position, i.e. it is indeed dominated by photoelectron statistics.
- c) The energy resolution saturates at low temperatures. According to ref. (5) the light output of the crystal should increase linearly down to temperatures of about 243 K. Thus, the observed saturation is due to a reduction of the quantum efficiency and amplification of the phototube at low temperatures.
- d) The energy resolution follows the  $1/\sqrt{E}$  law to a very good approximation.
- e) The good timing characteristics remained unchanged as the fast component of the scintillation light is not affected by temperature.
- f) The  $\text{BaF}_2$  crystals proved to be mechanically stable against thermal changes. The crystal was cooled and heated several times with temperature gradients of 5 to 7 deg/h without any observable damage.

The efficiency of the investigated crystal is comparable to the  $\text{NaI}(\text{Tl})$  modules of the Heidelberg-Darmstadt crystal ball detector. For these modules an energy resolution better than 8% at 662 keV and 6% at 1173 keV was guaranteed; the optimum values which were finally obtained were 7.6 and 5.8% (7,8). However, these crystals show deviations from the  $1/\sqrt{E}$  law resulting in an energy resolution of 5.3 and 4.4% at 1.8 MeV and 4.4 MeV, respectively. Thus, the present results for  $\text{BaF}_2$  at 273 K are already superior above about 2 MeV while the data measured at 243 K are comparable or better in the entire energy range.

Optimum results for big  $\text{NaI}(\text{Tl})$  detectors were reported by Sandorfi and Collins (9), who quoted 6.9% at 662 keV and 3.2% at 6.13 MeV

using sophisticated methods for gain stabilization, anti-Compton suppression and surface compensation. The present results at 6.13 MeV are at least of the same quality but cannot be compared directly because of the different crystal size. However, with optimized stabilization and anti-Compton shields it should be possible to construct a high energy gamma-ray spectrometer with better energy resolution than present NaI(Tl) detectors, but with the superior time resolution of 0.5 ns characteristic for BaF<sub>2</sub> detectors.

- (1) Nucl. Instr. Meth. A259 (1987) 583
- (2) K. Wisshak, F. Käppeler, H. Müller, Nucl. Instr. Meth. A251 (1986) 101
- (3) F.A. Beck, Proc. Int. Conf. on Instrumentation for Heavy Ion Nuclear Research, Oak Ridge, TN, October 22-25 1984, ed., D. Shapira, (Harwood Academic Publishers 1985) p. 129
- (4) Harshaw radiation detector catalogue
- (5) P. Schotanus, C.W.E. van Eijk, R.W. Hollander, J. Pijpelink, Nucl. Instr. Meth. A238 (1985) 564
- (6) K. Wisshak, F. Käppeler, Nucl. Instr. Meth. 227 (1984) 91
- (7) W. Weiter, Diplomarbeit, Heidelberg (1981) unpublished
- (8) V. Metag, et al., Lecture Notes in Physics, vol. 178, ed. W. v. Oertzen (Springer, Heidelberg, New York, Tokyo, 1983)
- (9) A.M. Sandorfi, M.T. Collins, Nucl. Instr. Meth. 222 (1984) 479

### 5.1.3. ELECTRONIC COMPONENTS FOR THE 4 $\pi$ BaF<sub>2</sub> DETECTOR

H. Müller

The following survey lists those components for the 42 electronic channels of the 4 $\pi$  BaF<sub>2</sub> detector which have been newly developed. Most of these serve to complement commercial equipment as to adapt it to our particular requirements. As each electronic channel contains 10 to 15 adjustable parameters, special emphasis was laid on high stability performance. Voltage Divider for Photomultiplier: For optimum energy and time resolution the voltage divider (Fig. 1) was carefully adapted to the photomultipliers (Thorn EMI 9823). The resistor chain is enclosed in an aluminum housing of 350 cm<sup>3</sup> and produces ~ 4 W at 2.3 kV cathode voltage. The potentials of the first and last dynodes are fixed by temperature compensated Zener diodes. The potential of the focus electrode and the first dynode are adjustable to optimize signal output. The inductivities of the connections between dynodes are neutralized to reduce oscillations and to improve the signal rise time. All parts are on printed circuit and are arranged concentrically around the PM socket, thus minimizing the

Voltage Divider for PM THORN EMI 9823

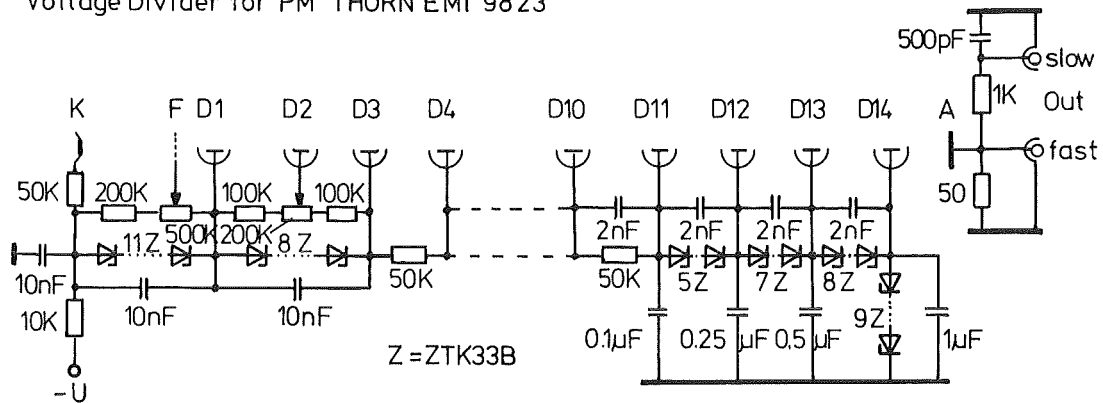


Fig.1 Voltage divider chain optimized for BaF<sub>2</sub> scintillator crystals and Thorn EMI 9823 photomultiplier tubes

connections. The voltage divider exhibits good temperature stability and resolution over long periods of time. Fast and slow outputs are provided for timing and energy measurements, respectively.

In order to facilitate the development, manufacturing and checking of the voltage divider chains a test stand (Fig. 2) was built. It consists of a photomultiplier socket that is supplied with high voltage. The voltage dividers can be attached to it as to a real photomultiplier. The potential of each dynode can be directly measured via a rotary switch and a digitized readout. At the same time the current through the resistor chain is also displayed. The setup is enclosed in a plexiglass shield with

Testunit for PM- Voltage Divider

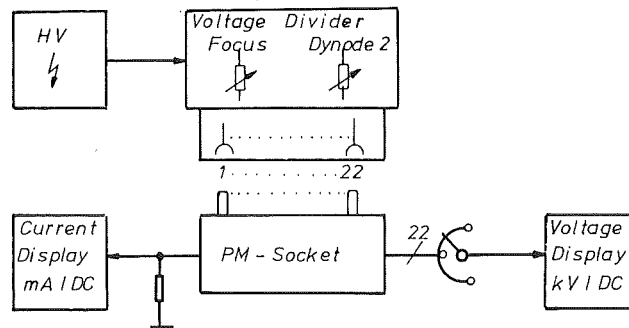


Fig. 2 Test unit for voltage divider chains

a high voltage switch to allow for measurements under realistic conditions.

Cable Amplifier: The photomultiplier signals have to be transferred to the electronics via 40 m long cables. On this way, frequency-dependent losses tend to deteriorate spectrum resolution and linearity. Therefore, an amplifier based on the components HA-2542 and HA-5002 was developed for the energy signal derived from the anode (Fig. 3). With an amplification of 2.5 on  $50\Omega$  the signal to noise ratio as well as the cable feedback to the signal source could be improved. A corresponding amplifier for the fast signal using SMD techniques and microwave transistors is under development.

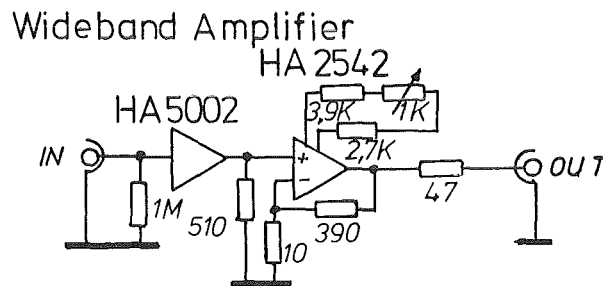


Fig. 3 Wideband amplifier for the energy signals of the  $4\mu\text{BaF}_2$  detector

Fast 42-fold OR: For the combination of the timing signals of all 42 electronic channels a fast OR was designed consisting of fast diodes (HP 5082-2800) and an operation amplifier in SMD technique (Fig. 4). NIM input signals of  $-700\text{ mV}$  and  $20\text{ ns}$  width create output signals of  $-1.8\text{ V}$  on  $50\Omega$  with a rise time of  $3\text{ ns/V}$  which can be used with NIM and ECL electronics.

#### 42Channel Fast OR

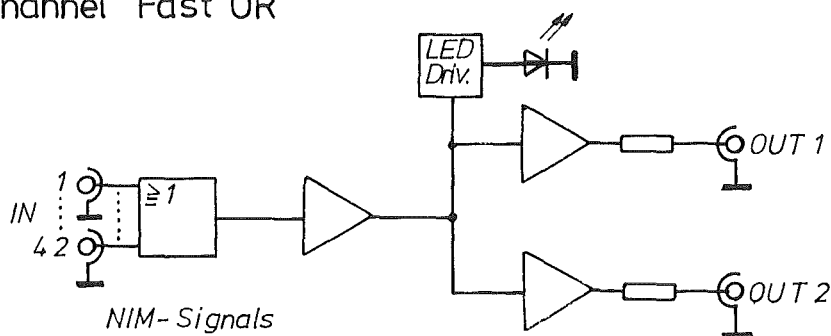


Fig. 4 A 42 channel fast OR

Channel Identifier: The information on sum energy and time of flight for each accepted event in the  $4\pi$  BaF<sub>2</sub> detector is complemented with the information which of the 42 channels contributed to it. To this end, the various channel addresses must be added to the digitized signals between ADC and computer. This is achieved in the following way (Fig. 5) :

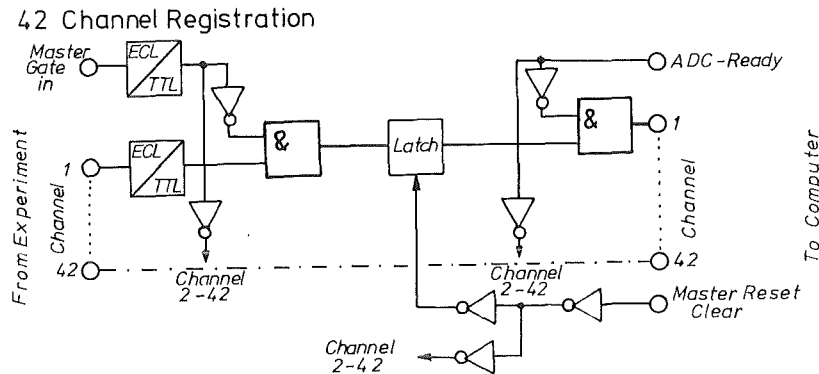


Fig. 5 42-fold channel identifier

Each electronic channel is connected to the identifier. Every input signal is combined with the master gate in a logic AND to set an electronic switch. After a certain waiting time following each event, the logic status defined by the switches, is transferred to the computer synchronous with the ADC-READY signal. After a certain transfer time the switches are reset and the ADC is cleared for the next event.

Coincidence Interface for 2 ADC (Fig.6): For the two-dimensional spectrum accumulation of energy versus time-of-flight both ADC outputs have to be unified by means of a coincidence between the two ADC-READY signals. As

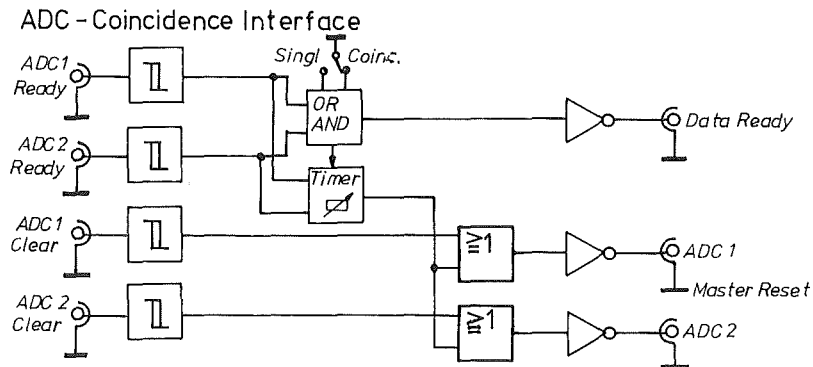


Fig. 6 Coincidence interface for 2 ADC

the ADCs are not synchronous, the first READY signal starts a waiting time which can be selected up to 10 $\mu$ sec. If the second ADC fires within this time, the event is accepted and stored by combining both bit patterns; otherwise the ADC are reset.

#### 5.1.4 ACCEPTANCE DETECTOR FOR THE MAGNETIC SPECTROGRAPH "LITTLE JOHN"

G. Gantenbein, J. Kiener, H.J. Gils, S. Zagromski

The break-up of 156 MeV  ${}^6\text{Li}$ -projectiles is studied at the Karlsruhe Isochronous Cyclotron at small reaction angles (1). The energy and the emission angles of both reaction products in the binary break-up  ${}^6\text{Li} \rightarrow \alpha + d$  are measured with the magnetic spectrograph "Little John". For an increase of the acceptance solid angle and for more precise measurement of the relative emission angle of the fragments a multiwire proportional chamber (MWPC) was designed and built (2). Its position measurement of the penetrating particles enables to determine the emission trajectory before entering the spectrograph.

The detector has a sensitive area of 30 x 50 mm<sup>2</sup> and consists of 5 wire planes mounted on epoxy frames and glued with araldite (see Fig. 1). For the central plane (anode) we used 10  $\mu$ m tungsten wires; the wires of the other planes made of the same material have a diameter of 50  $\mu$ m. The wires are separated by 1 mm, the planes are spaced 5 mm apart. From the diameter and distance of the wires a transparency of 80% is estimated.

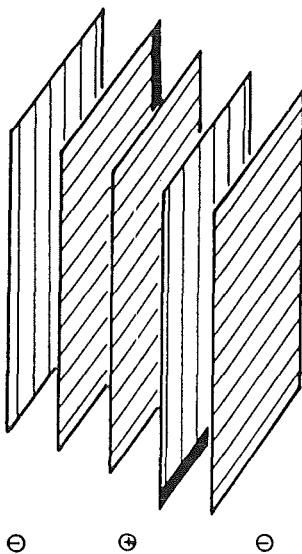


Fig. 1  
View of the wire planes

In order to measure two particles in coincidence the anode and the corresponding position planes are logically divided into two parts. Both anode signals of the detector are used to start different TPHCs, which are stopped by the delayed signals of the position-wires. The position dependent delay is provided by delay line chips fixed directly at the epoxy frames (4 ns delay per wire). Each position plane delivers two position-signals (one at each end). Altogether the detector has 8 output channels. The electronics for two channels is schematically drawn in Fig. 2. For the gas atmosphere we used isobutane at two different pressures (4.7 mbar and 15 mbar), which were electronically controlled and stabilized to within 0.1 mbar (3).

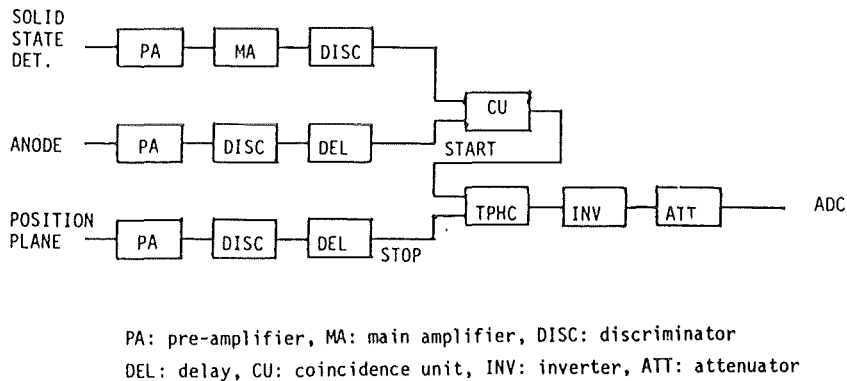


Fig. 2 Electronic set-up for test purposes

First, the chamber was tested with the 9 MeV proton beam of the Erlangen tandem accelerator. With the help of a solid state detector placed behind the MWPC it was possible to determine the efficiency of the MWPC. For 15 mbar we observed an efficiency above 95% with a counting rate of about 800 Hz per 0.75 mm<sup>2</sup> of the sensitive area (see Fig. 3). The measured efficiency at various voltages agrees with general expectations (Fig. 4). The detector was stable at counting rates up to 40 kHz on some fraction of the whole sensitive area. Improvements have to be worked out concerning the differences in efficiency between position planes and anodes, which is somewhat higher for the anodes. The position resolution, measured to be 3.5 - 4.0 mm, should increase if constant-fraction-discriminators will be used in future instead of simple discriminators.

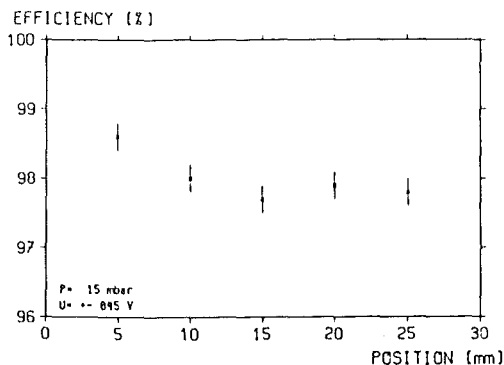


Fig. 3 Efficiency at various positions

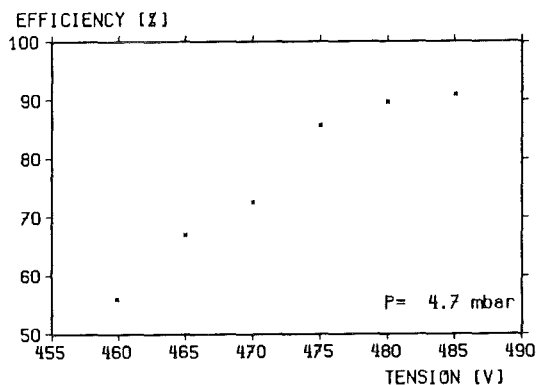


Fig. 4 Efficiency versus voltage

- (1) J. Kiener, H.J. Gils, N. Heide, H. Jelitto, H. Rebel, S. Zagromski, this report, contrib. 1.4.6
- (2) Physikalische Nachweisgeräte, Dr. H. Stelzer, D-6101 Messel
- (3) M. Heinz, unpublished results, Kernforschungszentrum Karlsruhe (1983)

#### 5.1.5 A MODIFICATION OF THE MAGNETIC SPECTROGRAPH "LITTLE JOHN" FOR HIGH ANGULAR RESOLUTION MEASUREMENTS

R. Rudeloff\*, S. Zagromski, A. Lehmann\*, H.J. Gils, W. Eyrich\*, H. Schlösser\*, J. Kiener, H. Wirth\*,

The differential cross section of  ${}^6\text{Li}$  scattering using the 156 MeV beam of the Karlsruhe Cyclotron shows a very narrow diffraction structure for excitation strengths with defined angular momentum. The distance between maxima and minima of the giant resonances in medium and heavy nuclei studied in our experiments is only about  $\Delta\theta = 1^\circ$ . Therefore one can, in principle, measure neighbouring maxima and minima simultaneously by use of the magnetic spectrograph "Little John". This is an advantage to avoid systematic errors in the study of giant resonances. Moreover it obviously helps to save measuring time. The necessary subdivision of the angular acceptance can either be provided by using position sensitive acceptance detector systems (1) or by measuring the angles of the scattered particles in the region of the focal plane. This is illustrated in Fig. 1, which



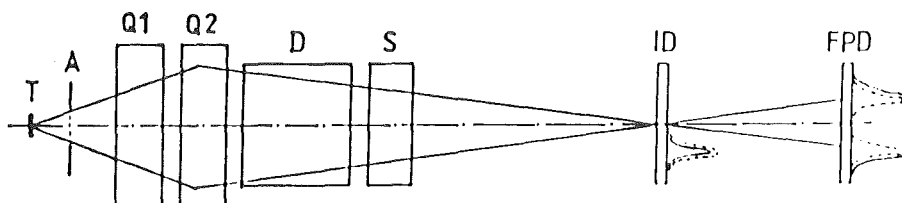


Fig. 1 Scheme of the trajectories of the scattered particles at fully opened acceptance slits

shows schematically the trajectories in horizontal direction for widely opened acceptance slits.

We tested the second method by installing an intermediate detector (ID) in front of the standard focal plane detector system (FPD). This has the advantage to allow also measurements at very small scattering angles, including zero degree. Due to the available long distance between the sextupole and the focal plane of  $\sim 2$  m and due to the flexible focussing conditions the position of the intermediate detector could be optimized. For a sufficient subdivision of the angular acceptance a distance of about 60 cm between ID and FDP was chosen. A decrease of the energy resolution caused by angular straggling is avoided when focussing the scattered particles to the ID.

Fig. 2 shows first experimental results from  ${}^6\text{Li}$  scattering on  ${}^{12}\text{C}$ , which confirm the estimate based on ion optics. The peaks at 0.00 MeV and 4.44 MeV excitation energy are plotted for two different positions of the acceptance slits corresponding to an angular shift of  $\Delta\theta = 1.2^\circ$ . These spectra were obtained with a horizontal acceptance of  $0.15^\circ$ . The centers of the peaks on the ID (Figs. 2a and b) are constant for both settings as expected. Only their different intensity ratios give evidence for the angular shift. Figures 2c and d show the situation on the FPD. The centers are shifted as expected from Fig. 1.

The relative distance and the FWHM of the peaks provide a rough estimate that the ID allows a subdivision of the acceptance in scattering angle intervals of  $\Delta\theta = 0.3^\circ$ .

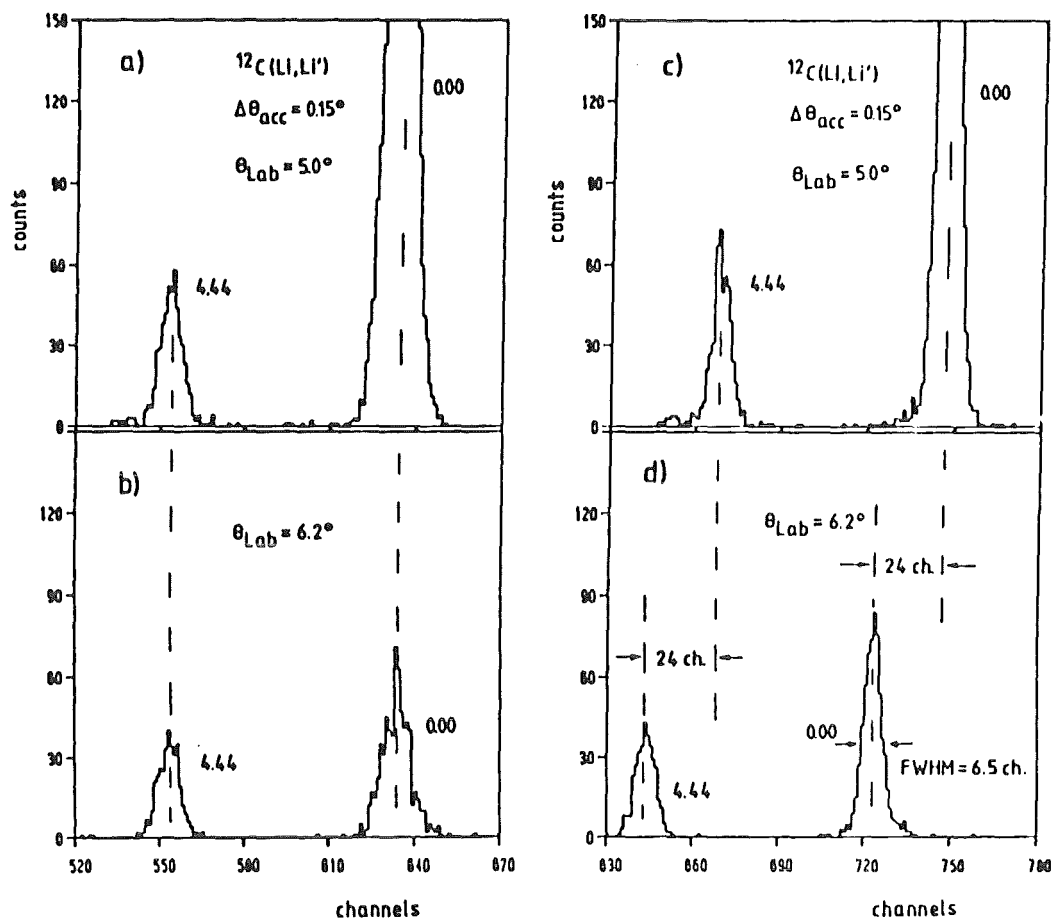


Fig. 2  $^{12}\text{C}(\text{}^6\text{Li}, \text{}^6\text{Li}')^0$  spectra obtained with different positions of the acceptance slits. Left: Intermediate Detector (ID), right: Focal Plane Detector (FPD)

(1) G. Gantenbein, J. Kiener, H.J. Gils, S. Zagromski, this report, contrib. 5.1.4

\* Physikalisches Institut der Universität Erlangen-Nürnberg

5.1.6 PRODUCTION OF SUPERCONDUCTING TUNNEL JUNCTIONS FOR PARTICLE DETECTION

P.Jany, F.Finkbeiner, W.Heeringa, H.O.Klages, H.Skacel, T.Strobel

Superconducting detectors have a potentially high energy resolution power arising from the fact that in a superconductor the lowest lying excited electron states (quasi-particles) are separated from the ground state (Cooper-pairs) by a gap  $\Delta$  of the order of only 1 meV instead of 1 eV in semiconductors. Therefore the number of charge carriers produced by ionizing radiation is by a factor of 1000 higher. The achievable energy resolution of superconducting detectors is expected to be up to 50 times better than that of semiconductor particle detectors.

An ionizing particle that deposits its energy in a superconductor produces an excess of quasi-particles by Cooper-pair breaking. The best way to detect such an excitation is to use a superconducting tunnel junction. Figure 1 shows the current-voltage characteristic of a typical tunnel-junction (5). The junction is biased at a voltage  $V_B$  between 0 and  $2\Delta/e$ . An excess current occurs when an excitation is caused by an ionizing particle.

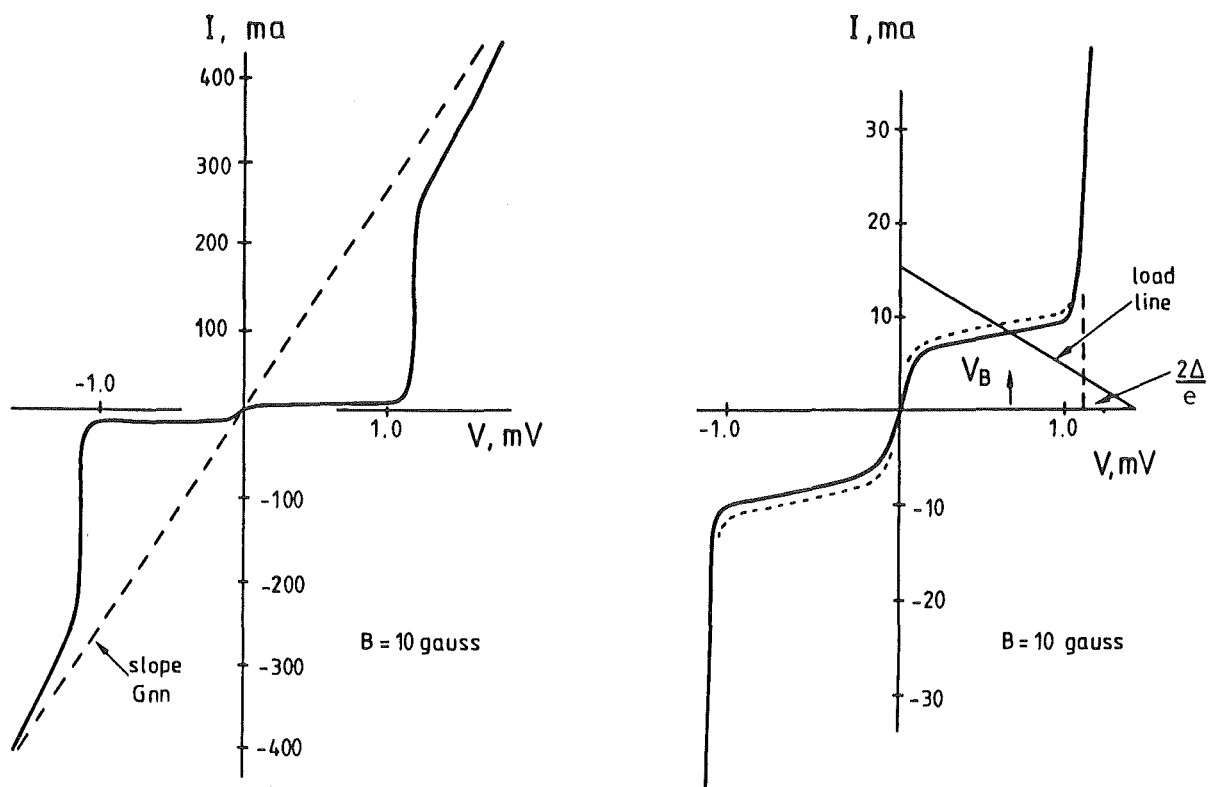


Fig.1: Current-voltage characteristic of a typical tunnel-junction according to (5)

Other groups have made such devices and detected pulses from  $\alpha$ -particles and X-rays (1-5). In our institute work is going on to install the

experimental set-up to produce and study this kind of detectors. In first experiments we produced aluminium tunnel-junctions. We use a Varian UHV chamber to evaporate aluminium through a galvanotype nickel mask on sapphire substrates. The insulating tunnel barrier is formed by the natural oxide. A glow discharge oxidation process is in preparation. The junction area is  $150 \times 150 \mu\text{m}^2$  with contact leads of  $30 \mu\text{m}$  leading to gold contacts. These gold contacts are produced before in another evaporation chamber which has been built for this purpose. The tunnel -junctions are mounted in a copper holder with fixed micro-spring contacts and cooled down to 300 mK in a cryostat, which is described in contribution 5.2.1 of this report

To develop the techniques of signal detection and noise reduction the tunnel-junctions will be first illuminated with light pulses from luminescence or laser diodes through fiber optics. Afterwards a variable energy X-ray source will be installed.

There would be a wide range of possible applications for this new kind of detectors with an energy resolution superior to conventional semiconductor detectors.

- (1) G.H.Wood, B.L.White, Can.J.Phys. 51 (1973) 2032
- (2) M.Kurakado, J.Appl.Phys. 55 (1984) 3185
- (3) D.Twerenbold, A.Zehnder, J.Appl.Phys. 61 (1987) 1
- (4) F.v.Feilitzsch, TU München, priv. communication
- (5) N.E.Booth, Nucl.Phys.Lab. Oxford Uni., Ref.19/87

#### 5.1.7 MWPC SET-UP FOR NEUTRON INDUCED REACTIONS ON $^{12}\text{C}$

S.Scheib, P.Doll, G.Fink, H.O.Klages

As reported in the 1985 annual report (1) a large solid angle detector system consisting of multiwire proportional chambers and plastic  $\Delta E$ - and E-scintillation detectors has been set up to investigate neutron induced reactions on nuclei leading to charged particles in the exit channel. In figure 1 one can see the improved set-up consisting of four MWPC's, two  $\Delta E$  plastic scintillation detectors (1 mm NE102A) and two circular E-scintillation detectors (17.5 mm NaI, diameter 140 mm) with an entrance window of  $75 \mu\text{m}$  aluminium. Because proton energy spectra for incident neutron energies less than 50 MeV suffer from energy loss straggling of the protons in the air gap between the target and the E detector a vacuum chamber has been constructed. Four target positions cover an angular range from  $4.8^\circ$  to  $30.1^\circ$  in the laboratory system. The charged particles have to travel through 26 cm air at most. We will use  $125 \mu\text{m}$  polyethylene ( $\text{CH}_2$ ) and  $100 \mu\text{m}$  carbon as targets on each target position.

A new multiwire proportional chamber has been constructed as monitor to measure the flux and the spatial distribution of the polarized neutron beam from POLKA (2). Charged particles produced by a  $\text{CH}_2$ -converter enter the gas

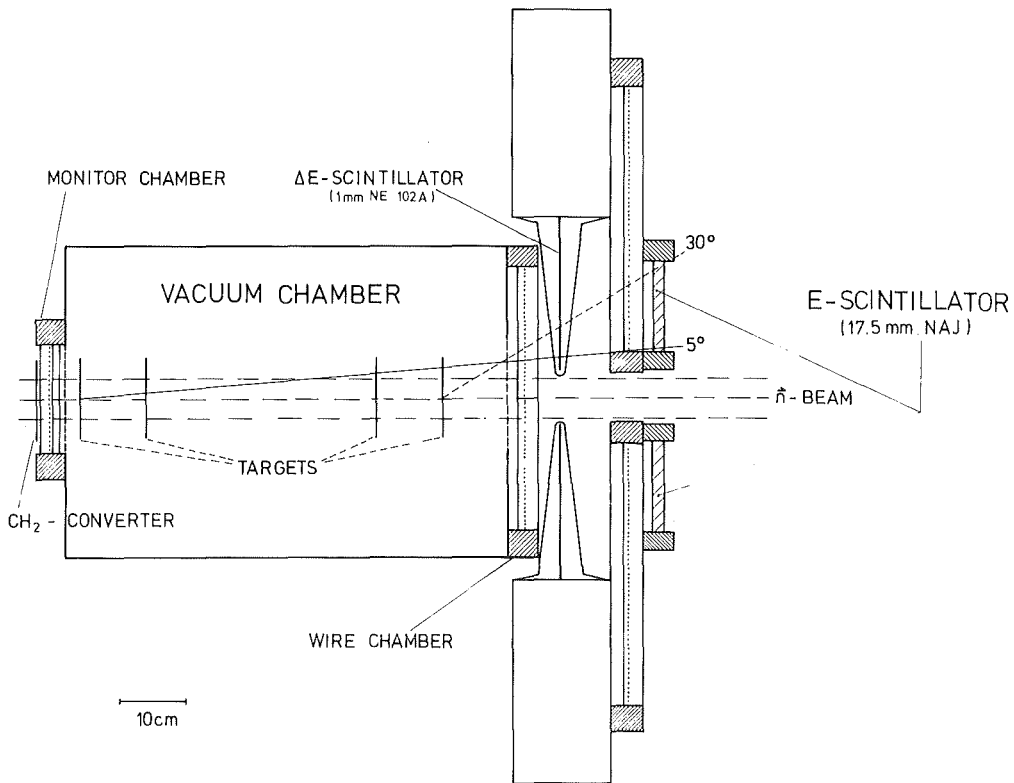


Fig.1: Schematic view of the set-up

volume of the chamber which consists of an x and y wire plane of 72 gold plated tungsten wires having a diameter of 20  $\mu\text{m}$  and a wire spacing of 2 mm. Each anode wire plane is centered between two cathode planes made of 3  $\mu\text{m}$  aluminized mylar foil. The two crossed anode wire planes cover an area of 164 x 164  $\text{mm}^2$ . The distance between the anode and cathode plane is 5 mm. The read-out of the anode wires is made by a 50  $\Omega$  delay line. The monitor has been tested with several argon-isobutane-freon (13B1)-methylal gas mixtures.

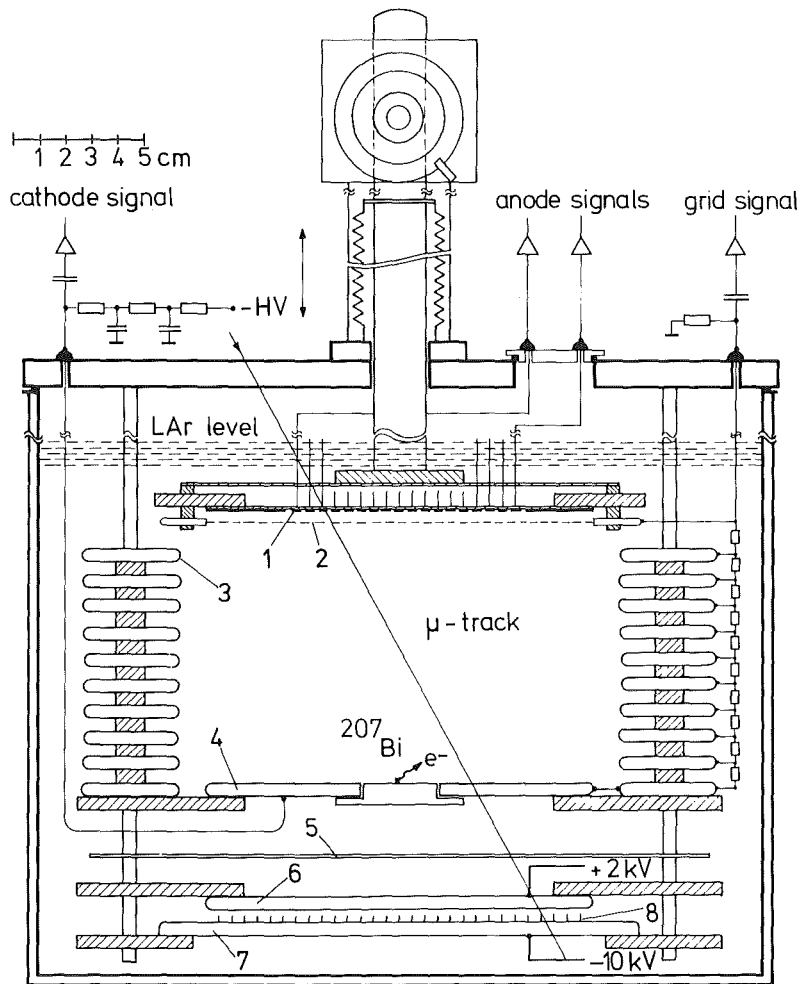
The authors would like to thank K.Kärcher and A.Höhne for their support.

- (1) P.Doll et al., KfK report 3969 (1985) p.155
- (2) H.O.Klages et al., NIM 219 (1984) 269

### 5.1.8 LIQUID ARGON TIME PROJECTION CHAMBER

G.Giorginis, D.Mann, S.Wölfle, H.Gemmeke, R.Maschuw, B.Zeitnitz

Work on the liquid argon time projection chamber has been continued. Fig.1 shows the chamber construction. Especially long term stability against signal decrease due to outgassing impurities has been investigated. A convenient method for purification was developed using electron injection into the liquid by corona discharge. The purification cell was mounted below the drift chamber as shown in Fig.1. The injected electrons are attached to impurity molecules which are collected on the electrodes. Fig.1 demonstrates the method, showing the signal recovering after electron injection.



- |                      |                        |                                  |
|----------------------|------------------------|----------------------------------|
| 1.segmented anode    | 5.shielding electrode  | □ stainless steel and resistors  |
| 2.Frisch grid        | 6.purification anode   | ▨ plastics insulator             |
| 3.field shaping ring | 7.purification cathode | ▲ ultra high vacuum feed through |
| 4.cathode            | 8.tungsten tips        |                                  |

Fig.1: Schematic cross section of the LAr TPC. The purification cell consists of the parts 6 to 8.

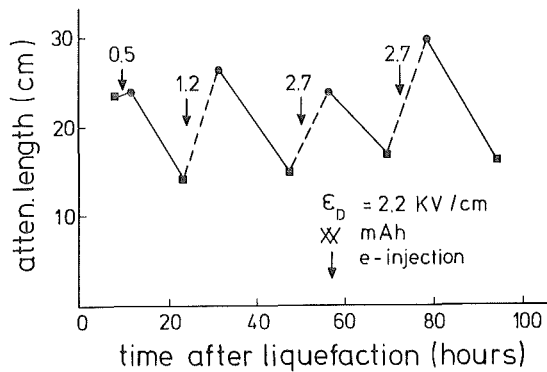


Fig.2: Attenuation length as function of time before (squares) and after (circles) purification.

5.1.9 IONIZATION CHAMBERS USING ROOMTEMPERATURE LIQUIDS

J.Engler, H.Keim, M.Cettert, A.Hoss, J.Knapp

R&D work on ionization chambers using molecular, room temperature liquids was pursued along different lines of investigations.

- A grid ionization chamber has been built as a test and monitor device. It uses the conversion electrons of a <sup>207</sup>Bi source. With this chamber the radiation hardness of liquid ionization chambers has demonstrated for the first time. The pulse-height dependence on radiation doses is shown in Fig.1. At extreme rates we observe a decrease in charge output. We explain the effect as volume formation of electronegative compounds. At medium dose rates, however, we observe an increase of the signal demonstrating that the liquid becomes purified.

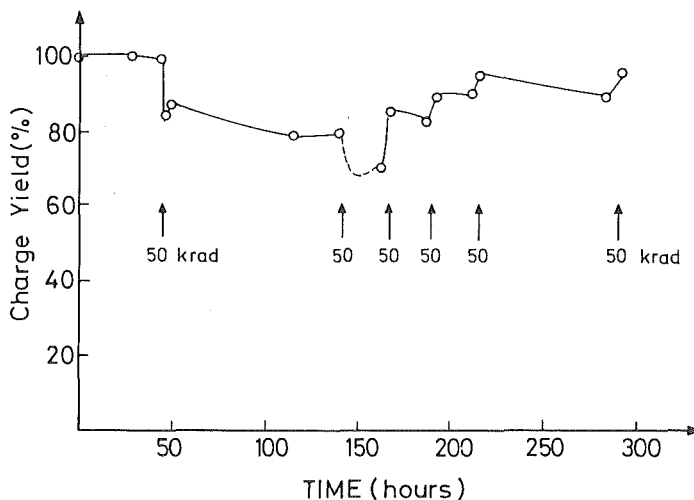


Fig.1: Signal yield in a chamber using tetramethylsilane. The first two doses were applied in 3 seconds each. The last four in 10 minutes each.

- Construction of 3 modules of an U-TMS calorimeter has been continued. All Uranium plates are encapsuled and tested against leakage. A cosmic ray test of a module is actually under way.
- Two pure hydrocarbon liquids, neopentane and isononane have been purified and tested with cosmic ray muons and  $^{207}\text{Bi}$  electrons. In Fig.2 the muon signals at two voltage settings are shown for neopentane.

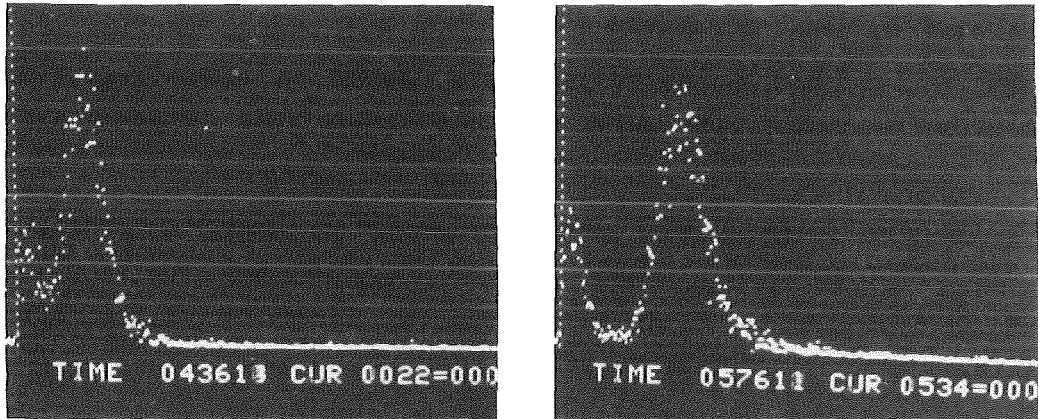


Fig.2: Cosmic muon signal in a neopentane chamber at two voltage settings of 2 kV and 6 kV.



## 5.2 INSTRUMENTATION

### 5.2.1 A $^3\text{He}$ EVAPORATION CRYOSTAT

T.Strobelt, W.Heeringa, P.Jany

To study the behaviour of superconducting thin film tunnel junctions as particle detectors, a  $^3\text{He}$  cryostat has been designed and constructed. Superconducting junctions can be employed as photon or particle detectors if they are cooled well below the transition temperature, see also contr. 5.1.6 of this report. We plan to produce junctions of Al, In and Sn with critical temperatures of 1.2 K, 3.4 K and 3.7 K, respectively. Therefore we decided to build a  $^3\text{He}$  evaporation cryostat, with which a lowest temperature of about 0.3 K can be reached.

The lay-out of the cryostat is shown in fig.1. It contains a large experiment chamber of about  $900\text{ cm}^3$ . The  $^3\text{He}$  is precooled and liquified in a  $^4\text{He}$  bath which is pumped to 1.3 K. This bath can be continuously filled through a needle valve.

The cryostat can be operated either in single shot mode or in continuous mode. In the first case the operation time is more than one day. In the second case the  $^3\text{He}$  is circulated through a capillary tube of 120 cm length and 0.10 mm diameter. Easy maintenance was achieved by the use of a turbomolecular pump instead of an oil diffusion pump in the  $^3\text{He}$  system.

In the first runs a lowest temperature of  $340 \pm 40\text{ mK}$  was achieved. The temperature was measured with carbon resistors. More accurate temperature sensors will be installed in the near future.

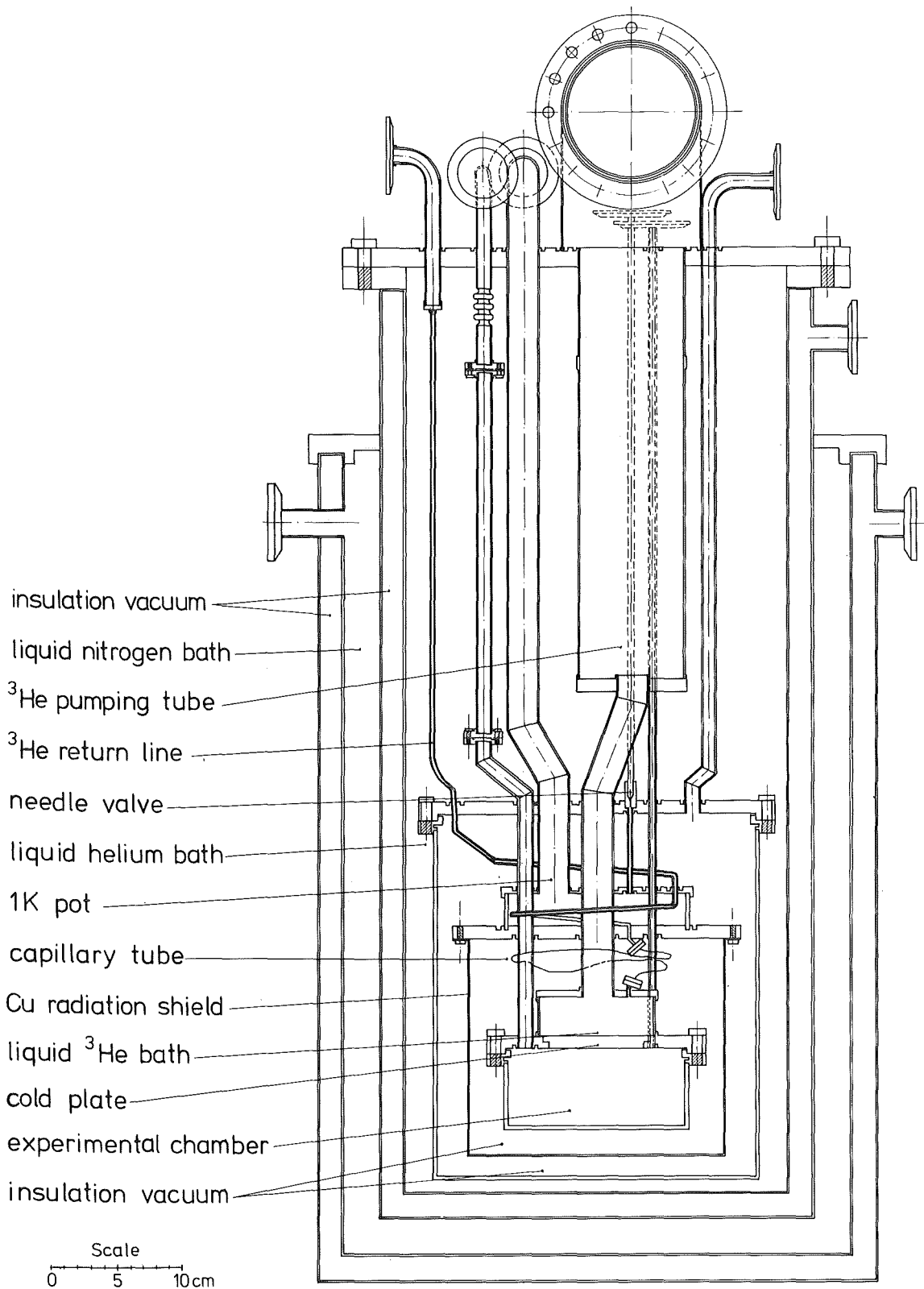


Fig.1: Layout of the  $^3\text{He}$  cryostat.

### 5.2.2 SCALER-MULTIPLEXER: THE FIRST LAYOUT ATTEMPT USING THE SOPHISTICAD LAYOUT-SYSTEM

G.Schmalz

The Scaler-Multiplexer is part of the electronics used by the neutrino experiment which is installed in the Rutherford Appleton Laboratory, Chilton, GB.

The layout of the printed board of this device was realized with the interactive layout system SophistiCAD, running on a 68000-Processor and an additional graphic Processor with a high resolution colour display. The result is shown in fig.1.

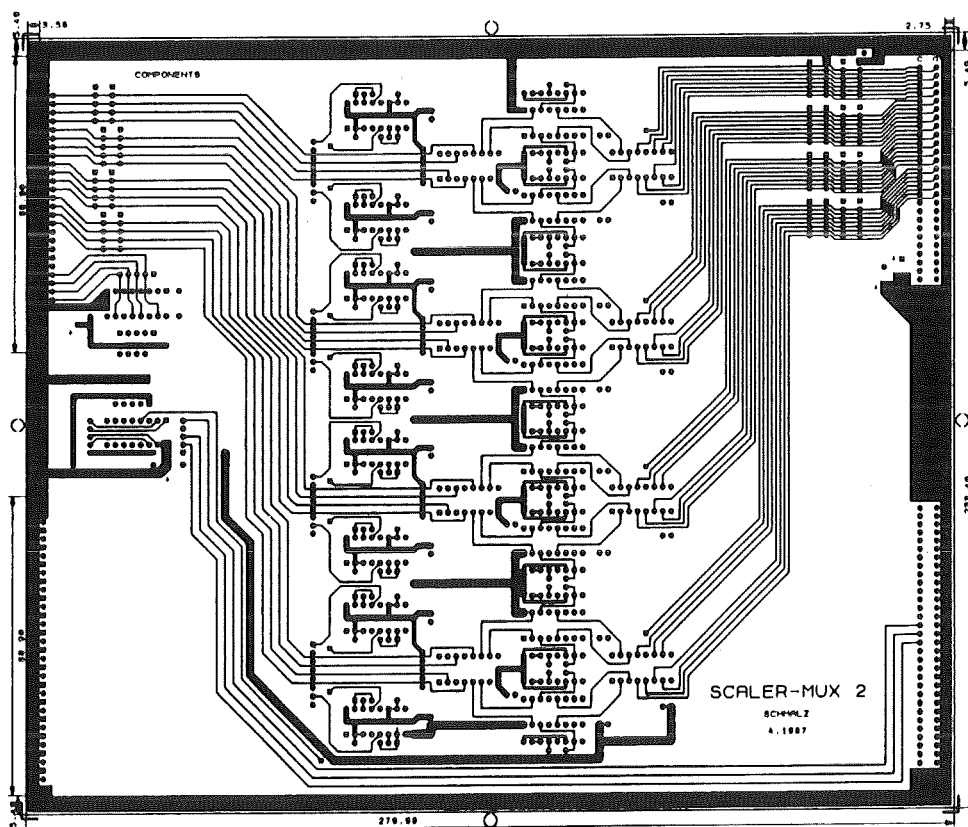


Fig.1: Component-Side of the Sc-Mux.

5.2.3 A CAMAC CONTROLLED LINEAR GATE

H. Müller

The complexity of the 4n BaF<sub>2</sub> detector requires on line data selection to avoid overloading of the data accumulation system. Therefore, a fast decision on the relevance of an event will be made using the fast component of the scintillation light from all modules. But once an event is accepted, the true total energy is determined only from those modules which were really hit in order to optimize the signal to noise ratio.

For this purpose a linear gate was built that can be used along with the CAMAC electronics for timing and logic signals (Fig. 1). Four linear gates were integrated in a CAMAC module of 1/25 width. The input signal (~2 μsec wide) is delayed by 200 ns and fed into an operation amplifier LH 0032, whose gain and offset can be tuned via a 8 bit DAC. The gain can be changed over a range from 1 to 1.3 thus leaving the bandwidth of the amplifier almost unaffected. This is an essential feature, as the high voltage is chosen to yield equal pulse height in the fast component; therefore, proper adjustment of the energy signals is performed via the gain of the linear gate. The offset can be varied by 25 mV with a resolution of 100 μV. The so adjusted signal is fed to a buffer amplifier LH 0033 and then to an analogue switch AM 1000 with an ON resistance of ~30Ω adapted to the output. A second output with high resistivity serves for monitoring. The width of the gate signal is determined by a timer (SN 7412 N) whose time constant delay can be set by a 8 bit DAC up to ~ 10 μsec.

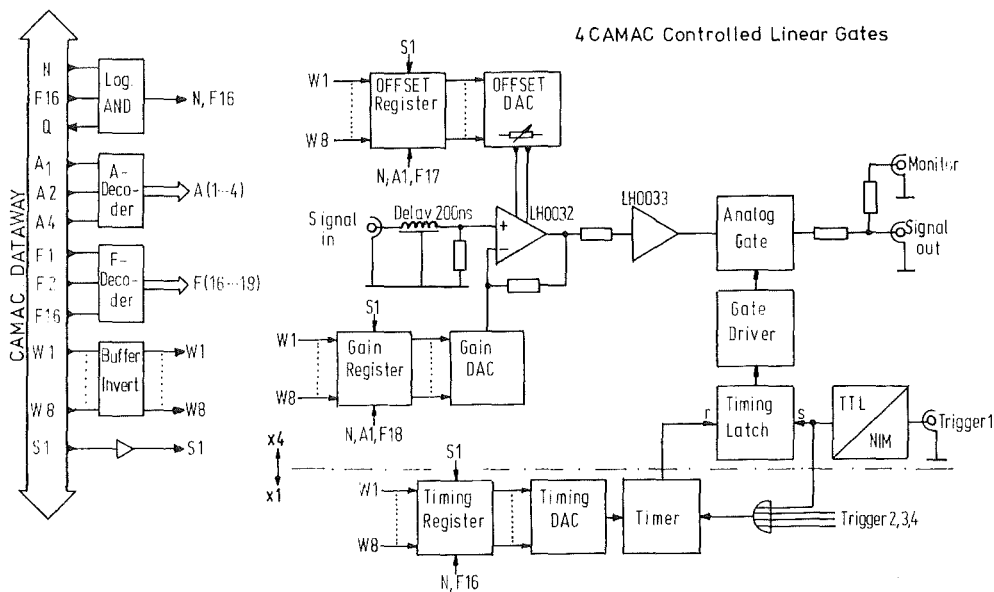


Fig. 1 Block diagram for the CAMAC controlled linear gates

The design has considered the possibility that the adjustable ranges for gain, offset and gate width may not always satisfy the experimental requirements. For this reason the DAC are built from digital switches (HEF 4066) and metal film resistors of the E 24 series so that the possible ranges can easily be modified by exchanging the metal film resistors.

#### 5.2.4 EXTENSION AND IMPROVEMENT OF THE DATA ACQUISITION SYSTEM FOR THE MAGNETIC SPECTROGRAPH "LITTLE JOHN"

S. Zagromski, H.J. Gils, D. Manger, J. Kiener

The data acquisition system for the magnetic spectrograph "Little John" and for other charged particle experiments at the cyclotron (1) was extended and improved with respect to the multi-group coincidence branch. This branch consists of 16 ADCs (Laben-models 8116 and 8215), 4 local ADC-Control-Units (Fig. 1, Mod. 8232), 1 Master-Control-Unit (Mod. 8233), 1 Double-Parallel-Datatransfer-Unit (Mod. 8171) and two Camac-Interfaces (Mod. 5911). The data are sent to two independently working computers PDP 11/73 which are Camac-modules, working in the respective Camac-crates. One computer is used for fast data-transfer to magnetic tape and the second one performs on-line processing.

The ADC system was designed and built by LABEN (Italy) according to our specifications. Final tests and improvements were done at KfK when the complete system was mounted. Advantages of this system for measurements in nuclear physics are high quality of the 13 bit-ADCs (successive approximation method, small conversion time of 9  $\mu$ s and small integral nonlinearity of 0,025%) and flexibility in coincidence requirements.

Groups of ADCs which fire in a preselectable time interval represent a coincidence group. Valid coincidence groups are also preselectable by Camac, where each of the ADCs may be combined with any one or more of the other ADC's. Coincidence groups are encoded for reconstruction and transmitted event by event to the computers. A buffer of 512 words (24bit) in the Master-Control-Unit may be selected by Camac. ADCs that fire, but do not fit in any preselected coincidence group, may be transmitted in separate data packages to the computers.

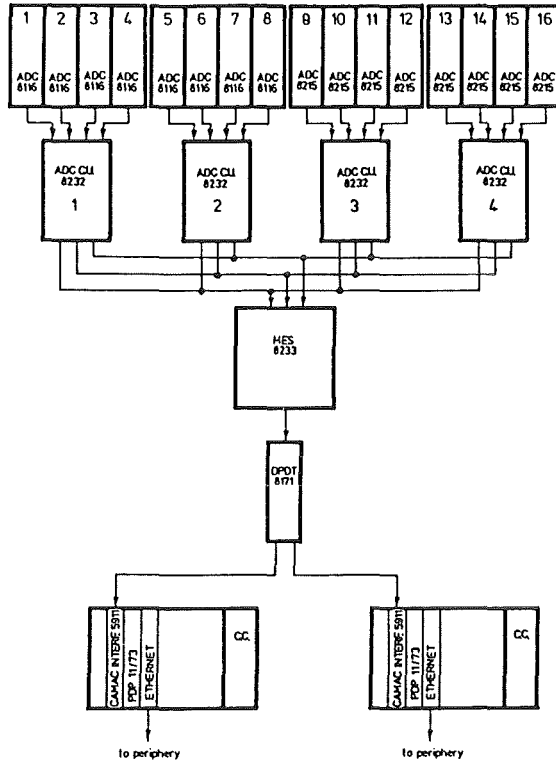


Fig. 1 Block scheme of the ADC system

- (1) H.J. Gils, J. Bialy, H. Schlösser, S. Zagromski, Report KfK 3969, Kernforschungszentrum Karlsruhe (1985) 176

### 5.3 ACCELERATORS

#### 5.3.1 OPERATION OF THE KARLSRUHE ISOCHRONOUS CYCLOTRON (KIZ)

F. Schulz, H. Schweickert

During the period of report the isochronous cyclotron KIZ was in full operation (Tables 1 and 2). The 6800 h of beam time available for our users is one of the largest numbers we could ever deliver per year. But even with that almost continuous round the clock operation we could not fulfill all the beam time requirements. 1986/87 our machine was overbooked by more than 20 %. Therefore there was only little time available for improvements of components and subsystems:

- The 90°-bending element for the injected beams coming from the ion source building was exchanged with an advanced achromatic system giving better possibilities to adjust the injected beam on to the axis of the beam guiding elements inside the magnet.
- The components of the high energy external beam guiding system are now all connected for implementation of the Simatic Logic. The switch over to the new PDP-11/73 based control and monitor system (see 5.3.4) was delayed because of manpower problems.
- An additional axial slit was installed in the SW-Dee in order to improve the beam quality for extraction. First results show that using this new slit the extraction efficiency for  $\alpha$ -particles could be increased from 50 % to 60 %. This is especially important for the high intensity extraction of  $\alpha$ -particles for the dual beam experiments.
- The old energy degrader in the beam line right after the extraction was replaced by a new one. Fig. 1 shows a photograph of the new beam line segment before installation. The degrader consists of Be-plates whose thickness varies from 2 mm to 4 mm in steps of 0.25 mm.

Cyclotron Operational	With Internal Ion Source		With external Ion Source		Total	
For Experiments Beam Development Testing new Components Developments for Isotope Production	2830 h	33.9 %	3982 h	47.6 %	6812 h	83.9 %
	392 h	4.7 %	272 h	3.3 %	665 h	8.0 %
<b>Total Time of Operation with the Beam on Targets</b>	<b>3222 h</b>	<b>39.5 %</b>	<b>4255 h</b>	<b>50.9 %</b>	<b>7477 h</b>	<b>89.1 %</b>
Scheduled shut-down for Maintenance, Repair and Installation	307 h	3.7 %	68 h	0.8 %	375 h	4.5 %
Unscheduled Shut-down	243 h	2.9 %	265 h	3.2 %	508 h	6.1 %
<b>Total Shift Time</b>	<b>3772 h</b>	<b>45.1 %</b>	<b>4588 h</b>	<b>54.9 %</b>	<b>8360 h</b>	<b>100 %</b>

\* Polarized Deuterons 2395 h;  ${}^6\text{Li}^{3+}$ -Ions (156 MeV) 1860 h

Table 1: Beam statistics of KIZ from July 1986 to June 1987

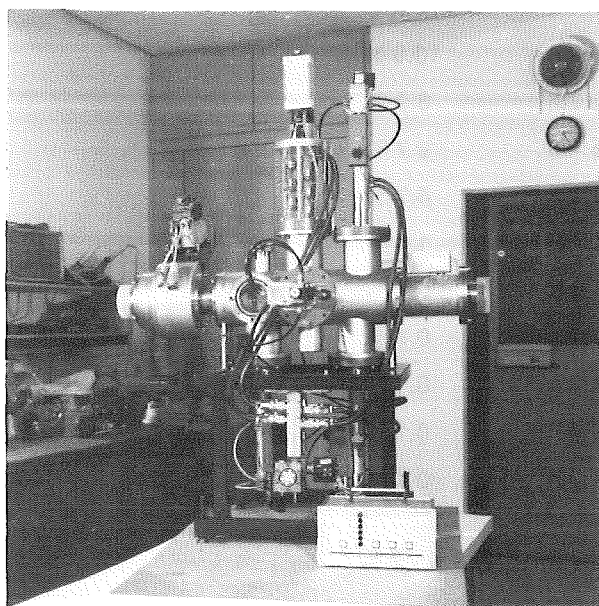
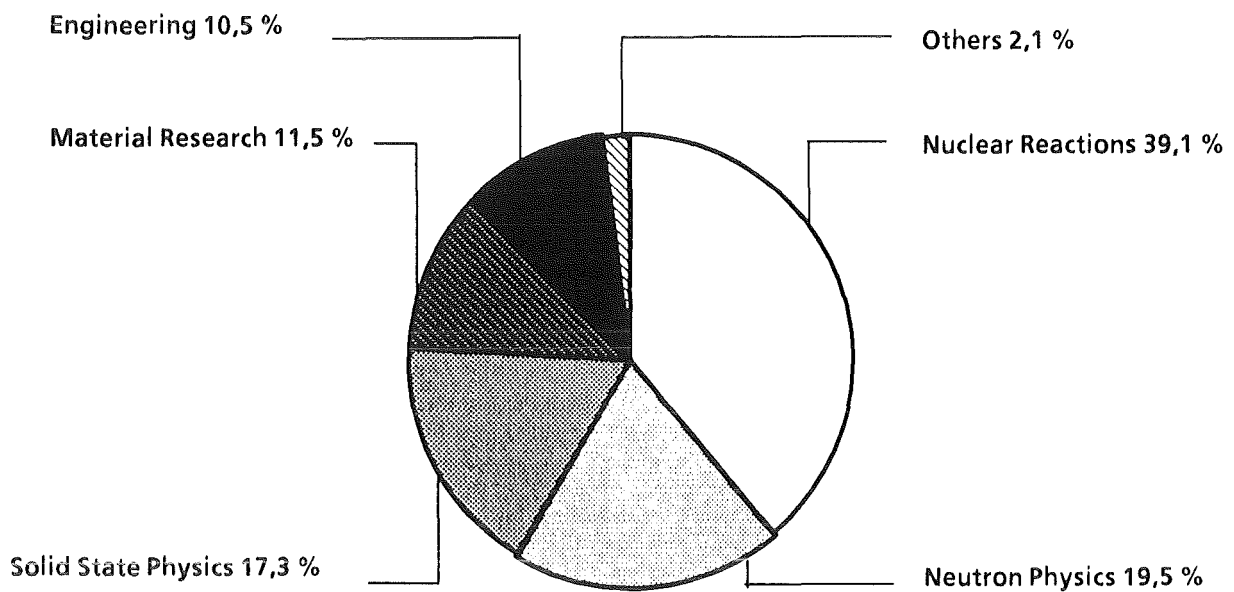


Fig. 1

New beam line segment right after extraction before installation. The beam enters from the right side through a capacitive probe, a beam stop and a diaphragm unto the energy degrader. Behind the degrader a ZnS screen and fast closing valves are installed.





### Internal Users

Institut für Kernphysik III	1263.6 h	18.5 %
Institut für Kernphysik I	1203.4 h	17.6 %
Institut für Material u. Festk.-Forsch.	604.6 h	8.8 %
Institut für Radiochemie	15.0 h	0.2 %
Institut für Heiße Chemie	1.0 h	0.1 %
	<hr/>	<hr/>
	3087.6 h	45.3 %

### External Users

Universität Tübingen	879.1 h	12.9 %
Universität Erlangen	688.5 h	10.0 %
Freie Universität Berlin	556.2 h	8.2 %
Technische Universität München	456.4 h	6.7 %
Max-Planck-Institut Heidelberg	321.2 h	4.7 %
Universität Ulm	98.7 h	1.4 %
Universität Münster	56.8 h	0.8 %
Technische Hochschule Darmstadt	7.7 h	0.1 %
Universität Bonn	4.5 h	0.1 %
Universität Heidelberg	3.4 h	0.1 %
DKFZ Heidelberg	1.2 h	0.1 %
	<hr/>	<hr/>
	3073.7 h	45.2 %
Irradiation of Machine Parts	651.0 h	9.6 %
	<hr/>	<hr/>
Total	6812.3 h	100 %

Table 2: Use and users of KIZ from July 1986 to June 1987

### 5.3.2 OPERATION OF THE COMPACT CYCLOTRON (KAZ)

J. Möllenbeck, H. Schweickert

During the period of report the cyclotron was operated for isotope production and activation of machine parts as well as for basic research. Only about 50 % of the maximum available machine time is now booked.

The availability of the machine was again excellent and no major breakdown occurred during operation. The mean breakdown rate is now lower than 4 % with respect to the scheduled operational time.

A short shutdown period around New Year was used to extend the energy range for the beams to be extracted for the machine parts irradiations from 20-30 MeV up to 20-40 MeV.

The lifetime of the D-insulators could be considerably improved by changing the mechanical design and by using better insulator materials. By this, the service intervals could be extended by a factor of 3 which results in a considerable reduction of the dose to the operational staff.

### 5.3.3 STATUS OF EXTERNAL ION SOURCES

H.P.Ehret, R. Ernst, L. Friedrich, E. Huttel, J. Kaltenbaek,  
F. Schulz, L. Wiss, P. Ziegler, U. Zimmermann

Further attempts have been undertaken to get a polarized beam of higher quality.

One turbopump has been shifted from the hexapole chamber to the dissociator chamber and the leakage from the dissociator to the hexapole chamber was reduced in order to reduce atomic beam losses by gas scattering. As a result the atomic beam intensity was not increased but the molecular background was reduced by 50 %, thus the 2200 l/s pumping capacity is not a limiting factor.

The emittance of the horizontal beam has been measured (Fig. 1). A cylindrical beam is now achieved by a spherical deflector and a focus in the middle of the deflector can be deduced from the emittance diagram.

A He refrigerator cooling of the atomic beam designed by SENTEC had been installed. This design and several modifications failed because of recombination in the Macor accommodator. A Teflon accommodator had a short lifetime of several hours only. Fig. 2 shows the resulting beam intensity as a function of the temperature, confirming the same behaviour as reported by the groups at ETH and SIN. But the optimum of the gas flow

reduced to half the value typical for LN<sub>2</sub> operation, thus the gain due to the larger hexapole acceptance and ionizer efficiency was cancelled. We decided to operate the source with LN<sub>2</sub> cooling and start an own He-refrigerator-cooled atomic beam development seperately.

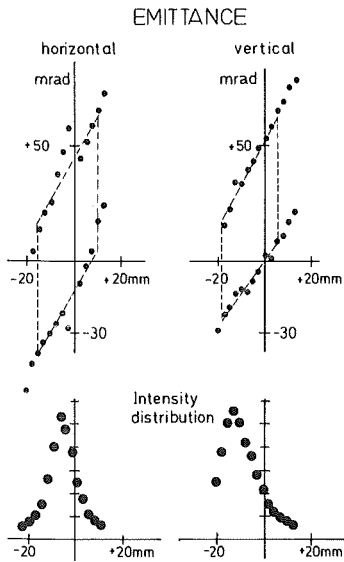


Fig. 1: The measured emittance corresponds to a polarized beam of 10 keV, about 1000 mmxmrads and 30  $\mu$ A

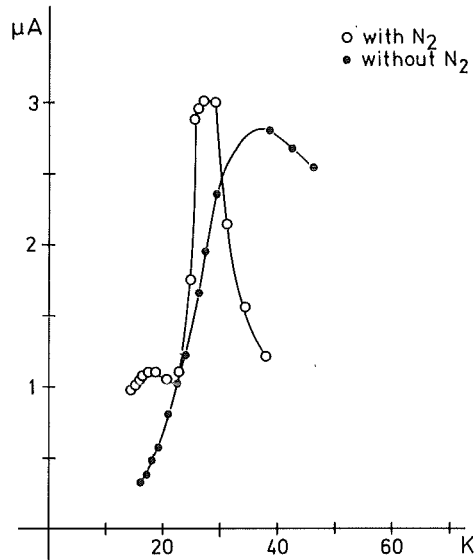


Fig. 2: Intensity of the polarized deuterons as a function of the nozzle temperature with and without N<sub>2</sub> added to the D<sub>2</sub> gas

The present state of the ECR source LISKA is characterized by the charge state distribution (CSD) given in Fig. 3. From the CSD of the <sup>7</sup>Li ions an intensity of the <sup>6</sup>Li<sup>3+</sup> ions of about 15  $\mu$ A can be deduced of which 0.2  $\mu$ A can be extracted from the cyclotron. The CSD was measured behind a

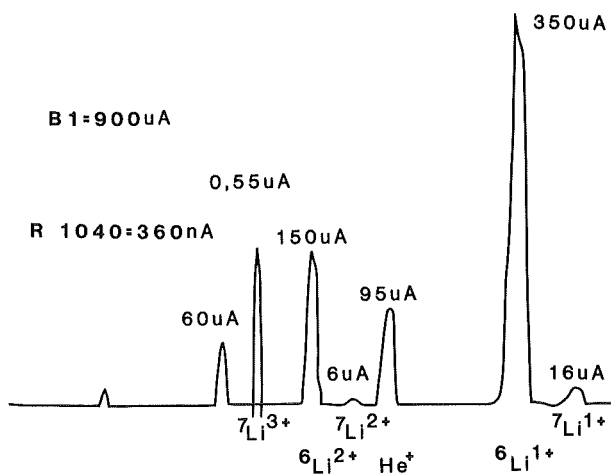


Fig. 3  
Charge state distribution of the Li ions from Liska

double focusing  $90^\circ$  magnet installed directly behind the source, replacing a Wien filter and an electrostatic deflector and comprises 75 % of the total current delivered by the source.

The  ${}^6\text{Li}^{3+}$  yield was optimized using a first stage ECR which ionizes the Li vapor instantly after leaving the oven. The microwaves are coupled into this stage through  $0.2 \times 20$  mm slits. Fig. 4 shows the present configuration of this first stage. A small amount of the buffer

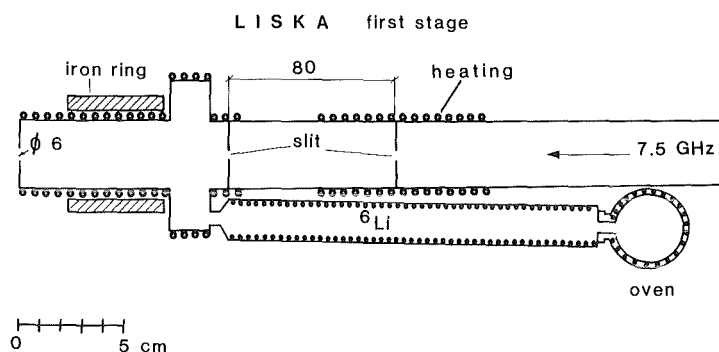


Fig. 4  
Liska, first stage

gas He is still needed to stabilize the plasma. This new first stage showed to be very helpful to optimize the CSD and the Li consumption. It will be subject of further improvements.

#### 5.3.4 THE NEW COMPUTER CONTROL SYSTEM OF THE KIZ BEAM LINES

J. Bialy, J. Eulenfeld, H. Heinzmann, W.R. Kappel, M. Schmitt,  
T.J. Thouw

The new Computer Control System to control and monitor the Karlsruhe Isochronous Cyclotron (KIZ) beam line elements is a powerful and flexible distributed intelligence system of modular design, both in the hard- and software.

The main components of the control system are:

1. A complete PDP-11/73 computer (including disk, backup tape etc.).
2. Stand alone "Starburst" computers (PDP-11/73 CPUs in a Camac modul), including Camac crate based, control and monitor, I/O modules.
3. Siemens Simatic Logic Programmiers plus their bus oriented I/O modules.
4. Micro processors for dedicated special functions.
5. A 10 Mbit/s base band Ethernet Local Area Network (LAN), slow/fast Ethernet interface moduls and controllers.

6. Completely table driven software written in Fortran for the PDP's, including off-line dialog programs for generating the touchpanel pictures, database, blockdiagrams, tables etc.
7. Flexible and compressed database with auto generated database pointers for up to 1024 database entries.
8. General communication software PDP/SIMATIC which allows user defined communication codes.

System control on this system is done via one operator consol consisting of a keyboard and CRT for startup and message display, touchpanels for all knob assignments, simple actions and complex "procedures", potentiometer knobs for analog actions such as vario TV cameras and power supplies control. Also part of the control consol are the b/w and color display monitors which show the blockdiagrams, magnet currents values, beam diagnostic information, vacuum and interlock situation.

Live update and display, using blockdiagrams and alphanumeric text, for all crucial elements down to the bit level is accessible through easy touchpanel handling.

The various PDP's and Logic Programmers do actions as defined by the control software so that each local system can be used for almost every purpose.

PDP computers communicate through the Ethernet Network using standard Ethernet interfaces and Decnet protocol, whereas the communication between the PDP's and the Logic Programmers/Micro Processors is a byte string, transmitted between RS-232 interconnections.

The dialog between all the computers of the entire system is entirely transparent to the operator.

Almost all of the off/on-line control software is written in Fortran and the on-line part consists mainly of completely table driven and "quasi independent" modular tasks.

Interrupt handling plus tasks priority structure allows fast response to operator controlled or operator independent system actions, at any time. The tasks communicate and synchronizise with each other by using Significant Event flags, task "busy" and "buffer" flags, buffers, plus fast and slow wait loops.

Data and tables are stored in dynamic regions, allowing tasks to access data simultaneously by window technique.

Flags, pointers and other important data are stored in a global common area, which again is a dynamic region attached to all tasks at run time.

Both the hard and software are so flexible that almost every possible future expansions can be incorporated by off-line tables expansion and/or by adding "quasi-independent" additional tasks, without recompiling or relinking the existing system.

A rudimentary version of the system, which will already have all the basic structures mentioned above, will be tested and debugged in October 1987.

## 5.4 APPLICATIONS

### 5.4.1 ELEMENTAL AND TRACE ELEMENT DISTRIBUTION IN MEDICAL SAMPLES: ANALYSIS BY PROTON INDUCED X-RAY EMISSION

C. Spieker\*, D. Heck, W. Zidek\*, T. Stratmann\*,  
D.P. v. Bassewitz\*\*, H. Losse\*, H. Vetter\*, H. Zumkley\* (1)

The analysis of trace elements is performed by proton-induced X-ray emission. The process is most effective if the velocity of the exciting particles - protons - is similar to the velocity of the electron on its orbit in the simple atomic model of Bohr. For K-shell electrons of the elements with  $15 \leq Z \leq 40$  this requires proton energies of a few MeV available from electrostatic Van-de-Graaff accelerator machines. After knocking out the K-shell electron the empty place is filled up by electrons jumping from higher orbits with simultaneous emission of characteristic X-rays, which are registered with a cooled Si(Li) detector. By a set of electrodes the beam can be swept across the specimen surface. Therefore, this method yields an excellent correlation of trace element distribution within the morphological structure of organic tissue. In the present study the sweep went along a line perpendicular to the arterial wall layers (aortic, renal and heart muscle) of normotensive and spontaneously hypertensive rats. Along this line all elements are recorded simultaneously. These are P, S, Cl, K, Ca, Fe, Cu, Zn, Br and Sr. The trace element content of the aortic wall and the renal artery of 22 spontaneously hypertensive and 11 normotensive rats and of human heart muscle was investigated.

The results demonstrate that Zn was only detected in the muscle-containing layers of the arteries. There was no different distribution between hypertensive and normotensive rats. However,  $Ca^{2+}$  was mainly detected in the smooth muscle-containing tunica media of hypertensive rats. Thus by comparison of Zn and  $Ca^{2+}$  distributions in the tissue, a better identification of the different layers of the arterial wall could be achieved. The results of this study reveal that trace element analysis with PIXE yields valuable additional information on trace element distribution in organic tissue.

(1) Meth. and Find. Exptl. Clin. Pharmacol. 8 (1986) 363

\* Med. Univ. Poliklinik, Münster

\*\* Gerhard Domagk Institut für Pathologie, Münster

5.4.2 Ca<sup>2+</sup>-METABOLISM IN ARTERIES OF SPONTANEOUSLY HYPERTENSIVE RATS:  
ASSESSMENT BY PROTON INDUCED X-RAY EMISSION (PIXE)

C. Spieker\*, D. Heck, W. Zidek\*, H. Losse\*, H. Vetter\* (1)

Changes of intracellular Ca<sup>2+</sup> metabolism have been discussed to be of importance for the pathogenesis of essential hypertension. In the present study the particle induced X-ray emission was used to get information on the spatial distribution of Ca<sup>2+</sup> in aortas and renal arteries of hypertensive (SHR) and normotensive rats.

Our findings demonstrate a significant Ca<sup>2+</sup> elevation in the aorta and renal artery of SHR versus normotensive rats (3317±734 µg Ca<sup>2+</sup>/g tissue vs. 1623±569 µg Ca<sup>2+</sup>/g tissue and 3432±1867 µg Ca<sup>2+</sup>/g tissue vs. 1050±554 µg Ca<sup>2+</sup>/g tissue, respectively).

(1) Journal of Hypertension 4(suppl. 5) (1986) 122

\* Med. Univ. Poliklinik, Münster

5.4.3 DISTRIBUTION OF TRACE ELEMENT CONCENTRATIONS IN MORRIS  
HEPATOMA 7777

T. Cichocki\*, D. Heck, L. Jarczyk\*\*, E. Rokita\*\*,  
A. Strzalkowski\*\*, M. Sych\* (1)

In Morris hepatoma 7777 and liver samples the concentrations of the elements Cl, K, Ca, Fe, Cu, Zn and Br, and their localization were determined by the micro-PIXE (proton induced X-ray emission) method with a spatial resolution of less than 15µm. Higher average concentrations of Ca and Br and lower of Fe were observed in tumor in comparison with liver. The Cu content in the liver of a tumor bearing rat was distinctly lower than in a control liver. High, narrow peaks were found in the distributions of Ca, Fe and Zn concentrations.

(1) Cancer Letters (in print)

\* Academy of Medicine, Kraków, Poland

\*\* Institute of Physics, Jagellonian University, Kraków, Poland



#### 5.4.4 ELEMENTAL COMPOSITION OF HUMAN AORTA IN MARFAN SYNDROME

T. Cichocki\*, D. Heck, L. Jarczyk\*\*, E. Rokita\*\*,  
A. Strzalkowski\*\*, M. Sych\* (1)

The distribution of concentrations as well as mean contents of P, S, Cl, K, Ca, Fe, Cu, Zn and Br were determined in a wall of human aorta affected by Marfan syndrome (MS). The mean contents of Cl, Fe and Cu were twice as high and the K level was one order of magnitude lower in aorta with MS when compared with reference atherosclerotic cases. Identical distributions of concentrations obtained for P and Ca confirm the presence of Ca-P crystalline deposits, however, their number is lower than in aorta without MS matched with age.

(1) Pathologica (in print)

\* Academy of Medicine, Św. Anny 12, Kraków, Poland.

\*\* Institute of Physics, Jagellonian University, Kraków, Poland

#### 5.4.5 TRACE ELEMENT METABOLISM IN LIVER CELLS AFTER COPPER SULFATE UPTAKE

D. Heck, A. Ochs\*, H. Thom\*\*, H.P. Buscher\* (1)

The importance of copper in liver cirrhoses is still unclear. This we want to brighten up in an in-vitro experiment. Hepatocytes are cultured on foils to form cellular monolayers, which are exposed to CuSO<sub>4</sub> solution. The trace elements P, S, Cl, K, Ca, Fe, Cu, Zn and Br are determined by PIXE, sweeping the proton microbeam in two dimensions across selected regions of the cell cultures. The concentration averages over positions covering the interior of hepatocytes or the intercellular gaps are formed and the behaviour of the various trace elements is studied in dependence on the copper solution exposure time. In some cases cell nuclei are identified and evaluated separately.

(1) Nucl. Instr. Meth. B (in print)

\* Medizinische Universitätsklinik II, Freiburg

\*\* Institut für organische Chemie und Biochemie der Universität,  
Freiburg

#### 5.4.6 THREE-DIMENSIONAL LITHIUM MICROANALYSIS BY THE ${}^7\text{Li}(p,\alpha)$ REACTION

D. Heck (1)

To investigate the corrosive behaviour of lithium in stainless steel, an analysis method is required, which gives lithium as well as the heavier constituents of the attacked steel with a positional resolution in the micrometer range. In the Karlsruhe ion microprobe the combination of the  ${}^7\text{Li}(p,\alpha)$  reaction with PIXE (for heavier elements) and with RBS (for carbon and oxygen) covers all interesting elements. With 3 MeV proton impact energy just above the broad reaction cross section maximum, the alpha particle count rate is optimized. The horizontal and vertical sweeping of the proton microbeam ( $\approx 2.5 \mu\text{m}$  diameter) across the specimen together with the energy loss of the alpha-particles on their way through the specimen to the detector reveal a three-dimensional lithium concentration distribution in the micrometer range. In the investigated samples of stainless steel the positional correlation of lithium with oxygen and chromium indicates the formation of lithium chromate complexes at the expense of the chromium content in the neighbouring zone.

(1) Nucl. Instr. Meth. B (in print)

#### 5.4.7 REPROCESSING OUTPUT VERIFICATION BY K-EDGE DENSITOMETRY

R. De Meester\*, H. Eberle, S. Johnson\*\*, L. Koch\*,  
I. Michel-Piper, H. Nackaerts\*\*\*, H. Ottmar, (1)

A K-edge densitometer is described which is used to analyse the U and Pu concentrations in reprocessing output samples. The isotopic composition of Pu is determined by gamma spectroscopy combined with the isotope correlation technique. Results of a field test and subsequent application for routine analysis for fissile material control purposes indicate that this method is highly accurate and reliable.

(1) Nucl. Safeguards Technology 1986, IAEA, Vienna (1987) Vol. 1, 233

\* European Institute for Transuranium Elements, Karlsruhe

\*\* Int. Atomic Energy Agency, Vienna

\*\*\* Euratom Safeguards Directorate, Luxembourg

5.4.8 FIELD DEMONSTRATION OF AN X-RAY DENSITOMETER FOR URANIUM AND  
PLUTONIUM INPUT VERIFICATION IN REPROCESSING

H. Ottmar, H. Eberle, L. Koch\*, R. De Meester\*,  
E. Kuhn\*\*, (1)

Experimental results and operational experience from the field demonstration of a combined K-edge/K X-ray fluorescence densitometer for uranium and plutonium input verification measurements are presented and discussed. The feasibility of fast input assay is demonstrated from measurements on representative dissolver solutions. Some practical aspects relevant for applications in international safeguards are outlined.

(1) Nucl. Safeguards Technology 1986, IAEA, Vienna (1987) Vol. 1, 201

\* European Institute for Transuranium Elements, Karlsruhe

\*\* Int. Atomic Energy Agency, Vienna

5.4.9 ENERGY-DISPERSIVE X-RAY TECHNIQUES FOR ACCURATE HEAVY ELEMENT  
ASSAY

H. Ottmar, H. Eberle, P. Matussek, I. Michel-Piper, (1)

Energy-dispersive X-ray techniques have been employed in two different ways for the accurate determination of element concentrations in specimens: 1. spectrometry of fluorescent characteristic X-rays as widely applied in the various modes of the traditional XRF analysis technique, and 2. spectrometry of the energy-differential transmittance of an X-ray continuum at the element-specific absorption-edge energies. The paper mainly focuses on the second technique of X-ray absorption-edge spectrometry and describes its application to the measurement of uranium and plutonium in process solutions from the reprocessing of spent nuclear fuels.

(1) Advances in X-Ray Analysis 30 (1987) 285

#### 5.4.10 DEMONSTRATION OF NDA TECHNOLOGY FOR REPROCESSING INPUT ANALYTICAL MEASUREMENTS

H. Ottmar, H. Eberle, L. Koch\*, (1)

A versatile, nondestructive system for the measurement of uranium and plutonium concentrations in process solutions from the reprocessing of spent nuclear fuels has been developed at KfK and successfully demonstrated in a hot cell environment at the European Institute for Transuranium Elements, Karlsruhe. The NDA system incorporates the proven X-ray techniques of K-edge densitometry and fluorescence analysis of K series X-rays. The feasibility of direct nondestructive uranium and plutonium assay in reprocessing input solutions using this system is demonstrated from measurements on actual dissolver solutions. The performance of the system is evaluated by comparing the results with those of parallel analyses performed by the conventional isotope dilution mass-spectrometry technique.

(1) J. of the Inst. of Nucl. Mat. Manag. Vol. XV (1986) 632

\* European Institute for Transuranium Elements, Karlsruhe

#### 5.4.11 EVALUATION OF HIGH-RATE PULSE PROCESSING IN K-EDGE DENSITOMETRY

H. Eberle, P. Matussek, I. Michel-Piper, H. Ottmar, (1)

Different pulse processing systems have been tested at high counting rates for K-edge densitometry measurements with a continuous X-ray beam. The total input counting rates presented to the gamma detector have been varied between 10 kcps and 100 kcps. This paper describes the results of the measurements, in particular the influence of high counting rates on the spectral resolution, on the pile up behaviour, on the throughput rate, and on the K-edge densitometry results.

(1) EUR 11041 EN, ESARDA 21 (1987) 179

#### 5.4.12 DESIGN OF A WAVELENGTH-DISPERSIVE PREFILTER FOR IMPROVED SENSITIVITY OF EDXRFA

P. Matussek, I. Michel-Piper

In energy-dispersive X-ray fluorescence (EDXRF) measurements on thick samples like liquids usually more than 99% of the total counts recorded by the detector are useless events arising from scattering of the excitation radiation in the sample. Since only a limited total pulse rate can be adequately handled by the pulse processing systems, this situation is detrimental to both the measurement precision for the analyte and to the detection capability at lower concentrations. For energy-dispersive L-XRFA there exists, however, a possibility to circumvent this problem to some extent without resorting to specially prepared thin samples. The solution consists of an energy-selective filter inserted into the beam path between sample and detector.

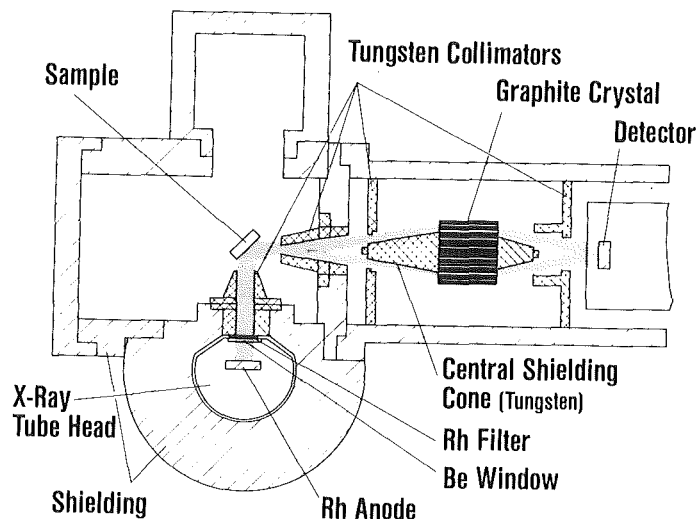


Fig. 1 Layout of a L-XRF system with improved sensitivity.

Following a suggestion of Berdikov et al. (1) we are currently setting up an improved energy-dispersive L-XRF system as schematically shown in Fig. 1. In this arrangement a cylindrical graphite crystal is located between sample and detector. It transmits only a relatively narrow energy band with the  $L\alpha$  X-rays from the actinide elements (13 - 15 keV). This filter with its central beam stop not only prevents the scattering radiation to reach the detector, but also shields the detector against the self-radiation from radioactive samples. In this set-up L X-rays from the actinides will efficiently be excited by means of an X-ray tube equipped

with a rhodium anode. With this configuration we expect to lower the detection limits to less than 0.1 mg/l for actinides in radioactive samples, which will make L-XRFA applicable, for example, to the uranium and plutonium analysis in a number of process solutions from various waste streams in a reprocessing plant.

- (1) V.V. Berdikov, O.I. Grigor'ev, B.S. Iohin, Nucl. Instr. Meth. 155 (1978) 313

#### 5.4.13 PARTICIPATION IN THE INTERLABORATORY EXERCISE REIMEP-86 FOR THE DETERMINATION OF THE $^{235}\text{U}$ ABUNDANCE IN $\text{UF}_6$ SAMPLES

H. Eberle, P. Matussek

The purpose of the Regular European Interlaboratory Measurement Evaluation Programme (REIMEP) is, like other programmes of similar type, to demonstrate the interlaboratory spread of measurements and to allow the participants to compare their measurement results to a certified value and to the results of other laboratories. Extending previous programmes the REIMEP-86  $\text{UF}_6$  exercise was not restricted to a particular measurement technique but included for the first time both mass spectrometry and gamma-ray spectrometry as representatives for destructive (DA) and non-destructive (NDA) measurement techniques. In case of the gamma-ray spectrometric assay the comparison with the routinely used and well established mass-spectrometric analysis provides the chance to demonstrate the potential of this NDA technique and to recognize the limitations for its application.

Highly accurate NDA determinations of the  $^{235}\text{U}$  abundance by means of gamma-ray spectrometry are only possible when the measurements are performed relative to well characterized calibration standards. An internationally certified reference material for NDA  $^{235}\text{U}$  abundance measurements is available since 1985 as EC-NRM-171/NBS SRM-969 from CBNM, Geel and NBS, Washington. It consists of a set of 5 well specified  $\text{U}_3\text{O}_8$  samples covering the range of  $^{235}\text{U}$  abundances from 0.3% to 4.5%. Our measurements of the REIMEP-86  $\text{UF}_6$  sample have been performed relative to this reference material.

The REIMEP-86  $\text{UF}_6$  sample was shipped in a well characterized monel can containing about 80 g  $\text{UF}_6$  as a solid sample. The areal density of the  $\text{UF}_6$  material of 8.2 g/cm<sup>2</sup> provided more than 99.9% of the 185 keV gamma

radiation perpendicular to the sample surface as compared to an infinitely thick sample. In such a quasi-infinite-thickness geometry the 185 keV gamma radiation originating from the decay of  $^{235}\text{U}$  serves as a direct measure for the  $^{235}\text{U}$  abundance. However, corrections have to be applied for the different matrix composition of the reference material and the unknown  $\text{UF}_6$  sample ( $\text{U}_3\text{O}_8 - \text{UF}_6$ ), for the different gamma attenuation in the container walls, and for counting losses due to pile-up and dead-time effects in the counting electronics.

In order to evaluate the accuracy limits of the method and to identify possible, so far unknown sources of systematic errors, very careful measurements have been performed to keep the influence of all measurement parameters affecting the assay accuracy as small as possible. The thickness of the container walls have been determined by means of an ultrasonic thickness gauge and by a precision micrometer (Zeiss Passameter) with error limits of 2  $\mu\text{m}$  and 0.5  $\mu\text{m}$ , respectively. In total, 61 measurements have been performed using a high-resolution GeLi detector. This results in about 50 million 185 keV gamma-ray counts accumulated in the gamma-ray spectra within a measurement time of 520 hours. 340 hours hereof were spent for the calibration, 180 hours for the measurement of the unknown  $\text{UF}_6$  sample. Pile-up and dead-time effects have been corrected by feeding an analog pulse from a counting-rate controlled pulser into the preamplifier of the gamma detector. After all corrections the  $^{235}\text{U}$  abundance of the  $\text{UF}_6$  sample was determined to

$$3.5005 \pm 0.0031 \% \text{ } ^{235}\text{U},$$

where the total error is given at the 2 $\sigma$  level i.e., the true  $^{235}\text{U}$  abundance value is expected to be within the error limits given with a probability of 95%. The certified  $^{235}\text{U}$  abundance value of  $3.5001 \pm 0.0010 \% \text{ } ^{235}\text{U}$  reported by CBNM after completion of the REIMEP-86 exercise compares very well with our result.

The long counting time required for gamma-spectrometric  $^{235}\text{U}$  abundance assays is inherent to the method due to the comparatively low surface-radiation intensity of the 185 keV gamma rays in low enriched uranium materials. In our case the contribution of the counting statistics to the total relative error of 0.09 % was about 0.07 %, whereas all other uncertainties (wall thickness,  $^{235}\text{U}$  abundance of the reference material) added up to 0.06%. However, the use of a larger sample of about 250 g  $\text{UF}_6$  as compared to only 80 g  $\text{UF}_6$  in the REIMEP-86 sample would have reduced

the counting time required for the indicated precision by more than a factor of 10.

Summarizing the results of the REIMEP-86 UF<sub>6</sub> exercise we note that gamma-spectroscopic <sup>235</sup>U abundance measurements can deliver results with a relative accuracy in the order of 0.1 % at 2σ when the assay system is calibrated with the EC-NRM-171 reference material. These error limits can be achieved within counting times of about 12 hours for large samples containing about 250 g low enriched uranium material. It was estimated that a counting time of only one hour is required for a relative assay accuracy of 0.2 % at 2σ using 250 g samples. This counting time and the achievable accuracy seems to be a good compromise for practical applications. The assay of samples with natural or depleted uranium will result in correspondingly longer counting time. The obvious disadvantages of the gamma-spectrometric <sup>235</sup>U abundance assay, namely the relatively large amount of sample material required, and the comparatively long counting time is partly compensated by the fact that this NDA technique necessitates no chemical preparation of the sample and only minimum handling of the sample material: Fill 250 g of the material to be assayed into a well specified sample container and start the measurement.

#### 5.4.14 ENERGY-DISPERSIVE XRF ANALYZERS FOR URANIUM MONITORING IN A REPROCESSING PLANT

I. Michel-Piper, H. Ottmar

Energy-dispersive X-ray fluorescence analysis (EDXRFA) is being considered as a potential technique for the in-line monitoring of uranium in a number of process streams within a reprocessing plant for spent nuclear fuels. The respective instrumentations, which should be designed as simple and reliable as possible, must be able to detect uranium concentrations down to 10 mg/l at the presence of typical fission product activity levels up to about 10<sup>9</sup> Bq/l.

In order to assess the principal capabilities and limitations of the different variants of EDXRFA, we carried out a number of comparison measurements with different test equipments in which both the mode of excitation and the type of the detector has been varied (1). To meet the requirements for instrument simplicity, only configurations using isotopic sources for exciting the fluorescence of either L- or K-X rays were



considered in the present studies. Three different detectors were employed for the spectroscopy of the fluorescent L-X rays: a 30 mm<sup>2</sup> x 5 mm Si(Li) detector cooled with liquid nitrogen, and a 25 mm<sup>2</sup> x 0.3 mm Si detector and a Xe gas proportional counter, both operated at room temperature. We found, however, that the proportional counter showed very poor performance for measurements on samples with a substantial amount of fission products. For this reason we have abandoned this type of detector as a practical alternative. For the spectroscopy of the K-X rays we employed a standard Ge detector system with a planar 200 mm<sup>2</sup> x 10 mm detector cooled with liquid nitrogen.

The performance of the different configurations has been evaluated from measurements on actual process solutions with respect to their detection capability and their sensitivity to interfering radiation from fission products and actinides. Table 1 summarizes the detection limits for uranium (for other actinide elements they would be about the same) obtained within a counting time of 10 min from 1 ml samples. For the detection limits we used the criteria that the net peak signal should be 3 times the standard deviation of the background below the X-ray peak. The detection limits are given for solutions containing no fission products, and for solutions with a fission product activity of about 10<sup>9</sup> Bq/l.

For L-XRFA the lowest detection limits were obtained with a <sup>109</sup>Cd source ( $t_{1/2} = 453$  d). Acceptable detection limits, however, are also achieved with <sup>241</sup>Am as excitation source. According to our experiences <sup>241</sup>Am is best used in the direct excitation mode with a suitable converter foil placed between source and sample. The minimum uranium concentration detectable via the K-X rays fluorescence by means of a <sup>57</sup>Co source is about 5 times higher than that obtained from L-X rays excited by a <sup>109</sup>Cd source.

Direct interferences of gamma and X-rays from fission products do neither exist for the La nor for the K $\alpha_1$  uranium X-rays. However, the presence of fission products causes an increase of the average continuous background level. This was found to be negligible for K-XRFA, but not for L-XRFA arrangements using isotopic sources for excitation. The detection limits from the latter configurations therefore slightly deteriorated for solutions containing fission products as indicated in Table 1. Of course, the impact of fission products is largest, but still tolerable, for the low-resolution Si detector operated at room temperature.

Table 1. Detection limits for uranium (sample volume 1 ml, counting time 10 min).

Excitation Source	Detector	X-Ray Analyzed	Total Detector Count.Rate (kcps)	Detection Limit (mg U/l)	
				Pure Solution	With $10^9$ Bq/l Fiss.Pr.
$^{57}\text{Co}$ $1.5 \cdot 10^9$ Bq	HpGe	$K_{\alpha 1}$	20	10	10
$^{241}\text{Am}$ , $1.85 \cdot 10^{10}$ Bq Direct Excitation 0.1 mm Cu-Filter	Si(Li) Si, 20°C	$L_{\alpha}$	50	2.8	2.9
		$L_{\alpha}$	10	3.8	4.2
$^{241}\text{Am}$ , $1.85 \cdot 10^{10}$ Bq Direct Excitation 0.2 mm Sn-Converter Foil	Si(Li) Si, 20°C	$L_{\alpha}$	17	2.8	3.0
		$L_{\alpha}$	4	3.8	4.2
$^{241}\text{Am}$ , $1.85 \cdot 10^{10}$ Bq Indirect Excitation Sn Secondary Target	Si(Li) Si, 20°C	$L_{\alpha}$	3	4.5	6.0
		$L_{\alpha}$	1	11	16
$^{109}\text{Cd}$ $7.4 \cdot 10^8$ Bq	Si(Li) Si, 20°C	$L_{\alpha}$	12	2.0	2.1
		$L_{\alpha}$	12	4.7	4.8

Based on the performance characteristics of the different XRF configurations, and taking into account the operational aspects relevant for in-line application, it appears reasonable to propose a fairly simple XRF analyzer for the envisaged application, in which L-X rays excited with a long-lived isotopic source ( $^{241}\text{Am}$ ) are spectroscopied with a non-cooled Si detector.

- (1) I. Michel-Piper, H. Ottmar, Report KfK 4159, Kernforschungszentrum Karlsruhe (1986), 216

#### 5.4.15 APPLICATION OF THE HYBRID X-RAY INSTRUMENT FOR THE MEASUREMENT OF THORIUM-PLUTONIUM MIXED SOLUTIONS

H. Eberle, S.-T. Hsue\*

The major aqueous process used to recover and purify plutonium at the Los Alamos Plutonium Facility is anion exchange in nitric acid. A weakness of this process is its inability to cleanly separate the thorium impurity from plutonium, which results in a continuous recycling and buildup of the thorium. Alternative processes are available to separate thorium; however, these tedious and time consuming options should be used only when the level of thorium impurity clearly justifies them. An assay method is needed to determine the trace amounts of thorium in the plutonium product solutions. Nondestructive assay is preferred because chemical determination of trace amounts of thorium is difficult as well as time consuming.

For this application, a technique is needed that can determine Th/Pu weight ratios of approximately 0.001 (or even lower) with reasonable precision and accuracy. Our investigation is intended as a study of the feasibility of tailoring the Hybrid Instrument to the assay of plutonium-thorium mixed solutions at small Th/Pu ratios.

A set of standards was prepared for the experiment, with Pu/Th ratios ranging from 50 to 1000. The concentration of the major element plutonium was determined with the K-edge densitometry part of the Hybrid Instrument.

The filtered X-ray continuum of the X-ray tube used for the XRF measurements preferentially excites thorium atoms relative to plutonium atoms when the accelerating voltage is lowered to values not far above the plutonium absorption-edge energy. To determine the optimum operating voltage for the XRF analysis in the Hybrid Instrument, data were collected for one sample at 125, 130, 140 and 150 kV accelerating voltage. The optimum precision for the ThK $\alpha_1$ /PuK $\alpha_2$  ratio, which is determined by the peak to background ratio and the net peak areas of the X-rays, was found at about 130 kV (1). Figure 1 shows the measured ThK $\alpha_1$ /PuK $\alpha_2$  ratio as a function of the known Th/Pu ratio. With one exception, the data points fall on a straight line.

Several conclusions can be made from this feasibility study on applying the Hybrid Instrument for thorium-plutonium mixed solutions:

- The optimum accelerating voltage for measuring the Th/Pu ratio is about 130 kV. This voltage offers the best peak-to-background ratio and the best measurement precision. However, a two-pass assay is required. One

for XRF and one for densitometry. A compromise would use a voltage of 135 kV for both XRF and densitometry.

- At optimum operating conditions, the detection limit ( $P = 3\sqrt{B}$ ) for thorium is about 25 mg/l for a 1000 s assay.
- The minimum Th/Pu ratio that can be assayed by the Hybrid Instrument with reasonable precision is about 1/1000. At this ratio, a precision of 5 % can be achieved for a 1000 s assay of thorium concentrations greater than about 0.2 g/l.
- With the use of slightly larger sample volumes and less collimation, the detector counting rates can be increased by a factor of 2 or 3, thereby improving the measurement precision by a factor of about 1.5.

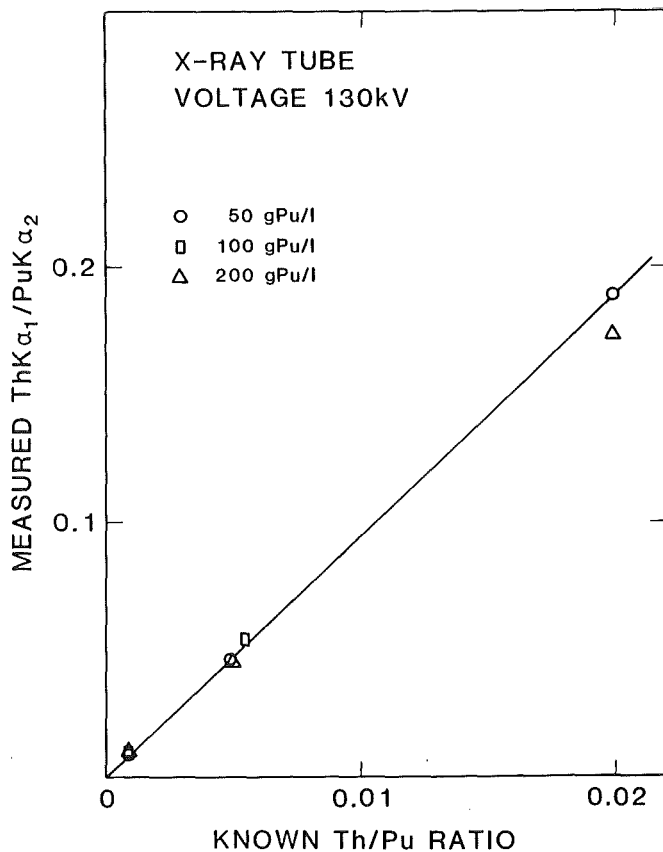


Fig. 1  
Measured ThKa<sub>1</sub>/ PuKa<sub>2</sub>  
ratio as function of  
known Th/Pu ratio.

(1) S.-T. Hsue, H. Eberle, Report LA-11002-MS (1987)

\* Los Alamos National Laboratory, Los Alamos, New Mexico, USA

#### 5.4.16 A COMPARISON OF METHODS FOR THE NET PEAK AREA DETERMINATION FROM XRF SPECTRA OF THE KFK HYBRID INSTRUMENT

H. Eberle

Spectroscopy of small peaks located on a very high background level and/or positioned on a very nonlinear background continuum always leads to problems in the delineation of the true background and in the determination of the true net peak area. These conditions exist, for example, for the  $\text{PuK}\alpha_1$  - line in the XRF-spectra of the KfK Hybrid K-edge/K-XRF solution assay system, in which undiluted and highly radioactive reprocessing input solutions from dissolved LWR fuels are analysed for their U and Pu concentration. Since the respective measurements are used for accountancy and safeguards purposes, it is of great importance that the determinations are free from systematic errors.

In the present operation of the Hybrid Instrument the XRF part is used for the determination of the U/Pu ratio only. This information is deduced from the measured intensity ratio of fluorescent uranium and plutonium K X-rays which are located on a relatively broad bump of backscattered X-rays from the primary X-ray beam.

The present software of the Hybrid Instrument uses background counts from windows adjacent to the X-ray peaks for the determination of the net peak areas (1). This method, however, tends to give rise to systematic errors at lower concentrations with correspondingly lower peak-to-background ratios. Therefore two alternative methods for the net peak area detection were investigated:

- calculation of the background using a digital filter (2), and
- generation of a continuous background baseline (3).

The three different procedures have been tested on a series of XRF spectra measured with the Hybrid Instrument. An original LWR dissolver solution with a uranium concentration of 226.9 g/l, and with a U/Pu ratio of 96.7, has been diluted in several steps down to a concentration of about 1 gU/l. In this way a set of seven reference solutions with a constant U/Pu ratio has been generated. On each solution a series of repeat measurements with a counting time of 1000 s each has been carried out.

The quantity for the comparison was the U/Pu ratio, which has been determined from the ratio of net peak counts in the uranium and plutonium  $\text{K}\alpha_1$  X-rays at 98.44 keV and 103.76 keV, respectively. This evaluated ratio should have been constant for all spectra taken at the different concentrations.

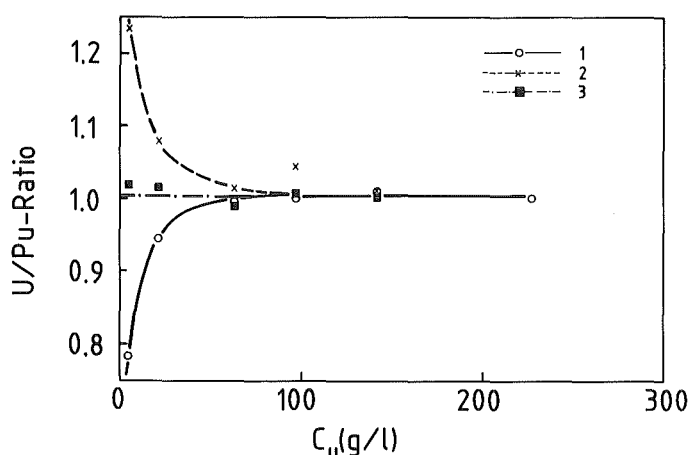


Fig. 1  
Dependence of the U/Pu-ratio on the major element uranium. For data analysis the Hybrid Instrument's software (1), digital filtering of the spectrum (2) and the analytical generation of a continuous background baseline (3) was used.

The results obtained from the different methods for net peak area determination are graphically displayed in Fig. 1. Only the procedure from Ref. 3 shows a linear behaviour of the U/Pu - ratio over a wide range of concentration  $C_U$  of the major element uranium. This method is therefore recommended for use in XRF measurements with the Hybrid Instrument if lower concentrations are involved.

- (1) H. Eberle, H. Ottmar, Report JOPAG/04.86-PRG-128, Kernforschungszentrum Karlsruhe (1986).
- (2) P.J. Statham, Analytical Chemistry 49 (1977) 2140.
- (3) Y. Kawarasaki, Nucl. Instr. Meth. 133 (1976) 335.

#### 5.4.17 PRODUCTION OF ISOTOPES FOR MEDICAL APPLICATIONS

K.H. Assmus, S. Augstein, V. Bechtold, H.D. Dennerlein,  
H. Dohrmann, D. Erbe, E. FoBhag, A.Hanser, R. Hüfner, N. Kernert,  
W. Maier, A.Martin, H. Ripp, U. Sahm, S. Uhlemann



The Karlsruhe compact cyclotrom ( $CP42H^-$ ) is routinely used for the production of radioactive isotopes for medical diagnostics. The status of the various products is as follows.

#### Ultra pure $^{123}I$

With the new target system the amount of  $^{123}I$  produced could be increased by 30 % compared to last year. The target and the chemical units were operating without any failures. The 50  $\mu m$  window at the high pressure gas

target was replaced routinely after 5000  $\mu\text{Ah}$ . The quality of the  $^{123}\text{I}$  concerning nuclide purity and chemical purity is remarkably high. Several independent checks of the Karlsruhe  $^{123}\text{I}$  quality in USA, Japan, France and Germany demonstrate the quality standard. As an example Table 1 shows the results measured by the Physikalisch-Technische Bundesanstalt (PTB) in Braunschweig.

**Physikalisch-Technische Bundesanstalt**

**Prüfschein**

Vorgang: Bestimmung der Verunreinigungen in einer  $^{123}\text{I}$ -Lösung

Kennzeichnung: Jod/Rb-Charge 193/5 vom 03.12.1986

Antragsteller: Kernforschungszentrum Karlsruhe  
Postfach 3640, 7500 Karlsruhe 1  
Auftragsnummer: 425/01286540/0061

Gesch.-Nr. der PTB: 6.32-23810.86

Die Aktivitäten der Verunreinigungen in einer  $^{123}\text{I}$ -Lösung wurden mit einem kalibrierten Reinstgermanium-Spektrometer der Physikalisch-Technischen Bundesanstalt am 11. Dezember 1986 gemessen. Die auf das Nuklid  $^{123}\text{I}$  bezogenen Meßwerte der Aktivitätsverhältnisse  $A_i/A$  ( $^{123}\text{I}$ ) zum Bezugszeitpunkt 11.12.1986, 22.30 h, sind in Spalte 2 der Tabelle auf Blatt 2 angegeben. Spalte 3 enthält die Halbwertszeiten der Radionuklide, die benutzt wurden, um die Aktivitätsverhältnisse in Spalte 4 zum gewünschten Bezugszeitpunkt 03.12.1986, 8.00 h, zu errechnen.

Die Zuordnung der Linie bei der Energie  $E = 140,5 \text{ keV}$  zum Nuklid  $^{99}\text{Ho}/^{99}\text{Tc}^m$  ist als nicht vollständig gesichert anzusehen, da keine weiteren Linien für eine Auswertekontrolle zur Verfügung standen.

Die Aktivität von  $^{123}\text{I}$  betrug am 11.12.1986, 22.30 h,  
( $8,2 \pm 0,4$ )  $\cdot 10^3 \text{ Bq}$

- 2 -

Nicht ohne Erlaubnis der PTB zu reproduzieren. Die Prüfergebnisse dürfen nur innerhalb der Gültigkeitsdauer verwendet werden. Anträge oder Änderungen beziehen sich auf die Geschäftsverteilung der Physikalisch-Technischen Bundesanstalt, Bundesallee 100, Postfach 3111, D-3300 Braunschweig.

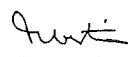
Physikalisch-Technische Bundesanstalt

Blatt 2 zu Prüfschein 6.32-23810.86

Spalte 1	2	3	4
Nuklid	$A_i/A$	T 1/2	$A_i/A$
	11.12.86, 22.30		03.12.86, 8.00.
$^{48}\text{V}$	$1,4(4) \cdot 10^{-3}$	15,974 d	$3,9(9) \cdot 10^{-8}$
$^{95}\text{Nb}$	$0,9(27) \cdot 10^{-4}$	35,0 d	$2,1(7) \cdot 10^{-8}$
$^{95}\text{Tc}^m$	$9,8(20) \cdot 10^{-3}$	61 d	$2,1(4) \cdot 10^{-7}$
$^{96}\text{Tc}$	$3,6(3) \cdot 10^{-2}$	4,28 d	$2,9(3) \cdot 10^{-6}$
$^{99}\text{Ho}/^{99}\text{Tc}^m$	$3,7(4) \cdot 10^{-3}$	2,7476 d	$6,6(7) \cdot 10^{-7}$
$^{119}\text{Tc}^m$	$1,9(9) \cdot 10^{-3}$	4,69 d	$1,3(6) \cdot 10^{-7}$
$^{121}\text{Te}$	1,81(10)	17 d	$5,1(3) \cdot 10^{-5}$
$^{124}\text{I}$	$2,8(6) \cdot 10^{-3}$	4,18 d	$2,3(6) \cdot 10^{-7}$
$^{125}\text{I}$	0,34(4)	59,3 d	$7,6(8) \cdot 10^{-6}$
$^{132}\text{Te}/^{132}\text{I}$	$10(5) \cdot 10^{-4}$	3,204 d	$1,2(6) \cdot 10^{-7}$
$^{205}\text{Bi}$	$5,5(14) \cdot 10^{-3}$	15,31 d	$1,6(4) \cdot 10^{-7}$
$^{206}\text{Bi}$	$9,0(9) \cdot 10^{-3}$	6,243 d	$4,9(5) \cdot 10^{-7}$

Die in Klammern angegebenen Werte der Meßunsicherheiten beziehen sich jeweils auf die letzte Ziffer der Meßwerte und gelten für ein Vertrauensniveau von 99%.

Braunschweig, 15.01.87  
Im Auftrag



Dr. K. Debertin  
Direktor und Professor




Table 1: Measurement of the Iodine-123 quality by the Physikalisch-Technische Bundesanstalt in Braunschweig. The impurities are shown in column four.

Parallel to the routine production a new hot cell was built which houses the chemical unit for the iodine raw-product and the distribution of the iodine batches. Fig. 1 shows the "Glass-tunnel" with the hot cell in the rear and the quality control center in the front.

The iodine production system KIPROS which was sold to a pharmaceutical company in Japan last year, went into operation on schedule and is since operating in a routine regime. In August 1988 a second iodine production system is to be delivered to a pharmaceutical company in USA.

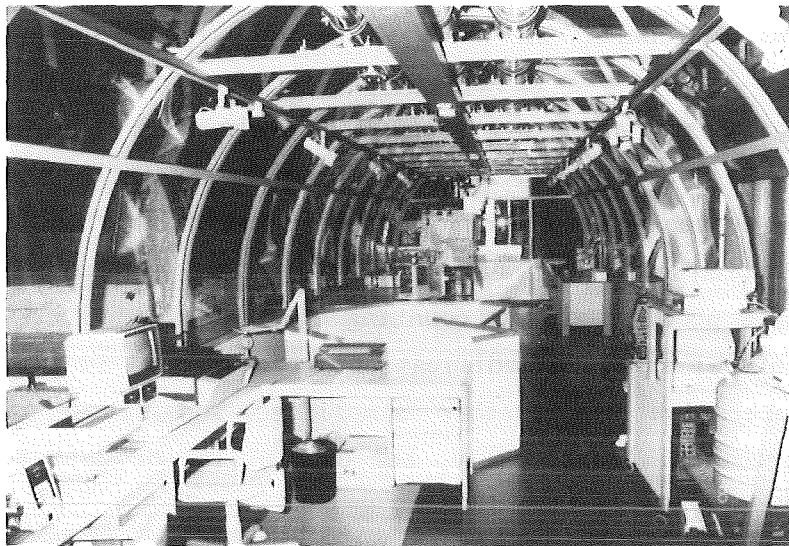


Fig. 1 The 'Glasstunnel' for the production of ultra pure iodine. The iodine-123 is pumped from the target via a stainless steel pipeline in to the hot cell in the rear. The quality control center is located in the front.

### $^{81}\text{Rb}/^{81\text{m}}\text{Kr}$ generator

Due to a great effort in marketing the production of the generators had to be increased by 40 % compared to last year. The main part of the production is still used for generators for lung ventilation studies in hospitals. A small amount of rubidium is delivered to the mass separator facility in order to produce ultra pure  $^{81}\text{Rb}$  for blood flow measurements and myocardial imaging. KfK is world wide the only producer of the latter product. This work is done in collaboration with several research hospitals in Germany.

### $^{81}\text{Rb}/^{81\text{m}}\text{Kr}$ liquid generator

The design of the prototype is finished. Components are tested and were modified if necessary. The software of the control unit was checked out. Ergonomic studies were carried out by an industrial designer. This work is not finished until now. The clinical tests of the system are scheduled for late 1987.



#### 5.4.18 BLOOD FLOW MEASUREMENTS USING ULTRA-PURE- $^{81}\text{Rb}$

U. Baßler, J. Bialy, J.W. Peters, M. Schmitt, H. Schweickert

During the time of report, the hardware as well as the software of the system described in last year's report were further tested and developed.

Clinical tests of the system were started at the Medizinische Hochschule Hannover (MHH) last autumn. During these tests some hardware changes became necessary to ensure reliable operation. So, especially, the air circulation of the system had to be improved significantly to avoid temperature problems of the counting electronics.

Also several software modifications were adapted in the past year. Mainly, the operation was further simplified and better adjusted to clinical requirements. Additionally, the possibility of data transmission to other computer systems, like IBM PC, was added.

Besides these more technical problems also nuclear medical tests were carried out. Although most of these medical tests, due to the clinical and legal boundaries, were made within the clinical routine diagnostics, we also had the possibility to participate in some more elaborate and complicated procedures. One of these was a liver transplantation of a pig, carried out by the MHH transplantation team for training. Pure  $^{81}\text{Rb}$  was injected into the transplantate liver and the  $^{81}\text{Rb}/^{81\text{m}}\text{Kr}$  ratio as equivalent to the blood flow was monitored throughout the operation. Fig. 1 shows the results of our measurements. The signifi-

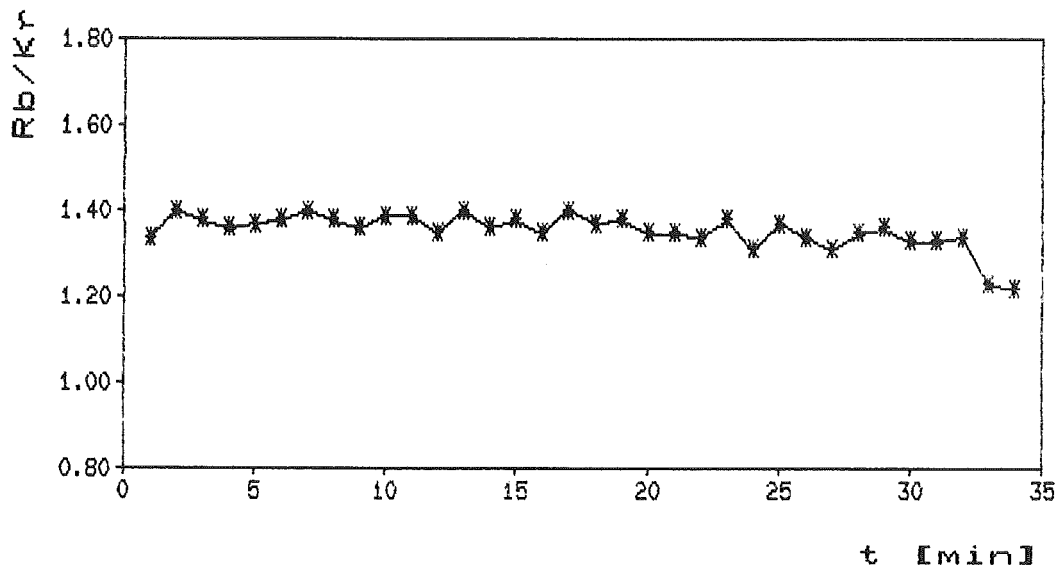


Fig. 1 Results of blood flow measurement in a transplanted liver

cant decrease after 32 minutes corresponds to the death of the animal and thus to a blood flow of zero.

The first results of the clinical tests also show that our system is not only suitable for blood flow measurements, but that it also makes a lot of new diagnostic methods possible. So many biological functions might be measured more precisely using more than just one radioactive tracer. Different substances can be labeled with different nuclides and their interaction can be studied better than with available systems. These new possibilities will be studied in more detail.

#### 5.4.19 RADIONUCLIDE TECHNIQUE FOR MECHANICAL ENGINEERING (RTM)

R. Blank, E. Bollmann, P. Fehsenfeld, B. Gegenheimer, P. Herrmann,  
H. Holler, A. Kleinrahm, H. Roth, B. Schüssler

The production of thin layer activated machine parts for industry and research institutes has been increased by 40 % compared to the preceding year. The volume of production planned for the year 1988 had already been reached in 1986. The application of the advanced radionuclide technique in mechanical engineering (RTM) for on-line wear and corrosion measurements has been considerably expanded. Several international companies in the chemical, in the large marine diesel engine and in the truck engine manufacturing industries have started using RTM advantageously for solving problems in research, development and plant condition monitoring.

The new irradiation facility installed recently at the compact cyclotron has been intensively used for activation service. An example of an application, a railway brake disk in irradiation position in front of the cyclotron beam tube is shown in Fig. 1. RTM diagnostics has been applied successfully for developing reliable, wear resistant brake disks for high speed trains.

Work in development of RTM has been carried out in new fields of application such as textile and tool machinery as well as in thin layer activation of ceramic materials. The experiments have been performed in cooperation with the Institut für Textiltechnik, Denkendorf, with Fachhochschule Darmstadt and with the Institut für Materialforschung IMF I/KfK.

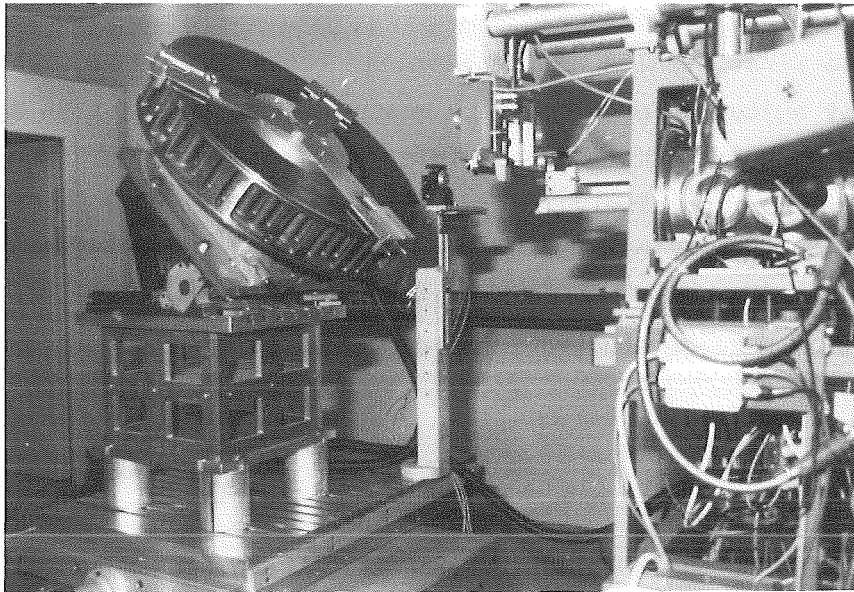


**Fig. 1** Railway brake disk in irradiation position in front of the cyclotron beam tube. RTM diagnostics has been applied successfully for developing reliable, wear resistant brake disks for high speed trains

## 6. LIST OF PUBLICATIONS

### 6.1 PUBLICATIONS AND REPORTS

- ANSELMANT, M.; BEKK, K.; HANSER, A.;  
HOEFFGEN, H.; MEISEL, G.; GOERING, S.; REBEL,  
H.; SCHATZ, G.  
Charge radii and moments of tin nuclei by  
laser spectroscopy.  
KfK-4071 (April 86)  
Physical Review C, 34(1986) S.1052
- ANSELMANT, M.; CHONGKUM, S.; BEKK, K.;  
GOERING, S.; HANSER, A.; MEISEL, G.; REBEL,  
H.  
Isotope shift of a series of Sr isotopes.  
Zeitschrift fuer Physik D, 3(1986) S.421-22
- ANSELMANT, M.; BEKK, K.; CHONGKUM, S.;  
GOERING, S.; HANSER, A.; HOEFFGEN, H.;  
KAELBER, W.; MEISEL, G.; REBEL, H.  
Charge radii and moments of strontium nuclei  
by laser spectroscopy.  
Zeitschrift fuer Physik A, 326(1987)  
S.493-500
- BAO, Z.Y.; KAEPELER, F.  
Neutron capture cross sections for s-process  
studies.  
Atomic Data and Nuclear Data Tables, 36(1987)  
S.411-51
- BAUR, G.; BERTULANI, C.A.; REBEL, H.  
Coulomb dissociation as a source of  
information on radiative capture processes of  
astrophysical interest.  
Internat.Symp.on Weak and Electromagnetic  
Interactions in Nuclei, Heidelberg, July 1-5,  
1986  
KfK-4032 (Januar 86)  
Nuclear Physics A, 458(1986) S.188-204
- BEER, H.  
A measurement of the  $^{139}\text{La}$  capture cross  
section and a study of the s-process at magic  
neutron number 82.  
Astronomy and Astrophysics, 162(1986)  
S.330-32  
In: Qaim, S.M. [Hrsg.]  
Progress Report on Nuclear Data Research in  
the Federal Republic of Germany for the  
Period April 1, 1985 to March 31, 1986  
NEANDC(E)-272 U Vol. 5(June 1986) S.8  
INDC(Ger)-29/LN + Special
- BEER, H.; PENZHORN, R.D.  
The  $^{40}\text{Ar}$  capture cross section and the  $^{40}\text{Ar}$   
solar abundance.  
In: Qaim, S.M. [Hrsg.]  
Progress Report on Nuclear Data Research in  
the Federal Republic of Germany for the  
Period April 1, 1985 to March 31, 1986  
NEANDC(E)-272 U Vol. 5(June 1986) S.5  
INDC(Ger)-29/LN + Special
- BEER, H.  
Measurement of the capture cross sections of  
 $^{156}\text{Dy}$  and supra(194m,196,198)Pt.  
In: Qaim, S.M. [Hrsg.]  
Progress Report on Nuclear Data Research in  
the Federal Republic of Germany for the  
Period April 1, 1985 to March 31, 1986  
NEANDC(E)-272 U Vol. 5(June 1986) S.10  
INDC(Ger)-29/LN + Special
- BEER, H.; PENZHORN, R.D.  
Measurement of the neutron capture cross  
section of  $^{40}\text{Ar}$  and an s-process analysis  
from  $^{34}\text{S}$  to  $^{42}\text{Ca}$ .  
Astronomy and Astrophysics, 174(1987)  
S.323-28
- BOEHRER, A.  
Clustertopologie multihadronischer Ereignisse  
in der  $e^+e^-$ -Annihilation.  
KfK-4251 (April 87)
- BRADY, F.P.; DOLL, P.; FINK, G.; HEERINGA,  
W.; HOFMANN, K.; KLAGES, H.O.; NITZ, W.;  
WIJCZYNSKI, J.  
Analyzing powers of elastic and inelastic n-d  
scattering between 16 and 50 MeV.  
Kondo, M. [Hrsg.]  
Polarization Phenomena in Nuclear Physics :  
Proc.of the 6th Internat.Symp., Osaka, J,  
August 26-30, 1985  
Journal of the Physical Society of Japan,  
55(1986) Suppl. S.864-65
- BUECHE, G.; DOLL, P.; FRIEDRICH, L.; [HRSG.]  
Annual report on nuclear physics activities  
July 1, 1985 - June 30, 1986.  
KfK-4159 (Dezember 86)
- CELLO-COLLABORATION  
A search for single photons at PETRA.  
DESY-86-050 (Mai 86)  
LAL-86-11 (Mai 86)  
Physics Letters B, 176(1986) S.247-54  
(Contributed Paper)  
23rd Internat.Conf.on High Energy Physics,  
Berkeley, Calif., July 16-23, 1986
- CELLO-COLLABORATION  
Search for light leptoquark bosons.  
23rd Internat.Conf.on High Energy Physics,  
Berkeley, Calif., July 16-23, 1986  
DESY-86-063 (Juli 86)  
Physics Letters B, 178(1986) S.452-56
- CELLO-COLLABORATION; FLUEGGE, G.  
Excited lepton search.  
DESY-86-012 (Februar 86)  
LAL-85-50 (Februar 86)  
Physics Letters B, 168(1986) S.420-26
- CELLO-COLLABORATION  
Search for excited quarks in  $e^+e^-$   
interactions with the CELLO detector.  
(Contributed Paper)  
23rd Internat.Conf.on High Energy Physics,  
Berkeley, Calif., July 16-23, 1986  
DESY-86-100 (September 86)  
Physics Letters B, 181(1986) S.178-84
- CELLO-COLLABORATION  
Determination of  $\alpha_{\text{sub}(s)}$  and  $\sin^2\Theta_{\text{sub}(w)}$   
from measurements of the total hadronic cross  
section in  $e^+e^-$  annihilation.  
DESY-86-133 (October 86)  
Physics Letters B, 183(1987) S.400-11
- CELLO-COLLABORATION  
A measurement of the muon pair production in  
 $e^+e^-$  annihilation at  $38.3 \leq \sqrt{s} \leq 46.8$  GeV.  
Physics Letters B, 191(1987) S.209-16

CELLO-COLLABORATION

A measurement of the muon pair production in  $e^+e^-$  annihilation at  $38.3 \leq \sqrt{s} \leq 46.8$  GeV.  
DESY-87-005 (Januar 87)

CELLO-COLLABORATION

A search for hadronic events with low thrust and an isolated lepton.  
DESY-87-016 (Februar 87)  
Physics Letters B, 193(1987) S.157-62

CELLO-COLLABORATION

Search for production of charged higgs particles.  
DESY-87-30 (April 87)  
Physics Letters B, 193(1987) S.376-82

CELLO-COLLABORATION

Searches for supersymmetric particles with the CELLO detector at PETRA.  
DESY-87-013 (Februar 87)  
Zeitschrift fuer Physik C, 35(1987) S.181-99

CICHOCKI, T.; HECK, D.; JARCZYK, L.; ROKITA, E.; STRZALKOWSKI, A.; SYCH, M.

Proton microbeam study of calcium-phosphate complexes in human arteries.  
4th Internat. Conf. on Particle Induced X-Ray Emission and its Analytical Applications, Tallahassee, Fla., June 9-13, 1986  
Nuclear Instruments and Methods B, 22(1987) S.210-13

CORVI, F.; BASTIAN, C.; WISSHAK, K.  
Neutron capture in the 1.15-keV resonance of  $^{56}\text{Fe}$  using Moxon-Rae detectors.  
Nuclear Science and Engineering, 93(1986) S.348-56

In: *Qaim, S.M. [Hrsg.]*  
Progress Report on Nuclear Data Research in the Federal Republic of Germany for the Period April 1, 1985 to March 31, 1986  
NEANDC(E)-272 U Vol. 5(June 1986) S.6  
INDC(Ger)-29/LN + Special

DOLL, P.; EBERHARD, V.; FINK, G.; GARRETT, R.; HAESNER, B.; HEERINGA, W.; HOFMANN, K.; JANY, P.; KECSKEMETI, J.; KLAGES, H.O.; KRUPP, H.; WOELFL, CHR.; WILCZYNSKI, J.  
np scattering experiments and  $n-^3\text{He}$  experiments from 1 to 50 MeV.  
Oryu, S. [Hrsg.]  
Proc. of the Internat. Workshop on Few Body Approaches to Nuclear Reactions in Tandem and Cyclotron Energy Regions, Tokyo, J, August 22-24, 1986  
Singapore: World Scientific 1987 S.109-17

DOLL, P.; GARRETT, R.; HALE, G.M.; HEERINGA, W.; JANY, P.; KLAGES, H.O.; MAIER, CHR.  
Analyzing powers of the elastic  $n-^3\text{He}$  scattering from 1-2 MeV and from 16-50 MeV.  
Kondo, M. [Hrsg.]  
Polarization Phenomena in Nuclear Physics:  
Proc. of the 6th Internat. Symp., Osaka, J, August 26-30, 1985  
Journal of the Physical Society of Japan, 55(1986) Suppl. S.876-77

DOLL, P.; FINK, G.; FINLAY, R.W.; FORD, T.D.; HEERINGA, W.; KLAGES, H.O.; SCHMALZ, G.; SKACEL, H.; KRUPP, H.; MAIER, CHR.  
The Karlsruhe polarized neutron facility POLKA.  
Proc. of the Internat. Nuclear Physics Conf., Harrogate, GB, August 25-30, 1986  
Harrogate: Institute of Physics 1986 Vol. 1 S.536

EBERLE, H.; OTTMAR, H.  
Operations manual for the KfK hybrid K-edge/K-XRF densitometer.  
JOPAG/04.86-PRG-128 (April 86)

ENGLER, J.; KEIM, H.; WILD, B.  
Performance test of a TMS calorimeter.  
KfK-4085 (Juni 86)  
Nuclear Instruments and Methods A, 252(1986) S.29-34

ENGLER, J.; KEIM, H.; MUELLER, C.  
A track chamber using liquid TMS.  
KfK Preprint No 86-1  
Nuclear Instruments and Methods A, 254(1987) S.311-16

EYRICH, W.; HOFMANN, A.; LEHMANN, A.; MUEHLDOERFER, B.; SCHLOESSER, H.; WIRTH, H.; GILS, H.J.; REBEL, H.; ZAGROMSKI, S.  
Investigation of isoscalar giant resonances in  $^6\text{Li}$  scattering.  
Proc. of the Internat. Nuclear Physics Conf., Harrogate, GB, August 25-30, 1986  
Harrogate: Institute of Physics 1986 Vol. 1 S.71

EYRICH, W.; HOFMANN, A.; LEHMANN, A.; MUEHLDOERFER, B.; SCHLOESSER, H.; WIRTH, H.; GILS, H.J.; REBEL, H.; ZAGROMSKI, S.  
E0 strength in  $^{12}\text{C}$  from  $^6\text{Li}$  scattering.  
Physical Review C, 36(1987) S.416-19

FEHSENFELD, P.; KLEINRAHM, A.; BOLLMANN, E.  
Radionuklidtechnik im Maschinenbau zur Verschleiss- und Korrosionsmessung in Industrie und Forschung.  
KfK-Nachrichten, 18(1986) S.224-34

FINK, G.; DOLL, P.; GARRETT, R.; HEERINGA, W.; HOFMANN, K.; KLAGES, H.O.; KRUPP, H.  
Measurement of the np differential cross section from 22 to 50 MeV.  
Sasakawa, T. [Hrsg.]  
Few Body Systems in Particle and Nuclear Physics: 11th Internat. IUPAP Conf., Tokyo and Sendai, J, August 24-30, 1986  
Sendai: Tohoku Univ., 1986. - S.396-97  
(Research Report of Laboratory of Nuclear Science, Tohoku University: Suppl.; 19(1986))

FINK, G.; KRUPP, H.; DOLL, P.; EBERHARD, V.; GARRETT, R.; HEERINGA, W.; KLAGES, H.O.  
Status of neutron-proton scattering experiments and phase-shift analysis up to 50 MeV neutron energy.  
Proc. of the Internat. Nuclear Physics Conf., Harrogate, GB, August 25-30, 1986  
Harrogate: Institute of Physics 1986 Vol. 1 S.525

GIORGINIS, G.; WOCELE, J.; KIONTKE, S.; MASCHUW, R.; ZEITNITZ, B.  
A three dimensional He-recoil MWPC for fast polarized neutrons.  
Nuclear Instruments and Methods A, 251(1986) S.89-94

GOEL, B.; HEERINGA, W.  
Polarisation and depolarisation mechanisms in ICF targets.  
Velarde, G. [Hrsg.]  
4th Internat. Conf. on Emerging Nuclear Energy Systems (ICENES 4), Madrid, E, June 30 - July 4, 1986 Proc.  
Singapore: World Scientific 1987 S.412-16

- HANSER, A.; STOLL, H.P.  
Produktion von reinem Rubidium-81 durch  
elektromagnetische Isotopentrennung und seine  
Anwendungsmoeglichkeit in der  
Nuklearmedizin.  
KfK-Nachrichten, 19(1987) S.83-88
- HECK, D.; OCHS, A.; KLEMPNOW, A.; MAIER,  
K.P.; KRATT, C.  
Trace element distributions in human liver  
lobules determined with micro-PIXE.  
Braetter, P. [Hrsg.]  
4th Internat. Workshop on Trace Element  
Analytical Chemistry in Medicine and Biology,  
GSF Neuherberg, April 21-23, 1986 Proc.  
Trace Element - Analytical Chemistry in  
Medicine and Biology  
Berlin [u.a.] : Walter de Gruyter & Co., 1987  
Vol. 4 S.367-74
- HECK, D.; OCHS, A.; KLEMPNOW, A.; MAIER,  
K.P.; KRATT, C.  
Localized changes of trace element  
concentrations within diseased human liver  
lobules.  
4th Internat. Conf. on Particle Induced X-Ray  
Emission and its Analytical Applications,  
Tallahassee, Fla., June 9-13, 1986  
Nuclear Instruments and Methods B, 22(1987)  
S.196-200
- HEERINGA, W.; MAIER, CHR.; SKACEL, H.  
Exchange of polarized targets in a high  
magnetic field and at mK temperatures.  
Internat. Workshop on Polarized Sources and  
Targets, Montana, CH, January 13-17, 1986  
Helvetica Physica Acta, 59(1986) S.795-98
- HEERINGA, W.  
Polarization of solid deuterium-tritium fuel  
for nuclear fusion.  
KfK-4168 (November 86)
- HEERINGA, W.; KLAGES, H.O.; MAIER, CHR.  
Performance and improvement of the Karlsruhe  
polarized target facility KRYPTA.  
Kondo, M. [Hrsg.]  
Polarization Phenomena in Nuclear Physics :  
Proc. of the 6th Internat. Symp., Osaka, J,  
August 26-30, 1985  
Journal of the Physical Society of Japan,  
55(1986) Suppl. S.1100
- HINTERBERGER, F.; ROSSEN, P. VON; CIERJACKS,  
S.; SCHMALZ, G.  
High resolution resonance study of the  $^{12}\text{C}+\text{n}$   
total cross section in the region of  $^{13}\text{C}$   
 $T=3/2$  states.  
Zeitschrift fuer Physik A, 326(1987) S.407-12
- HOLUB, E.; HILSCHER, D.; INGOLD, G.; JAHNKE,  
U.; ORF, H.; ROSSNER, H.; ZANK, W.P.;  
SCHROEDER, W.U.; GEMMEKE, H.; KELLER, K.;  
LASSEN, L.; LUECKING, W.  
Preequilibrium neutron emission in fusion of  
 $^{16}\text{O}+^{12}\text{C}$  at 25 MeV per nucleon.  
Physical Review C, 33(1986) S.143-52
- HSUE, S.T.; EBERLE, H.  
Application of the hybrid X-ray instrument  
for measurement of thorium-plutonium mixed  
solutions.  
LA-11002-MS (July 87)
- JELITTO, H.  
Experimentelle Untersuchungen des Aufbruchs  
von 156 MeV  $^6\text{Li}$ -Ionen unter extremen  
Vorwaertswinkeln mit dem Karlsruher  
Magnetspektrographen 'Little John'.  
KfK-4259 (Mai 87)  
Dissertation, Universitaet Heidelberg 1987
- KAEPPELER, F.; NAQVI, A.A.; AL-OHALI, M.  
The isomeric ratio of  $^{85}\text{Kr}$  at a thermal  
energy of  $kT = 54$  keV.  
In: Qaim, S.M. [Hrsg.]  
Progress Report on Nuclear Data Research in  
the Federal Republic of Germany for the  
Period April 1, 1985 to March 31, 1986  
NEANDC(E)-272 U Vol. 5(June 1986) S.8  
INDC(Ger)-29/LN + Special
- KAEPPELER, F.; NAQVI, A.A.; AL-OHALI, M.  
Stellar Krypton cross sections at  $kT=25$  and  
52 keV.  
Physical Review C, 35(1987) S.936-41
- KLAGES, H.O.; BRADY, F.P.; DOLL, P.; GARRETT,  
R.; HANSMEYER, J.; HEERINGA, W.; HIEBERT,  
J.C.; HOFMANN, K.; JANY, P.; KRUPP, H.;  
MAIER, C.; NITZ, W.; WILCZYNSKI, J.  
Few-nucleon experiments with fast polarized  
neutrons.  
Conf. on Neutron-Nucleus Collisions: a Probe  
of Nuclear Structure, Gloucester, Ohio,  
September 5-8, 1984  
Young, P.G. [Hrsg.]  
Nuclear Data for Basic and Applied Science :  
Proc. of the Internat. Conf.,  
Santa Fe, N.M., May 13-17, 1985  
Los Alamos: Los Alamos National Laboratory  
1986. -  
Vol. 1 S.869-77
- KLAGES, H.O.; HOFMANN, K.; NITZ, W.; VOELKER,  
G.; DOLL, P.; FINK, G.; GARRETT, R.;  
HEERINGA, W.; KOIKE, Y.  
Neutron-deuteron elastic scattering in the  
energy range up to 50 MeV.  
Berman, B.L. [Hrsg.]  
The Three-Body Force in the Three-Nucleon  
System : Proc. of the Internat. Symp.,  
Washington, D.C., April 24-26, 1986. -  
S.313-14  
(Lecture Notes in Physics; 260)
- KLAGES, H.O.  
ND elastic scattering, breakup reactions and  
the search for three-nucleon forces.  
Berman, B.L. [Hrsg.]  
The Three-Body Force in the Three-Nucleon  
System : Proc. of the Internat. Symp.,  
Washington, D.C., April 24-26, 1986. - S.203  
(Lecture Notes in Physics; 260)
- KLAGES, H.O.  
Neutron-deuteron elastic scattering and  
breakup experiments.  
Sasakawa, T. [Hrsg.]  
Proc. of the 11th Internat. IUPAP Conf. on  
Few-Body Systems in Particle and Nuclear  
Physics, Tokyo, J, August 24-30, 1986  
Amsterdam : North Holland 1987 S.353c-364e
- KLAGES, H.O.; HOFMANN, K.; NITZ, W.; DOLL,  
P.; GARRETT, R.; HEERINGA, W.; KRUPP, H.  
Analyzing power of the  $^2\text{H}(n,n)d$  (FSI) breakup  
reaction from 20 to 50 MeV.  
Berman, B.L. [Hrsg.]  
The Three-Body Force in the Three-Nucleon  
System : Proc. of the Internat. Symp.,  
Washington, D.C., April 24-26, 1986. -  
S.311-12  
(Lecture Notes in Physics; 260)
- KLAY, N.; KAEPPELER, F.; RUPP, G.  
The  $\beta^-$ -branch in the decay of supra(79m)Se.  
In: Qaim, S.M. [Hrsg.]  
Progress Report on Nuclear Data Research in  
the Federal Republic of Germany for the  
Period April 1, 1985 to March 31, 1986  
NEANDC(E)-272 U Vol. 5(June 1986) S.7  
INDC(Ger)-29/LN + Special

- KOZIK, T.; BUSCHMANN, J.; GROTOWSKI, K.; GILS, H.J.; HEIDE, N.; KIENER, J.; KLEWE-NEBENIUS, H.; REBEL, M.; ZAGROMSKI, S.; COLE, A.J.; MICEK, S.  
Intermediate mass fragments in the reaction  ${}^6\text{Li} + {}^{46}\text{Ti}$ , at  $E/A=26$  MeV.  
Spring Meeting of Nuclear Physics Sections of the Deutsche Physikalische Gesellschaft, Nederlandse Natuurkundige Vereniging, Belgische Natuurkundige Vereniging, Societe Belge de Physique, Dansk Fysisk Selskab, Groningen, NL, March 23-27, 1987  
Verhandlungen der Deutschen Physikalischen Gesellschaft, R.6, Bd.22 (1987) A-6.6  
Zeitschrift fuer Physik A, 326(1987) S.421-28
- KRUPP, H.; DOLL, P.; EBERHARD, V.; HEERINGA, W.; KLAGES, H.O.; WOELFL, CHR.; WILCZYNSKI, J.  
The np spin correlation parameter  $A_{sub}(yy)$  in the energy range 17 to 50 MeV.  
Sasakawa, T. [Hrsg.]  
Few Body Systems in Particle and Nuclear Physics : 11th Internat. IUPAP Conf., Tokyo and Sendai, J, August 24-30, 1986  
Sendai : Tohoku Univ., 1986. - S.398-99  
(Research Report of Laboratory of Nuclear Science, Tohoku University : Suppl. ; 19(1986))
- KRUPPA, A.T.; LOVAS, R.G.; BECK, R.; DICKMANN, F.  
Breathing cluster model for nuclei of two s-wave clusters.  
Physics Letters B, 179(1986) S.317-21
- KRUPPA, A.T.; BECK, R.; DICKMANN, F.  
Electromagnetic properties of  ${}^6\text{Li}$  in a cluster model with breathing clusters.  
Physical Review C, 36(1987) S.327-45
- KUESTER, H.  
Recent results on new particle searches at PETRA.  
KfK-4110 (Juli 86)  
21th Rencontre de Moriond on Perspectives in Electroweak Interactions and Unified Theories,  
Les Arcs, F, March 9-16, 1986
- MAIER, CHR.; REPPENHAGEN, D.; DOLL, P.; FINLAY, R.W.; FORD, T.D.; KLAGES, H.O.  
Spin-spin interaction in neutron-nucleus scattering.  
Proc.of the Internat.Nuclear Physics Conf., Harrogate, GB, August 25-30, 1986  
Harrogate: Institute of Physics 1986 Vol.1 S.10
- MASCHUW, R.  
Search for neutrino oscillations with KARMEN.  
Fackler, O. [Hrsg.]  
'86 Massive Neutrinos in Astrophysics and in Particle Physics : Proc.of the 6th Moriond Workshop, Tignes, F, January 25 - February 1, 1986  
Gif-sur-Yvette : Ed. Frontieres, um 1986. - S.293-99
- MAYER, P.  
Suche nach instabilen Photinos.  
KfK-4211 (April 87)
- NAQVI, A.A.; KAEPPeler, F.; DICKMANN, F.; MUELLER, R.  
Fission fragment properties in fast neutron induced fission of  ${}^{237}\text{Np}$ .  
Physical Review C, 34(1986) S.218-25  
In: Qaim, S.M. [Hrsg.]  
Progress Report on Nuclear Data Research in the Federal Republic of Germany for the Period April 1, 1985 to March 31, 1986  
NEANDC(E)-272 U Vol. 5(June 1986) S.11  
INDC(Ger)-29/LN + Special
- NEUDOLD, M.  
Ein Multiprozessorsystem zur Messdaten-Aufnahme bei Kernphysikalischen Experimenten.  
KfK-4183B (Dezember 86)
- OEHLSCHLAEGER, J.; MOHN, H.U.; CORCALCIUC, V.  
Rechnerprogramm zur Auswertung einfacher Reaktionsmodelle des Aufbruchs nuklearer Projektile.  
KfK-4275B (Juni 87)
- PLANETA, R.; KLEWE-NEBENIUS, H.; BUSCHMANN, J.; GILS, H.J.; REBEL, M.; ZAGROMSKI, S.; KOZIK, T.; FREINDL, L.; GROTOWSKI, K.  
The nonelastic projectile break-up cross section from particle-gamma coincidence measurements for the  ${}^6\text{Li}+{}^{40}\text{Ca}$  reaction at 156 MeV.  
Nuclear Physics A, 448(1986) S.110-22
- PLANETA, R.; BELERY, P.; BRZYCHCZYK, J.; COHILIS, P.; EL MASRI, Y.; GREGOIRE, GH.; GROTOWSKI, K.; MAJKA, Z.; MICEK, S.; SZCZODRAK, M.; WIELOCH, A.; ALBINSKI, J.  
Element distributions after binary fission of  ${}^{235}\text{U}$ .  
Physical Review C, 34(1986) S.512-22
- REBEL, M.  
Investigations of nuclear projectile break-up reactions - a laboratory approach of nuclear astrophysics.  
Internat. Summer School 'Symmetries and Semiclassical Features of Nuclear Dynamics', Poiana Brasov, R, September 1-13  
KfK-4158 (Oktober 86)
- REUSCHER, M.  
Prototypuntersuchung zum Nachweis Neutrino-induzierter Ereignissignaturen im Bereich von 5-50 MeV im Szintillationsdetektor KARMEN 1.  
Dissertation, Universitaet Karlsruhe 1986
- SOSIN, Z.; KOZIK, T.; MICEK, S.; GROTOWSKI, K.  
A gas ionization chamber for on-line heavy ion identification.  
Nuclear Instruments and Methods A, 249(1986) S.344-48
- SPIEKER, C.; HECK, D.; ZIDEK, W.; STRATMANN, T.; BASSEWITZ, D.P.VON; VETTER, M.; ZUMKLEY, H.  
Application of proton-induced-X-ray emission (PIXE) to the determination of trace elements in biological samples.  
Trace Elements in Medicine, 3(1986) S.87-89
- WALTER, G.; BEER, H.; KAEPPeler, F.; REFFO, G.; FABBRI, F.  
The s-process branching at  ${}^{79}\text{Se}$ .  
Astronomy and Astrophysics, 167(1986) S.186-99
- WILD, B.  
Funktionstest eines TMS-Kalorimeters.  
KfK-4119 (Oktober 86)
- WISSHAK, K.; KAEPPeler, F.; MUELLER, H.  
Prototype crystals for the Karlsruhe 4m barium fluoride detector.  
Nuclear Instruments and Methods A, 251(1986) S.101-07
- WISSHAK, K.; GUBER, K.; KAEPPeler, F.  
Gamma-ray spectroscopy with a cooled barium fluoride crystal.  
Nuclear Instruments and Methods A, 259(1987) S.583-85

## 6.2 CONFERENCE CONTRIBUTIONS

Internat. Symp. on Weak and Electromagnetic Interactions in Nuclei, Heidelberg, July 1-5, 1986

BAUR, G.; BERTULANI, C.A.; REBEL, H.  
Coulomb dissociation as a source of information on radiative capture processes of astrophysical interest.

BEER, H.  
Competition of neutron capture and beta decay at the  $^{85}\text{Kr}$  and  $^{151}\text{Sm}$  branchings, a means to estimate the s-process pulse conditions.

KLAY, N.; KAEPPELER, F.  
The stellar beta decay rate of  $^{79}\text{Se}$ .

2nd IAP Workshop Advances in Nuclear Astrophysics, Paris, F, July 7-11, 1987

BEER, H.  
s-process studies using single and pulsed neutron exposures.

KAEPPELER, F.  
Status of the classical s-process.

KAEPPELER, F.; NAQVI, A.A.; AL-OHALI, M.  
Stellar cross sections at  $KT=52$  KeV: the example of  $^{85}\text{Krsupra}(m)$ .

18th Meeting of the European Group for Atomic Spectroscopy (EGAS), Marburg, July 8-11, 1986

ANSELMANT, M.; BEKK, K.; CHONGKUM, S.;  
GOERING, S.; HANSER, A.; KAELEBER, W.;  
LIEWEHR, W.; MEISEL, G.; REBEL, H.; SCHATZ,  
G.; THOMPSON, R.C.  
Recent laser spectroscopy activities at KfK.

23rd Internat. Conf. on High Energy Physics, Berkeley, Calif., July 16-23, 1986

APEL, W.D.; CELLO-COLLABORATION  
Measurement of the total hadronic cross section in  $e^+e^-$  annihilation between center of mass energies of 14 and 47 GeV.

CELO-COLLABORATION  
A search for single photons at PETRA.

CELO-COLLABORATION  
Search for light leptoquark bosons.

CELO-COLLABORATION  
High pt jet formation in untagged photon-photon collisions.

CELO-COLLABORATION  
Study of inclusive leptons from b-quark production in  $e^+e^-$  annihilations at energies above 43 GeV.

CELO-COLLABORATION  
Search for the zino in  $e^+e^-$  interactions.

CELO-COLLABORATION  
Search for excited quarks in  $e^+e^-$  interactions with the CELLO detector.

CELO-COLLABORATION  
Search for winos and higgsinos in  $e^+e^-$  interactions.

CELO-COLLABORATION  
Search for charged and neutral heavy leptons in  $e^+e^-$  interactions.

CELO-COLLABORATION  
Search for scalar electrons and photinos in  $e^+e^-$  interactions.

CELO-COLLABORATION  
Measurement of the muon pair asymmetry in  $e^+e^-$  annihilations at  $38.3 \leq \sqrt{s} \leq 46.8$  GeV.

CELO-COLLABORATION  
High order, high momentum transfer QED tests and search for excited electrons.

CELO-COLLABORATION  
Comparison of the lowest energy jet in three-jet events at 44 GeV with the average jet in two-jet events at 14 GeV.

CELO-COLLABORATION  
Measurement of the total hadronic cross section in  $e^+e^-$  annihilation between center of mass energies of 14 and 47 GeV.

35th Annual Denver Conf. on Applications of X-ray Analysis, Denver, Colo., August 4-8, 1986

OTTMAR, H.; EBERLE, H.; MATUSSEK, P.;  
MICHEL-PIPER, I.  
Energy-dispersive X-ray techniques for accurate heavy element assay.

Few Body Systems in Particle and Nuclear Physics : 11th Internat. IUPAP Conf., Tokyo and Sendai, J, August 24-30, 1986



FINK, G.; DOLL, P.; GARRETT, R.; HEERINGA, W.; HOFMANN, K.; KLAGES, H.O.; KRUPP, H.  
Measurement of the np differential cross section from 22 to 50 MeV.

KRUPP, H.; DOLL, P.; EBERHARD, V.; HEERINGA, W.; KLAGES, H.O.; WOELFL, CHR.; WILCZYNSKI, J.  
The np spin correlation parameter  $A_{sub}(yy)$  in the energy range 17 to 50 MeV.

Internat. Nuclear Physics Conf., Harrogate, GB, August 25-30, 1986

DOLL, P.; FINK, G.; FINLAY, R.W.; FORD, T.D.; HEERINGA, W.; KLAGES, H.O.; SCHMALZ, G.; SKACEL, H.; KRUPP, H.; MAIER, CHR.  
The Karlsruhe polarized neutron facility POLKA.

EYRICH, W.; HOFMANN, A.; LEHMANN, A.; MUEHLDOERFER, B.; SCHLOESSER, H.; WIRTH, H.; GILS, H.J.; REBEL, H.; ZAGROMSKI, S.  
Investigation of isoscalar giant resonances in  ${}^6\text{Li}$  scattering.

FINK, G.; KRUPP, H.; DOLL, P.; EBERHARD, V.; GARRETT, R.; HEERINGA, W.; KLAGES, H.O.  
Status of neutron-proton scattering experiments and phase-shift analysis up to 50 MeV neutron energy.

MAIER, CHR.; REPPENHAGEN, D.; DOLL, P.; FINLAY, R.W.; FORD, T.D.; KLAGES, H.O.  
Spin-spin interaction in neutron-nucleus scattering.

Internat. Summer School 'Symmetries and Semiclassical Features of Nuclear Dynamics', Poiana Brasov, R, September 1-13

REBEL, H.  
Investigations of nuclear projectile break-up reactions - a laboratory approach of nuclear astrophysics.

41. Tagung der Deutschen Gesellschaft fuer Verdauungs- und Stoffwechselkrankheiten, Hannover, 2.-4. Oktober 1986

OCHS, A.; HECK, D.; KLEMPNOW, A.; KRATT, C.; MAIER, K.P.; SCHAEFER, H.; GEROK, W.  
Differenzierung von Haemochromatose und sekundaeerer Siderose durch Protonen induzierte Roentgenemission (PIXE).

7. Internat. Lebersymposium 'Leberzirrhose', im Rahmen der Basler Leberwoche, Basel, CH, 17.-21. Oktober 1986

OCHS, A.; KLEMPNOW, A.; HECK, D.; KRATT, C.; SCHAEFER, H.; MAIER, K.P.  
Inhomogeneous copper distribution in advanced cirrhosis in Wilson's disease detected by proton-induced X-ray emission (PIXE) compared with rubeanic acid staining.

11th Internat. Conf. on Cyclotrons and their Applications, Tokyo, J, October 20-24, 1986

BECHTOLD, V.; FEHSENFELD, P.; SCHWEICKERT, H.  
Industrial applications of the Karlsruhe compact cyclotron.

20th SNEAP (Symp. of Northeastern Accelerator Personnel), Notre Dame, Ind., November 3-6, 1986

ERNST, A.  
The 2 and the 3.75 MeV van de Graaff - accelerators at the KfK and their control system.

IAEA Internat. Symp. on Nuclear Material Safeguards, Wien, A, November 10-14, 1986

DE MEESTER, R.; EBERLE, H.; JOHNSON, S.; KOCH, L.; MICHEL-PIPER, I.; NACKAERTS, H.; OTTMAR, H.  
Reprocessing output verification by K-edge densitometry.

OTTMAR, H.; EBERLE, H.; KOCH, L.; DE MEESTER, R.; KUHN, E.  
Field demonstration of an X-ray densitometer for uranium and plutonium input verification in reprocessing.

4ieme Rencontre entre Astrophysiciens et Physiciens Nucleaires, Bruxelles, B, 8-9 Decembre 1986

BEER, H.  
Neutron capture reactions - status and techniques of measurement and astrophysical impact.

25th Winter Meeting on Nuclear Physics, Bormio, I, January 19-24, 1987

HEIDE, N.; CORCALCIUC, V.; GILS, H.J.; REBEL, H.; ZAGROMSKI, S.; SRIVASTAVA, D.K.; SAMANTA, C.  
Manifestation of the internal momentum distribution in  ${}^6\text{Li}$  break-up reactions?

Workshop on Modern Optics, Lasers and Laser Spectroscopy for Radioactive Isotopes, Kanpur, IND, January 23-29, 1987

MEISEL, G.; BEKK, K.; REBEL, H.; SCHATZ, G.  
Atomic beam, optogalvanic and stored ion spectroscopy for radioactive isotopes.

Workshop on Break-up Phenomena in Nuclear Physics, Calcutta, IND, February 9-11, 1987

REBEL, H.  
Our interest in nuclear break-up.

REBEL, H.  
Coulomb break-up studies - access to information on radiative capture processes of astrophysical interest.

22th Rencontre de Moriond on Perspectives in Electroweak Interactions and Unified Theories, Les Arcs, F, March 8-15, 1987

JUNG, H.  
Aspects of the CELLO single photon experiment.

Fruehjahrstagung DPG, Atomphysik, Kurzzeitphysik, Molekuelphysik, Plasmaphysik, Massenspektrometrie, Goettingen, 16.-20.Maerz 1987  
Verhandlungen der Deutschen Physikalischen Gesellschaft, R.6, Bd.22 (1987)

KAELBER, W.; MEISEL, G.; BEKK, K.; REBEL, H.  
Laserspektroskopie an Thorium-Ionen in einer Hochfrequenz-Ionenfalle.

Fruehjahrstagung DPG, Teilchenphysik, Zuerich, CH, 18.-20.Maerz 1987

ENGLER, J.; GELLERT, M.; KEIM, H.  
Ionisationskammer fuer Fluessigkeiten bei Raumtemperatur.

FUSTER, J.; CELLO-COLLABORATION  
Search for charged higgs at PETRA.

GAMERDINGER, K.; CELLO-COLLABORATION  
Energie-Korrelationen in multihadronischen Ereignissen der  $e^+e^-$ -Physik.

HANSMEYER, J.; CELLO-COLLABORATION  
Modellunabhaengige Grenzen fuer die Kopplungskonstante  $\alpha_{sub}(s)$  der starken Wechselwirkung.

JUNG, H.; CELLO-COLLABORATION  
Single photon Experiment bei CELLO.

MAYER, P.; CELLO-COLLABORATION  
Suche nach instabilen Photinos mit dem CELLO Detektor.

Spring Meeting of Nuclear Physics Sections of the Deutsche Physikalische Gesellschaft, Nederlandse Natuurkundige Vereniging, Belgische Natuurkundige Vereniging, Societé Belge de Physique, Dansk Fysisk Selskab, Groningen, NL, March 23-27, 1987  
Verhandlungen der Deutschen Physikalischen Gesellschaft, R.6, Bd.22 (1987)

BEER, H.; MACKLIN, R.L.  
A stopwatch for the time duration of the s-process neutron irradiations.

DIETZEL, R.; EYRICH, W.; HOFMANN, A.; LEHMANN, A.; MUEHLIDORFER, B.; SCHLOESSER, H.; WIRTH, H.; GILS, H.J.; REBEL, H.; ZAGROMSKI, S.  
Investigation of isoscalar giant resonances in  ${}^6\text{Li}$ -scattering.

DOLL, P.; EBERHARD, V.; FINLAY, R.; FORD, T.; HEERINGA, W.; KLAGES, H.O.; REPPENHAGEN, D.; VOLLMER, A.  
Measurement of the analyzing power of neutron induced reactions on  ${}^3\text{He}$ .

DOLL, P.; EBERHARD, V.; FINLAY, R.; FORD, T.; HEERINGA, W.; KLAGES, H.O.; KRUPP, H.; REPPENHAGEN, D.; WOELFL, CHR.  
Experimental studies of the nucleon-nucleus spin-spin interaction.

DOLL, P.; EBERHARD, V.; FINK, G.; FINLAY, R.; HEERINGA, W.; KLAGES, H.O.; KRUPP, H.; REPPENHAGEN, D.; VOLLMER, A.  
Backward angle n-p analyzing power  $A_{sub}(y)$  at energies from 17 MeV to 50 MeV.

DOLL, P.; FINK, G.; FINLAY, R.W.; HAUPENTHAL, M.; KASTEN, B.; KLAGES, H.O.; SCHIELER, H.; SMEND, F.; WICKE, G.  
Neutron capture studies using pulse-shape-discrimination (PSD) techniques in a large NaI(TL).

GIORGINIS, G.; MANN, D.; WOELFLE, S.; GEMMEKE, H.; MASCHUW, R.; ZEITNITZ, B.  
The Karlsruhe liquid argon time projection chamber.

HEIDE, N.; CORCALCIUC, V.; GILS, H.J.; REBEL, H.; ZAGROMSKI, S.; SRIVASTAVA, D.K.  
Experimental study of  ${}^6\text{Li}$  break-up at large relative momenta of the fragments.

JELITTO, H.; BUSCHMANN, J.; GILS, H.J.; KIENER, J.; REBEL, H.; ZAGROMSKI, S.; SAMANTA, C.  
Projectile break-up reactions of 156 MeV  ${}^6\text{Li}$  at small relative momenta.

KARMEN-COLLABORATION  
Status of the KARMEN neutrino experiment.

KELLER, K.; GENTNER, R.; LASSEN, L.; LUECKING, W.; SCHRECK, R.; GEMMEKE, H.  
Angular momentum dissipation in  ${}^{32}\text{S} + {}^64\text{Ni}$  collisions at 7.5 MeV/u.

KLAY, N.; KAEPPELER, F.  
The stellar  $\beta$ -decay rate of  ${}^{79}\text{Se}$ .

KLAY, N.; BEER, H.; BOERNER, H.; KAEPPELER, F.; SCHATZ, G.; KRUSCHE, B.  
The level scheme of  ${}^{176}\text{Lu}$  and its astrophysical implications.

KOZIK, T.; BUSCHMANN, J.; GROTOWSKI, K.; GILS, H.J.; HEIDE, N.; KIENER, J.; KLEWE-NEBENIUS, H.; REBEL, H.; ZAGROMSKI, S.; COLE, A.J.; MICEK, S.  
Intermediate mass fragments in the reaction  ${}^6\text{Li} + {}^{46}\text{Ti}$ , at  $E/A=26$  MeV.

ROESCH, W.; RICHTER, A.; SCHRIEDER, G.;  
BELLM, D.; GENTNER, R.; KELLER, K.; LASSEN,  
L.; SEIBERT, U.; CASSING, W.; GEMMEKE, H.;  
SCHUELL, D.  
Preequilibrium emission of neutrons in the  
system  $^{40}\text{Ar} + ^{40}\text{Ca}$  at 15 and 20 MeV/amu.

SCHLOESSER, H.; LEHMANN, A.; EYRICH, W.;  
HOFMANN, A.; MUEHLDOERFER, B.; WIRTH, H.;  
GILS, H.J.; REBEL, H.; ZAGROMSKI, S.  
Optimization of the magnetic spectrograph  
'Little John' to study giant resonances.

WIRTH, H.; EYRICH, W.; HOFMANN, A.; LEHMANN,  
A.; MOOSBURGER, M.; MUEHLDOERFER, B.;  
SCHLOESSER, H.; GILS, H.J.; REBEL, H.;  
ZAGROMSKI, S.  
Measurement of the ( $^6\text{Li}$ ,  $^6\text{He}$ ) reaction to  
study spin-isospin-transfer strength.

WISSHAK, K.; KAEPPELER, F.; GUBER, K.  
The Karlsruhe  $4\pi$  barium fluoride detector.

Conf. on Nuclear Structure and Particle  
Physics, Birmingham, GB, April 1-3, 1987

REBEL, H.; BEKK, K.; MEISEL, G.; SCHATZ, G.  
The odd-even staggering of nuclear charge  
radii from atomic beam laserspectroscopy of  
Pb, Sn and Sr isotopes.

Workshop on Muon Catalyzed Fusion and Fusion  
with Polarized Nuclei, Erice, I, April 3-9,  
1987

HEERINGA, W.  
Prospects for polarizing solid DT.

Workshop on Nuclear Astrophysics, Schloss  
Ringberg, Tegernsee, April 21-24, 1987

KAEPPELER, F.; KLAY, N.; BEER, H.; SCHATZ, G.  
Experimental studies of thermal effects  
during s-process nucleosynthesis.

REBEL, H.  
Coulomb dissociation as a source of  
information on radiative capture processes of  
astrophysical interest.

Internat. Symp. on Collective Phenomena in  
Nuclear and Subnuclear Long Range  
Interactions in Nuclei,  
Bad Honnef, May 4-7, 1987

EYRICH, W.; HOFMANN, A.; LEHMANN, A.;  
MOOSBURGER, M.; MUEHLDOERFER, B.; SCHLOESSER,  
H.; WIRTH, H.; GILS, H.J.; REBEL, H.;  
ZAGROMSKI, S.  
Investigation of giant resonances in  
 $^6\text{Li}$ -scattering and ( $^6\text{Li}$ ,  $^6\text{He}$ ) reactions.

24th European Cyclotron Progress Meeting,  
Nice, F, May 11-12, 1987

BECHTOLD, V.; FEHSENFELD, P.; HANSER, A.;  
MOELLENBECK, J.; SCHWEICKERT, H.; THOUW, T.  
Industrial applications of the Karlsruhe  
compact cyclotron.

9th Annual Meeting of the European Safeguards  
Research and Development Association  
(ESARDA), London, GB, May 12-14, 1987

EBERLE, H.; MATUSSEK, P.; MICHEL-PIPER, I.;  
OTTMAR, H.  
Evaluation of high-rate pulse processing in  
K-edge densitometry.

Internat. Europhysics Conf. on High Energy  
Physics, Uppsala, S, June 25 - July 1, 1987

APEL, W.D.; CELLO-COLLABORATION  
Search for heavy leptons.

APEL, W.D.; CELLO-COLLABORATION  
A model independent study of the shape of the  
third jet in  $e^+e^-$  annihilation into  
multihadrons at 35 GeV.

APEL, W.D.; CELLO-COLLABORATION  
The  $K^0_{(s)}K^0_{(s)}$  final state in  $\gamma\gamma$   
interactions.

APEL, W.D.; CELLO-COLLABORATION  
Study of the  $ee\gamma$  and  $\mu\mu\gamma$  final states and  
search for excited leptons in  $e^+e^-$   
interactions.

APEL, W.D.; CELLO-COLLABORATION  
Tests of QED in the  $e^+e^-$  annihilation into  
two, three and four photons.

CELLO-COLLABORATION  
Single photon search with the CELLO detector.

7. PERSONNEL

Head of the Institute IK I: Prof.Dr.B.Zeitnitz

Scientific and Technical staff:

Apel, W.-D., Dr.	Hucker, H.	Vollmer, A.
Bayer, R.	Husson, L., Ing.	Wild, P.
Böhrer, A.	Jany, P., DP	Wochele, J., DP
Cattai, A., Dr.	Jung, J., DP	Wölfle, S.
Deutsch, G.	Keim, H.	Wölfl, Chr., DP
Dittmann, R.	Klages, H.O., Dr.	Wolf, J.
Doll, P., Dr.	Kleinfeller, J., Dr.	Ziegler, P.
Drexlin, G., DP	Knapp, J., Dr.	
Eberhard, V.	Knopf, M.	
Engler, J., Dr.	Mann, D.	
Fink, G., DP	Markofsky, T.	
Finkbeiner, F.	Maschuw, R., Dr.	
Flügge, G., Prof.Dr.	Mayer, P.	
Fries, D.C., Prof.Dr.	Mielke, H.-H.	
Gabriel, P.	Müller, C.	
Gamerdinger, K., DP	Müller, H., Prof.Dr.	
Gettert, M.	Müller, W.	
Gemmeke, H., Dr.	Plischke, P., Dr.	
Giorginis, G., Dr.	Ranitzsch, K.H., Dr.	
Grandegger, W., DP	Raupp, F., Dr.	
Grimm, A.	Reppenhagen, D.	
Gumbsheimer, R., DI(FH)	Riegel, M.	
Haedinger, U.,	Scheib, S.	
Hagert, H.,	Schieler, H.	
Hahn, M.,	Schmalz, G., DI	
Hansmeyer, J., Dr.	Schmidt, F.K., Dr.	
Hauber, S.	Schneider, H., Dr.	
Hauptenthal, M.	Seufert, R.	
Heeringa, W., Dr.	Skacel, H.	
Hesselbarth, J.	Spohrer, G.,	
Hoss, A.	Strobelt, T.	

Head of the Section III: Prof.Dr.Gerd Schatz

Scientific and Technical staff:

Antoni, I.	Kiener, J., DP
Beer, H., Dr.	Klay, N., DP
Bekk, K.,Dr.	Köhler, A.
Eberle, H.,Ing.	Matussek, P., DP
Feurer, B.	Meisel, G., Priv.Doiz.,Dr.
Friederich, H.-M.	Michel-Piper, I., DI(FH)
Gerstenhöfer, Th.,DP	Müller, H.
Gils, H.J.,Priv.Doiz.,Dr.	Oehlschläger, J., DMath
Göring, S., DP	Ottmar, H., Dr.
Hanser, A., Dr.	Rebel, H.G.,Prof.Dr.
Heck, D.,Dr.	Rupp, G.
Heide, N., DP	Schmidt, K.A., DP
Jelitto, H., Dr.	Voss, F., Dr.
Kälber, W., DP	Wisshak, K., Dr.
Käppeler, F., Dr.	Zagromski, S., DI(FH)

Guest scientists:

Chongkum, S., Dr.  
Corcalciuc, V., Dr.  
Dembczynski, J., Prof.Dr.  
Grotowski, K., Prof.Dr.  
Kozik, T., Dr.  
Ratynski, W., Dr.  
Zhao, W., Dr.

Head of the Cyclotron Laboratory: Dr. H. Schweickert

Scientific and Technical Staff:

Acharya, H.	Heidenreich, K.	Peters, J., DP
Assmus, K.	Heinzmann, H., DI	Rämer, Chr., Ing.
Baßler, U.	Heitz, E.	Ripp, H.
Bauer, G.	Herrmann, P.	Roth, H.
Bechtold, V., Dr.	Hirth, W.	Sahm, U., Dr.
Bialy, J., DP	Höllmüller, S.	Schimpf, P.
Biber, J.	Holler, H.	Schmitt, M.
Blank, R.	Hüfner, R., Dr.	Schönstein, E.
Bollmann, E., DP	Huttel, E., Dr.	Schüssler, B.
Dennerlein, H.D.	Kaltenbaek, J.	Schütz, R.
Dohrmann, H., Ing.	Kappel, W.-R., Ing.	Schulz, F., Ing.
Dressel, M.	Kauther, P.	Schweickert, H., Dr.
Dressen, R.	Kernert, N., DP	Seidel, H.
Ehret, E.-P.	Kessel, M.	Seitz, J.
Erbe, D.	Kirste, E.	Seufert, H.
Erdel, E.	Kleinrahm, J., Dr.	Sheikh, S.
Ernst, R.	Klinger, G.	Staub, M.
Fehsenfeld, P., Dr.	Kögel, B.	Stöbener, E., Ing.
Feuerstein, P.	Konrad, J.	Thouw, T., Dr.
Fischböck, T.	Krieg, U.	Uchatius, R.
Foßhag, E., Dr.	Lang, R.	Uhlemann, S.
Franz, J.	Maier, W.	Wiss, L.
Friedrich, L., Dr.	Mangold, D.	Ziegler, P.
Gegenheimer, B.	Mayl, R.	Zimmermann, H.
Günther, O.	Möck, W.	Zimmermann, U.
Heger, V.	Möllenbeck, J., Ing.	